A GENERALIZED SIZING METHOD FOR REVOLUTIONARY CONCEPTS UNDER PROBABILISTIC DESIGN CONSTRAINTS

A Thesis
Presented to
The Academic Faculty

by

Taewoo Nam

In Partial Fulfillment
of the Requirements for the Degree
Doctor of Philosophy in the
School of Aerospace Engineering

Georgia Institute of Technology
May 2007

A GENERALIZED SIZING METHOD FOR REVOLUTIONARY CONCEPTS UNDER PROBABILISTIC DESIGN CONSTRAINTS

Approved by:

Professor Dimitri N. Mavris,
Committee Chair
School of Aerospace Engineering
Georgia Institute of Technology

Professor Vitali V. Volovoi
School of Aerospace Engineering
Georgia Institute of Technology

Professor Daniel P. Schrage
School of Aerospace Engineering
Georgia Institute of Technology

Mr. Craig L. Nickol
Langley Research Center
National Aeronautics and Space Administration

Dr. Danielle S. Soban
School of Aerospace Engineering
Georgia Institute of Technology

Date Approved: April 2, 2007

To my wife, Joung Yun

for her patience, perseverance, sacrifice, and support

but most of all for her unending love

ACKNOWLEDGEMENTS

I would first like to thank my advisor, Professor Dimitri Mavris, for his support throughout my entire graduate studies. His technical expertise, unflagging ardor, and persistent encouragement were the bedrock of this work. My gratitude extends to my entire committee for their guidance and valuable comments regarding my endeavor.

This research would not have been possible of it were not for the financial support provided by NASA and the Department of Defense under the University Research, Engineering and Technology Institutes (URETI) program. I am also grateful for the financial support that I have received from the Handeul Scholarship Foundation.

My fellow graduate students have been of great help in completing this document. Specifically, I would like to thank Taeyun Choi for providing his fuel cell propulsion system analysis model and tireless proofreading. My appreciation extends to all other URETI team members, especially Davis Balaba, Eric Upton, Bhuan Agrawal, and Blake Moffitt for their suggestions and assistance. I thank to Kelly Griendling, Jean Charles Domercant, Dongwook Lim, Santiago Balestrini, and Henry Won for reviewing various versions of my thesis manuscripts. Special thanks are in order for Kyunghoon Lee for his magical assistance with all things LaTeX. I am also very appreciative of the valuable comments given to me by Mr. Mark Water, known as a great wizard of ASDL.

The final version of this document would not be what it is, had it not been for the professional proofreading done by Mrs. Osburg. I am also in debt to Dr. Chae, Dr. Lillie, Dr. Cheon, Mr. McKeon, and Dr. Ahn for their friendship and support. They have made my time in Atlanta more enjoyable.

A very special thanks has to go to Mr. Hoffschwelle, who mentored me while I

was at KAI. To me, he shall remain as the one who most influenced my career in aerospace engineering by inspiring me to love studying airplanes.

The last but not the least, I would like to thank my family and loved ones. No word can sufficiently express how thankful I am of my parents and parents-in-law enough for their unending love and support. I have been a long way from home for a long time. Particularly, the last five years have been the hardest they had to endure, without me being able to support them as much as they deserved. Finally, my wife, Joung Yun, my daughter, Jihye, and my son, Jiung; without your encouragement and love, I could never have achieved this. I am a lucky man and *proud to be called your husband and your father*.

Thanks everyone,

Atlanta, Georgia, Spring 2007

TABLE OF CONTENTS

LIST OF TABLES

LIST OF FIGURES

SUMMARY

Internal combustion (IC) engines that consume hydrocarbon fuels have dominated the propulsion systems of air-vehicles for the first century of aviation. In recent years, however, growing concern over rapid climate changes and national energy security has galvanized the aerospace community into delving into new alternatives that could challenge the dominance of the IC engine. A critical element required to pursue alternative energy flight is a quantitative assessment environment for aircraft sizing and synthesis that provides insight into the system-wide responses of these technologies and system architectures, thereby increasing the possibility of arriving at more informed decisions.

Nevertheless, traditional aircraft sizing methods have significant shortcomings for the design of such unconventionally-powered aircraft. First, traditional aircraft sizing methods are specialized for aircraft powered by IC engines, and thus are not flexible enough to assess revolutionary propulsion concepts that produce propulsive thrust through a completely different energy conversion process. Another deficiency associated with the traditional methods is that a user of these methods must rely heavily on experts' experience and advice for determining appropriate design margins. Aircraft sizing achieves its goal by imposing two primary constraints: matching available power to required power and available energy to required energy. These constraints have always been assumed to be deterministic in the context of traditional sizing methods and even under the more recent probabilistic design paradigm. In reality, significant uncertainty, including unsettled performance requirements and

environmental regulations, changes in drag and weight due to evolving airframe design, and lack of accuracy of subsystem performance prediction may permeate design parameters and contributing analyses associated with these constraints. The traditional approach to mitigate the risk associated with such uncertainty is to add design margin quantified by the empirical knowledge of experienced engineers. Such an approach, however, may result in either significant risk or unnecessary increases in weight and cost. Furthermore, the introduction of revolutionary propulsion systems and energy sources is very likely to entail an unconventional aircraft configuration, which inexorably disqualifies the conjecture of such "connoisseurs" as a means of risk management. Motivated by such deficiencies, this dissertation aims at advancing two aspects of aircraft sizing: 1) to develop a generalized aircraft sizing formulation applicable to a wide range of unconventionally powered aircraft concepts and 2) to formulate a probabilistic optimization technique that is able to quantify appropriate design margins that are tailored towards the level of risk deemed acceptable to a decision maker.

A more generalized aircraft sizing formulation, named the Architecture Independent Aircraft Sizing Method (AIASM), is achieved by modifying several assumptions of the traditional aircraft sizing method. First, fuel is generalized as a concept of on-board energy which can originate from a gamut of energy sources. Each source is categorized as consumable energy or non-consumable energy. In addition, the propulsion system is modeled as an integration of multiple power-paths, each of which is characterized by three parameters: the specific energy of the energy source, the specific power and efficiency maps of power transfer devices. Lastly, generalized weight decomposition and weight differential equations are employed to model the fuel consumption behavior of the revolutionary concepts that, unlike the IC engine, may sequester and retain specific by-products from being emitted during flight.

In the course of the development of AIASM, a couple of expedients useful for the

first-order estimation of aircraft performance are also developed: a set of generalized Breguet range equations and the Non-dimensional Aircraft Mass (NAM) Ratio Diagram. The generalized Breguet range equations can estimate the ferry range of an aircraft powered by alternative energy-propulsion architectures with little information pertinent to the aircraft. Utilizing the generalized Breguet range equations as well as the intrinsic duality between the mass of on-board energy sources and the mass of the propulsion systems, the NAM Ratio Diagram identifies the performance frontiers in terms of range and velocity, which are achievable with a given energy-propulsion system architecture.

Along with advances in deterministic aircraft sizing, a non-deterministic sizing technique, named the Probabilistic Aircraft Sizing Method (PASM), is developed. The method allows one to quantify adequate design margins to account for the various sources of uncertainty via the application of the chance-constrained programming (CCP) strategy to AIASM. The CCP aims to find an optimum solution that minimizes the objective function within the *probabilistically* feasible space, in which each point satisfies a set of non-deterministic constraints in accordance with the target probabilities chosen by a decision maker. The PASM mathematically formulates an aircraft sizing problem into an optimization problem whose goal is to minimize the expectation of the objective function values subject to multivariate, nonlinear, individual or joint probabilistic constraints. In this context, the three design variables, power, wing area, and fuel (energy) quantity, are manipulated until all probabilistic constraints are satisfied with equal or higher probabilities than the target. In this way, PASM can also provide insights into a good compromise between *cost* and *safety*. The proposed methods are verified by applying them to two aircraft sizing studies for a fuel cell-powered general aviation (GA) aircraft and a Solar-Powered High Altitude Long Endurance (SPHALE) aircraft with a Regenerative Fuel Cell (RFC) system.

CHAPTER I

INTRODUCTION

Since the Wright brothers' first flight, aerospace endeavors have achieved enormous advancement in technology, both commercial and military. The fabric-covered wooden frame and skid of the "Wright Flyer" has been replaced with metal or advanced composite material and retractable landing gear systems, respectively. Their descendants no longer lie down on the wing to control an airplane but sit in a "glass cockpit" supported by an fully integrated avionics system. Despite such prodigious development of aviation, one thing has not changed: *machine-flights depend almost entirely on internal combustion engines that consume hydrocarbon fuels.* Although the advent of the jet engine ushered in a new era of aviation, its thrust is produced by ultimately the same physics and sources: *exothermic reaction of a fossil fuel derived from oil-fields.* Only a few momentous events, for instance the Solar Challenger's flight across the English Channel solely by solar power in 1981, have reminded the aerospace community of the obvious but not always apparent fact that aircraft can fly via different energy sources.

About half a century ago, atomic energy and hydrogen were envisioned for aircraft propulsion, respectively, and attempts were made to experiment with replacing the hydrocarbon fuels with nuclear or liquid hydrogen for high-speed aircraft [1, 2]. For reasons that were valid at that time, these efforts did not lead to practical applications and were not actively pursued. Despite incessant subsequent efforts to fuel aircraft with alternative energy sources, the dominance of internal combustion (IC) engines had been deemed unbeatable. In recent years, however, alternate energy sources and revolutionary propulsion systems have been attracting renewed attention. An

Figure 1: Examples of unconventionally powered and propelled aerospace systems

ample anthology of literature [3, 4, 5] that foresees the future of aviation commonly advocates the transition to alternative energy sources to power the next generation aircraft, with fossil fuels becoming less reliable. AeroVironment's Helios, funded by the National Aeronautics and Space Administration (NASA), accentuated the great potential of solar energy by establishing a new altitude record for non-rocket-powered aircraft of 96,863 feet in 2001 [6]. Particularly, hydrogen has also been rigorously re-examined for applicability to both jet engines and fuel cells [7].

1.1 Promoters for Energy Alternatives

In the sense that crude oil is a finite resource, the search for alternative energy sources has been predestined since the inception of the *oil economy*. It would be a very logical inference that the cost and availability of conventional aviation fuels will ultimately increase up to a point which is unattractive to aviation. However, the rigorous research of recent years has reached well beyond the level of a "mundane" response for the cliché. In fact, several issues concerning the environment, technology, economics, and national energy security have coalesced into an impetus, which is fostering the search for alternative energy flights.

1.1.1 Mounting Concern for the Environment

The first issue is increased public concern over the environmental impact of engine emissions, which have adverse effects on global warming, ozone depletion, and local air quality. Global warming is referred to as the gradual increase in temperatures on the Earth's surface. Scientists have amassed compelling evidence that recent warming coincides with rapid growth of anthropogenic greenhouse gases such as carbon dioxide, water vapor, methane, nitrous oxide, and ozone. According to a recent report by the National Research Council (NRC), the average surface temperature of the earth has risen 0.4 - 0.8°C over the last century [8]. Moreover, climatologists at NASA's Goddard Institute for Space Studies (GISS) in New York City noted that the 2005 calendar year marks the highest global annual average surface temperature in more than a century and the past four years were identified as belonging to the top five warmest years worldwide over past century [9]. This growing evidence indicates that such a strong underlying warming trend is continuing and even speeding up. The estimation about future global temperature trends depends heavily on assumptions concerning population and economic growth, land use, technological changes, energy availability, and fuel mix [10]. Estimates for this century range from 1 to 3.5°C, any of

which is the greatest average rate of warming in the last 10,000 years [10]. Although this appears as a tiny perturbation, such a change in the global mean may result in a substantial variation in regional temperature and weather, which could have appalling ramifications on the ecological system and human life[1].

Aviation is believed to be less responsible for global warming than some other human activities[2]. Nevertheless, the impact of aircraft emissions on the earth's atmosphere and climate has caught the attention of transportation planners and policymakers for several reasons. First, jet aircraft are the primary source of greenhouse gases that are deposited directly into the upper atmosphere [10]. According to the Intergovernmental Panel on Climate Change (IPCC) and other experts, some of these jet emissions have a greater warming effect than they would have if they were released in equal amounts at the surface by, for example, automobiles [13]. Secondly, the impact of carbon dioxide emissions on the atmosphere can be amplified two- to fivefold by other gases and particles[3] emitted from jet engines. Lastly, aviation is one of the fastest growing contributors to climate change, with global air passenger travel projected to grow at a rate of 5 percent per annum through 2015 [13]. Such a solid growth in aviation, the IPCC predicted, will increase the radiative forcing from aircraft by up to a factor of 11 by 2050, compared with a predicted increase of roughly a factor of two in total anthropogenic forcing [10]. The IPCC recently concluded that the consequential increase in aviation emissions, concomitant to such an escalating demand for air travel, "would not be fully offset by reductions in emissions achieved through technological improvements on conventional propulsion systems alone [13]."

Another concern related to aircraft emissions is ozone depletion. The stratospheric

[1]According to a recent analysis [11], global warming of more than 1°C, relative to 2000, will constitute "dangerous" climate change as judged from likely effects on sea level and extermination of species.

[2]Carbon dioxide and water emitted from aircraft engines account for only 3% of total anthropogenic green house gas emissions [12].

[3]They include water vapor, nitrogen oxide and nitrogen dioxide (collectively termed NO_x), sulfates, and soot.

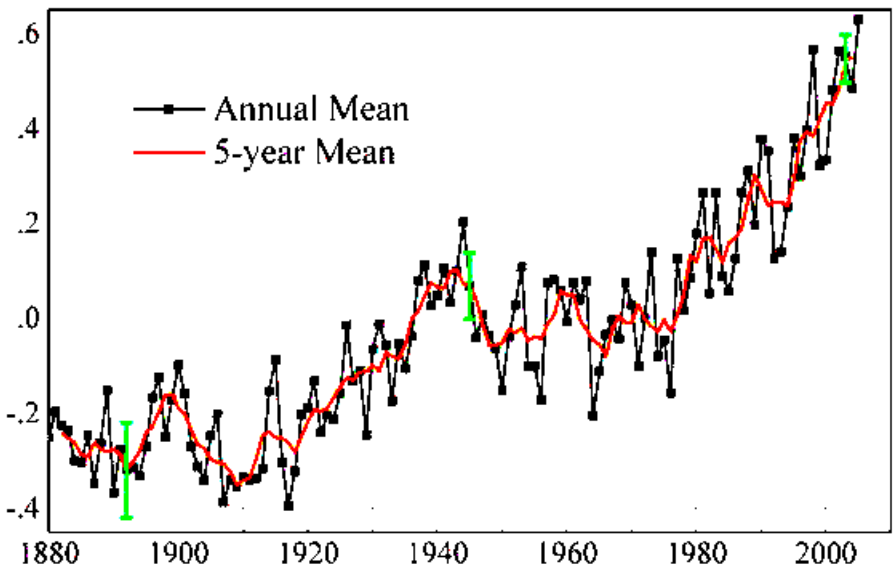

Figure 2: global land-ocean temperature anomaly (°C). Error bars are estimated with 2σ (95% confidence) uncertainty. [9]

ozone layer absorbs ultraviolet radiation that can cause skin cancer. Although ozone-depleting substances (ODS) such as chlorofluorocarbons (CFCs) and halons are controlled under the Montreal Protocol, the Earth's protective ozone layer is persistently being diluted. It has been reported that aircraft emissions can alter the chemistry of the stratosphere, resulting in changes in the concentration of ozone [14]. These changes, in turn, may indirectly affect the total amount of ozone and global climate through coupling with radiative and dynamic atmospheric processes [15]. NO_x emissions by aircraft can affect atmospheric ozone in either positive or negative ways, depending on the altitude at which they are emitted [16]. Although there is considerable uncertainty in the estimates of the actual impact, it is generally agreed that emissions at altitudes above 50,000 to 55,000 feet will degrade the ozone layer to some degree [17]. Several analyses [18, 19, 20] indicate that water emissions from a fleet of large commercial supersonic aircraft operating in the stratosphere would significantly deplete ozone, even if NO_x could be reduced to very low levels.

In addition to effects on the global environment, concerns over degradation in local air quality in the vicinity of airports are growing due to increasing air traffic, increasing urbanization, increasing public, and regulatory attention [21]. Oxides of nitrogen (NO_x), carbon monoxide (CO), and unburned hydro carbon (HC) are the main concerns of aircraft engine emissions for local air quality.

With growing concern about aviation's effects on the global atmosphere and local air quality, relevant regulations are now more stringent, and new regulations are being prepared. Present aircraft emissions regulations apply only to the landing and take-off cycle, known as the LTO cycle, up to an altitude of 900 meters. In the United States, the first regulation on vented fuel, smoke and exhaust (NO_x, HC, CO) emissions was promulgated by the U.S. Environmental Protection Agency (EPA) in 1973, and was revised in 1976, 1980, 1982 and 1984 [22]. In 1997, the two-staged voluntary NO_x standard and CO standard of the International Civil Aviation Organization (ICAO) was codified into the United States law to align with the international emission regulation [23]. In order to further reduce the NO_x emission, the ICAO made a more stringent standard which aims for 16% average reduction for the engines certified after December 31, 2003, and EPA amended the existing standards for NO_x emissions of new commercial aircraft engines 2005 to align with the new ICAO standard. [24]. Instead of developing the standard for CO_2, the ICAO is currently considering a market-base measurement, which includes voluntary measures, emissions-related levies, and emission trading to achieve environmental goals at a lower cost and in a more flexible manner [17].

In response to this, from 1998 to 1999, a series of high-level studies exploring aircraft with unconventional propulsion systems, which focused on reducing aircraft emissions and noise was jointly performed by NASA Langley Research Center (LaRC) and NASA Glenn Research Center (GRC) [25]. Such efforts culminated in the Quiet

Green Transport (QGT) study, one of the initial studies undertaken by the Revolutionary Aerospace Systems Concepts (RASC) Program [25, 26].

1.1.2 Technological Advancement

One thing that held back earlier efforts at seeking alternative energy sources is that the propulsion systems and energy storage systems required for the use of non-hydrocarbon fuel were not mature. A rapid leap in revolutionary propulsion system technology during the past decades, however, has reopened the possibility of operating aircraft on alternative energy sources. For example, the first photovoltaic (PV) cell built by Charles Fritts in 1883 was only around 1% efficient [27], and the first commercial solar cells developed by Hoffman Electronics-Semiconductor Division in 1955 barely exceeded 2% [28]. However, efficiencies of state-of-the-art PV cells are higher than 20%.

Although the current technologies are not immediately ready for commercial applications, continuing ample investment on developing alternative propulsion technology in aerospace as well as other sectors will collectively bring forward feasible and viable aircraft applications. For example, recent efforts in fuel cell propulsion systems are being driven mainly by automobile communities. Aviation sectors will also benefit from such advances in fuel cell technology and electrical components, promoted by automotive and other transportation sectors.

1.1.3 Economic Aspects

A continuous decrease in alternative energy costs due to technological advances, in concert with a steep increase in oil prices in recent years, has been also pushing the advent of commercially viable alternative energy sources forward. As depicted in Figure 3, world oil prices have increased significantly over the past two years relative to historical levels. Crude oil prices, which hovered in the $15-25 per barrel range from the mid-1980s until 2002, have been above $40 since February 2005. Future oil prices

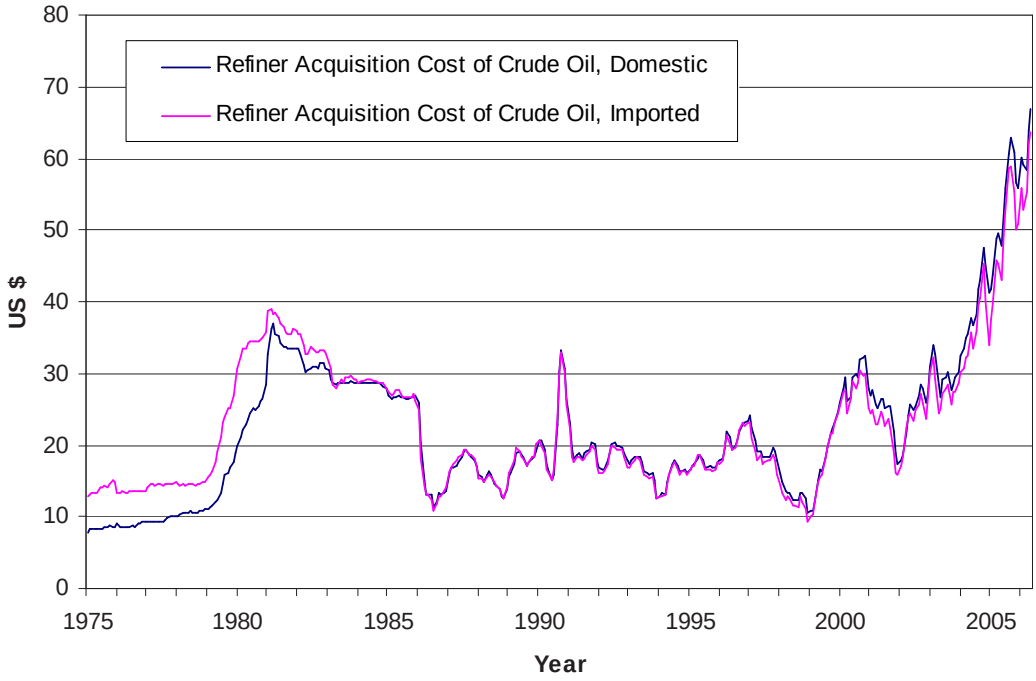

Figure 3: History of crude oil, refiner acquisition cost. The source data [29] were published by the U.S. Department of Energy

are not easy to predict, heavily depending on capricious factors such as geopolitical instability and weather as well as a fundamental driver: supply-demand. Considering rapid world-oil-demand growth driven by all areas of economic activity, many analysts agree that the recent soaring oil prices are not a passing phenomenon like previous oil crises. As far as supply is concerned, the ever-increasing production of crude oil is believed to be approaching its peak[4]. The peak is defined as the apex of worldwide oil production, that occurs when half of the ultimately recoverable reserves have been extracted according to Hubbert Bell Curve [31]. When this resource-limited peak is reached, oil production will start a gradual, but relentless decline that will trigger a cataclysmic rise in oil prices [32]. The date of the global peak heavily depends on the

[4]According to a DOE report published in 2004 [30], no major new field discoveries have been made in decades. Presently, world oil reserves are being depleted three times as fast as they are being discovered.

size of Middle-East reserves, estimations of which are notoriously unreliable [33]. The most optimistic estimate is that the peak of production will be 20 to 25 years from now [34]. Most studies expect crude oil production to peak much earlier, sometime around the year 2015, or even earlier [33]. "Whether the peak occurs sooner or later is a matter of relative urgency, but does not alter a central conclusion; the United States needs to establish a supply base for its future energy needs using its significant oil shale, coal, and other energy resources [30]."

In contrast, the cost of renewable energy has been significantly lowered. For example, the cost of wind power in the U.S. was $.80 per KWh in 1980, but $0.04 per KWh today [35]. The prices of solar cells have even more drastically decreased over a half century. The first commercial solar cells developed by Hoffman Electronics-Semiconductor Division in 1955 cost $1,785 per watt (in 1955 dollars) [28]. The costs dropped down to $100 a watt in 1976, and they sell for less than $3 a watt today. The costs are "expected to continue declining 5 percent annually, even if there are no technology breakthroughs. [36]" In addition to decreases in price tags on alternative energy, increases in oil prices will further narrow the gap, after which alternative energy sources will become increasingly competitive.

1.1.4 National Energy Security

Growing concerns about national energy security have made the search for alternative energy source even more apropos. Dependence upon foreign oil may undermine the national economy and energy security. Today, the U.S. imports 60% of its crude oil supply, and U.S. dependence on foreign sources of oil will increase as domestic resources are exploited [37]. In particular, the U.S. transportation network relies heavily on petroleum from overseas as an energy source [12]. Air travel uses around 10% of total energy consumed by the U.S. transportation network [38], and in 2002, the U.S. imported 62% of its petroleum from overseas. Demand for the transportation

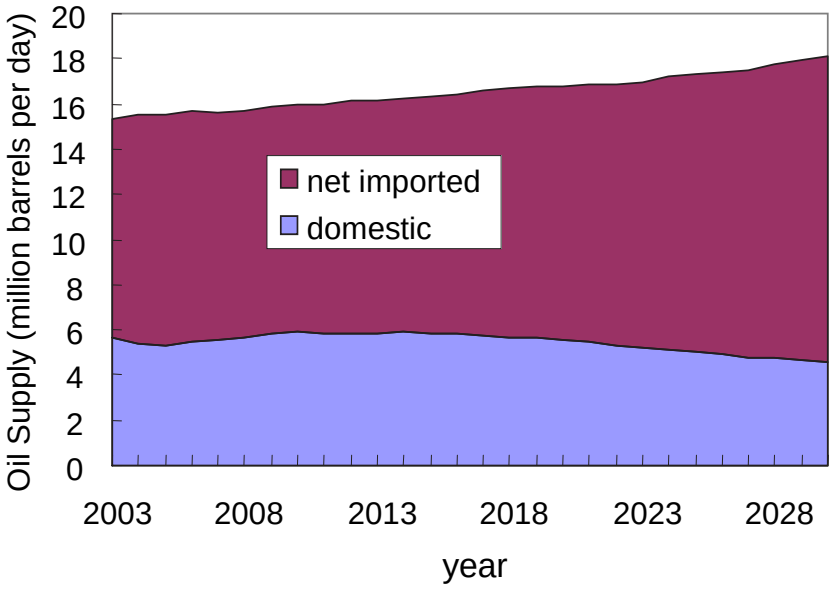

Figure 4: U.S. oil supply sources [38]

sector is expected to continue to increase at a rate between two and three percent per annum until at least 2010 whilst domestic production is forecast to remain relatively static until 2030 [38]. The ramification is that import dependence is only likely to get worse (forecast to be at 68% by 2030 [38]), as shown in Figure 4.

Most of the world's oil reserves are concentrated in the Middle East, and over two-thirds are controlled by the members of OPEC whose "self-appointed mission is to manipulate prices by turning the production spigots up and down [39]." A recent analysis [40] indicates that "oil price shocks and price manipulation by OPEC have cost the U.S. economy dearly, about $7 trillion from 1973 to 2000, which is as large as the sum total of payments on the national debt over the same period." Furthermore, each of the oil market upheavals was followed by a recession. With growing U.S. imports and increasing world dependence on OPEC oil, the U.S. economy would be vulnerable to future price shocks [41]. In addition to increased economic vulnerability, dependence on foreign energy sources(particularly on oil imported from the Middle East, a very volatile region of the world) increases the political burden on the U.S.

government. Senator Joseph R. Biden says: "that dependence means we pay a huge price militarily for access to a resource that we cannot do without. One estimate suggests we pay as much as $825 billion a year in security expenditures to project our influence and secure access to oil [42]."

To address these challenges, in 2001 President George W. Bush announced the National Energy Policy [43] envisioning a comprehensive long-term strategy that includes promoting domestic energy resources such as natural gas, coal, nuclear, and renewable energy sources. In addition, the Energy Policy Act of 2005 [44], and the U.S. Department of Energy (DOE) Strategic Plan [45] also call for developing a diverse portfolio of domestic energy supplies as well as improving energy efficiencies. Furthermore, the President's "Advanced Energy Initiative" announced in 2006 provides for a 22% increase in research by the U.S. Department of Energy to find clean alternatives to oil [46].

Efforts to alleviate the national economy's addiction to oil are also being made across Europe. Such approaches include flourishing windmills in Denmark and "a renewed debate in Britain about reversing promises to cut back on nuclear energy supplies [47]." Most impressive, the Swedish government announced in February 2006 national plans to be world's first "oil-free economy" by 2020 without building a new generation of nuclear power stations [48]. In addition, governments of many countries are espousing cutting-edge research to develop sustainable energy sources to reduce their dependence on imported energy sources.

1.1.5 Unconventional Missions

The development of revolutionary aerospace concepts such as high altitude, extremely long endurance aircraft and vehicles designed for planetary exploration that are not feasible with conventional propulsion systems has provided a need for revolutionary propulsion technologies. High Altitude Long Endurance (HALE) platforms such as

Helios and HeliPlat [49] have been envisioned as a possible alternative to communication satellites. They could also monitor weather, track hurricanes, and make substantial contributions in disaster management via more precisely directing emergency resources [6]. In addition, their remote sensing capability, continuously available over extended time periods of weeks and months, inspires several commercial applications such as "precision" agricultural management and wildfire monitoring that have a need for near real-time high-spatial resolution imagery [50]. In comparison to orbital satellites, "atmospheric satellites" would offer better observational resolution, local persistence, and the capability of reuse [51]. However, such great potential is stymied by a conspicuous technological barrier: such a long endurance capability cannot be achieved with a conventional propulsion architecture and fuel. The U.S. Air Force tanker KC-10 Extender would be the apotheosis of a conventional propulsion aircraft designed for carrying as much fuel as permitted. The aerial refueling tanker, derived from the civilian DC-10-30 airliner, carrying 365,000 lbs. fuel [52], offers an "unrefueled" range of 11,500 nautical miles, holding the record for the world's longest-ranged aircraft. However, even this aircraft cannot stay airborne more than two days without refueling. Therefore, alternative propulsion system architectures and energy sources suitable for such an unconventional mission must be pursued.

Burgeoning interest in the exploration of terrestrial planets is also promoting the research of alternative propulsion aircraft. The idea of performing scientific observations on Mars or Titan using a winged-platform has persisted because of the clear advantages associated with an airborne platform. Just like on Earth, airborne observations would complement ground-based and space-based observations, permitting higher resolution than possible with space-based platforms and greater coverage than possible with ground-based platforms [53]. Airplanes offer an additional advantage over other airborne platforms such as balloons in that it can be maneuvered to specific locations of interest [53]. This advantage has brought winged-platforms onto the

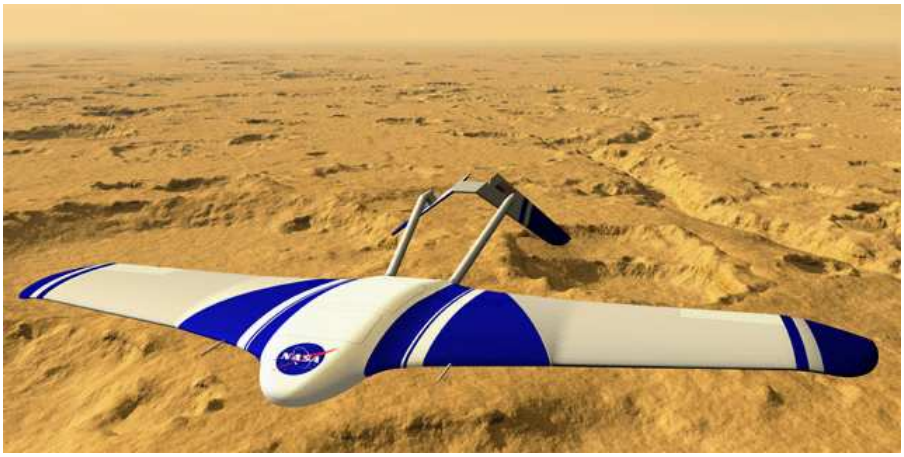

Figure 5: ARES platform for Mars exploration [57]

table with other alternative concepts for atmospheric explorations of Mars and Titan. For Mars exploration, a concept of winged-platform, shown in Figure 5, was embodied for the Aerial Regional-scale Environmental Survey (ARES) of Mars mission [54]. This Mars Scout mission was proposed to provide high-value scientific measurements in the areas of atmospheric chemistry, surface geology and mineralogy, and crustal magnetism [53]. The feasibility of atmospheric flight by an airplane on Titan was also investigated for a post-Cassini mission [55]. Nevertheless, there are several technical challenges associated with a terrestrial airplane, many of which arise from significantly different flight environments. Particularly their atmospheric properties such as density, temperature, and composition invoke a great challenge. For instance, the thin, carbon dioxide Martian atmosphere does not allow conventional air-breathing propulsion systems, which forces NASA researchers to investigate alternative propulsion systems [56].

1.2 Energy Sources for Aviation

Although the recent issues described in the previous section address the need of the search for new aviation fuels, alternative-energy flights have been pursued for a long

time in aviation history. This section provides a compendium of the previous efforts and the current research status for alternative energy sources focusing on hydrogen, solar, and nuclear power as well as the evolution of conventional fuels.

1.2.1 Conventional Aviation Fuels

Conventional aviation fuels are classified into two general categories: aviation gas and aviation turbine fuels, both of which are hydrocarbon liquids obtained from crude oil. Aviation gas, often called avgas, is a gasoline-based fuel." Since the fledging aviation engines first used to power flight were built based on the automotive gasoline piston engines of the day, it is a natural outcome that they were fueled with automotive gasoline [58]." Such a gasoline-based fuel has been improved for antiknock properties by increasing the octane rating over the years. Currently, these types of fuel are used mainly for reciprocating piston engine aircraft and light helicopters[5].

The advent of jet turbine engines introduced another type of aviation fuel. Aviation turbine fuels, often called "jet fuel" are kerosene-based. A major problem with gasoline is its higher volatility, characterized by a low "flash point," the temperature at which it produces fumes that can be ignited by an open flame [59]. Gasoline has a flash point of around -45 degrees Celsius [60], which makes the aircraft vulnerable to catching fire in the event of an accident or combat. Jet fuel has much higher flash point than avgas (e.g. minimum 38°C for Jet A [61]), which results in less risk of fire during handling on the ground and higher survivability in crashes. Compared with reciprocating engines that prefer a low flash point to improve their ignition characteristics, continuous combustion turbine engines are less sensitive to a flash point of fuel, and work properly on kerosene. In addition to its higher safety, jet fuels yield fewer losses due to evaporation at high altitudes. These types of fuel are used for

[5]Currently the two major grades in use internationally are Avgas 100 and Avgas 100LL, 'low lead' version of the former [58].

powering jet and turboprop aircraft for both commercial and military applications[6].

These conventional aviation fuels produced from crude oil have powered virtually all machined flight for over a century. The ascendancy is not a result of fortuitous circumstances but recognitions of their inherent advantages, principally their high (both volumetrically and gravitationally) energy content as well as competitive prices, over other energy sources. Nevertheless, the advantages, as discussed in §1.1, have been gradually eclipsed by their adverse impacts on the environment and national energy security.

1.2.2 Hydrogen

Hydrogen as a substitute for conventional hydrocarbon fuel has attracted strong interest from the aviation community for more than half a century for several reasons. First, hydrogen has three times higher energy content per unit mass than conventional hydrocarbon fuels (120MJ/Kg vs. 40MJ/Kg, in lower heating value) [32]. Secondly, hydrogen can be extracted from fossil fuels such as coal, oil or natural gas, or can be obtained via electrolyzing water [12], which may drastically palliate national energy security concerns. Strictly speaking, hydrogen is not an energy source in itself but rather an energy carrier. That is to say that it must, itself, be made from a primary energy source, which is not necessarily imported. The ability to source such a great deal more primary energy domestically or to diversify energy supply sources has great potential to help reduce the U.S. energy security challenges [12]. Lastly, hydrogen has the potential of drastically alleviating emissions problems [32]. Should hydrogen be sourced from fossil fuels coupled with carbon sequestration or generated from renewable energy sources such as wind, solar, and geothermal energy, the net carbon emissions, in the sense of "well to wing," could be reduced to near zero [12].

[6]Two main grades of turbine fuel in use in civil commercial aviation: Jet A-1 and Jet A, both are kerosene type fuels. There is another grade of jet fuel, Jet B, which is a wide cut kerosene (a blend of gasoline and kerosene) but it is rarely used except in very cold climates. Three grades of turbine fuel in use in military aviation include JP-4, JP-5, and JP-8.

Despite their noteworthy advantages, several drawbacks of the use of hydrogen as an aviation fuel exists. First, its low volumetric energy density (about three times lower than that of conventional aviation fuels) necessitates larger and heavier fuel tanks, which are likely to offset significantly the advantages of its lower energy mass density. In addition, development of technologies to ensure sufficient safety as well as the assurance of the public is a big challenge. The construction of infrastructures related to hydrogen production, distribution, and storage also may bring on numerous technical, economic, and political problems.

Hydrogen can power an airplane via two different energy conversion processes: thermodynamic conversion through combustor or electrochemical conversion through fuel cell systems. The aboriginal research of hydrogen as an aviation jet fuel is found in a report [62] by Silverstein and Hall of the NACA-Lewis Flight Propulsion Laboratory published in 1955, which identified the potential of the use hydrogen as an aviation fuel. Their research gave a birth to an experimental program[7] that was intended to demonstrate the feasibility of burning hydrogen in a turbojet engine at a high altitude in the next year. In the same year, Lockheed's Advanced Development Projects organization, better known as Kelly Johnson's Skunk Works, was awarded a contract to build two prototype reconnaissance aircraft designated as CL-400 that would be capable of cruising at Mach 2.5 at an altitude of 100,000 feet [2]. In spite of the success in developing practical solutions to the problems encountered in handling cryogenic liquid fuel, the program was terminated with no aircraft built. In the light of technological advancements in the past several decades, however, in recent years hydrogen fueled jet aircraft have met with a renewed interest in the United States. Europe also commenced an industry-wide investigation entitled "Cryoplane - Liquid

[7]A U.S. Air Force B-57 twin-engine medium bomber was modified to carry liquid hydrogen in a tank located under the left wing tip and made the first flight by hydrogen in 1956. The converted aircraft climbed up to altitude and speed specified for the test using conventional JP fuel for both engines. Upon reaching test conditions, the convertible J-65 turbojet engine on the left-hand side switched over to hydrogen fuel. [2]

Hydrogen Fueled Aircraft System Analysis" in 2000 [7].

In addition to its use as a *jet* fuel, hydrogen could be used as the fuel source for *fuel cells*. Fuel cells are electrochemical devices that convert the chemical energy of a reaction directly into electrical energy [63]. The electrochemical process, as opposed to a combustion process, is not limited by Carnot cycle efficiency, and fuel cell systems have the potential to achieve significantly higher efficiencies than IC engines do.

There are many varieties of fuel cells including proton exchange membrane fuel cell (PEMFC) and solid oxide fuel cell (SOFC), but they are all related by a single common chemistry; generating electrical energy by the electrochemical oxidation of fuel [63]. While most fuel cells operate on pure hydrogen, some cells can operate on hydrogen-rich fuels such as methanol. "Hydrogen fuel cells can also be operated on other hydrocarbon fuels if a reformer, which acts as a mini-refinery to separate the hydrogen from the other elements in the fuel, is used along with the fuel cell [64]." The use of a reformer or direct methanol fuel cell could eliminate concerns over hydrogen production and storage, but would result in higher in-use emissions, compared to those of a hydrogen fuel cell [64].

Fuel cells have already been used to power electrical systems of spacecraft on every manned space flight of NASA [65]. Capitalizing on enormous advancement in specific power and power density in recent years, fuel cells began to be considered for aeronautical applications [5]. Several pioneering attempts by industry and academia have already been made to fly an airplane on fuel cell-based electric propulsion systems as demonstrated with AeroVironment's Hornet and Global Observer[8] shown in Figure 6, as well as a fuel cell-powered UAV designed and constructed by Georgia Institute of Technology [67]. Currently fuel cells are mostly envisioned for low speed and long endurance applications, in which propellers driven by electric motors produce thrust.

[8] After three years development, AeroVironment commenced flight testing of a subscale prototype of the liquid hydrogen-powered UAV having eight electric motors mounted along a 50 ft wing in 2005 [66].

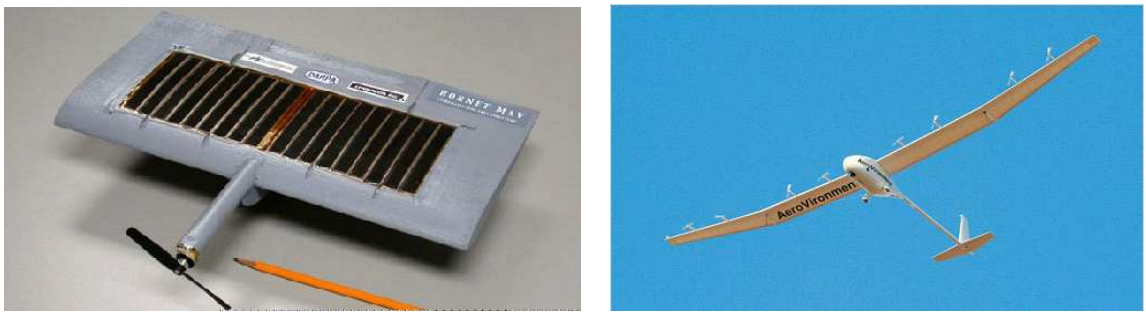

Figure 6: AeroVironment's fuel cell-powered aircraft: the Hornet (left) and Global Observer (right)

Fuel cells are also proposed as a power plant for magnetoplasma jet engine (called "magjet") that is capable of air-breathing flight in the supersonic and hypersonic regime [68].

1.2.3 Solar Energy and Beam Power

Solar-powered aircraft have also attracted the attention of several agencies over the past several decades because of their promising potential in military and civilian applications. This type of aircraft utilizes electric energy transformed from solar rays via PV cells. The most appealing feature of solar energy is that it can be obtained continuously during flight, and thus could yield a nearly fuel-less, emissions-free flight. Furthermore, if PV cells produce and store sufficient extra energy during the daytime for flight at night, solar-powered aircraft could possibly fly for a virtually unlimited duration. Another noteworthy advantage of a solar powered propulsion system over air-breathing engines is that available power is nearly insensitive to the variation of air density. Since the solar ray is attenuated as it travels through the atmosphere, its strength at high altitude is considerably higher than that at sea level. These two primary advantages of solar power are greatly valued for high altitude long endurance missions.

Table 1 compares characteristics of various PV cells commercially available. Sunpower single crystal silicon PV cells are widely used for airplane applications such as Pathfinder and Helios because of their superior specific power and efficiency.

Table 1: Characteristics of solar cells [69]

Cell Type	Manufacturer	Weight/Area (Kg/cm^2)	Pmax	Efficiency (%)	Cost/Watt ($)
Si	SunPower	0.000081	0.01984	21.50	$10.32 \sim 12.90$
Si	Mitsubishi	0.00122627	0.013054	13.10	6.03
Si	Sanyo	0.000051	0.00748	7.48	Unknown
GaAs-Dual	SpectroLabs	0.084	0.0295	19.62	Unknown
GaAs-Triple	SpectroLabs	0.084	0.0383	25.47	12.24

A number of solar-powered aircraft have been developed over several decades in the United States as shown in Figure 7. The first solar aircraft was Sunrise I built by Astro Flight and flown during the winter of 1974-75. It weighed 27.5 pounds, had a 32-foot wing span, and was powered by 450 watts provided from the solar cells [70]. By the fall of 1975, Astro Flight constructed an improved version called Sunrise II. This effort was followed by the development of the first manned solar-powered aircraft, Gossamer Penguin, which used the solar panels from Sunrise II. Following Gossamer Penguin, Dr. Paul MacCready's Solar Challenger, the solar cells of which could deliver over 4000 W at altitude and 2500 W at sea level, crossed the English Channel on July 7, 1981. In the same year, a classified program looked into the feasibility of long-duration, solar-electric flight above 65,000 feet, giving a birth to HALSOL (High-Altitude Solar Energy) built by AeroVironment. HALSOL proved the aerodynamics and structures of the approach, but subsystem technologies, principally for energy storage, were inadequate for the intended mission [71]. HALSOL was mothballed for ten years but later evolved into Pathfinder [71] in NASA's Environmental Research Aircraft and Sensor Technology (ERAST) Program [72], which also spawned the

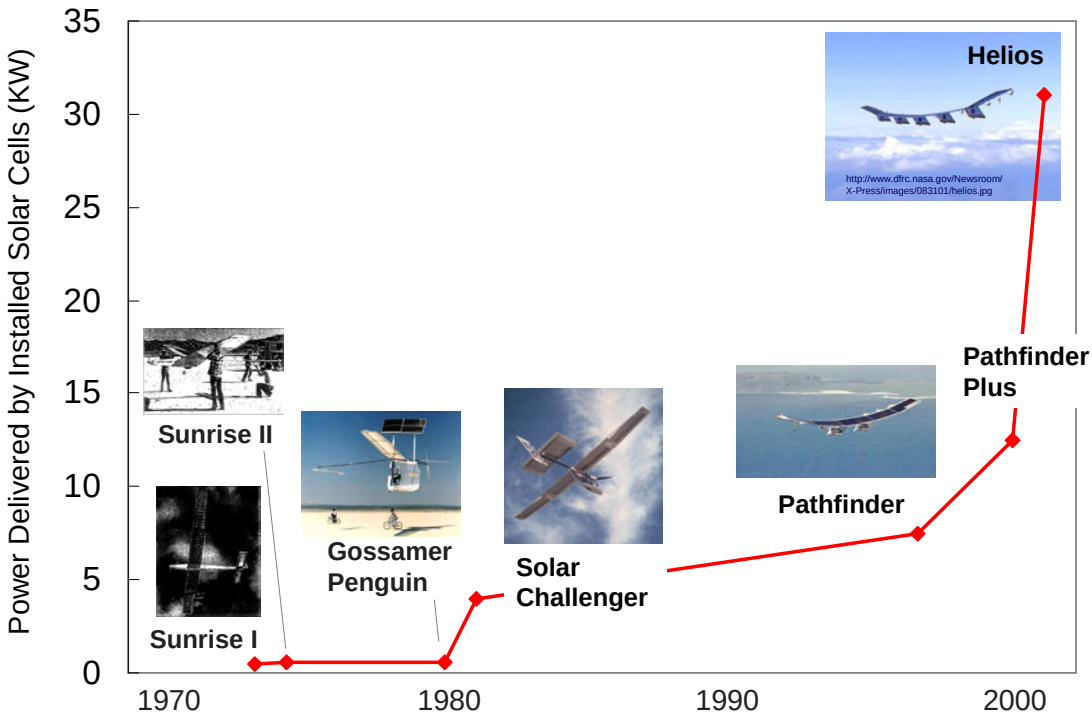

Figure 7: Evolution of solar-powered aircraft

development of the Centelios and Helios vehicles.

Despite the loss of the Helios in 2003, NASA has been pursuing a variety of options to continue the further development of solar and energy storage system technology for airborne applications [6]. These efforts are expected to lead to even more revolutionary HALE UAV aircraft capable of flying routinely as reliable "atmospheric satellites" on critical scientific and civil missions by 2010-2015 [6]. The European Space Agency is also promoting the development of a solar-powered airplane, the Solar Impulse, for which design and assembly are planned in 2007, followed by a first flight attempt in 2008 [73]. In addition, solar power remains a promising energy source for the application of atmospheric flights on terrestrial planets where solar intensity is sufficiently high. For instance, a group of NASA researchers [74, 75] proposed a solar-powered aircraft designed to explore the atmospheric environment of Venus.

1.2.4 Nuclear

Despite the appalling aftermath of its failure, nuclear energy has long been attractive to aerospace propulsion engineers. The most fundamental and compelling reason for the utilization of nuclear power in aerospace applications is that the nuclear explosive is the most compact of all known energy sources so far [76].

The attempt to operate aircraft on atomic power antedated efforts made to use hydrogen and solar power. Development of a nuclear-turbojet powered airplane was initiated by the Nuclear Energy for the Propulsion of Aircraft (NEPA) Project, launched by the United States Air Force (USAF) in 1946, and the follow-up Aircraft Nuclear Propulsion (ANP) Program, controlled by the joint Atomic Energy Commission (AEC) and USAF [77]. By the time President Kennedy delivered a statement canceling the program on March 28, 1961, about $1 billion had already been devoted to the development of a nuclear-powered aircraft for nearly 15 years [78]. In light of the advent of large commercial aircraft such as the Boeing 747, thanks to considerable advances in the airframe and engine, the USAF sponsored a conceptual study [1] for assessing whether an aircraft of one million pounds, with logical extensions of the technology, would allow for a useful payload capability with a fully shielded nuclear reactor installed. Annexed to the research, NASA also continued a low-level effort [79, 80] to determine and solve the major obstacles to practical, safe, and economical nuclear aircraft. However, to date, no aircraft has ever flown with atomic energy.

In contrast to their abortive efforts, nuclear power has been successfully implemented in the application of the U.S. Navy's combatant fleet. Currently, all submarines and nine aircraft carriers of the Navy's aircraft carriers are nuclear-powered [81]. In addition, nuclear power has been widely used in space missions[9].

[9]Since 1961, the United States has successfully flown 41 radioisotope thermoelectric generators (RTGs) and one reactor to provide power for 24 space systems [82]. The former Soviet Union has reportedly flown at least 35 nuclear reactors and at least two RTGs to power 37 space systems [82].

In recent years, nuclear power has been reinvestigated for extremely long endurance reconnaissance flights [83] as well as space exploration [84, 85]. The use of nuclear technology in the aerospace sector faces formidable barriers of public acceptance, however, especially if employed in airplanes. Therefore, the development of nuclear powered aircraft is contingent upon resolving a paramount safety issue and acquiring public acceptance.

1.2.5 Other Alternatives

In addition to solar energy, hydrogen, and atomic energy, several energy sources have been envisioned for alternative aviation fuels. Bob Saynor et al. [86] examined, in their research named "The Potential for Renewable Energy Sources in Aviation (PRESAV)" Project, the feasibility of several energy sources and identified Synthetic Fischer-Tropsch kerosene and biodiesel as those that warrant further detailed studies.

Liquid methane has also been considered one of the options for aircraft engines. However, the use of liquid methane would result in a minimal reduction in pollutants. Moreover, the methane production peak is expected to occur a few years after the crude oil production peak [32]. Considering the expected price escalation, the complexity and cost of changing the infrastructure, methane is not considered to be a viable alternative.

A cohort of researchers also introduced an interesting non-chemical propulsion concept of beaming power, which is based on wireless transmission of electrical energy, thus ending up with a nearly fuel-less, emissions-free flight with extremely long endurance capability. Compared with solar-powered aircraft, the operation of which is heavily limited by geographic location, especially latitude, due to the availability of solar light, the operation of beaming powered aircraft is more likely to be flexible. Motivated by such potential advantages, researchers in several countries flew a variety of model aircraft using beamed microwave energy twenty years ago [87]. However, the

intrinsic nature of the microwave beam causes it to dissipate with distance, resulting in a commensurate decrease in power delivered to the target. With only lasers left as a potentially feasible option for practical power beaming, a group of researchers proposed the concept of a laser-powered transportation system [88]. Beamed power has been rigorously reinvestigated for many potential aerospace applications, including high-altitude airships, extra-terrestrial robotic rovers and aircraft, and small or swarming unmanned aircraft [84, 87].

Batteries and ultra capacitors are also being increasingly considered as preferable energy storage systems for a certain class of aircraft. Despite their remarkable power draw capability, the poor energy density of batteries and ultra capacitors have stymied them from appearing as a promising energy carrier for airplanes and even automobiles. Capitalizing on remarkable technological advancement in the past decade, however, batteries, especially lithium-polymer batteries, have shown their great potential as demonstrated by small radio-controlled (RC) aircraft and Micro Aerial Vehicles (MAVs). Batteries are expected to expand their usage such as booster power to subsidize primary power source as envisioned for the Boeing's Fuel Cell Demonstrator Airplane [89] and a rechargeable energy source to sustain overnight flights for an extremely long endurance solar-powered aircraft as demonstrated in AC Propulsion's solar powered unmanned aerial vehicle, the "SoLong [90]," shown in Figure 8.

Figure 8: Examples of battery-powered aircraft: Boeing's Fuel Cell Demonstrator [89] (left) and AC Propulsion's SoLong [91] (right)

1.3 Motivation

When consent to transition to alternative energy sources is given, the following questions immediately arise: when will the transition happen?; what alternative energy sources should take the place of hydrocarbon?; and how can the transition be achieved? [2] Answering the questions is relevant, but not the scope of this research. In fact, those three questions are casting numerous research doubts on the whole society, because the transition is expected to bring tremendous impact on all aspects of the entire world. Fortunately, rigorous research during the past decades has led to a large consensus that hydrogen is very likely to be the answer to the second question.

A transition from hydrocarbon fuels to hydrogen, or any other alternative, is expected to be a very complex, enormously expensive and arduous process even if all the necessary technologies were already available [32]. It must also be noted that the transition involves not only the development of new vehicles but also the construction of infrastructures related to the production and distribution of alternative energy, thereby inexorably affecting various aspects of our society and ecosystem. For example, zero-emissions aircraft, which store virtually all by-products on-board, are often conceived of as being nearly innoxious to our environment. Although the air-vehicle itself can approach the idea of an emissions-free energy source well, emissions are still produced during the production of the energy source and in the manufacture of the energy production plant and vehicle [31]. Therefore, in order to develop technically feasible, economically viable, environmentally acceptable new energy sources and aircraft systems, the government, academia, and private industry beyond the aerospace sector must interact as a whole and vigorously implement a holistic strategy addressing these challenges through increased levels of inter-agency collaboration [92].

To facilitate such large scale collaboration, a quantitative assessment environment that provides insight into the system-wide responses of alternative technology and policy evolution scenarios, as illustrated in Figure 9, would be valuable, thereby

increasing the possibility of arriving at more informed decisions. One critical aspect of such a quantitative assessment environment is *aircraft sizing*, which determines the overall size of aircraft and installed engines. Providing such a fundamental basis for most design and analysis activities, including internal layout, cost analysis, signature analysis, and system effectiveness analysis, it is considered a prerequisite task during the conceptual design phase. For instance, one of the results of aircraft sizing, the initial estimation of thrust or power required, is a primary input in the preliminary investigation of the engine company, especially if a new propulsion system is jointly developed. Therefore, aircraft sizing is the gateway that bridges technologies of the alternative propulsion systems and alternative energy sources to the assessment of impacts on our environment and economy.

As discussed in §1.1, an alternative aviation energy source is being pursued to address not only global issues entailing a worldwide transition of the primary energy source, but also emerging scientific or military needs seeking a specific solution for an unique mission. Nevertheless, aircraft sizing is still regarded as a critical capability that is required to select the most appropriate energy source and system architecture in performing the given mission.

Through a century of aircraft development, the traditional method for aircraft sizing has fully matured, and it is well understood. Nevertheless, it is doubtful that traditional aircraft sizing methods are immediately applicable to the sizing of revolutionary aircraft powered by a wide range of alternative energy sources, which is the aboriginal motivation that initiated this research.

1.4 Dissertation Overview

This introductory chapter has discussed the impetus toward the transition to alternative aviation energy sources, promoted by a combination of environmental, technological, economic, and national security issues. It has also reviewed that such rigorous

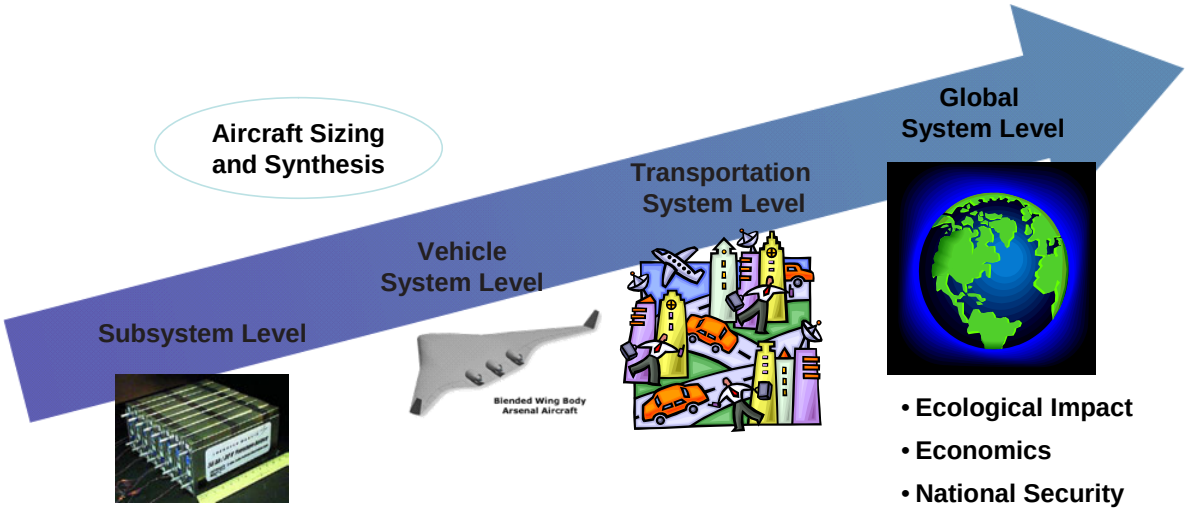

Figure 9: A notional system of system analysis structure for assessing the impacts of alternative energy sources on all of society

efforts of implementing alternative energy (fuel) sources to aviation may necessitate improving aircraft sizing methods, which originally motivated this research.

The remainder of this dissertation is organized as described in Figure 10. Chapter II surveys and summarizes the literature regarding the aircraft sizing process as it exists today and the efforts of many researchers to improve the aircraft sizing process to apply it to aircraft operating on alternative energy sources. The literature survey also identifies the deficiencies of current practice in the designs of alternative propulsion aircraft, which warrant the need for an advanced aircraft sizing method, as conceived in the previous chapter.

Identifying what capabilities the emerging method must possess to fill the gap between the traditional sizing method and the emerging unconventional aircraft concepts, Chapter III establishes the research objective of this dissertation. The next logical step is to identify research questions to be answered in order to achieve the research objective. This effort crystallizes the research questions into how to develop two capabilities: 1) aircraft sizing methodology independent of the architectures of

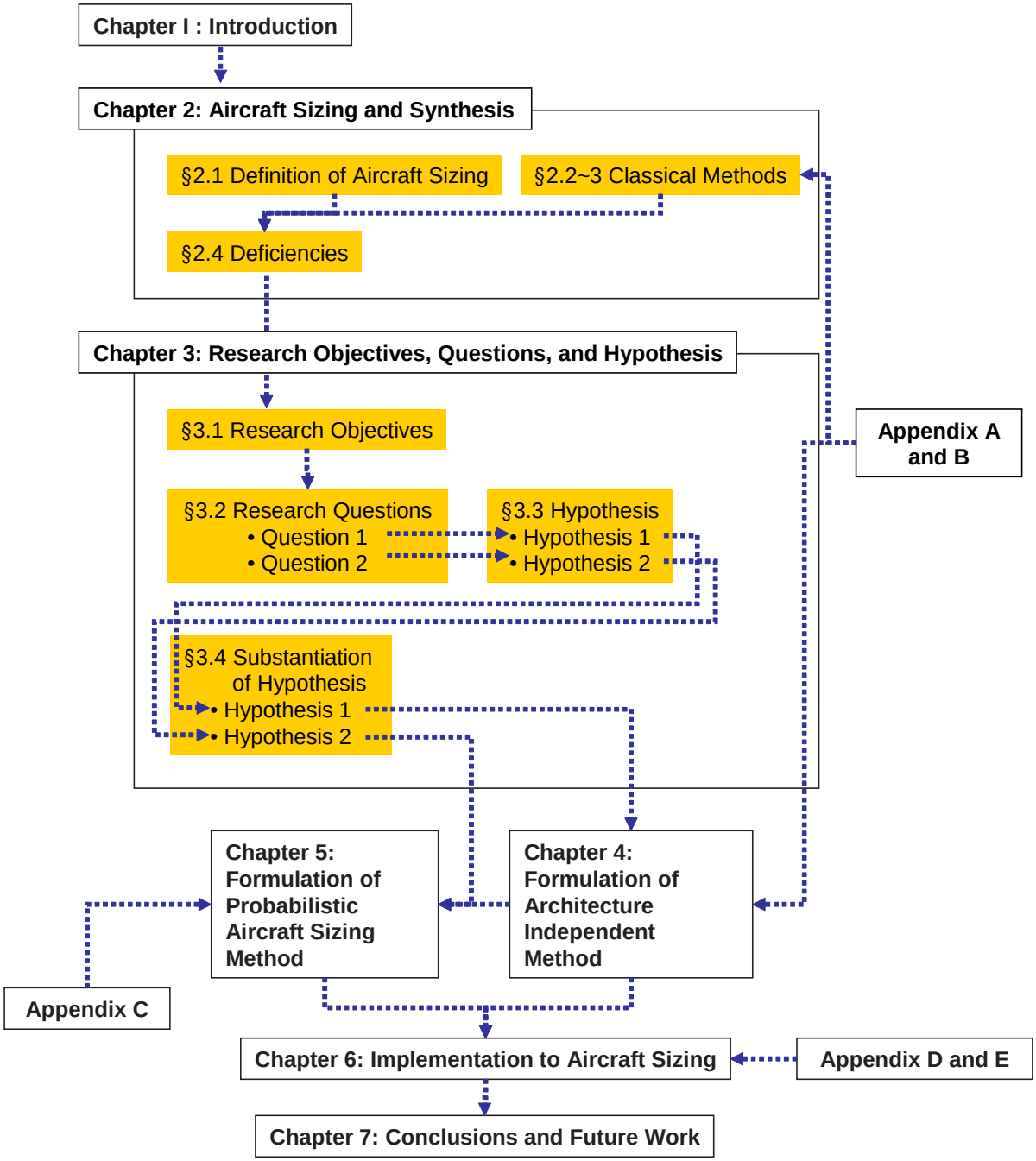

Figure 10: Thesis structure overview

energy and propulsion systems; and 2) intelligent allocations of opposite design margins against uncertainty. Subsequently, the hypotheses for the corresponding research questions are surmised and translated into appropriate mathematical representations.

Built upon the substantiation of the hypotheses, Chapter IV and Chapter V present the formulation of the Architecture-Independent Aircraft Sizing Method (AIASM) and the Probabilistic Aircraft Sizing Method (PASM), respectively, as the solutions to the research questions. In the course of the development of AIASM, Chapter IV also introduces two expedients useful for first-order estimations of aircraft performances: generalized Breguet range equations and the Non-dimensional Aircraft Mass (NAM) ratio diagram. In addition to PASM, Chapter V also discusses several solution techniques suitable for solving the formulated problem and several extended topics such as the application to multidisciplinary design optimization problems and probabilistic sensitivity analysis techniques to enhance the proposed method.

In order to demonstrate the usefulness of these methods, Chapter VI presents the implementation of the proposed method into the sizing of fuel cell-powered electric general aviation aircraft and solar-powered electric HALE aircraft with regenerative fuel cell propulsion. Finally, Chapter VII provides the conclusion of this research and discusses future work envisioned to reinforce the proposed methods.

CHAPTER II

AIRCRAFT SIZING AND SYNTHESIS

Discussion of the previous chapter has directed our focus to aircraft sizing. The primary purpose of this chapter is to review classical aircraft sizing methods as well as recent efforts to improve them and to identify the deficiencies in their applications to alternative-energy flights. §2.1 contains a compendium of definitions and underlying physics of aircraft sizing. Subsequently, §2.2 reviews traditional aircraft sizing methods. §2.3 extends the discussion to how the traditional methods account for the implication of uncertainty inherent to the aircraft sizing process. Upon all the discussions, the last section summarizes the shortcomings of traditional sizing methods.

2.1 Definition of Aircraft Sizing and Synthesis

One of the imperative tasks performed during the conceptual design phase, aircraft sizing is well known to the aerospace community. Therefore, reminding readers of the meaning and concept of aircraft sizing tends to be commonplace. Nevertheless, the clarification of its definition is crucial in elucidating the remainder of this dissertation.

According to Raymer [93], "aircraft sizing is the process of determining the take-off gross weight and fuel weight required for an aircraft concept to perform its design mission." However, this definition does not contain sufficient affinity for the word, "sizing." If determining aircraft weight is a main concern, it should rather be called "weight estimation." In addition, his definition unevenly emphasizes mission fuel estimation, which is important, but not predominant in the process. DeLaurentis [94] describes aircraft sizing as "a mathematical algorithm that determines the size and

weight of an aircraft based on a specified mission and contributing disciplinary analyses." This definition states the process is to determine the aircraft size as well as its weight, which inspires another question: what is the aircraft size?

This question may be answered by reflecting on how an airplane comes onto the design board from the creative imagination of designers. At the beginning of conceptual design, designers create and evaluate various configurations and select one or several baseline configurations for detailed evaluations. Each of the conceptual designs is created at first in the form of a simple sketch that conveys general ideas for the airplane, leaving the following significant questions: 1) how big the aircraft should be; 2) how powerful the engine should be; and 3) how heavy the aircraft will be. Three quantities: aircraft size, thrust and weight, given as the answers to the above questions, are essentially important in evaluating the "goodness" of a configuration, because they strongly affect the cost, including acquisition cost and operation cost. In addition, these three quantities are prerequisite information to follow-on design activities. For instance, without knowing the size of the aircraft, control surface sizing and internal layout are not possible. Another important aspect is that the three questions should be answered simultaneously since they are interdependent. If the aircraft size needs to be changed, the aircraft weight changes, and thus, the required thrust must change because drag and weight increase, which in turn increases aircraft weight due to bigger engines. The chain of this impact propagation will keep moving on until the quantities converge toward a solution, which is the objective of the aircraft sizing process.

The next logical question would be the following: what drives these three quantities to a converged solution? Or, what is the criteria of the convergence of the solution? The aircraft must achieve three criteria: power (or thrust) matching, energy matching, and volume matching. Power matching is referred to as a balancing

act between the required power and the available power. The required power is dictated by the point performance requirements that specify the ability of performing certain maneuvering motions such as take-off, climb, sustained turn, instantaneous turn, acceleration, cruise, approach, and landing. The required energy is dictated by the mission performance requirements that specify the ability of performing a series of motions. In other words, the point performance requirements establish the demand for producing force or power, while the mission performance requirements establish the demand for containing energy. Volume matching is referred to as a balance between the required volume and the available volume. Traditionally, volume balance is verified through more detailed studies of the internal arrangement after aircraft geometry is initially established through the aircraft sizing process. In the case of traditional aircraft design, however, the volume balance is implicitly secured to a certain degree via the application of "familiar" (in the sense of "evolutionary," not "revolutionary") configurations and empirical weight estimations without the direct assessment of volume balance, simply because all existing aircraft, whose weight data are used to construct the regressed equations, contain all subsystems, structures, and fuel. In addition, it is not too far-fetched to regard the aircraft being designed as a small perturbation from the historical trend. For this putative reason, this section focuses on thrust balance and fuel balance.

In this process, aircraft size and thrust are what the designer can control, while aircraft weight is what is to be computed accordingly, which means aircraft size and thrust are design variables of the aircraft sizing process. In this context, changing the size is referred to as photographically scaling up or down the notional configuration, which results in a geometry of the final configuration that is not necessarily *congruent* to but *similar* to the initial configuration. In such a sense, aircraft size can be determined by setting wing area. Similarly, changing thrust is referred to as scaling "rubberized" engines. Therefore, aircraft sizing is to determine two scales of the given

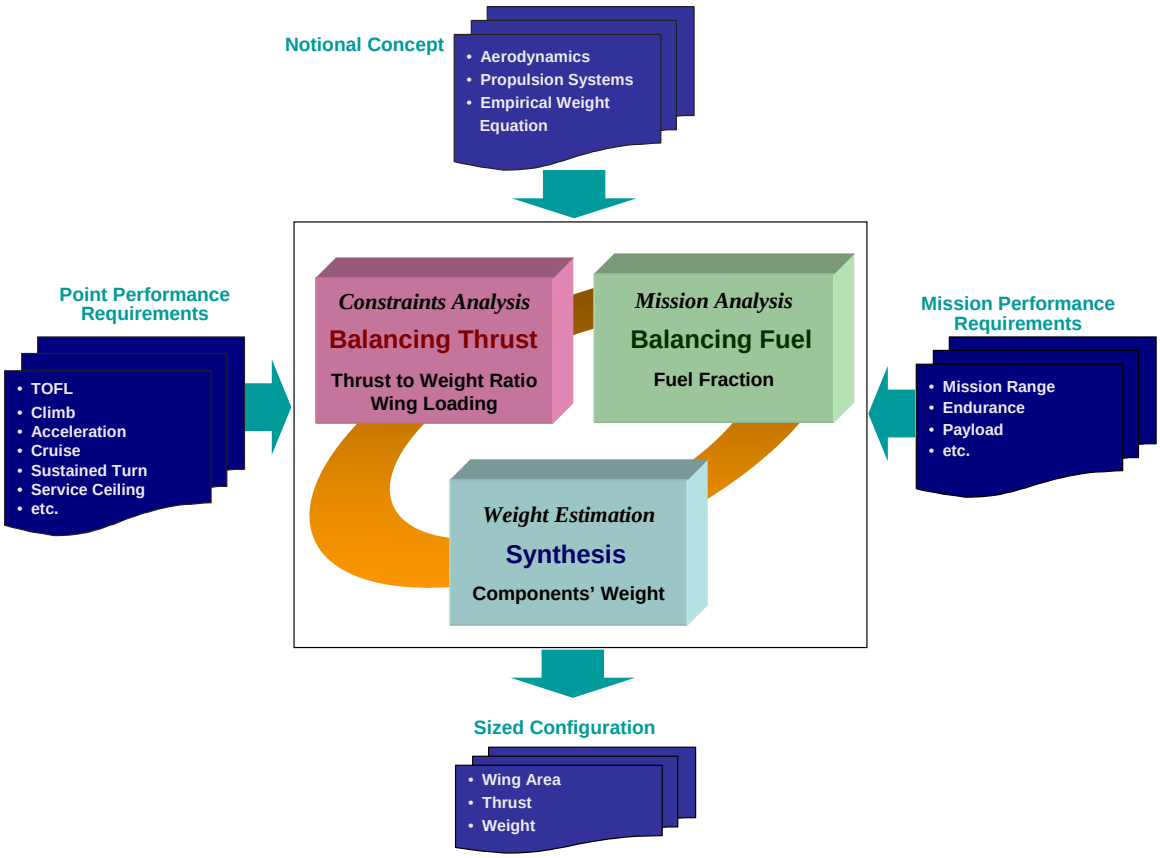

Figure 11: Illustration of the fundamental concept of aircraft sizing

concept: a geometric scale that is dictated by the wing area and a propulsive scale that is dictated by the amount of engine thrust.

Aircraft sizing is often misconceived as aircraft configuration optimization, which seeks an optimum aircraft shape yielding the minimum aircraft weight and cost. Aircraft sizing is to determine the scale of the given configuration and not to attempt to modify the given configuration. Instead, aircraft sizing is a crucial element of configuration optimization. Most multidisciplinary design optimization (MDO) studies find optimum aircraft design by wrapping around an aircraft sizing code with an optimization tool. Nevertheless, an optimization technique may be involved with the aircraft sizing process. Because a myriad of combinations of geometric scales and propulsive scales may satisfy design constraints, an optimization process is required to find the

best combination of the two scales. However, it must be noted that the optimization process tries to modify neither aircraft shape nor propulsion system characteristics, but two scaling parameters. In summation, aircraft sizing is defined herein as:

> *an analytical process that determines the best combination of two scales of a baseline configuration, a geometric scale that is dictated by the wing area and a propulsive scale that is dictated by the amount of engine thrust so that the resultant aircraft should satisfy the three criteria: matching power, energy, and volume.*

Thus, the aircraft sizing problem can be formulated as a deterministic constrained optimization problem, in which the objective function, denoted as f, is minimized by varying design variables, denoted as $\mathbf{x}$, subsect to a set of design constraints as follows:

$$\begin{aligned} \min_{\mathbf{x}} \quad & f \\ \text{s.t.} \quad & T|_{available} \geq T|_{required} \\ & W_F|_{available} \geq W_F|_{required} \end{aligned} \tag{1}$$

where T and W_F denote the amount of thrust and fuel, respectively. The design variables denoted as $\mathbf{x}$ typically include available thrust ($T|_{available}$), wing area (S), and available fuel ($W_F|_{available}$).

In general, take-off gross weight or design gross weight is selected as the objective function of an aircraft sizing problem. The objective of aircraft sizing may differ depending on the mission objective of the aircraft and the scope of the design study. The ultimate figure of merit (FoM) for military aircraft would be the mission effectiveness or the exchange ratio of the aircraft. The FoM for commercial transport is often chosen among monetary metrics such as Return of Investment (ROI) and the average yield per Revenue Passenger seat Mile ($/RPM). However, the selection of such metrics as the objective function entails the integration of relevant analyses with aircraft sizing processes. “The difficulty in using economic cost as a design FoM

in aerospace vehicle design is that cost arises in a myriad of forms and can be quite complicated to estimate in its totality. This makes it unwieldy for use as a day-to-day design FoM in an engineering environment unless only the top few factors contributing to cost are tracked while the remaining many factors are ignored. These top few factors contributing to cost are well known in the aerospace industry and are strongly correlated to vehicle gross and empty weight. Therefore, aircraft weight is a good index on cost, and by extension, a good FoM for vehicle design [95]."

The first constraint in Eq. (1) represents the criterion of power balance, and the second one represents the criterion of energy balance. The available power in the power balance criterion is dictated by the characteristics of the propulsion system, and the required power is dictated by the performance requirement and airframe design. The available energy in the energy balance criterion is dictated by the amount of onboard fuel, and the required energy is dictated by the mission requirements, airframe design, and the efficiency of the propulsion system.

The mathematical formulation of the aircraft sizing process is based on an application of Newton's Second Law to the motion of an airplane, of which three-dimensional geometric characteristics and the properties of internal systems and structures are abstracted as a handful of parameters such as drag polars and mass properties. In reality, however, an aircraft is a complex system whose subsystems must meet physical and functional compatibility requirements for each other so that the whole system can work in harmony. "The recomposition of these elements into an integrated whole is known as synthesis [96]." In such a sense, implementing proper synthesis increases the realism of aircraft sizing by accounting for the interconnections between the designs of elements. Synthesis comes along with aircraft sizing in many different ways. Jenkinson et al. [97] views synthesis as the designers' effort to make an initial configuration for the aircraft sizing process balanced and workable by incorporating knowledge from all pertinent disciplines. Experienced design engineers are likely to come up with a *less*

controversial, initial configuration of a notional aircraft that avoids any foreseeable technical issues by their engineering intuitions and previous experience. For example, they try to put the wing at a "right location" in consideration of many aspects such as stability and control, landing gear arrangement, and structural integrity. They also might consider various aspects regarding cockpit design such as vision envelopes and signatures as well as aerodynamic characteristics, although they do not precisely assess the design.

Another important aspect of synthesis with respect to aircraft sizing is to provide guidance for a more realistic estimation of components' weight. For instance, the weight of the landing system can be more accurately calculated along with determining its geometric size to provide sufficient ground clearance.

The degree of synthesis is limited by available information and design maturity. The scarcity of information on the aircraft system in the conceptual design phase makes only very low level of synthesis practical. However, the interconnections between major components must be captured and implemented into the aircraft sizing process. For example, the amount of power extraction from the main engine for subsystems may be significant for some aircraft equipped with a high electric power-demanding payload. In such a case, power extraction must be properly taken into account for sizing the propulsion system and the amount of required fuel. Otherwise, the results of aircraft sizing will not be realistic.

2.2 Traditional Sizing Methods

A copious anthology of literature presents different aircraft sizing methods. Some authors [98] discuss the aircraft sizing process in the course of explaining the development of configuration such as the aircraft shape, notably wing geometry. If only the parts regarding aircraft sizing from the textbooks are compared, however, a remarkable confluence in their logic and approach is found, despite some differences

in details such as terminology and the sequence of the process. Therefore, review of the traditional methods herein is focused on one representative method by adding notable differences from other methods. Mattingly's method is selected as just such a paragon method.

2.2.1 Overall Process of Aircraft Sizing

The overall process of Mattingly's method is pictorially described in Figure 12. The process is initiated by developing a notional concept. Determining the two scales, represented by wing area and thrust, of the given concept is the goal of the process. With its specific dimensions left undetermined, the initial concept encapsulates three major attributes related to aerodynamics, propulsion, and empty weight that are the basic inputs of the process. Therefore, those data must be prepared by preceding analyses before the process gets started. The process is comprised of three major parts: constraint analysis, mission analysis, and weight estimation. Constraint analysis establishes thrust balance by selecting thrust-to-weight ratio and wing load in the feasible solution region that avoids the violation of performance requirements. Mission analysis estimates the required fuel amount normalized by the take-off gross weight, which leads to fuel balance. These analyses, however, do not directly determine the size of the aircraft but secure thrust balance and fuel balance, because the analyses provide the information of wing area and thrust in normalized-by-weight forms, and aircraft weight is not yet determined at this point. Weight estimation combined by the information of the thrust-to-weight ratio and wing loading ultimately determined the three quantities: thrust, wing area, and aircraft weight.

2.2.2 Inputs of the Aircraft Sizing Process

As mentioned previously, the aircraft sizing process is performed with a specific air-vehicle concept in mind. The initial concept does not have to be contrived, but must be specific enough to address all attributes of an imaginary aircraft required for the

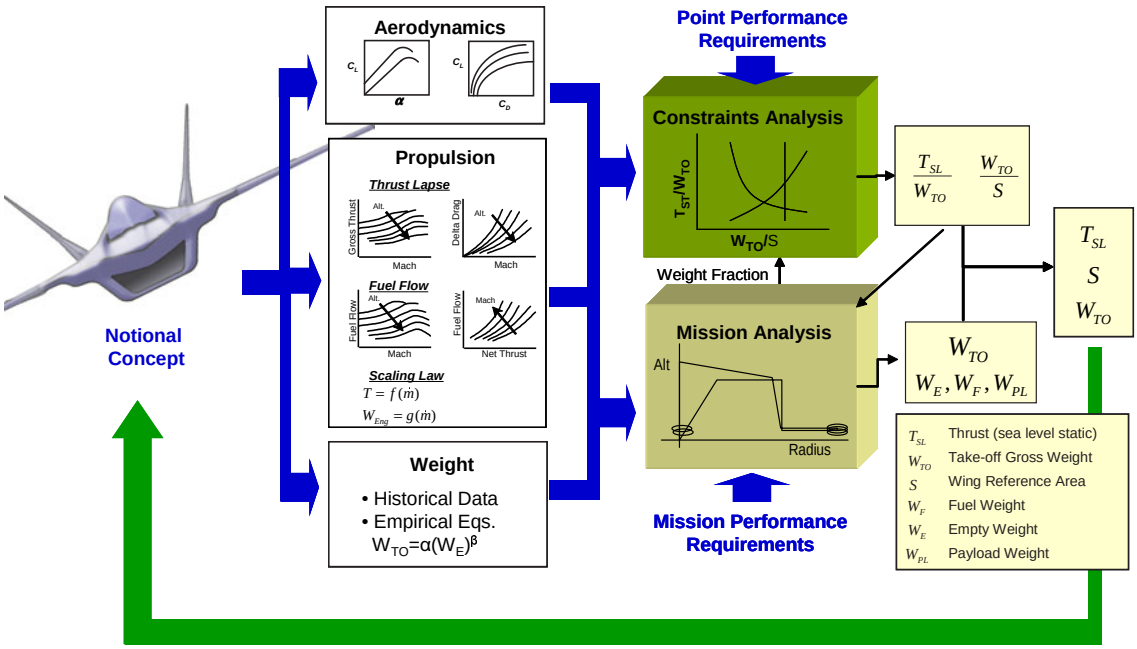

Figure 12: Mattingly's aircraft sizing process

sizing process. Most of such attributes are contained within the aircraft's external configuration and propulsion system characteristics. The former is developed based largely on engineering intuition and prior knowledge, and establishes basic aerodynamic characteristics, such as drag polar data and lift curves. The latter includes thrust and specific fuel consumption (SFC) variation with altitude, Mach number, and power settings. Most aircraft design projects begin with a rubberized engine that can be scaled up or down so that it matches the thrust required by the mission. Therefore, the thrust lapse behavior through flight conditions and power settings, other than the figure of the available thrust itself, is precisely what is required.

In addition, empirical weight equations that are able to estimate empty weight are also required. Such equations were generally developed from regression analysis of the data extracted from large numbers of existing aircraft. The large diversity in the aerodynamic configuration, structural layout, materials, including subsystems of today's aircraft, does not allow universal weight equations, hence the weight equations were developed from a certain type of aircraft. Therefore, it is crucial to select correct

weight equations that are properly customized to the class to which the aircraft belongs.

Data sets of aerodynamics, propulsion, and weight equations described above are the input data of the aircraft sizing process and their fidelity ultimately determines the level of fidelity of aircraft sizing.

2.2.3 Thrust Balance

Ibrahim [99] proposed a method that determines wing load and thrust-to-weight ratio using semi-empirical relationships for performance measures, such as take-off distance, maximum rate of climb at sea level, maximum level speed, and landing distance, developed from historical data of military jet trainers and light attack airplanes. His method starts with developing an assumption regarding the response of a performance measure with respect to thrust to weight ratio and wing loading, each denoted as T_{SL}/W_{TO} and W_{TO}/S, respectively. For example, the author propositioned the following relationship between take-off ground run denoted as S_{TD} and design parameters.

$$S_{TD} \propto \frac{(W_{TO}/S)}{\sigma^{1.8}(T_{SL}/W_{TO})C_{Lmax.TO}} \tag{2}$$

where $C_{Lmax.TO}$ and σ denote the maximum take-off lift coefficient and ambient air density ratio, respectively. For a designated level of technology, it is assumed that the order of magnitude of the maximum lift coefficient in the take-off configuration for a category of aircraft remains the same. Accordingly,

$$S_{TD} \propto \frac{(W_{TO}/S)}{\sigma^{1.8}(T_{SL}/W_{TO})} \tag{3}$$

Finally, based upon this relationship, a regression analysis from a historical database of military jet trainers and light attack airplanes results in a linear equation describing the take-off distance in terms of T_{SL}/W_{TO} and W_{TO}/S as follows:

$$S_{TD} = 167 + 1.029\frac{(W_{TO}/S)}{\sigma^{1.8}(T_{SL}/W_{TO})} \tag{4}$$

The author developed semi-empirical equations for other performance constraints in a similar way. This method provides a comparatively accurate estimation of required thrust and wing loading only when a large amount of sample data for existing aircraft built with similar level of technologies is available. Thus, this method is not immediately applicable to the design of aircraft built with an unconventional configuration and/or a different level of technologies, for which sufficient historical data do not exist.

Mattingly [100] proposes a more systematic approach known as the constraint analysis for thrust balance. The equations of constraint analysis can be derived directly from the consideration of dynamic equilibrium of aircraft motion as shown in Figure 13. The velocity of free stream air has an angle of attack (AoA) to the wing chord line (WCL). Lift (L) and drag ($D + R$) forces are normal and parallel to this velocity, respectively. Thrust (T) is at an angle (ϕ) to the WCL. The application of Newton's Second Law to the aircraft motion yields the two following equations that describe the relationship of the net forces versus acceleration perpendicular and parallel to the velocity vector, V, respectively.

$$T\cos(AoA+\phi) - W\sin\theta - (D+R) = \frac{W}{g_o}a_{\parallel} = \frac{W}{g_o}\frac{dV}{dt} \tag{5}$$

$$L + T\sin(AoA+\phi) - W\cos\theta = \frac{W}{g_o}a_{\perp} \tag{6}$$

where D is basic configuration drag; R is additional drag to D due to the changes of the configuration such as deflecting control surfaces, extracting landing gear, and installing ordnance such as weapons and external fuel tanks; h is the flight altitude; V is the free-stream velocity; and g_o is the gravity constant. Multiplying Eq. (5) by V leads to the following equation:

$$\{T\cos(AoA+\phi) - (D+R)\}V = W\{V\sin\theta + \frac{d}{dt}\left(\frac{V^2}{2g_o}\right)\} \tag{7}$$

Note that for most flight conditions the thrust vector is very nearly aligned with the direction of flight, so that the angle ($AoA + \phi$) is very small, which allows one

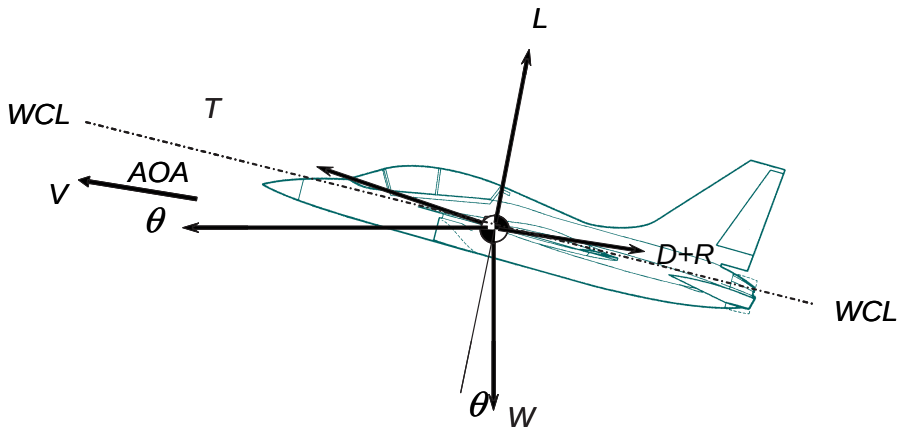

Figure 13: Forces on aircraft [100]

to assume $\cos(AoA + \phi) \approx 1$. In addition, $V \sin\theta$ is simply the time rate of change in altitude (h), known as the rate of climb (for positive values) or the sink rate (for negative values), given as

$$V \sin\theta = \frac{dh}{dt} \tag{8}$$

Combining Eq. (7) and Eq. (8) yields the following equation.

$$(T - (D + R))\, V = W \frac{dh}{dt} + \frac{W}{g_o} \frac{d}{dt} \left(\frac{V^2}{2} \right) \tag{9}$$

This equation describes the *dynamic equilibrium* between power input and the rate of change in the potential energy of the aircraft. The left-hand side of the equation represents the rate of net mechanical energy input to the aircraft, which is often called excess power. The right-hand side of the equation represents the time rate of change in the sum of kinetic energy and potential energy of the aircraft.

Dividing Eq. (9) by aircraft weight, W, gives another equivalent equation:

$$\frac{(T - (D + R))}{W} V = \frac{d}{dt} \left(h + \frac{V^2}{2g_o} \right) \tag{10}$$

The left-hand side of the equation is called the *specific excess power*. This metric represents the ability of an aircraft to change its energy state, thus playing as one of

the important factors to determine the short range air combat capability of fighters. The right-hand side of the equation is called *energy height*, which is the sum of kinetic energy and potential energy normalized by the aircraft weight. Therefore, the equation states that the specific excess power of the aircraft equals the time rate of change in the energy height of the aircraft.

Starting with Eq. (10), Mattingly derived a general form of constraint equations, named the *Master Equation*, that provides the desired relationships between the thrust-to-weight ratio and wing loading as follows:

$$\frac{T_{SL}}{W_{TO}} = \frac{\beta}{\alpha}\left\{\frac{qS}{\beta W_{TO}}\left[K_1\left(\frac{n\beta}{q}\frac{W_{TO}}{S}\right)^2 + K_2\left(\frac{n\beta}{q}\frac{W_{TO}}{S}\right) + C_{D_o} + \frac{R}{qS}\right] + \frac{1}{V}\frac{d}{dt}\left(h + \frac{V^2}{2g_o}\right)\right\} \quad (11)$$

where β is the weight fraction; α is the thrust lapse ratio; q is the dynamic pressure; K_1 is the drag polar coefficient for the 2nd order term; K_2 is the drag polar coefficient for the 1st order term; C_{D_o} is the zero lift drag coefficient; and n is the load factor. With the *master equation*, Mattingly developed a number of constraint equations, each of which is customized to a specific performance constraint, such as take-off field length, climb, acceleration, and sustained turn. The mathematical expression of the tailored constraints is listed in Appendix A.

The beauty of this method is that it allows the designer to consider all performance constraints in one unified graphical environment. Most aerodynamic point performance measures, which include take-off field length, climb, acceleration, sustained turn, and approach speed, can be expressed as functions of thrust loading (T/W) at sea level, and wing loading (W/S) for a given aircraft geometry, thrust lapse behavior and set of flight conditions. Thus, the feasible solution region is circumscribed by a set of constraint curves that represent each performance requirement as depicted in Figure 14. The design point is generally selected at the location of the lowest thrust-to-weight ratio consistent with the greatest wing loading as illustrated in Figure 14(a), because lower thrust-to-weight ratios lead to smaller propulsion systems and greater

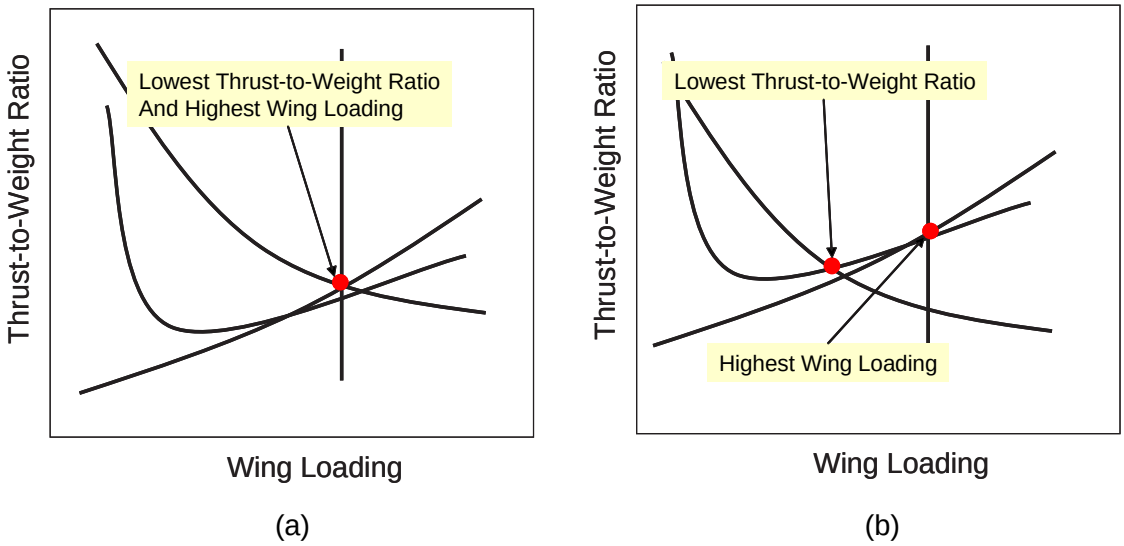

Figure 14: Notional constraint analysis diagrams

wing loading values lead to smaller wings [100], both of which always reduce aircraft weight and cost [93]. However, in some cases as illustrated in Figure 14(b), the lowest thrust-to-weight ratio may not be consistent with the greatest wing loading and a minimum point is not clearly identified. Such difficulty can be resolved when the whole sizing process is mathematically optimized [101]. Another important aspect is to consider the proper design margins for the design constraints. However, a plethora of redundant thrust will most likely increase the propulsion system weight, and thus the take-off gross weight as a consequence without the proportional benefit of reducing the risk. Therefore, the margins must be carefully determined so as to strike a good compromise between the risk and the impact on aircraft weight and cost.

2.2.4 Fuel Balance

Energy balance means the amount of on-board stored energy is no less than the amount of required energy to complete the mission. The equation that describes the amount of required energy can be established by integrating Eq. (9), as follows:

$$\int Pdt = \int (D+R)Vdt + \int Wdz_e \tag{12}$$

This equation states that the amount of energy added to the system by propulsive thrust work ($\int Pdt$) equals the sum of the amount of energy lost by the system due to work done by the system on its surroundings ($\int (D+R)Vdt$) and the increase in the conservative energy of the system ($\int W dz_e$) which is another representation of the energy conservation law that states: energy cannot be created or destroyed. Though containing the canonical idea of energy balance, this equation is not fairly practical to estimate the amount of required fuel as it is. First of all, since D, R, W, and V vary during the mission, it is not possible to obtain the simple closed form of Eq. (12). Furthermore, Eq. (12) describes the energy balance in terms of the mechanical energy of the aircraft as a point-mass with the exclusion of the energy conversion process taken inside of the aircraft. Therefore, even if we can estimate the amount of total energy by propulsive thrust work, $\int Pdt$, from Eq. (12), in general we cannot directly estimate from the information the amount of required fuel to complete the mission. This discussion reveals the need for another analysis that connects the time rate of fuel consumption ($\dot{W}_F$) to the time rate of input mechanical energy (P)[1]. The relationship is ultimately governed by thermodynamic laws, but can be described in simple form as follows:

$$\dot{W}_F = -c_t T \tag{13}$$

where c_t, and T stands for thrust-specific fuel consumption and thrust, respectively. By assuming that the rate at which aircraft weight diminishes ($\dot{W}$) equals the fuel flow ($\dot{W}_F$), Eq. (13) can be rewritten as

$$\frac{dW}{W} = -c_t \frac{T}{W} dt \tag{14}$$

For level flight, $L = W$ and $T = D$. Thus,

$$\frac{dW}{W} = -\frac{c_t}{V}\frac{D}{L} ds \tag{15}$$

[1] $(\cdot)$ notation represents differentiation with respect to time.

Making an assumption that c_t, V, and L/D are constant with their representative values during flight, Eq. (13) can be considered a first-order ordinary differential equation, which is solved for the boundary conditions of $W(s = 0) = W_{initial}$ and $W(s = R) = W_{final}$ with

$$R = \frac{V}{c_t}\frac{L}{D}\ln\frac{W_{initial}}{W_{final}} \tag{16}$$

which is known as the Breguet range equation. For propeller aircraft, the Breguet range equation is given as

$$R = \frac{\eta_{pr}}{c_p}\frac{L}{D}\ln\frac{W_{initial}}{W_{final}} \tag{17}$$

where η_{pr} and c_p denotes propeller efficiency and power-specific fuel consumption, respectively. A simple estimation of the required fuel, presented by several authors including Wood [98], is just to account for the fuel amount consumed for the cruise mission using the modified Breguet range equation as follows:

$$\frac{W_F}{W_{TO}} = 1 - \frac{W_{final}}{W_{initial}} = 1 - \exp\left(\frac{Rc_p}{\eta_{pr}}\frac{D}{L}\right) \tag{18}$$

Since the greatest amount of fuel is consumed generally during cruise, this method is acceptable as a first order crude guess. However, in the design of aircraft that must perform a complicated mission, notably, combat aircraft, this approach may yield significant errors.

A more accurate approach is to compute the required fuel fraction by calculating the product of all the weight fractions of discretized mission segments as shown in Figure 15, which is widely used in most sizing methods including Mattingly's method. The weight fraction of each mission interval can be obtained by one of a set of integrating differential equations listed in Appendix B, which are developed from Eq. (14).

$$\frac{W_F}{W_{TO}} = 1 - \frac{W_{final}}{W_{initial}} = 1 - \prod_s \left(\frac{W^{(s)}_{final}}{W^{(s)}_{initial}}\right) \tag{19}$$

where $\prod$ is defined as a product operator that multiplies all the values associated with the variable in parentheses.

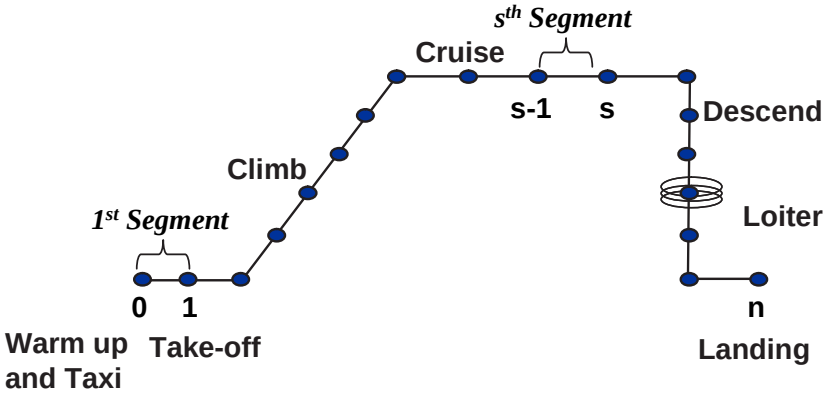

Figure 15: Discretized mission profile

2.2.5 Weight Estimation

The results from the two analyses are fed into the weight estimation module. Once the take-off gross weight as well as the T/W and W/S values are available, the amount of thrust and the wing area of the notional configuration can be established. The method of computing aircraft weight differs depending on the maturity of the design and the availability of the information. During early aircraft design, including most of the conceptual phase, simple empirical and parametric methods are widely used. Depending on the selected method, a different set of parameters may be required. However, the parameters used in such a method are limited to what can be predicted without detailed layout studies.

The simplest method is to estimate the take-off gross weight simply by multiplying payload weight by a constant, in general, four [98]. More detailed methods break down the take-off gross weight into several weight groups; for example, empty weight, fuel weight and payload weight. Then, each group weight is calculated by appropriate methods such as numerical analysis or statistical estimation. Payload weight is usually available from the requirements; fuel weight is calculated by a mission analysis; and empty weight is estimated from a historical database. If most components and parts are modeled, then the element to element method may be used. This method

computes the aircraft weight by summing up the weight of all elements of an aircraft.

The first method is oversimplified. In contrast, the last method is not practical, since the aircraft components and parts are not designed at the time of aircraft sizing. Thus, the second method is widely used for aircraft sizing. The fundamental idea of this approach is that aircraft weight can be broken down into two parts: fixed weight (W_{fix}) independent of the take-off gross weight such as the weight of the crew and payload, and variable weight (W_{var}) dependent on the take-off gross weight such as the weight of structures and subsystems. The former is known from the requirements and the latter can be predicted from a statistical database and/or relevant analyses. Therefore, a weight decomposition equation can be stated in generic form as follows [102]:

$$W_{TO} = W_{fix} + W_{var} \tag{20}$$

Then, Eq. (20) can be reformed as follows:

$$W_{TO} = \frac{W_{fix}}{1 - \frac{W_{var}}{W_{TO}}} \tag{21}$$

The take-off gross weight can be computed by Eq. (21), when the ratio of W_{fix} to W_{TO} can be estimated by utilizing statistical data. Components that W_{fix} and W_{var} account for may differ depending on the type of the aircraft. In general, W_{fix} includes the weight of the payload and the crew, and W_{var} includes empty weight and fuel weight. Then, Eq. (21) can be reformed as follows [103]:

$$W_{TO} = \frac{W_{PL} + W_{crew}}{1 - \frac{W_E}{W_{TO}} - \frac{W_F}{W_{TO}}} \tag{22}$$

Even though Eq. (22) is one of the most common expressions of the take-off gross weight calculation, Eq. (21) must not be overlooked because it more effectively shows the bedrock idea of using a statistical database for the take-off gross weight in generic form.

Multiple ways of estimating empty weight are available, depending on the availability of historical data. The simplest one is using a fixed ratio of empty weight to

the take-off gross weight. For example, Anderson [103] determined the empty weight fraction as 0.62 for the design of five-passenger, propeller-drive, business transport aircraft from an observation that the empty weight fractions of 19 airplanes covering the time period from 1930 to the present show a remarkable consistency of clustering around 0.62. However, this oversimplified method works only when the estimated weight is very close to the weight of the reference airplanes, because the empty weight fraction is affected by the aircraft weight. Thus, this method must be limited to an initial guess for the empty weight fraction. The accuracy of empty weight estimation may be improved by estimating the empty weight as a function of the take-off gross weight.

$$\frac{W_E}{W_{TO}} = \Gamma(W_{TO}) \tag{23}$$

However, this method is still too oversimplified to capture the impact of changes in wing area or engine thrust to aircraft weight. Therefore, a more advanced method is to compute empty weight as a function of engine thrust, wing area, and some other design parameters ($\mathbf{p}$) as well as the take-off gross weight as follows:

$$W_E = f(W_{TO}, T_{SL}, S, \mathbf{p}) \tag{24}$$

A more complex method is to estimate the weight of components or subgroups separately.

$$W_E = \sum W_{comp_i} \tag{25}$$

Selection of a method among various methods strongly depends on the availability of historical data. In general, a more detailed decomposition is preferred. However, it must be noted that employing a more detailed analysis does not necessarily improve the accuracy of weight prediction [104]. A more complex analysis requires more detailed information on the airplane. If accurate information is not properly provided, the results may be biased. Similarly, higher fidelity tools do not necessarily yield more accurate results, unless the aircraft design is matured enough to provide sufficiently

accurate information required for the tools[2]. Therefore, the fidelity of analyses must keep pace with the maturity of designs, and the decision on a weight estimation method must be carefully made though prudent consideration of various factors.

2.2.6 Actual Value-Based Approach and Weight Specific Parameter-Based Approach

The aircraft sizing process generally includes three parts: point performance analysis, mission performance analysis, and aircraft weight estimation. There are two distinct ways of implementing these parts: the actual value-based approach and the weight specific parameter-based approach. The former uses actual values for thrust (power), wing area, and fuel quantity to establish thrust (power) balance and fuel balance, while the latter (Mattingly's method also belongs to this category) uses the parameters normalized or inversely normalized by aircraft weight, which are thrust-to-weight ratio, wing loading, and fuel fraction.

In the actual value-based approach, one must estimate the take-off gross weight for computing point performances and mission performances. For example, the required thrust for level flight is given as lift-to-drag ratio times aircraft weight. Therefore, the process must iterate the three variables through constraint analysis and mission analysis as well as weight analysis until the solution is reached at the thrust and power balance as shown in Figure 16. In contrast, the weight specific parameter-based approach establishes thrust (power) and fuel balance in terms of thrust required per unit aircraft weight and the amount of fuel required per unit aircraft weight. Therefore, thrust balance and fuel balance can be established independently of the computation of aircraft weight, which means that the constraint analysis and the mission analysis do not need to be repeated due to updates of aircraft weight. Even

[2]One example is that an initial weight estimation using an element-to-element method often yields larger errors than a parametric method based on historical data in actual aircraft development programs, even though the former is done by investing a substantial man-hours in engineering work including state-of-the-art computer-aided design and intensive structure analysis.

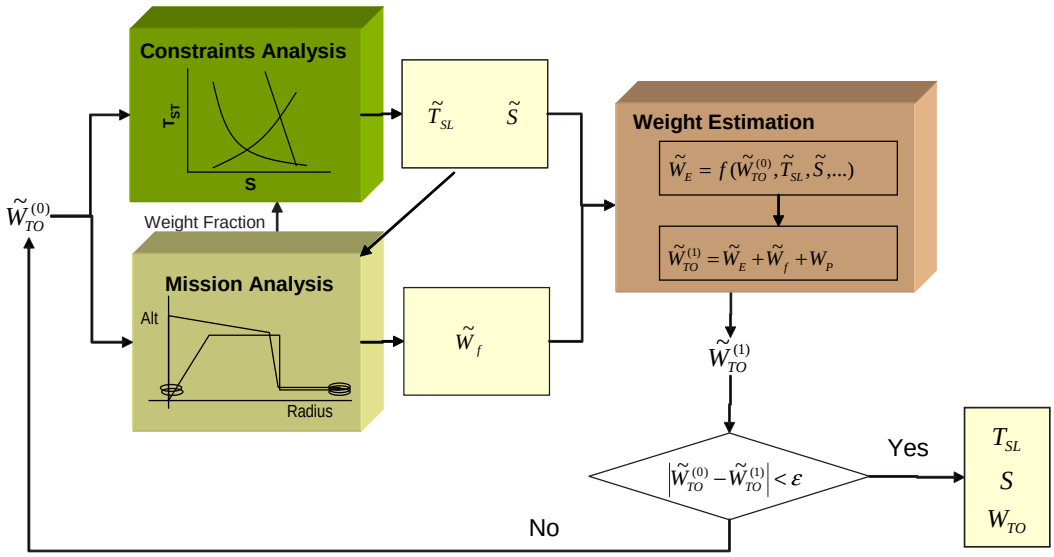

Figure 16: Iterative process of actual-value-based sizing approach

if an iteration process is required to estimate aircraft weight, it is restricted to the inside of the weight estimation module as shown in Figure 17. This benefit may not be noticeable for a one-time run, but it would be substantial for such applications that require a large number of simulations. If one wants to employ an optimization process to find a solution to thrust, wing area, and fuel quantity that minimizes aircraft weight, however, the benefit of the weight specific parameter-based approach over the actual value-based approach is no longer valid because the optimizer iterates the variables in anyway.

2.2.7 Iteration of the Aircraft Sizing Process

In addition to iterative processes described above, overall iteration is required for several reasons. First, the designer would want to improve aircraft design by changing the aircraft configuration and/or propulsion system design if the solution obtained from the process was not satisfactory. Alternatively, the designer would create an automated optimization environment by integrating the aircraft sizing process with disciplinary analyses to find optimum aircraft configuration and subsystem design

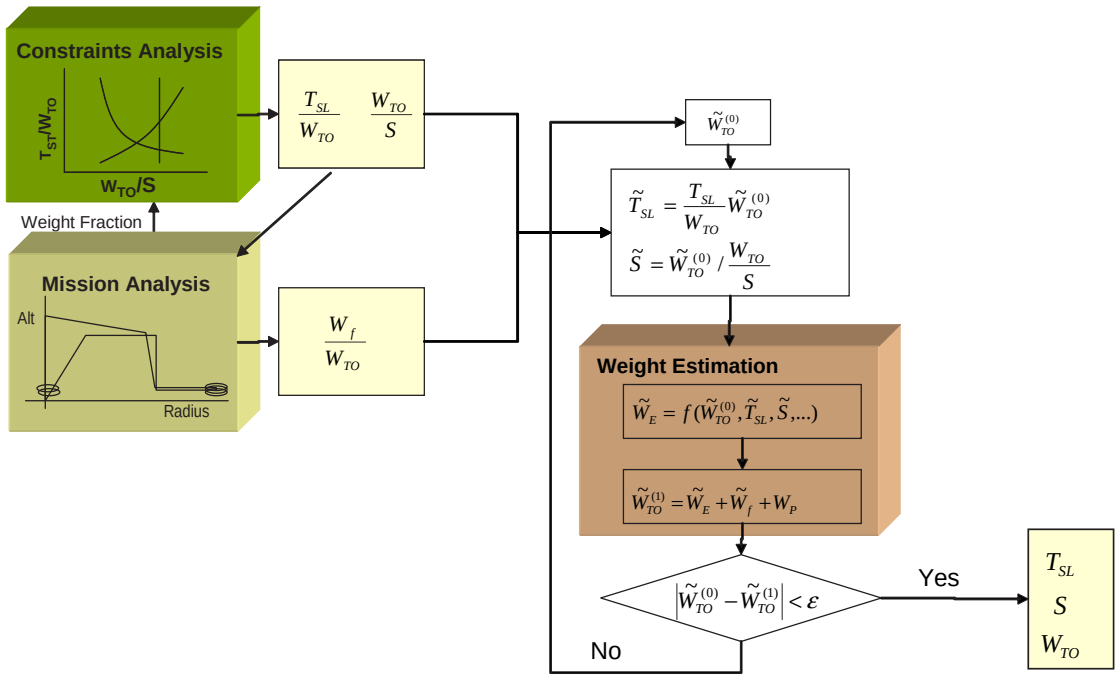

Figure 17: Iterative process of specific parameter-based sizing approach

parameters.

Another cogent reason for the overall iteration is that aerodynamic properties and propulsion system characteristics may change due to the scaling of aircraft geometry and engine thrust. Generally, aerodynamic characteristics stay constant in the process of scaling aircraft geometry up and down with the following the assumptions:

1. Aircraft is scaled photographically

2. Reynolds number effect is negligible within the range of scaling

However, these assumptions may not hold in certain situations. In the design of a subsonic commercial airline, fuselage geometry is usually determined by an internal layout subject to strict volume requirements for cabin design. If such fuselage sizing is already reflected on the notional configuration, changing only wing area makes more sense than photographically scaling the whole aircraft. Taking the former approach requires an update of aerodynamic properties at every change in the wing area of the

aircraft sizing process, since the aircraft geometry is not similar to the configuration of the previous iteration anymore [105]. Similarly, an assumption that the engine characteristics are only dependent on engine cycle and are not affected by scaling effects, is not always reliable. For instance, when more thrust is required than the level of a baseline turbofan engine, thereby enlarging engine geometry, fan tip speed will increase. As the tip speed of the fan approaches the divergence Mach number of its airfoil, aerodynamic losses will be substantial, and the real operating condition will diverge from what engine cycle analysis is based on. Therefore, once the aircraft sizing is done, one must assess the impact of the scaling effect on aerodynamics properties and engine characteristics and, if necessary, reiterate the whole aircraft sizing process after an appropriate update of aerodynamics properties and engine data.

2.3 Aircraft Sizing under Uncertainty

All design parameters involved in the aircraft sizing process can be neither accurate nor certain, particularly because aircraft sizing is performed during the pre-conceptual or conceptual design phase, when the least knowledge about the system is available. Therefore, how to account for the associated uncertainty sources is a crucial element in avoiding significant rework during the subsequent design processes.

2.3.1 Uncertainty Sources

A multitude of sources of uncertainty are involved in the aircraft sizing process. One significant source of uncertainty is the lack of model fidelity and the imprecise knowledge of the system. This type of uncertainty is unavoidable in the sense that it is impossible to develop a perfect mathematical representation of the behaviors of complex systems such as aircraft. Moreover, the desirable degree of fidelity is often compromised by the lack of time, resources, and the degree of design maturity, even when high fidelity models are available. Consequently, high fidelity models have

seldom been used during the early phases of aerospace systems design. Recent advancements in meta modeling have paved the way for accelerating the utilization of high fidelity models in conceptual design phases. Notwithstanding, the very act of approximation by meta models introduces yet another source of model uncertainty or errors. In addition, incomplete knowledge of the details of the system may also introduce a considerable amount of uncertainty. For instance, the precise amount of miscellaneous drag that accounts for additional parasite drag incurred by surface roughness, cavities, environment control systems, control surface gaps, and protuberances cannot be accurately calculated until a detailed description of their geometries, usually not available when aircraft sizing is performed, is established.

Another source of uncertainty is airframe design evolution. Modifications in the external configuration, often referred to as the Outer Mold Lines (OML), directly affect the aerodynamics of an aircraft. On the other hand, changes in the internal configuration may affect the weight of the aircraft. Such changes may collectively result in an increase or a decrease in the required power and energy for flight. The design changes may be attributed to various factors, most of which are motivated by the desire to resolve currently-known design issues. Performed in the embryonic stage of such a long evolution process, aircraft sizing inevitably involves uncertainty associated with design changes for the rest of the development period. While the majority of such changes occur during the conceptual design phase, the aircraft configuration continues to evolve after the aircraft is sized by efforts in the conceptual design phase, as shown in Figure 18, which summarizes the evolutionary process of the T-50 Golden Eagle developed for the Republic of Korea Air Force. As the design matures, the degrees of freedom to alter the design decrease, and the design is less likely to change. Nevertheless, both external and internal configuration of the aircraft will be subject to change through the first flight, even until production.

In addition to the airframe, the design requirements also evolve with time, which

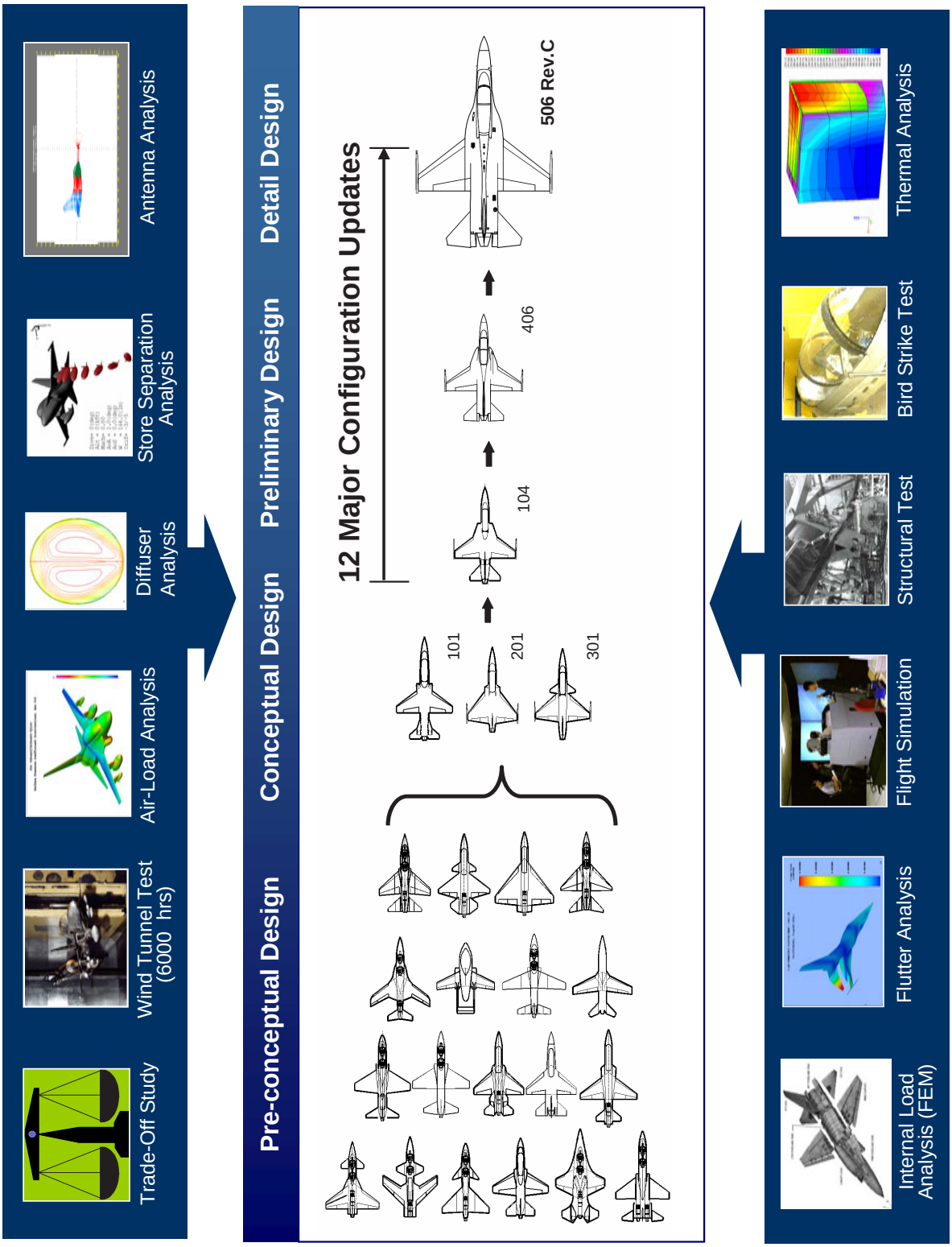

Figure 18: Design evolution of the T-50 Golden Eagle [106]

introduces another significant source of uncertainty in aircraft sizing. It is a popular misconception that design requirements are static. On the contrary, in almost all of the actual aircraft development programs, the requirements are seldom established firmly before design activities are initiated. They continue to evolve after being passed on to the design team. Particularly during the conceptual design phase, designers often explore the requirement space and the concept space while varying the requirements and design options in order to find a correct combination of capabilities and cost. In the light of such interactive trade-off studies, customers or decision makers may revise the initial set of design requirements. However, the evolution of design requirements continues even after the conceptual design phase. Since knowledge of the system increases with design maturity, valuable compromises between capabilities and cost, not previously recognized, may become critical. In addition, notable changes in the market or the operating environment may force the management to update their requirements.

Regulatory uncertainty refers to the risks inherent in obtaining any necessary licenses to construct or operate a project from the appropriate regulatory authority. Regulatory requirements may include safety regulations, environmental regulations, and maintenance regulations. Among those regulations, environmental regulations, in particular, emissions and noise regulations, have created significant uncertainty, causing consternation for airframe and engine designers. Historically, environmental regulations have become increasingly stringent, and this trend should continue in the future due to the necessity for environmental protection and quality of life. In addition, most airplanes and engines are very likely to have an extended period of service life. During this time, present environmental regulations could be re-examined in light of technological improvements, and new regulations could be enacted, thereby forcing early product retirement unless these potential scenarios are accounted for adequately [107].

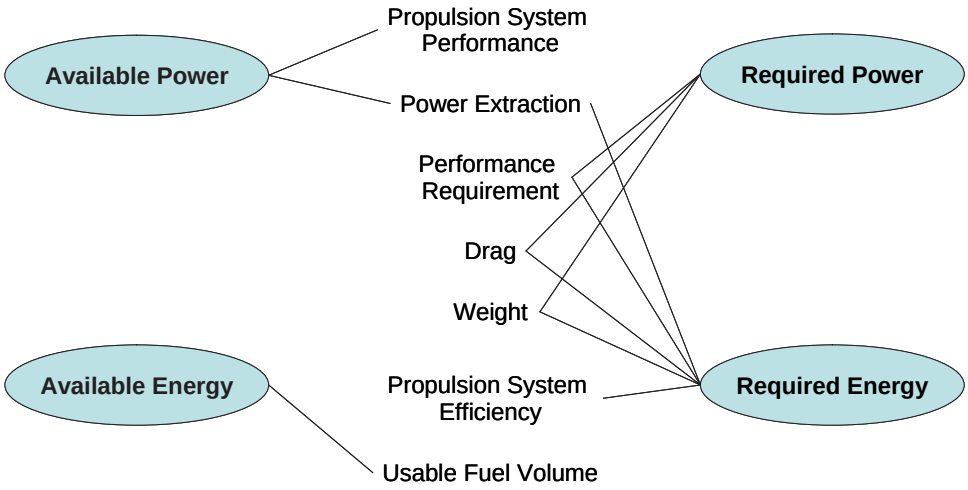

Figure 19: Impact of uncertainty on aircraft sizing

Implementing new technology also introduces uncertainty into the sizing process. "For complex systems, the search for feasible and viable solutions often requires the application of multiple new technologies,"[108] even though infusing technology may incur penalties in other disciplines as a "price" for the benefits. Generally, the impact of a technology, the "benefit" and the "price" cannot be precisely predicted in the conceptual design phase, especially if the technology is ranked low in terms of its technology readiness level (TRL), and if the propagation of technological impact is obscure. Revolutionary propulsion aircraft would be the case. Such advanced concepts will require years to develop, and the expected performance and system attributes could vary dramatically throughout their development. In addition to the uncertainty inherent in the propulsion system, the impact on other disciplines becomes more significant and less predictable.

2.3.2 Traditional Approaches to Aircraft Sizing Under Uncertainty

As outlined in Chapter I, various sources of uncertainty are involved with aircraft sizing. What does it mean to size an aircraft in the presence of such uncertainty? How can the full impact of uncertainty be correctly accounted for? In order to answer

these questions, one needs to return to the definition of aircraft sizing. The goal of aircraft sizing is to find the two scales, the geometric scale and the propulsive scale, that minimize the objective function, which is usually the take-off gross weight, while satisfying all requirements [109].

As illustrated in Figure 19, the sources of uncertainty permeate through both the "available" and "required" quantities, which indicates that both quantities must be treated as random variables, rather than deterministic design variables, for aircraft sizing. Therefore, the deterministic expression of the aircraft sizing problem given as Eq. (1) is rewritten as a probabilistic expression as follows:

$$\begin{aligned} \min_{\mathbf{x}} \quad & \tilde{f} \\ \text{s.t.} \quad & \tilde{P}_{available} \geq \tilde{P}_{required} \\ & \tilde{E}_{available} \geq \tilde{E}_{required} \end{aligned} \tag{26}$$

where ($\tilde{}$) indicates that the variable under the symbol is a random variable or a function of random variable(s). This problem is seeking an optimal solution of decision variables that minimize a probabilistic objective function under probabilistic constraints.

Even though the aerospace community has been cognizant of the significance of the probabilistic nature of design constraints and objective functions, a deterministic approach to aircraft sizing has been the dominant norm. The traditional approach to mitigate the risk associated with uncertainty is to add design margins as a hedge against foreseeable changes in the involved assumptions [107]. In the constraint analysis, designers choose the design point in the proximity of the active constraint curves, so that the movement of any of the constraint curves caused by revised estimates of aircraft and/or engine performance and requirements does not violate any of the design constraints. Then, the distance between the design point and a constraint curve represents the size of a design margin for the corresponding performance requirement(s). The margin for the mission performance requirements is usually not

considered in the aircraft sizing process in which the weight of aircraft is calculated with the assumption that the amount of available fuel equals that of required fuel. Such a margin, however, can be included by adding an allowance to the amount of required fuel. In fact, a military specification known as MIL-DTL-7700G reads that 5 percent penalty in fuel mileage must be accounted for in estimating the amount of required fuel. Nevertheless, this surplus fuel amount is intended to account for engines with "poorer-than-normal" fuel consumptions due to manufacturing tolerances on the production line or fuel mileage deterioration. Therefore, the allowance cannot be regarded as a design margin for uncertainty surrounding aircraft design activities such as the lack of analysis fidelity or changes in drag and weight due to design evolution.

The margin for mission performance is accounted for by maintaining the extra available fuel in the following design process. As stated earlier, the amount of available fuel, the same as that of required fuel, is assumed to be obtainable in the conceptual aircraft that is embodied by preliminary internal layout studies, a design task following aircraft sizing. Then, the amount of available fuel is verified by calculating the available fuel volume. If the confirmed amount of available fuel is less than the amount of required fuel, designers must take several measures to rectify this issue. The first is to rearrange the internal layout to acquire sufficient fuel volume. If these efforts end up failing, the designers may need to reshape the external configuration to accommodate more fuel volume or to resize the aircraft to satisfy the criterion of volume balance. On the other hand, if an extra amount of available fuel is identified, the designers may want to make the configuration slimmer to improve the aerodynamics and/or reduce the aircraft's weight. However, the designers usually try to maintain sufficient, but not extraneous, surplus fuel volume as a margin during the conceptual design phase. These activities continue throughout the preliminary design phase, when the external configuration and internal layouts continue to evolve,

and the amount of required fuel varies at every update of aerodynamics and weight databases, until a detailed internal arrangement is completed.

In summation, the traditional approach has been converting the probabilistic problem given as Eq. (26) to the following deterministic problem by adding predetermined design margin:

$$\begin{aligned} \min \quad & f \\ \text{s.t.} \quad & P_{available} = P_{required} + \Delta P \\ & E_{available} = E_{required} + \Delta E \end{aligned} \tag{27}$$

2.3.3 Recent Probabilistic Approaches to Aircraft Design

In the past decade, the aerospace community has made significant progress in nondeterministic approaches to aerospace systems design. In particular, the Aerospace System Design Laboratory (ASDL) at the Georgia Institute of Technology has advanced various probabilistic design methodologies. Mavris, Bandte, and DeLaurentis introduced a probabilistic approach called Robust Design Simulation (RDS) to aerospace systems design [110]. The method was originally developed for determining a robust design solution that is the most insensitive to noise (random) variables. Since its conception, the method has been implemented in many applications, including the conceptual design studies of a high-speed commercial transport (HSCT).

Even so, the RDS method is not entirely suitable for aircraft sizing under probabilistic constraints for several reasons. First, the uncertainty sources that the method can implement are limited to economic variables such as load factor, fuel cost, and learning curve. The propagated impact on system level metrics due to the variability of economic (noise) variables is still computed in a deterministically-sized aircraft. Secondly, the method seeks a solution that maximizes the probability of meeting a single, static, overall evaluation criterion. However, the constraints involved with aircraft sizing are multiple, interdependent, and probabilistic in nature.

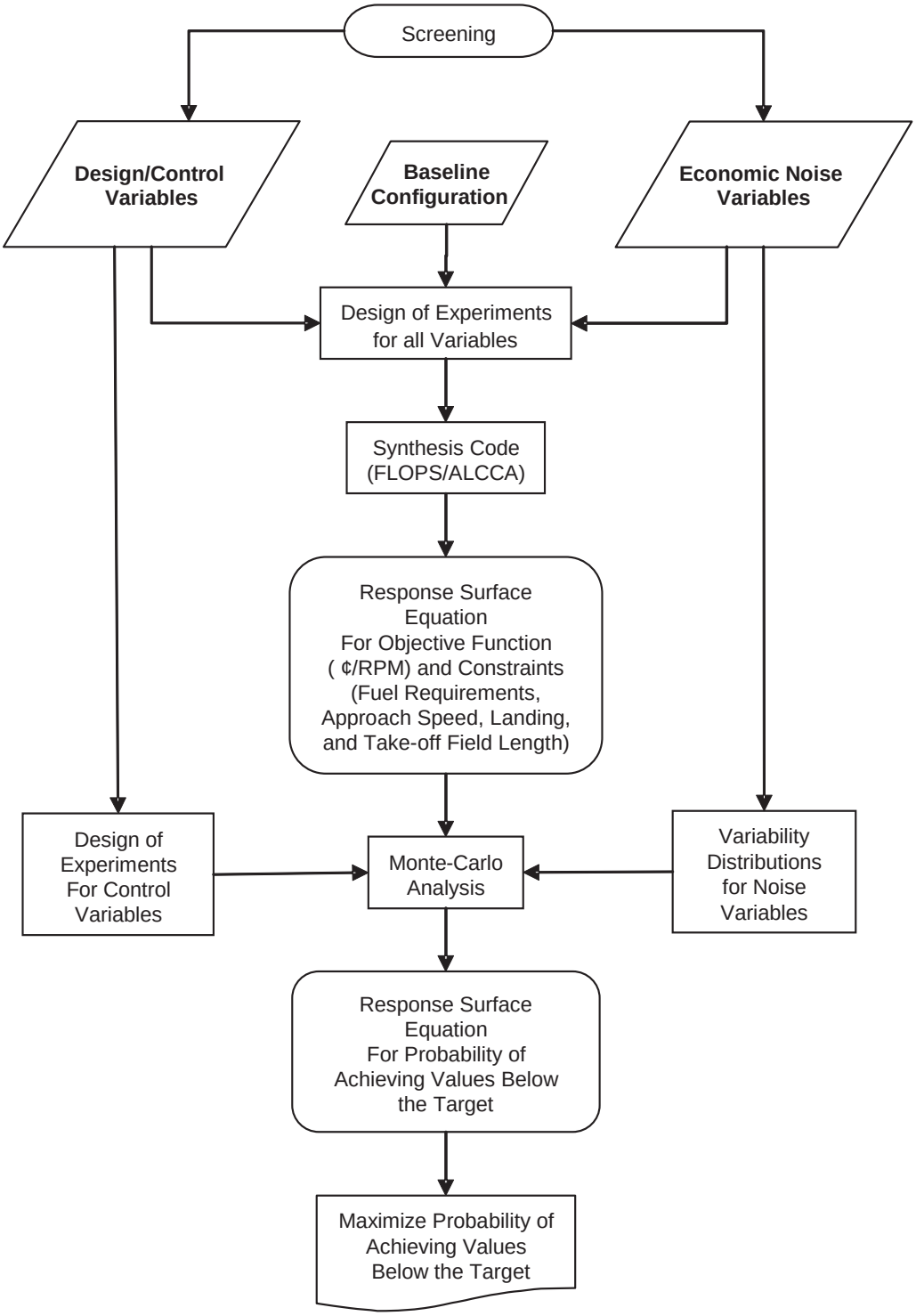

Figure 20: Overall process of Robust Design Simulation [110]

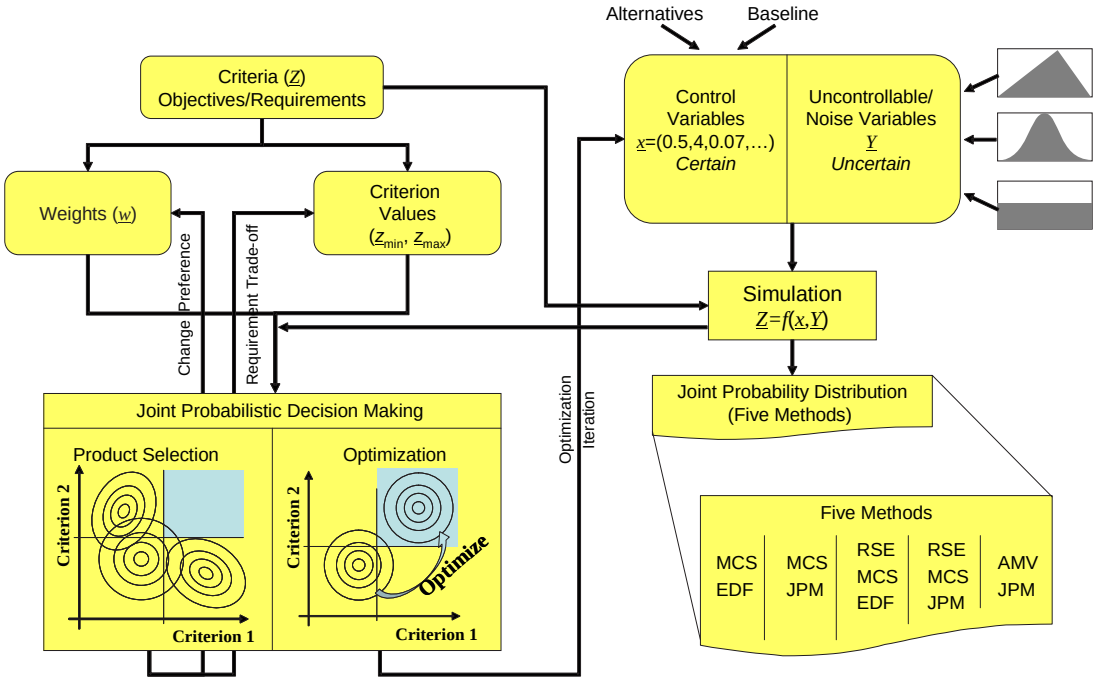

Figure 21: Bandte's JPDM process [112]

Bandte proposed the Joint Probabilistic Decision Making (JPDM) method, which is a probabilistic, multi-criteria optimization approach for aerospace system design [111]. Unlike RDS, JPDM utilizes the joint probability that the system can simultaneously satisfy multiple design criteria to find the design solution. The method was applied to various aerospace problems, such as the evaluation of the feasibility of design spaces, design optimization, and product selections. Still, this method is not immediately applicable to optimization problems with probabilistic constraints, such as probabilistic aircraft sizing. One of the primary reasons is the differences in types of the criteria according to which the probability of success is evaluated. The criteria used in JPDM are determined at fixed values, while the constraints used in the aircraft sizing problem are given as probabilistic multivariate functions of the decision variables.

Nam et al. [22] proposed a probabilistic method to identify the best propulsion system architecture under environmental and regulatory uncertainty associated with

NO_x, CO_2, and noise emissions. Such regulatory metrics are associated with design constraints for the design of an aircraft as well as a propulsion system. In the design constraints, the regulatory metrics appear as target values that associated performance measures as responses of design variables must satisfy. As discussed in §2.3.1, however, the regulatory metrics as target values of the associated constraints are subject to uncertainty such as future regulation changes. Under inherently probabilistic design constraints, their method aims to find the best propulsion system architecture, rather than an optimum solution for one architecture. The overall process of the method is illustrated in Figure 22. The performance measures including NO_x, CO_2, and noise emissions, which are functions of a set of design variables are approximated with a set of response surface equations. An optimization tool, wrapped with a Monte-Carlo simulation (MCS), solves a series of optimization problems, each of which is set up with randomly selected values of the regulatory constraints. A Cumulative Distribution Function (CDF) can be created from a sampling of the optimum deterministic solutions giving two pieces of information: the probability of success and expected optimum OEC range, which guides designers to select the best architecture among the options under consideration.

Although useful for the selection of a system architecture, this method is not appropriate for quantifying design margins for a given system architecture. A compelling reason is that the method simulates uncertainty and evaluates the propagated impacts on system design through a deterministic sizing tool, as depicted in Figure 23. Therefore, all the events that produce the CDFs in the figure represent a possible and desired design from a "wait and see" approach, in each of which designers wait until the uncertainty is clear, and then they deterministically size the aircraft. The consequence of the variation in the random variables in this approach is the variation in the size of the aircraft. If designers need to determine the size of aircraft without knowing the final settlement of the random variables in the future, they must take a

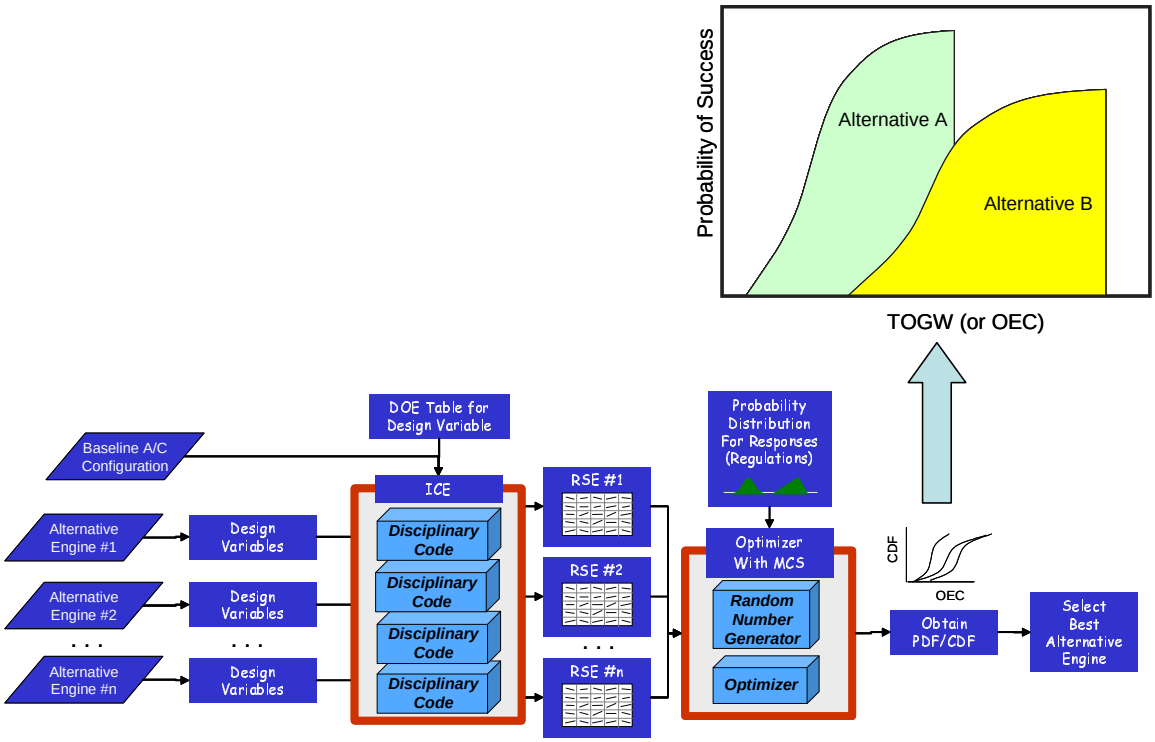

Figure 22: Nam's DSS method process [22]

"here and now" approach, as opposed to "wait and see" approach [113]. The consequence of the variation in random variables in this approach appears as a variation in the performance measures of the production aircraft, by which the feasibility of the design can be estimated.

Despite remarkable progress made in non-deterministic approaches for aerospace systems design in the past decade, no method provides a consolidated treatment of the probabilistic constraints associated with aircraft sizing.

2.4 Deficiencies in Traditional Sizing Methods

Traditional sizing methods have been successfully applied to thousands of aircraft designs and developments. However, the method confronts some serious challenges, as aerospace endeavors are pushing the envelope by pursuing unconventional concepts and implementing revolutionary technology.

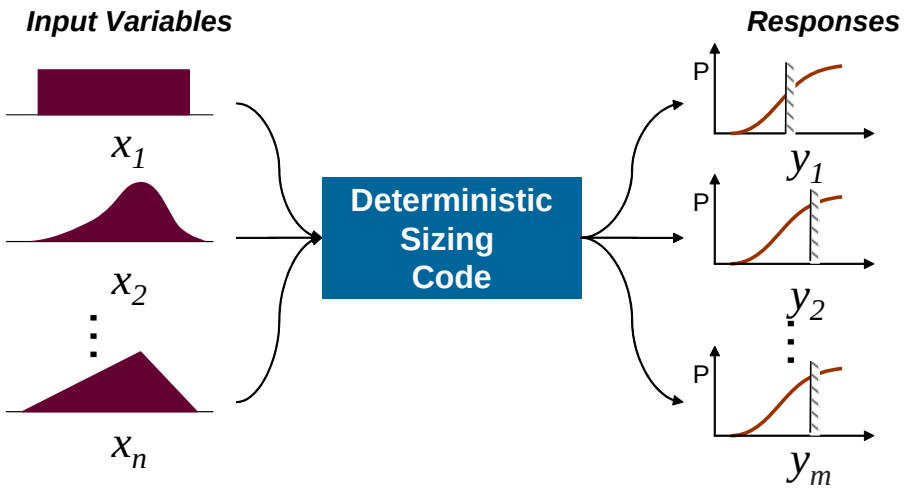

Figure 23: Simulation through deterministic sizing codes

2.4.1 Inflexibility toward Unconventional Concepts

One of the challenges is due to the inflexibility of traditional sizing methods for incorporating unconventionally-powered revolutionary concepts such as zero-emissions aircraft and regenerative propulsion aircraft. Traditional aircraft sizing methods are significantly specialized for aircraft powered by internal combustion engines.

A propulsion system is a device that produces propulsive thrust through a series of energy conversions. This process is typically affected by the design parameters of the system and operating conditions, such as Mach number, altitude, and ambient temperature. Because the technology behind traditional air-breathing combustion engines has matured, thrust lapses and SFC behaviors of traditional air-breathing combustion engines are well understood. Thus, aircraft design engineers need not track every detail of the internal energy conversion process inside the engine. Instead, they can obtain the thrust lapse, SFC behavior, and the scaling laws of a notional engine from well-established historical data by selecting the most suitable engine type and cycle, depending on the mission requirements. In addition, the propulsion system data can

also be created from physics-based legacy codes in which substantial knowledge obtained from several decades of engine development experiences was implemented. In contrast, emerging revolutionary propulsion systems have not yet been fully developed. They are continuously evolving, and thus, their thrust and fuel consumption behavior and scaling laws are not well established.

Another challenge, closely related to the above, is inflexibility of traditional analysis codes for revolutionary aircraft concepts. Most legacy codes that are used for conceptual aircraft design extensively refer to empirical or semi-empirical data, which may not work for this revolutionary propulsion aircraft. In addition, most aircraft sizing synthesis codes are specifically adjusted for conventionally powered aircraft, which leads to inflexibility for revolutionary propulsion systems such as zero-emissions aircraft and regenerative propulsion aircraft. Therefore, designers must reexamine the assumptions that the existing analysis models hold and determine whether the models are appropriate for the revolutionary propulsion system. Thereby, if necessary, new physics-based analysis environments must be developed.

Strictly speaking, however, the scarcity of historical database or immaturity of propulsion system analysis environments, themselves are not a deficiency in the traditional method, but must be referred to as limitation of implementing the method. The exact point where the traditional method fails is where emerging energy sources introduce coupling between propulsion component sizing and aircraft sizing. The successful integration of the propulsion system is one of critical aspects of aircraft development. Therefore, both physical and functional interfaces between the engine and airframe call for intensive engineering work including engine mounting; the connection of bleed air and mechanical power extraction; and the design of in-takes and diffusers. As far as aircraft sizing is concerned, however, airframe design generally does not have to be bothered by details of propulsion system design. Since both engine deck and engine scaling law is of interest to the propulsion system, the propulsion

system can be considered a sort of black-box. Nevertheless, certain emerging electric aircraft propulsion concepts introduce more ambiguous boundaries between the airframe, propulsion system, and energy storage. An example is an *ambient energy-harvesting* aircraft whose such energy-collecting components cannot be sized without considering the airframes geometry. Another example is a fuel cell wing [26], which produces aerodynamic lift as well as propulsive thrust. These problems can be solved by combining a partial or entire propulsion system sizing into aircraft sizing process, which can be achieved by constructing a more generalized formulation for modeling the propulsion system and integrating that into aircraft sizing formulation.

Another deficiency of the traditional sizing methods is their inflexibility in dealing with aircraft propelled by a set of different propulsion systems or hybrid propulsion systems. Except for a few aircraft such as KB-50J, a six-engine aerial refueling tanker equipped with four prop engines and two turbojet engines [114], most existing aircraft are equipped with a single engine or multiple identical engines. Therefore, the thrust available and fuel consumption for most conventional aircraft can be established by one engine deck. However, introducing new energy sources is very likely to call for hybrid propulsion systems for various reasons. First, economics appears as one of the most important factors. "The cost associated with infrastructure changes and the sustained use of legacy aviation systems logically demands a transition period as new energy sources are introduced [5]." Thus, an appropriate use of hybrid propulsion systems may facilitate timely introduction of fledgling new power systems. A hybrid system may also be preferred when some of the requirements are conflicting with each other, thereby any single propulsion system results in infeasible solutions. Especially electric propulsion system architectures may take advantage of integrating a combination of different types of power devices into a single propulsion system thanks to the versatility of electric power. For example, the combination of high specific-power devices such as lithium-polymer batteries and ultra-capacitors and high specific-energy

devices such as fuel cells may provide an optimum solution for an electric aircraft whose power profile has high peaks for short periods. If different types of propulsion systems and energy sources are equipped, and the power contribution rate of each propulsion system varies with flight conditions, then the traditional sizing formulation cannot handle this situation properly.

The last deficiency of the traditional sizing methods is related to the assumptions behind mission analysis. The most widely used mission analysis technique for conventional aircraft is based on the assumption that the time rate of change in aircraft weight equals the fuel flow, which leads to a historical equation known as the Breguet range equation. However, aircraft such as the Helios, which is equipped with regenerative power systems, maintains the same weight throughout the entire mission. Furthermore, more stringent emissions regulations in the future may force aerospace engineers to innovate propulsion systems so that the system can separate specific by-product components from engine emissions and store them on-board during flight. Furthermore, zero-emissions aircraft, which sequester and retain by-products on board during their operation and discharge them on the ground or at least a lower altitude, will get heavier as fuel burns. This behavior cannot be analyzed by the traditional mission analysis based on the Breguet range equation.

Most recent system-level studies [32, 115, 116, 117, 118] evaluate unconventional propulsion systems by retrofitting an existing aircraft and assessing the impact on aircraft performance without sizing the aircraft. The QGT study [26, 119] presented unconventionally powered aircraft sizing practices for two specific configurations: a conventional wing-tail combination with over-wing, hydrogen-fueled engines, and a blended wing-body concept powered by hydrogen fuel cells. The analyses were achieved with significant modifications to a traditional sizing code, the Flight Optimization System (FLOPS) code.

Smith and his colleagues [120] developed an electric aircraft sizing method suitable for battery powered electric aircraft. Harmats and Weihs [121] proposed a cohesive mathematical formulation for sizing of a high-altitude, long-endurance remotely piloted vehicle powered by a hybrid propulsion system combining solar power and internal-combustion engine. However, such methods were limited to certain types of propulsion systems and missions. A comprehensive, structured, generalized aircraft sizing method that is applicable to a wide range of unconventionally-powered aircraft has not yet been fully developed.

2.4.2 Inability to Account for Uncertainty

Another challenge is due to the inability of the traditional methods to account for uncertainty. Generally, uncertainty is greatest in the conceptual design phases because of the scarcity of information about the new product being designed [122]. The traditional approach to mitigate the risk associated with uncertainty is to add design margins, which generally cause direct and adverse impact on aircraft performance and cost. A question that immediately arises is how to quantify proper design margins. If extraneous margins are included, the solution may be to increase the weight and/or the cost without a proportional decrease in the associated risk. Therefore, determining the proper amount of design margins is crucial in achieving affordable risk with a minimal impact on aircraft cost.

In a traditional aircraft design environment, the appropriate margins are usually determined by experts based on their prior experience. Such a conjecture of "grey beards," however, may result in either a significant risk or unnecessary increases in weight and cost. Furthermore, this current practice with revolutionary concept design, whose solution is more likely to deviate from historical precedents, may conjure even more risk. Therefore, emerging revolutionary propulsion aircraft warrant the need for a novel, structured method that allows one to optimize the design with

the "correct" design margins, which tailor the risk to a level deemed acceptable by the decision maker. Nevertheless literature review has also shown that the various probabilistic approaches developed in the area of aerospace system design during the past decade are not able to fulfill such a need.

CHAPTER III

RESEARCH OBJECTIVE, QUESTIONS, AND HYPOTHESES

The literature review presented in Chapter I has identified an emerging need for a method that is capable of sizing aircraft powered by alternative energy sources. However, the continued review of traditional sizing methods as well as state-of-the-art design methods, presented in Chapter II, has revealed that existing methods are not able to fulfill the need. These observations resulted in the objective of this dissertation, which is presented in §3.1. Subsequently, §3.2 describes the research questions that must be answered to achieve the research objective, which is followed by a discussion of the hypotheses. The last section presents the mathematical representations of the hypotheses.

3.1 Research Objective

The objective of this dissertation is to develop a comprehensive, generalized, aircraft sizing formulation that is capable of:

1. *Sizing revolutionary aircraft concepts that are powered by a wide range of unconventional energy sources*

2. *Mitigating the risk associated with uncertainty to the level deemed acceptable by a decision maker*

The first part of the research objective encapsulates the original research motivation of this thesis: *introduction of alternative energy sources to aviation.* Therefore, the emerging method must possess a sufficient degree of generality to cope with various

types of propulsion system architecture utilizing different alternative energy sources. The second part is a logical adjunct to the first part, because the incorporation of alternative energy sources necessarily introduces uncertainty sources that traditional methods cannot properly handle as discussed in §2.4.2.

While no legacy code is publicly available for the analysis of revolutionary propulsion systems powered by alternative energy sources, a range of applicable analysis tools with varying levels of fidelity can be found in the literature. Therefore, the emerging sizing method must be made adaptable in order to to extend its applicability. Although not explicitly stated in the research objective, such a flexibility regarding analysis fidelity is pursued throughout the development of the new sizing method.

3.2 Research Questions

The aforementioned research objective can be fulfilled by developing sound solutions to the following two research questions.

- **Question 1**: *How can a generalized aircraft sizing method, independent of the architecture of energy storage and power generation, be formulated?*

This question is directly addressed by the efforts of pursuing the first capability of the emerging method, *capable of sizing aircraft powered by alternative energy sources*. The use of alternative energy sources, however, is very likely to accompany revolutionary, unconventional propulsion systems, energy storage systems, and energy reception systems (if applicable). Understanding the implication of the difference in the way of storing energy and producing power into aircraft sizing is as important as the difference in the properties of fuels (energy sources). Therefore, this research question is not just about addressing the issue of alternative energy sources, but is ultimately seeking an *architecture-independent* aircraft sizing formulation.

According to the SAE Dictionary of Aerospace Engineering [123], an architecture is defined as "the structure, functional, and performance characteristics of a system, specified in an implementation-independent way." Thus, "implementation-independency" implies consistency throughout individual product designs. For example, turbofan engines share a common structure regardless of the differences in the product-to-product details, compared with other type of engines, such as a turbojet, scramjet, and so forth. Similarly, alternative energy sources are also likely to have multiple options for incorporation into aircraft propulsion system architectures. For instance, hydrogen can fuel turbine engines as well as fuel cell power plants, each of which is associated with totally different architecture from another. Therefore, a new formulation must possess a common structure that is applicable to any architecture and is able to capture the impact on aircraft sizing due to the choice of an architecture.

In meeting the second part of the research objective, the following research question must be addressed.

- **Question 2**: *How can adequate design margins, required for mitigating the risk associated with uncertainty having minimal impacts on the design objective(s), be quantified in an aircraft sizing problem?*

As mentioned previously, the best way to mitigate the risk associated with uncertainty in a system design is to add proper design margins. Although the concept of robust design is intended to produce a design that is insensitive to randomness, robustness itself does not ensure the design will meet the design constraints with sufficient probabilities. Therefore, the emerging method must be able to intelligently allocate design margins that ensure the target probability of meeting the design constraints without committing too much cost on the design objective(s).

3.3 Hypotheses

The hypotheses presented herein are an attempt to answer the research questions given in the previous section. The hypotheses themselves serve as the cornerstones upon which the emerging method is constructed.

- **Hypothesis 1**: *A generalized aircraft sizing formulation that is independent of propulsion system architectures and energy sources can be formulated based on the traditional energy-based sizing approach by making the following modifications:*
  - *The propulsion system architecture is modeled as an integration of power-path(s), each of which is characterized by three parameters: the specific energy of the energy source, specific power, and efficiencies of power transfer devices.*
  - *Fuel is generalized as the source of energy on board a vehicle and is categorized into based on its nature of conversion: consumable and non-consumable.*
  - *Aircraft weight is decomposed into more generalized weight groups, which leads to a more general weight differential equation.*

The fundamental idea of aircraft sizing, which is represented by a power balance and an energy balance, is still valid for the sizing of revolutionary aircraft powered by alternative energy sources. In addition, the overall process of the traditional aircraft sizing method briefly outlined in Chapter II appears to be applicable to revolutionary aerospace vehicle concepts that operate on the consumption of alternative energy sources. Therefore, it is conjectured that the first research question can be answered by modifying the traditional methods as much as necessary rather than starting completely anew. Upon this recognition, Mattingly's method is selected as the bedrock

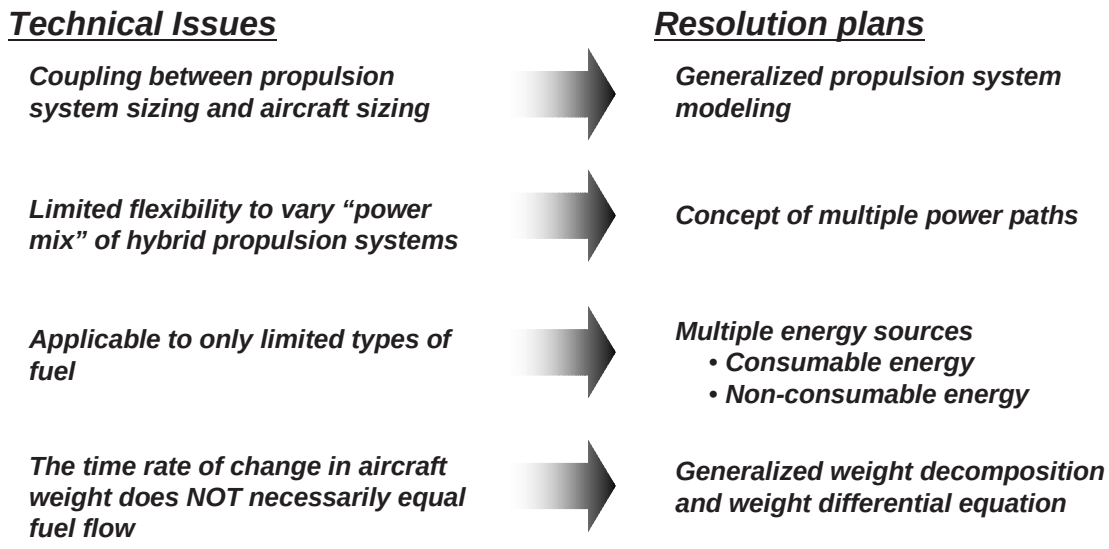

Figure 24: Strategy for a generalized sizing method

for a couple of reasons. Above all, the method is based on fundamental physics, Newton's Second Law, to which the emerging method also aspires. In addition, Mattingly's original formulation provides a structure that allows designers to employ a wide range of analysis tools of variable fidelity, unlike others that heavily depend on regressed equations developed from empirical data, which may not be valid for alternative energy-propulsion system architectures. Such an extensive applicability, however, outstandingly requires a considerable amount of modifications to the traditional formulation. The modifications can be addressed by seeking proper remedies to the deficiencies of traditional sizing methods identified in Chapter II, and summarized here as Figure 24.

The first modification is to generalize the concept of a propulsion system. Should the use of alternative energy sources be accompanied by the revolutionary, unconventional propulsion system architectures, the emerging method must have an architecture-independent structure that properly incorporates the sizing of propulsion systems into

the aircraft sizing process. Traditional aircraft sizing methods are applicable to internal combustion engine architectures consuming hydrocarbon fuels. With some modifications, their basic structures also seem applicable to certain propulsion systems using alternative fuels, whose architectures are similar to conventional propulsion system architectures. For example, a hydrogen-fueled jet engine has a significant proximity to its conventional counterpart. Nevertheless, the existing methods are mostly limited to what has been done in the past. Therefore, an architecture-independent formulation must be constructed based on the abstracted properties commonly found in all propulsion system architectures. Such abstracted properties must formally represent the following three attributes - fuel consumption, available power, and propulsion system's weight - that are the primary figures of merit of a propulsion system in view of aircraft sizing. This hypothesis is developed based on the belief that the abstraction of propulsion system architectures by specific energy of the energy source, the specific power, and the efficiencies of power transfer devices can properly capture the above three attributes.

The second modification is the generalization of the concept of fuel as an energy carrier. In addition to the propulsion system architectures, an architecture-independent method must have a proper means of capturing the attributes of various energy sources and their implications to aircraft sizing. As discussed in Chapter II, traditional aircraft sizing methods are, for the most part, specific to the use of conventional fuels, the weight of which gets reduced during flight due to consumption. However, this may not always be the case for certain alternative energy sources, whose weight remains constant in the process of power generation. Therefore, it is desirable to classify aircraft energy sources into two groups: *consumables* and *non-consumables*. A separate treatment of each group would allow the designer to properly capture the variation of energy source weight with flight. Henceforth, consumable energy is defined as a form of energy that is derived from a source whose weight is

reduced during power generation, such as traditional hydrocarbon fuels. Alternatively, non-consumable energy is defined as a form of energy derived from a source whose weight stays constant or changes negligibly during power generation, such as an electric battery, a nuclear battery, or human power.

The last modification is the incorporation of more generalized weight decomposition and weight differential equations. A revolutionary propulsion system with alternative energy source may debunk the primary assumption of traditional approaches to fuel balance: *the time rate of change in aircraft weight equals fuel flow*. This issue ensues from the use of a non-consumable energy source. The assumption may no longer be valid for certain types of aircraft that fly with only non-consumable energy sources, such as the Helios, which was conceived to use re-circulating hydrogen to fuel the regenerative fuel cell propulsion system, whose weight would not change throughout the entirety of its operation. An improper consideration of the aircraft's weight variation due to fuel consumption may result in a considerable error in the estimation of its mission range or the amount of energy sources, and thus consequential errors in its sizing. Since drawing non-consumable energy, by definition, does not result in any change in aircraft weight, the relationship between the time rate of change in consumable energy weight and aircraft weight is of interest. In addition, the relationship depends on how much of the by-products from the energy conversion process of a consumable source are emitted from the aircraft. Unless such by-products are fully and instantaneously expelled from the aircraft, as is the case of conventional propulsion systems, the time rate of change in aircraft weight would not necessarily equal the time rate of change in consumable energy weight. The weight of the by-products from most energy conversion processes would be reasonably in proportion to the weight of consumed fuel, the ratio of which can be determined by symbolic representation of a chemical reaction associated with the energy conversion process. Incorporating a generalized formulation that establishes the relationship between the time rate of

change in aircraft weight and the time rate of change in consumable energy weight would thusly allow the sizing of any kind of revolutionary aircraft concept, regardless of its energy-conversion mechanism.

- **Hypothesis 2**: *It is possible to determine adequate design margins that result in a solution satisfying all probabilistic constraints under consideration with a target probability, while searching for a design optimum.*

Although the initial problem statement of the probabilistic approach for aircraft sizing, given per Eq. (27) is a realistic representation of the real-world, in which one needs to make a decision for an optimal solution under uncertainty, it is not yet clearly defined. The most ambiguous of them all is how to interpret and implement the probabilistic constraints, and more specifically, how to determine the feasibility of the probabilistic constraints. One way of accounting for the probabilistic constraints is to find the design solution that, with 100% probability, satisfies all constraints on any realization of random parameters. However, such an extremely conservative solution is not likely to exist in reality. Furthermore, even if such a solution were to be found mathematically, the resulting impact on the objective function is expected to be prohibitive.

The underlying idea of this hypothesis is that the *adequateness* of design margins can be measured by two figures of merit: the probability of meeting non-deterministic constraints and their impacts on the design objective function. It is believed that a practical way to address the impact of uncertainty in the aircraft sizing process is to set design margins that tailor the probability of meeting the design constraints to the level deemed acceptable by decision makers. At the same time, it is desired that the impacts of such design margins on the objective function are minimized.

3.4 Substantiation of Hypotheses

The hypotheses verbally introduced in §3.3 are substantiated with mathematical interpretations that allow the intrinsic ideas to be assimilated into the emerging formulation. This section provides such a mathematical representation for each hypothesis.

3.4.1 Mathematical Representation of Hypothesis 1

The fundamental idea behind the first hypothesis is that the basis of the traditional energy-based sizing method is also valid for the sizing of unconventional energy-propulsion system architectures. The two axes of the traditional energy based sizing method - thrust balance (or power balance) and fuel balance (or energy balance) are based on the fundamental physics laws, Newton's Second Law and the Second Law of Thermodynamic Law, respectively. These two fundamental principles do not assume any specific energy source nor any specific propulsion system architecture, and thus are valid for describing the motion of any aircraft, regardless of its energy carrier and propulsion system architecture. Founded on the same cornerstones, however, the architecture-independent sizing formulation can be constructed by significantly modifying the old approaches. The three key modifications addressed by Hypothesis 1 are elaborated as follows.

3.4.1.1 Generalized Propulsion System

A generalized modeling of propulsion system architectures begins with the decomposition of the system itself. A propulsion system consists of a series of power generation or conversion devices, as depicted in Figure 25. Such devices can be categorized into a power generation device (PGD), a power transformation device (PTD), and a power output device (POD) - the last power transformation device.

All parameters which describe a given propulsion system in view of aircraft sizing - output power, fuel consumption, and system weight - can be represented by the following component-level parameters: specific energy of energy sources, specific power

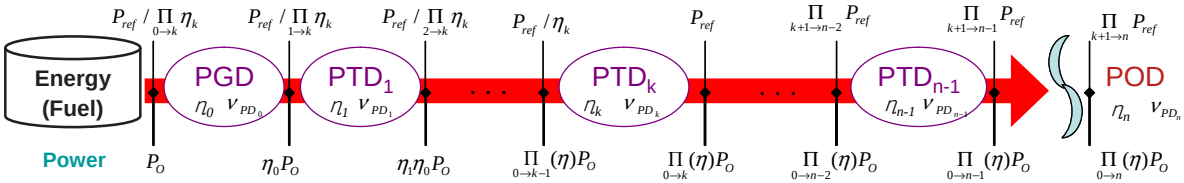

Figure 25: Generalized propulsion system model

of each power device, and the efficiency of each power device. Specific energy, denoted as ν_E, is the energy per unit weight of an energy carrier. The values of specific energy[1] for various energy sources are listed in Table 2.

The specific power of a power device, ν_{PD}, is the amount of output power produced by the device per unit weight. The efficiency, η, of the device is the ratio of the amount of output energy to input energy of each device. Then, the final propulsive power, P, is related to the first power input from the energy source, P_o as follows:

$$P = \eta_n \eta_{n-1} \cdots \eta_1 \eta_0 P_o = \Pi_\eta P_o \tag{28}$$

where Π_η denotes the overall efficiency of the propulsion system. This *tank-to-wing* efficiency is computed by multiplying the efficiencies of all energy conversion associated with a propulsive power generation process, that is $\Pi_\eta = \prod(\eta)$. The overall efficiency of an internal combustion engine is given as a multiple of thermal efficiency (η_{th}), the ratio of net output from thermal cycle to thermal energy input, and propulsive efficiency (η_p), the ratio of propulsive work to net output from thermal cycle as follows [126]:

$$\Pi_\eta = \eta_{th}\eta_p = \frac{V}{c_t \ LHV} \tag{29}$$

where c_t stands for thrust specific fuel consumption (TSFC) and LHV stands for lower

[1]The specific energy of chemical energy sources are often defined in terms of HHV (higher heating value) or LHV (lower heating value). The former is determined by bringing all the products of combustion back to the original pre-combustion temperature. The latter, also known as net calorific value, is determined by subtracting the heat of vaporization of the water in the by-product from the higher heating value results. The lower heating value is what is typically used for IC vehicle engine analysis.

Table 2: Energy contents

Fuel	Energy contents (MJ/Kg) [1)]	Reference
Coal [2)]	33.3	[124]
CO	10.9	[124]
Methane	50.1	[124]
Natural Gas [3)]	38.1	[124]
Propane	45.8	[124]
Gasoline [4)]	42.5	[124]
Diesel [5)]	43.0	[124]
JP-8	42.8	MIL-DTL-83133E
Hydrogen	120.1	[124]
Natural uranium	500,000	[125]

1) Lower heating value for chemical energy sources
2) Anthracite, average
3) Groningen (The Netherlands)
4) Average gas station fuels
5) Average gas station fuels

heating value. Fuel consumption, $\dot{W}_F$, is given as

$$\dot{W}_F = -\frac{P}{\nu_E \Pi_\eta} \tag{30}$$

Finally, the weight of a propulsion system (W_{PS}) is given as the sum of all power devices' weight (W_{PD_i}), each of which can be computed by dividing its sizing power by specific power (ν_{PS_i}) as follow:

$$W_{PS} = \sum_{i=1}^{n_{PD}} W_{PD_i} = \sum_{i=1}^{n_{PD}} \frac{P_{PD_i}}{\nu_{PD_i}} \tag{31}$$

Therefore, if the specific energy of the energy source and the specific power and the efficiency of each power device are established, then the system characteristics and behavior of the propulsion system can be fully described for the purpose of aircraft sizing.

Most aircraft propulsion systems also provide power for other subsystems such as cooling systems, hydraulic systems, and electric systems by means of engine bleed air

and mechanical power extractions. In order to capture the loss due to such power extraction, a small modification to the previous equation is needed. If P_{ext} is taken out at the k^{th} power device, then the modified efficiency, $\acute{\eta_k}$, of the power device can be expressed as follows:

$$\acute{\eta_k} = (\eta_k - \gamma) \tag{32}$$

where γ is the ratio of the amount of power extraction to the amount of input power of the power device.

3.4.1.2 Consideration of Multiple Energy Sources

In order to produce a generalized formulation, the aircraft is assumed to have multiple power-paths that have either consumable or non-consumable energy sources. Then, the total energy stored on-board, E, is the sum of these two types of energy as follows:

$$E = \sum_{i=1}^{n_{CE}} E_{CE}^{\langle i \rangle} + \sum_{j=1}^{n_{NE}} E_{NE}^{\langle j \rangle} \tag{33}$$

where n_{CE} is the number of power-paths of consumable energy, and n_{NE} is the number of power-paths of non-consumable energy. Therefore, the total weight of the on-board energy carriers, W_{energy} is

$$W_{energy} = W_{CE} + W_{NE} = \sum_{i=1}^{n_{CE}} W_{CE}^{\langle i \rangle} + \sum_{j=1}^{n_{NE}} W_{NE}^{\langle j \rangle} \tag{34}$$

It must be noted that this formulation calculates the energy weights in terms of power-paths and not energy types. For instance, if JP-8 is used for both a conventional jet engine and a fuel cell system that powers electric motors and propellers, then this system has two power-paths, and the required fuel weight for each of the two power-paths is estimated separately.

As new energy sources start to be utilized, hybrid propulsion systems and/or a combination of different types of propulsion systems that utilize multiple energy sources, may power future aircraft. Each of the power devices and their associated energy sources have different characteristics in terms of specific power and specific

energy. To reduce the weight of an aircraft, higher specific power and specific energy are always desired, but nature does not allow both in one source, as depicted in Figure 26. In general, higher specific energy may be favorable for range and endurance capability and higher specific power may be favorable for maneuvering capability. When multiple choices are available, designers may want to optimize the propulsion system architecture by properly mixing different types of power devices and energy sources. For instance, in the case of sizing an aircraft that is required to perform high-power demanding maneuvers for short periods during its mission, combining a high energy efficient primary power system with a booster would be a better approach than sizing the entire propulsion system with one combination of a power device and an energy source as demonstrated in previous research [83, 117][2]. However, the decision must be made based on a balanced consideration of the impact on producibility, reliability, and maintainability due to increased system complexity as well as cost.

The consideration of heterogeneous propulsion systems fueled by single or multiple energy source(s) entails a further modification of the generalized propulsion system model presented in §3.4.1.1. A mathematical representation for multiple power or energy sources can be developed by introducing the concept of *power-path*. A power-path is defined as a set of power devices along which a series of energy conversion processes take place. If a vehicle is powered by n_T different power-paths, each consisting of multiple energy sources and energy transformation devices (ETD) as depicted in Figure 27, the power available to the aircraft is given as the sum of the power from all individual power-paths.

$$P = \sum_{i=1}^{n_T} P^{\langle i \rangle} \tag{35}$$

[2]A similar concept for a hybrid propulsion system has been also premeditated for Boeing's Fuel Cell Demonstrator Airplane. According to Boeing [127], the aircraft will be powered by a hybrid fuel cell/battery propulsion system that combines lithium-ion batteries as a secondary power system with a PEMFC as a primary power source. The PEMFC system is sized to provide sufficient electrical power for level flight. For takeoff and climb, the batteries cut in to supply an additional boost.

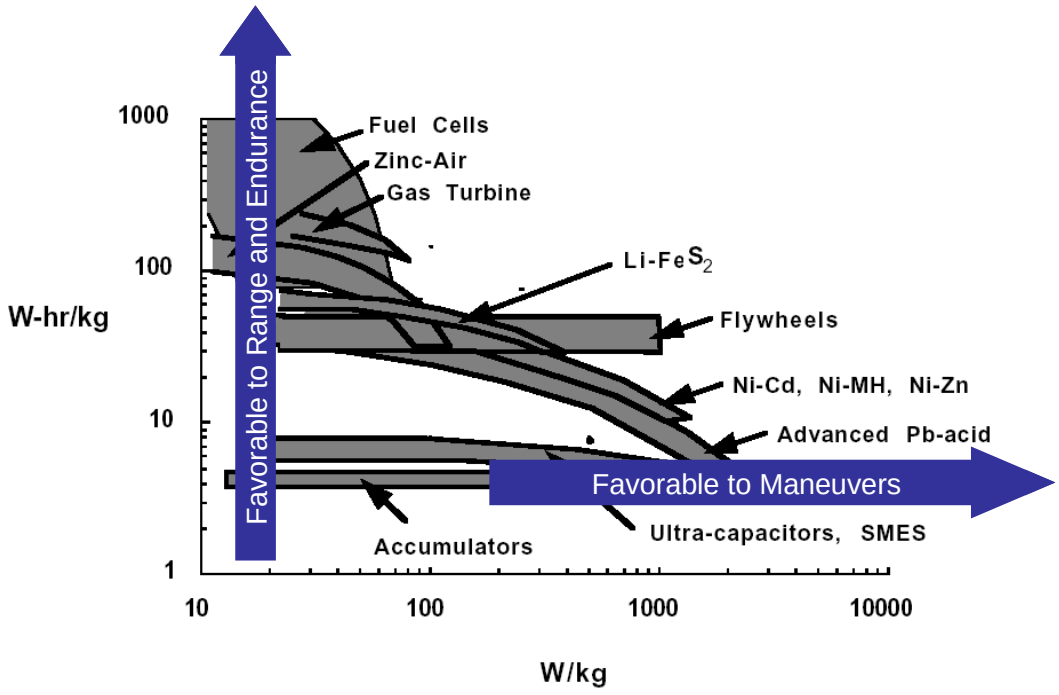

Figure 26: Comparison of specific energy and specific power for various power source technologies [128]

This expression can be modified by introducing a power fraction factor (τ) as follows:

$$P^{\langle i \rangle} = \tau^{\langle i \rangle} P \tag{36}$$

where,

$$\sum_{i=1}^{n_T} \tau^{\langle i \rangle} = 1, \ and \ \tau^{\langle i \rangle} > 0 \tag{37}$$

The first power input from the original energy source, $P_o^{\langle i \rangle}$, is eventually converted to the final propulsive power through multiple energy transformation processes. The final output power is given as the product of the efficiencies and $P_o^{\langle i \rangle}$ to account for the losses associated with each transformation/conversion.

$$P^{\langle i \rangle} = \Pi_\eta^{\langle i \rangle} P_o^{\langle i \rangle} \tag{38}$$

where $\Pi_\eta^{\langle i \rangle}$ represents the overall efficiency of the i^{th} power-path that is computed by the product of all efficiencies associated with the energy conversions.

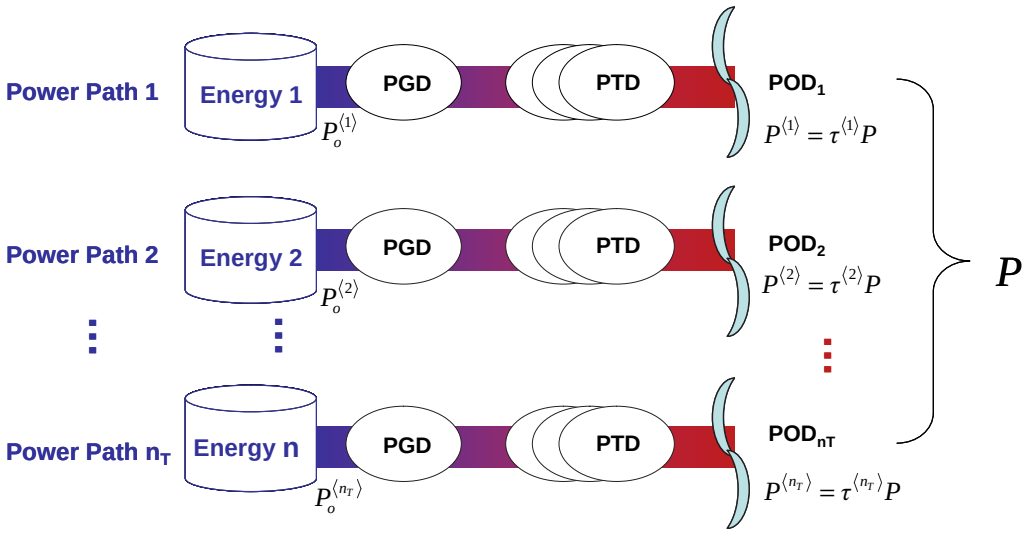

Figure 27: Multiple power-paths

3.4.1.3 Generalized Mission Analysis

In addition to the generalized conceptualization of fuel, a more generalized weight decomposition and weight differential equations are required to account for the impact of using of alternative energy sources. A more generalized weight decomposition has been developed as follows:

$$W = W_E + W_{PL} + W_{CE} + W_R \tag{39}$$

where W_R is the weight of the retained by-products from energy conversion. The non-consumable energy weight is included in the empty weight. Taking the derivative of Eq. (39) with respect to time produces the time rate of change in aircraft weight as

$$\dot{W} = \dot{W}_{CE} + \dot{W}_R \tag{40}$$

By assuming that the weight of the retained products is proportional to fuel consumption,

$$\dot{W}_R = -\mu \dot{W}_{CE} \tag{41}$$

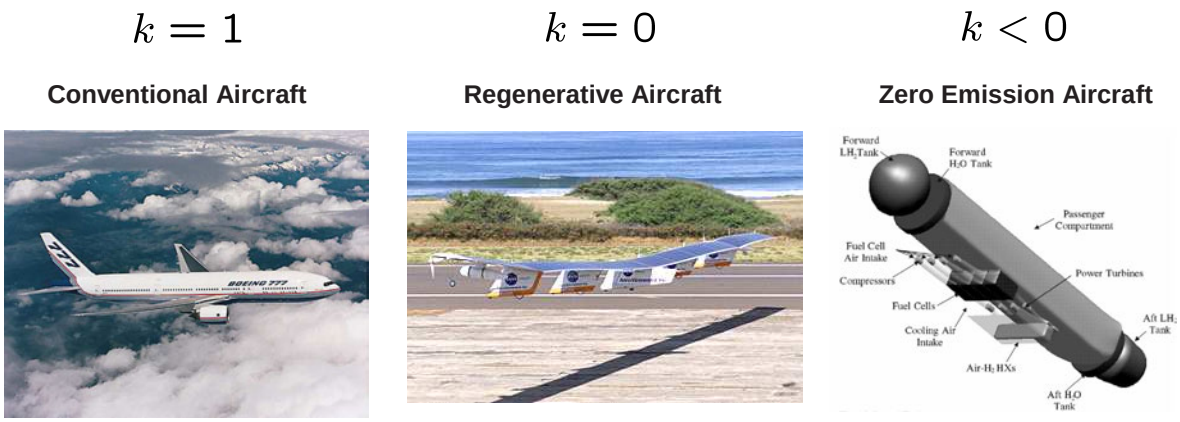

Figure 28: Typical k values, from left Boeing 777 [129], Helios [6], and Emissionless aircraft [119]

where μ is the retained-product-to-fuel ratio. Substituting Eq. (41) into Eq. (40) yields

$$\dot{W} = (1 - \mu)\dot{W}_{CE} \tag{42}$$

By introducing a constant k, the relationship between the time rate of change in the aircraft weight and the time rate of change in the consumable energy weight is given as

$$\dot{W} = k\dot{W}_{CE} \tag{43}$$

where

$$k = 1 - \mu \tag{44}$$

The value of k is determined by the characteristics of the given energy conversion process. Several typical k values are illustrated in Figure 28. In the case of traditional IC engines, k numerically equal one. If an aircraft is equipped with a regenerative fuel cell system as envisioned for the Helios[3], the aircraft's weight does not vary with fuel consumption, resulting in $k = 0$. In the case of a zero-emissions aircraft that

[3]The fuel cell systems designed for the Helios were of two types: regenerative and non-regenerative. However, the Helios never flew on a fuel cell propulsion system. The value of k would be zero if the former were equipped.

breathes external oxygen to burn hydrogen and store water on-board [26], the aircraft weight will grow as fuel burns, and thus, k is a negative number. If the aircraft is powered by multiple power-paths, k is given as

$$k = \sum_{i=1}^{n_{CE}} \frac{1 - \mu^{\langle i \rangle}}{\sum_{ii=1}^{n_{CE}} \frac{\tau^{\langle ii \rangle} \nu_{CE}^{\langle i \rangle} \Pi_{\eta}^{\langle i \rangle}}{\tau^{\langle i \rangle} \nu_{CE}^{\langle ii \rangle} \Pi_{\eta}^{\langle ii \rangle}}} \tag{45}$$

3.4.2 Mathematical Representation of Hypothesis 2

The key idea behind the second hypothesis is that the feasibility of the probabilistic constraints can be determined by the probability of meeting the constraints. For example, consider a probabilistic constraint, $g(\mathbf{x}, \boldsymbol{\xi}) > 0$, where $\mathbf{x}$ is a vector of decision variables and $\boldsymbol{\xi}$ is a vector of random parameters. Then, the design represented by $\mathbf{x}$ is considered to be located in a feasible region if and only if $\mathbb{P}[g(\mathbf{x}, \boldsymbol{\xi}) > 0] \geq \alpha$, where α is the target probability of meeting the constraints that is determined by management decisions. This implementation allows a means to determine the feasibility of the probabilistic constraints. Therefore, the aboriginal statement for the probabilistic sizing problem, given as Eq. (1), can be rewritten as follows:

$$\begin{aligned} \min_{\mathbf{x}} \quad & \tilde{f} \\ \text{s.t.} \quad & \mathbb{P}\left[\tilde{P}_{available} \geq \tilde{P}_{required}\right] \geq \alpha \\ & \mathbb{P}\left[\tilde{E}_{available} \geq \tilde{E}_{required}\right] \geq \alpha \end{aligned} \tag{46}$$

This equation mathematically formulates an aircraft sizing problem into an optimization problem whose goal is to minimize the objective function values subject to multivariate, nonlinear, individual or joint probabilistic constraints. In this context, the three design variables, power, wing area, and fuel (energy) quantity, are manipulated until all probabilistic constraints are satisfied with equal or higher probabilities than the target.

CHAPTER IV

FORMULATION OF THE ARCHITECTURE-INDEPENDENT AIRCRAFT SIZING METHOD

Research Question I described in Chapter III is seeking a generalized aircraft sizing formulation that is independent of the energy-propulsion system architecture of an aircraft. A fledging attempt to answer this question produced Hypothesis I, which includes the conceptual idea of the formulation. Building upon the substantiation of Hypothesis I presented in §3.4, this chapter presents the formulation of the Architecture-Independent Aircraft Sizing Method (AIASM) proposed as a solution to Research Question I.

The AIASM includes three parts: generalized constraint analysis, generalized mission analysis, and generalized weight estimation. The first section of this chapter presents the formulation of generalized constraint analysis. §4.2 introduces a set of generalized Breguet range equations. The equations are not only useful by themselves in quick estimations of range capability, but also provide a basis for facilitating the development of the more comprehensive generalized mission analysis presented in the following section. §4.4 discusses a more generalized weight estimation method. Based upon the mathematical formulations of the major three components, §4.5 describes the overall implementation process of AIASM. The rest of this chapter discusses a couple of extended topics. §4.6 presents a graphical tool that is able to compare the mission capability of multiple energy-propulsion system architectures in a unified visual environment. The last section presents an additional formulation required for the sizing of solar powered aircraft.

4.1 Generalized Constraint Analysis

Sharing the crux of Mattingly's constraint analysis method presented in §2.2.3, the generalized constraint analysis method is formulated upon the concept of generalized propulsion system modeling presented in §3.4.1. The most notable difference is that the new method establishes the static or dynamic equilibrium of motion for an aircraft in terms of *power* in lieu of *thrust*. The compelling reason for using power is that it is a more universal metric to represent the size of most emerging propulsion systems using alternative energy sources. In addition, power is a more convenient means by which hybrid propulsion system architectures are properly handled.

Formulation starts with the most simple case characterized by a single power-path propulsion system and a fixed external configuration, for which performance constraints can be visualized in a single design space comprised of power-to-weight ratio[1] and wing loading. Once the formulation for the simplest case is constructed, it is extended to more complicated cases with multiple power-paths and/or morphing configurations, leading to a multi-dimensional constraint analysis in a matrix form.

4.1.1 Formulation of a Single Constraint Analysis

Power balance states that the available power must be greater than or equal the required power, $P_{ava} \geq P_{req}$. The required power-to-weight ratio can be derived from Eq. (9) as follows:

$$\frac{P_{req}}{W_{TO}} = \beta \left\{ \frac{qS}{\beta W_{TO}} \left[K_1 \left(\frac{n\beta}{q} \frac{W_{TO}}{S} \right)^2 + K_2 \left(\frac{n\beta}{q} \frac{W_{TO}}{S} \right) + C_{D_o} + \frac{R}{qS} \right] + \frac{1}{V} \frac{d}{dt} \left(h + \frac{V^2}{2g_o} \right) \right\} V \qquad (47)$$

In general, the available power of a propulsion system varies depending on flight conditions (e.g. altitude, velocity, side slip) and power settings. Therefore, in order to size the propulsion system, we must have an invariant reference of the amount of power that represents the scale of a "rubberized" propulsion system. As such a reference,

[1] This term is often considered interchangeable with *power loading*. However, having an opposite connotation from power-to-weight ratio, *power loading* means the weight of the aircraft divided by engine power.

traditional methods often use the amount of maximum thrust and shaft power at the sea level static condition, for jet airplanes and propeller airplanes, respectively.

The choice of such a reference generally involves three decisions: a reference power device along the power-path; a reference operating condition; and a reference flight condition. The propulsive power used in Eq. (47) may not necessarily be the best choice for a metric that establishes power balance for most alternative propulsion systems. Particularly when the reference flight condition is set at a static condition ($V = 0$), the use of propulsive power as a reference immediately yields the conspicuous problem of the propulsive power always being zero, which makes the use of the propulsive power at a static condition impractical. Furthermore, the scale of the propulsion system may be better represented by the amount of power at a specific stage amid the energy conversion process rather than the output power at the final stage (the propulsive power). Therefore, the reference power must be carefully selected considering various aspects including characteristics of the propulsion system architecture and the availability of data. If an aircraft sizing process is conducted with a dedicated propulsion system analysis tool integrated with an aircraft sizing code, the choice of the sizing reference power is very likely to be "on-design" point of the propulsion system analysis.

If the k^{th} power device in Figure 29 is selected as the reference power device, then the available propulsive power is given as $P_{ava} = \Pi_{\eta}^{+} P_k$, where Π_{η}^{+} represents the product of efficiencies associated with the energy conversions following the stage of reference power, that is, $\prod_{k+1 \to n}(\eta)$. Note that P_k varies depending on flight conditions, which can be accounted for by introducing the power lapse ratio (α) that relates P_k to a reference power, denoted as P_{ref}, as follows:

$$P_k = \alpha P_{ref} \tag{48}$$

The value of P_k equals that of P_{ref} at an "on-design" point specified with engine-operating parameters, leading to $\alpha = 1$. For the aircraft propelled by a power-path,

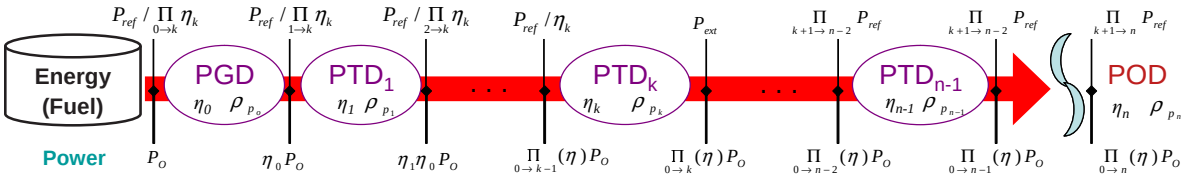

Figure 29: Reference Power in a power-path

the relationship between the reference power and the propulsive power is given as

$$P_{ava} = \alpha \Pi_{\eta}^{+} P_{ref} \tag{49}$$

For example, in the case of a propeller aircraft, if one chooses P_{ref} to be the maximum shaft power at the sea level static condition, then Π_{η}^{+} would be efficiency of the propeller, and α accounts for the variation of shaft power with mach number, altitude, and engine power settings.

By combining Eq. (47) and Eq. (49), the equation of power balance is written as

$$\frac{P_{ref}}{W_{TO}} \geq \frac{\beta}{\Pi_{\eta}^{+}\alpha}\left\{\frac{qS}{\beta W_{TO}}\left[K_1\left(\frac{n\beta}{q}\frac{W_{TO}}{S}\right)^2 + K_2\left(\frac{n\beta}{q}\frac{W_{TO}}{S}\right) + C_{D_o} + \frac{R}{qS}\right] + \frac{1}{V}\frac{d}{dt}\left(h + \frac{V^2}{2g_o}\right)\right\} V \tag{50}$$

This equation is a *power-based master constraint equation*, equivalent to Mattingly's "master equation" (Eq. (11) presented in §2.2). The equation defines the required reference power (P_{req}) in terms of aerodynamic coefficients, wing loading, rate of energy height, and other parameters. If the appropriate assumptions for each performance requirement are applied to this master equation, a corresponding constraint equation can be derived in a reduced form. A set of such tailored equations is included in Appendix A.

The weight fraction values (β) for mission segments are not available at this moment. Therefore, these values must be assumed reasonably for this analysis and should be updated by the mission analysis, if necessary. Once the constraint equations are developed, the feasible solution area can be graphically identified as bound by associated constraint curves.

4.1.2 Constraint Analysis Matrix

If the aircraft is powered by hybrid propulsion systems encapsulated by multiple power-paths, power balance must be considered for each power-path. The power constraint equation for multiple power-paths can be obtained by combining Eq. (50) with Eq. (36) as follows:

$$\frac{P_{ref}^{\langle i \rangle}}{W_{TO}} = \frac{\tau^{\langle i \rangle}\beta}{\Pi_{\eta}^{+\langle i \rangle}\alpha^{\langle i \rangle}} \left\{ \frac{qS}{\beta W_{TO}} \left[K_1 \left(\frac{n\beta}{q}\frac{W_{TO}}{S} \right)^2 + K_2 \left(\frac{n\beta}{q}\frac{W_{TO}}{S} \right) + C_{D_o} + \frac{R}{qS} \right] + \frac{1}{V}\frac{d}{dt}\left(h + \frac{V^2}{2g_o} \right) \right\} V \quad (51)$$

where $\tau^{\langle i \rangle}$ is a power fraction factor for i^{th} power-path. Multiple power-paths create the same number of constraint analysis domains, so the design point selection process becomes more complicated. An example of the constraint analysis for a notional aircraft propelled by two power-paths is illustrated in Figure 30. The propulsion system consists of the primary power-path that provides power throughout the entire mission and the secondary power-path that provides ancillary power on take-off, during climb, on missed approaches, and in emergency situations. The design point of the primary power-path is selected at the location of the lowest power-to-weight ratio. Then, the design point of the secondary power-path must be determined at a location along the vertical line, a-a, because wing loading of the aircraft must be maintained through all the constraint analysis domains. If a different wing loading on line b-b is selected, the power-to-weight ratio of the primary power-path increases, while the power-to-weight ratio of the primary power-path decreases. Another possible trade-off is to change the power fractions ($\tau^{\langle 1 \rangle}$, $\tau^{\langle 2 \rangle}$) of the two power-paths. The constraint curves of both the primary power-path and the secondary power-path are functions of $\tau^{\langle 1 \rangle}$ and $\tau^{\langle 2 \rangle}$. As the value of $\tau^{\langle 2 \rangle}$ increases, the primary power-path is allowed to have a lower power-to-weight ratio. Therefore, the optimum values of power distributions and aircraft sizing parameters may be found by employing an optimization process.

In addition, the method can be extended for the sizing of a *morphing* configuration. *Morphing* means herein reshaping aircraft external configuration with an aid of fully integrated embedded "smart" materials and actuators to achieve higher aerodynamic

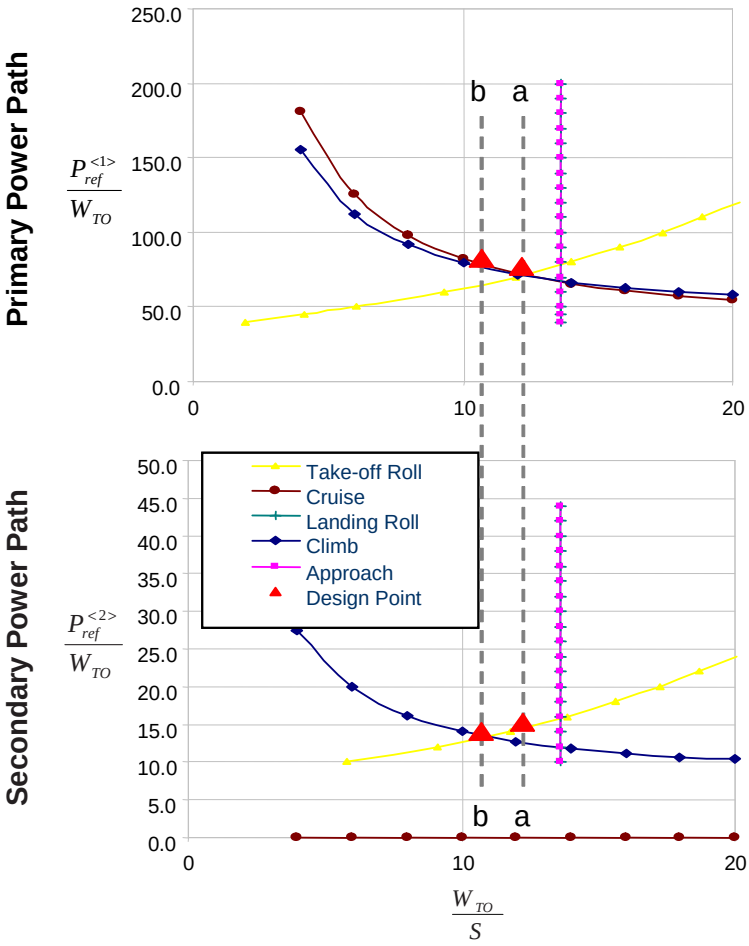

Figure 30: Design point selection of two power-paths

efficiency throughout most flight regions. An interesting aspect of morphing aircraft with regards to the constraint analysis is that multiple design values for wing loading may exist because the aircraft is able to vary wing area, as multiple design values for power-to-weight ratio should exist if an aircraft were powered by a hybrid propulsion system architecture. A constraint analysis as well as the comprehensive sizing practice of a morphing aircraft that reconfigure the wing to have two different values of wing area were demonstrated in Ref. [130].

Along with *aerodynamic morphing*, mission adjustability may benefit from *propulsion morphing*, which is built of a hybrid propulsion comprised of a high power sector

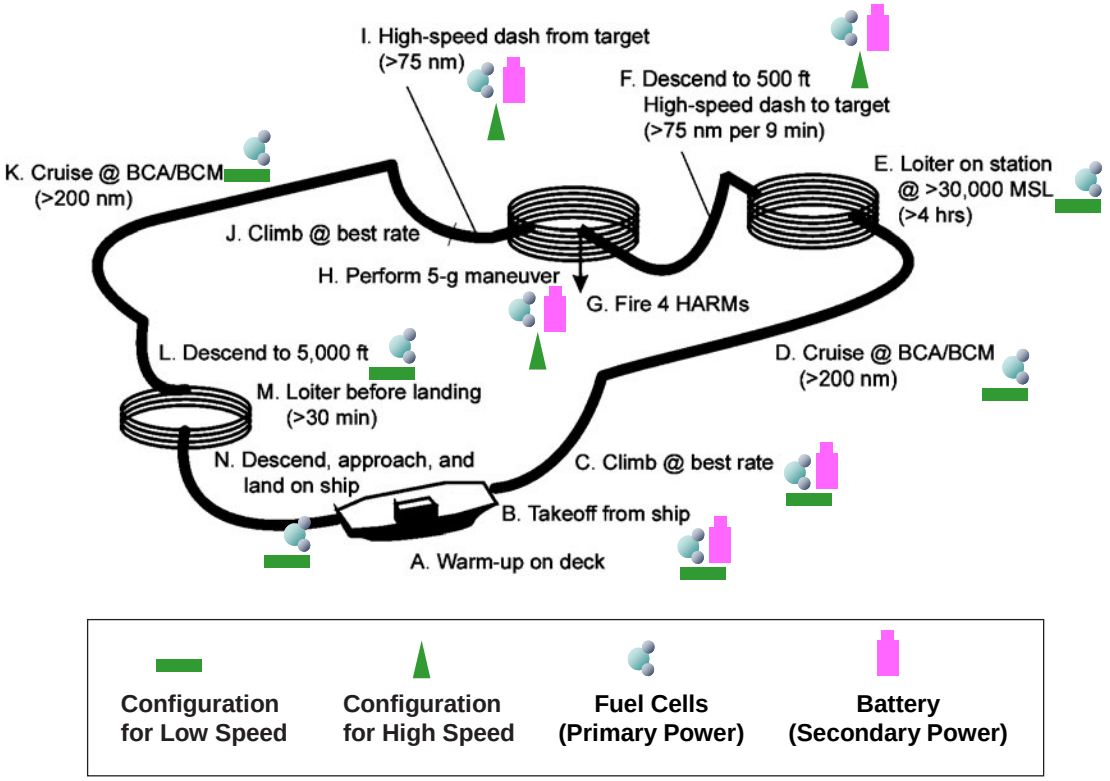

Figure 31: Approach to a notional UCAV design with a combination of *aerodynamic morphing* and *propulsion morphing*, (Source of the figure of mission profile: Ref. [130])

and a high energy sector. Figure 32 illustrates a notional extended constraint analysis setting for aircraft having a reconfigurable external configuration and propulsion system. The aircraft has two different configurations, each of which is preferred at low speed and high speed regions, respectively, and the propulsion system has two power-paths: fuel cells as a primary power and battery or super-capacitor as secondary power. Thus, the constraint analysis for the sizing of this morphing aircraft includes two power-to-weight ratio variables $(\frac{p_{ref}^{\langle 1 \rangle}}{W_{TO}}, \frac{p_{ref}^{\langle 2 \rangle}}{W_{TO}})$ as well as two wing loading variables $(\frac{W_{TO}}{S}^{\langle 1 \rangle}, \frac{W_{TO}}{S}^{\langle 2 \rangle})$, which create four combinatorial design spaces constrained by the following equation:

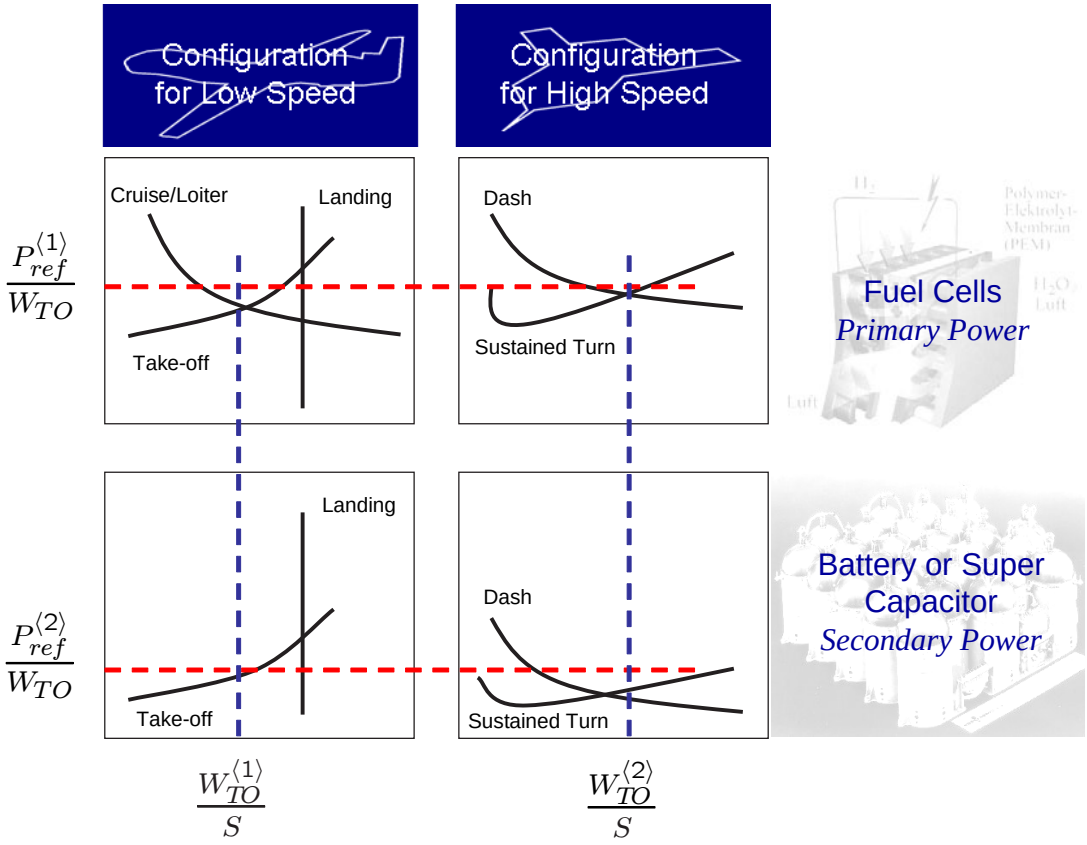

Figure 32: Notional constraint analysis setup for a morphing aircraft with hybrid power systems

$$\frac{p_{ref}^{\langle i\rangle}}{W_{TO}} = \frac{\tau^{\langle i\rangle}\beta}{\Pi_{\eta}^{+\langle i\rangle}\alpha^{\langle i\rangle}} \left\{ \frac{q}{\beta}\frac{S^{\langle j\rangle}}{W_{TO}} \left[K_1 \left(\frac{n\beta}{q}\frac{W_{TO}}{S}^{\langle j\rangle} \right)^2 + K_2 \left(\frac{n\beta}{q}\frac{W_{TO}}{S}^{\langle j\rangle} \right) + C_{D_o} + \frac{R}{qS} \right] + \frac{1}{V}\frac{d}{dt}\left(h + \frac{V^2}{2g_o} \right) \right\} V \tag{52}$$

Therefore, the constraint analysis is given in the form of a two-by-two matrix as depicted in Figure 32. It must be noted that in such a matrix, the values of wing loading must be the same along the column, and power-to-weight ratios must be the same along the row. The constraint curves vary due to the change in the power fractions of the two power-paths as well as aerodynamic characteristics of two configurations. Thus, an extended version of the optimization problem in which the power fractions and configuration are included as additional design variables is of interest.

4.2 Generalized Breguet Range Equations

The Breguet range equation is useful for various design assessments, providing qualified estimates of the cruise performance of an aircraft with only a few pieces of information about the modeled aircraft. As mentioned in §2.4.1, the classical Breguet range equation, as it is, would not work on certain unconventionally-powered air-vehicles. This section presents a set of generalized Breguet range equations that are also applicable to such aircraft. As useful as the classical Breguet range equation is for a quick estimation of the range capability, the development of the generalized Breguet range equations provides the basis of the generalized mission analysis presented in §4.3.

Compared with the original single Breguet range equation, multiple equations are formulated because the tendencies of the variation in aircraft weight due to fuel consumption could differ depending not only on the type of energy source but also how an alternative energy-propulsion system architecture treats the by-products from its power generation. The derivations of the generalized equations are made separately for consumable energy sources and also for non-consumable energy sources.

4.2.1 Flight by Consumable Energy

When an aircraft equipped with a consumable energy source flies, the amount of consumed energy for an infinitesimal period of time, dt, is given as:

$$dE_{CE} = -P_o dt = -\frac{P}{\Pi_\eta} dt \tag{53}$$

The change in the amount of consumable energy is proportional to the change in the weight of the energy source(s),

$$dE_{CE} = \nu_{CE} dW_{CE} \tag{54}$$

where ν_{CE} is the specific energy of the fuel in the power-path.

Combining Eq. (54) with Eq. (53) yields

$$dW_{CE} = -\frac{P}{\nu_{CE}\Pi_\eta}dt \tag{55}$$

Eq. (55) can be restated with respect to the time rate of change in aircraft weight from Eq. (43) as follows:

$$dW = -k\frac{P}{\nu_{CE}\Pi_\eta}dt \tag{56}$$

or

$$\frac{dW}{W} = \frac{-k}{\nu_{CE}\Pi_\eta}\frac{D}{L}ds \tag{57}$$

If k is not zero, assuming the lift-to-drag ratio (L/D) and overall efficiency (Π_η) are constant during flight, the integration of Eq. (57) leads to the following equation:

$$R = \frac{\nu_{CE}\Pi_\eta}{k}\frac{L}{D}\ \ln\left(\frac{W_{initial}}{W_{final}}\right) \tag{58}$$

where $W_{initial}$ and W_{final} denotes the aircraft's weight at the beginning and the end of the mission, respectively. The ratio of the initial weight to the final weight in Eq. (58) is given as a function of k and $\frac{W_{CE}}{W_{TO}}$ as follows:

$$\frac{W_{final}}{W_{initial}} = 1 - k\frac{W_{CE}}{W_{TO}} \tag{59}$$

Finally, combining Eq. (58) and Eq. (59),

$$R = \frac{\nu_{CE}\Pi_\eta}{k}\frac{L}{D}\ \ln\left(\frac{1}{1-k\frac{W_{CE}}{W_{TO}}}\right) \tag{60}$$

If the aircraft's weight does not change with flight, which is the case of $k = 0$, Eq. (57) yields a trivial solution, $W = constant$. To avoid this, a different approach is taken by modifying Eq. (55) as follows:

$$\frac{dW_{CE}}{W} = \frac{-1}{\nu_{CE}\Pi_\eta}\frac{D}{L}ds \tag{61}$$

Note that W is constant in the above equation, thus the equation can be solved by direct integration, leading to the following equation:

$$R = \nu_{CE}\Pi_\eta\frac{L}{D}\frac{W_{CE}}{W_{TO}} \tag{62}$$

This equation can also be derived from Eq. (60). As k approaches 0, $\ln\left(\frac{1}{1-k\frac{W_{CE}}{W_{TO}}}\right)$ is asymptotically approximated as $k\frac{W_{CE}}{W_{TO}}$ and Eq. (60) reduces to Eq. (62)

4.2.2 Flight by Non-consumable Energy

An aircraft powered by non-consumable energy would maintain the same weight throughout the mission unless it drops a payload. Therefore, the range equation can be developed by the same process applied to consumable energy with $k = 0$:

$$R = \nu_{NE}\Pi_{\eta}\frac{L}{D}\frac{W_{NE}}{W_{TO}} \tag{63}$$

4.2.3 Example Application to Zero-emissions Aircraft

The range of a notional aircraft powered by hydrogen fuel is computed using the generalized range equations. In the order of L/D, ν_{CE}, and Π_{η}, their numerical values are 15, 44.6×10^6 lbs ft/sec/lbs, and 0.3. Figure 33 illustrates the ratio of final to initial weight computed by Eq. (59). The case of $k = 0$ maintains the same weight, so the ratio is 1 for all consumable energy weight fractions. In the case of a positive k, as the consumable energy weight gets reduced, the aircraft weight also reduces. As the value for k increases, the rate of change in aircraft weight also increases, which leads to a further reduction in final aircraft weight. In contrast, in the case of a negative k, the aircraft weight increases with fuel burn, leading to a final weight greater than what the vehicle started with in the beginning.

Figure 34 plots the range versus consumable energy weight fraction for different values of k. It can be seen that as the consumable energy weight fraction increases, the range increases. In the case of $k = 0$, range is linearly related to energy weight fraction. As the numerical value of k grows, range increases more rapidly per consumable energy weight fraction, and exhibits a non-linear relationship.

Figure 35 shows how range, normalized by values at $k = 1$, varies with consumable energy weight fraction for different k values. The penalty of accumulating the weight

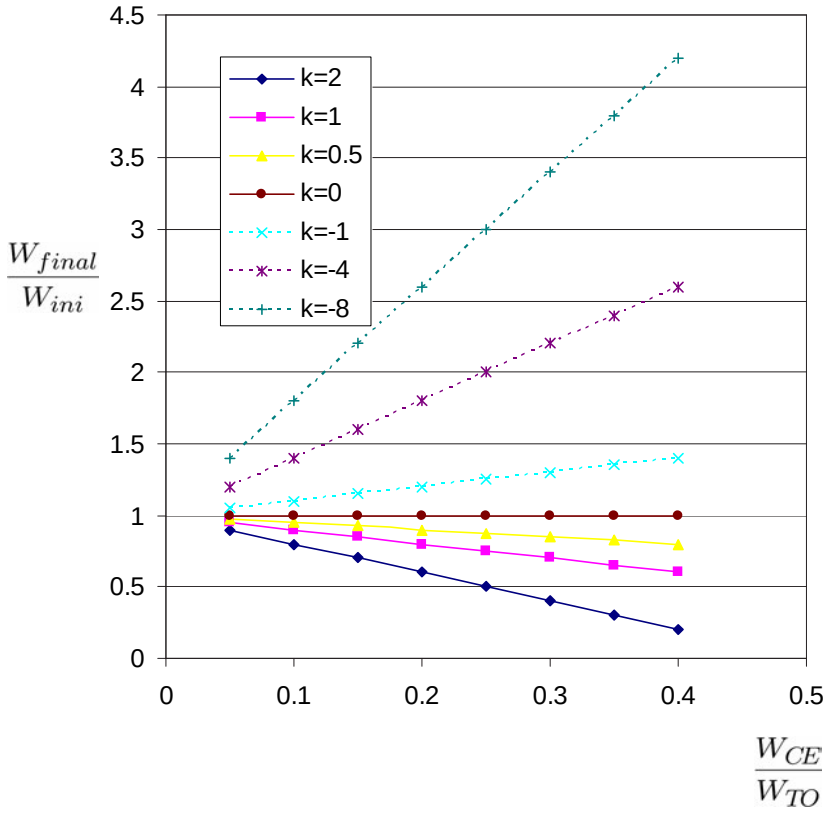

Figure 33: The ratio of final to initial vehicle weight vs. fuel fraction

of by-products grows as the fuel fraction increases, which means that the penalty associated with the accrued reaction product weight becomes more severe in longer-range aircraft.

The case where $k = -8$ is interesting because it is the case of a "zero emissions" aircraft that uses ambient air to oxidize hydrogen fuel and retains all by-products, essentially water, on-board. For an energy weight fraction of 0.1, the range at $k = -8$ is 70% of that of $k = 1$. Since the same aerodynamic efficiency and propulsion system efficiency are applied to this analysis, such a considerable difference is caused by the difference in the treatment of the by-products of the energy generating process. Therefore, in order to offset this penalty, significant improvements in the aerodynamics, structures, and propulsion technologies must be made for a viable development

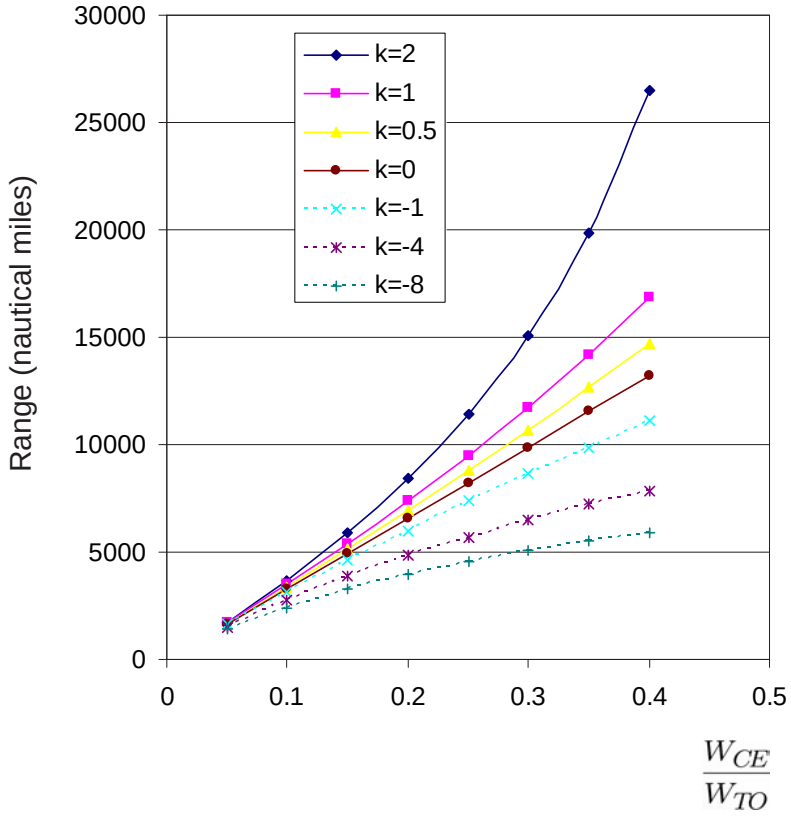

Figure 34: Range vs. fuel fraction

of a truly "zero emissions" aircraft.

For verification of the generalized Breguet range equations derived in this section, the equations are applied to the performance analysis of a 300-passenger, LH_2-fueled zero-emissions aircraft, whose mission range data are available in a study [119] performed by MSE Technology Applications, Inc. and NASA LaRC. The aircraft is propelled by electric ducted fan engines powered by a PSOFC (Planar Solid Oxide Fuel Cell) system. The fuel cells are operated on liquid hydrogen fuel, which is oxidized by ambient air induced by inlet ducts. The primary product of the electrochemical reaction is water vapor, which is stored in two spherical water tanks located in the front and back of the cabin.

The original study investigated the feasibility of the zero-emissions aircraft via two

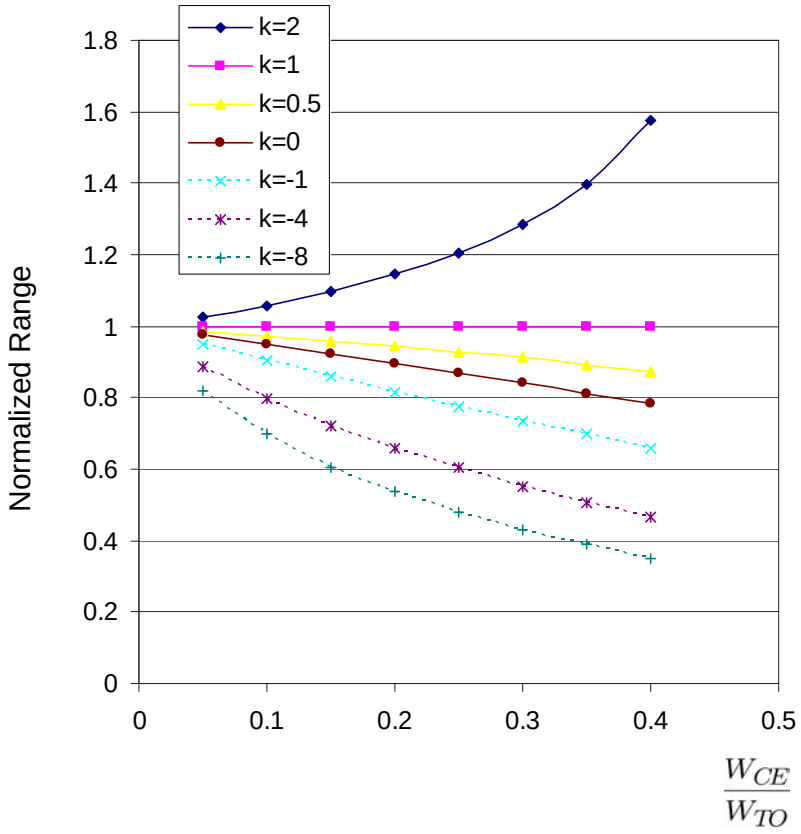

Figure 35: Normalized range vs. fuel fraction

sets of assumptions: a "Near-Term" (NT) scenario and a "Long-Term" (LT) scenario that describe the relevant assumptions regarding the aerodynamic parameters as well as the technologies related to the propulsion system, which include PSOFC electrochemical efficiency, PSOFC power density, propulsion fan efficiency, and percentage laminar flow. The NT scenario assumes electrochemical efficiency at cruise, motor efficiency, and fan efficiency at cruise 50%, 99%, and 85%, respectively, which yields an overall efficiency of 42.1%. In the LT scenario, the electrochemical efficiency at cruise and fan efficiency are raised to 60% and 87%, respectively. In addition, each scenario includes a technology adjustment parameter, named "Weight Reduction Factor," (WRF) that simulates possible levels of airframe weight reduction by the application of advanced materials.

The study analyzes the range performance of the zero emissions aircraft with a customized version of FLOPS modified by NASA LaRC, to account for the gaining of aircraft weight due to the storage of water. Table 3 lists a portion of their analysis results relevant to this study. Based on the information in Table 3, the input parameters of the generalized Breguet range equations were prepared. Overall efficiencies were computed by multiplying the electrochemical efficiency at cruise, motor efficiency, and fan efficiency at cruise. Fuel fraction was computed by dividing the amount of used fuel by take-off gross weight. The values of L/D were given as an average of the lower limit and the upper limit of the L/D ranges listed in Table 3. The value of k is given as 7.94 per the original study. With these parameters, the mission range was computed by the Generalized Breguet range equations. Table 4 lists the parameters and the results of this analysis.

The results of the generalized Breguet range equations are compared with the published results in Figure 36 that show the generalized Breguet range equations estimate the range of zero-emissions aircraft with fairly good accuracy. Except for a single case (the NT scenario with WRF=1), the range estimated by the generalized Breguet range equations is less than the results of FLOPS. The difference grows as the range increases, hence the maximum difference is found at 9.2% where the LT scenario is applied with WRF=3. These discrepancies are caused by several sources. The first is that the generalized Breguet range equation computes the range without considering non-cruise segments such as take-off, climb, and descent. Another source for the difference in the results is associated with an assumption of the generalized Breguet range equations: the overall efficiency of the propulsion system, lift-to-drag ratio are constant throughout the whole mission. Lastly in Alexander's study, the aircraft is allowed to dump out the water from takeoff up to 25,000 feet, because water emission would not be detrimental below that altitude. Such a procedure may either increase the range or reduce the aircraft weight. However, the generalized

Table 3: FLOPS analysis results of zero-emissions aircraft obtained by MSE and NASA LaRC [119]

Near Term Scenario

WRF	1	1.5	2	2.5	3
Wini(lbs.)	511,045	441,320	402,588	377,589	361,239
Wfinal(lbs.)	609,680	601,222	596,185	592,759	590,444
Wfuel(lbs.)	22,718	30,715	35,186	38,088	39,997
Unconsumed fuel(%)	25.50	22.30	21.30	20.80	20.50
Used fuel (lbs.)	16,925	23,866	27,691	30,166	31,798
Electrochemical efficiency(%)	50	50	50	50	50
Motor efficiency(%)	60	60	60	60	60
Fan efficiency(%)	99	99	99	99	99
L/D	24.3 - 24.7	23.3 - 24.5	22.8 - 24.4	22.4 - 24.5	21.9 - 24.5
Range(nmi)	2252	3599	4431	5019	5400

Long Term Scenario

WRF	1	1.5	2	2.5	3
Wini (lbs.)	447,979	372,101	333,251	308,993	292,678
Wfinal (lbs.)	610,414	600,330	595,002	591,460	589,003
Wfuel (lbs.)	28,973	38,093	42,731	45,634	47,592
Unconsumed fuel(%)	19.70	18.30	17.90	17.70	17.60
Used fuel (lbs.)	23,265	31,122	35,082	37,557	39,216
Electrochemical efficiency(%)	50	50	50	50	50
Motor efficiency(%)	60	60	60	60	60
Fan efficiency(%)	99	99	99	99	99
L/D	26.6 - 27.4	25.7 - 27.2	24.3 - 27.3	23.1 - 27.3	22.1 - 27.2
Range(nmi)	4834	7178	8547	9402	9975

Table 4: Input parameters and results of the generalized Range Equations of zero-emissions aircraft

Near Term Scenario					
WRF	1	1.5	2	2.5	3
Wce/Wto	0.033	0.054	0.069	0.080	0.088
overall efficiency	0.421	0.421	0.421	0.421	0.421
Average L/D	24.5	23.9	23.6	23.45	23.2
Range	2362	3526	4247	4757	5077
% difference	4.9	-2.0	-4.2	-5.2	-6.0

Long Term Scenario					
WRF	1	1.5	2	2.5	3
Wce/Wto	0.052	0.084	0.105	0.122	0.134
overall efficiency	0.517	0.517	0.517	0.517	0.517
Average L/D	27.0	26.5	25.8	25.2	24.7
Range	4728	6832	7949	8634	9059
% difference	-2.2	-4.8	-7.0	-8.2	-9.2

Breguet range equations are not able to capture such a detail. This example study concludes that a makeshift useful for estimations of the mission range with only handful information about the aircraft, the generalized Breguet range equations may produce considerable errors due to the assumptions associated with their development. These shortcomings will be overcome by the generalized mission analysis formulation that will be presented in the following section.

4.3 Generalized Mission Analysis

Unlike the generalized Breguet range equations, the generalized mission analysis method accounts for a variation in the propulsion system efficiency and aerodynamic parameters during the flight. In addition, the method provides proper equations for non-zero excess power conditions such as take-off, climb, acceleration, sustained turn, descent, and landing that had not been considered in the generalized Breguet range equations. Furthermore, the method is immediately applicable to hybrid propulsion

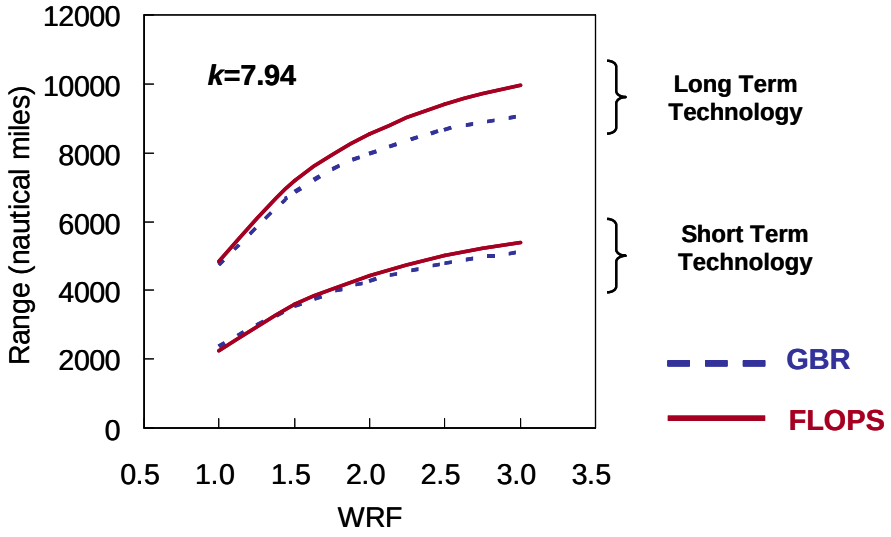

Figure 36: Range vs. WRF by a modified FLOPS and the generalized Breguet range (GBR) equations

system architectures.

The fundamental approach of the proposed method is similar to that of the traditional method. The mission profile is chopped into small legs, which allows us to assume that several parameters, such as the aerodynamic coefficients and the overall efficiencies of power-paths, are constant in each leg and simplify the associated equations a great deal compromising the analysis accuracy as little as possible. For each leg, the weight fraction or the amount of both consumable energy and non-consumable energy is calculated. By summing up the results, the amount of energy required to perform an entire mission can be estimated.

For the purpose of generality, the propulsion system is assumed to comprise multiple power-paths that use both consumable energy sources and non-consumable energy sources. The value of "k" is allowed to vary across the legs. The weight of the aircraft may or may not stay the same for a certain leg, while other parameters are set to their representative values in each leg. Accounting for the variation of aircraft weight due

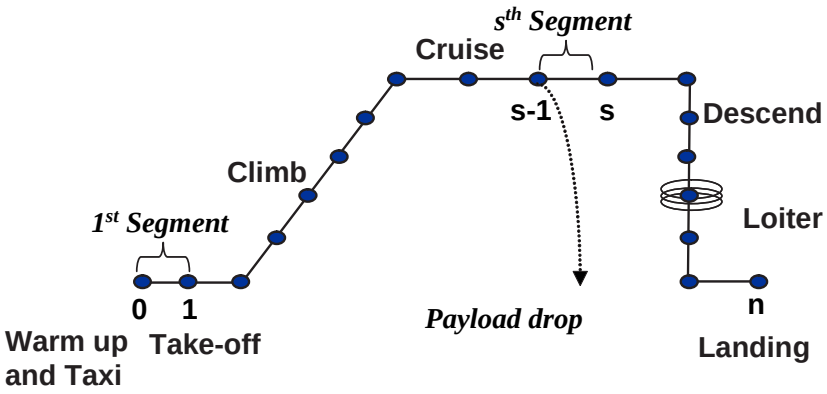

Figure 37: Discretized mission profile

to energy consumption in each leg, ensuing a considerable degree of complication in the mathematical formulation of the mission analysis, is found significantly to reduce the numerical error, which is discussed in the last part of this section.

4.3.1 Consumable Energy Sizing

Consumed energy is power multiplied by time:

$$dE_{CE}^{\langle i \rangle} = -p_o^{\langle i \rangle} dt = -\frac{\tau^{\langle i \rangle} P}{\Pi_\eta^{\langle i \rangle}} dt \tag{64}$$

The change in the amount of consumable energy is proportional to the change in the weight of energy sources.

$$dE_{CE}^{\langle i \rangle} = \nu_{CE}^{\langle i \rangle} dW_{CE}^{\langle i \rangle} \tag{65}$$

Combining Eq. (64) and Eq. (65) yields

$$dW_{CE}^{\langle i \rangle} = -\frac{\tau^{\langle i \rangle} P}{\nu_{CE}^{\langle i \rangle} \Pi_\eta^{\langle i \rangle}} dt \tag{66}$$

As mentioned before, two types of energy are being considered. The ways of calculating the amount of consumable energy differ, depending on how aircraft weight varies.

4.3.1.1 Variable Aircraft Weight ($k \neq 0$)

If aircraft weight changes in the mission leg, the amount of consumable energy consumed in the mission leg can be calculated based on the generalized weight differential equation presented in 3.4.1.3. Substituting Eq. (66) into Eq. (43) yields

$$\frac{dW}{W} = -\sum_{i=1}^{n_{CE}} \frac{k\tau^{\langle i \rangle}}{\nu_{CE}^{\langle i \rangle}\Pi_{\eta}^{\langle i \rangle}} \left(\frac{P}{W}\right) dt \tag{67}$$

By solving Eq. (67) for the s^{th} leg, the weight fraction of the leg obtained is

$$\frac{W^{(s)}}{W^{(s-1)}} = \exp\left(-\int_{t^{(s-1)}}^{t^{(s)}} \left(\sum_{i=1}^{n_{CE}} \frac{k\tau^{\langle i \rangle}}{\nu_{CE}^{\langle i \rangle}\Pi_{\eta}^{\langle i \rangle}} \left(\frac{P}{W}\right)\right) dt\right) \tag{68}$$

If the fragmented mission legs are small enough such that $k\tau^{\langle i \rangle}/\nu_{CE^{\langle i \rangle}}\Pi_{\eta}^{\langle i \rangle}$ can be assumed to be constant, then the above equations can be approximated as follows:

$$\frac{W^{(s)}}{W^{(s-1)}} = \exp\left(-k^{(s)}\Upsilon^{(s)}\Xi_{CE}^{(s)}\right) \tag{69}$$

where $\Upsilon^{(s)}$ is the weight specific mechanical energy, which is given as

$$\Upsilon^{(s)} = \int_{t^{(s-1)}}^{t^{(s)}} \left(\frac{P}{W}\right) dt \tag{70}$$

and $\Xi_{CE}^{(s)}$ is the overall power specific fuel consumption (OPSFC), which is equivalent to the power-specific fuel consumption (PSFC) of conventional combustion engines and given as

$$\Xi_{CE}^{(s)} = \sum_{i=1}^{n_{CE}} \frac{\tau^{\langle i \rangle}}{\nu_{CE}^{\langle i \rangle}\Pi_{\eta}^{\langle i \rangle}} \tag{71}$$

The ways of computing $\Upsilon^{(s)}$ differ, depending on the existence of excess power. In the case of positive excess power,

$$\frac{P}{W}dt = \frac{d(h + V^2/2g_o)}{1-u} = \frac{dz_e}{1-u} \tag{72}$$

where

$$u = \frac{D+R}{T} = nV\left(\frac{C_D + C_{DR}}{C_L}\right) / \sum_{i=1}^{n_T} \frac{\Pi_{\eta}^{+\langle i \rangle}\alpha^{\langle i \rangle}}{\beta} \frac{P_{ref}^{\langle i \rangle}}{W_{TO}} \tag{73}$$

Therefore, Eq. (70) can be rewritten as

$$\Upsilon^{(s)} = \int_{z_e^{(s-1)}}^{z_e^{(s)}} \frac{dz_e}{1-u} \simeq \frac{\Delta z_e^{(s)}}{1-u} \tag{74}$$

In the case of zero excess power, such that during cruise or a sustained turn, required power equals the total drag multiplied by free-stream velocity as follows:

$$\frac{P}{W}dt = \left(\frac{D+R}{W}\right) V dt \tag{75}$$

or

$$\frac{P}{W}dt = \left(\frac{D+R}{W}\right) ds \tag{76}$$

Therefore, Eq. (70) can be rewritten as

$$\Upsilon^{(s)} = \int_{t^{(s-1)}}^{t^{(s)}} \left(\frac{D+R}{W}\right) V dt \simeq \left(\frac{C_D + C_{DR}}{C_L}\right) V \Delta t \tag{77}$$

or

$$\Upsilon^{(s)} = \int_{s^{(s-1)}}^{s^{(s)}} \left(\frac{D+R}{W}\right) ds \simeq \left(\frac{C_D + C_{DR}}{C_L}\right) \Delta s \tag{78}$$

Then, the ratio of consumable energy weight used in the mission leg can be expressed as follows:

$$\frac{W_{CE}^{(s)}}{W_{TO}} = \frac{W^{(s-1)} - W^{(s)}}{kW_{TO}} = \frac{\beta^{(s-1)}}{k}\left(1 - \frac{W^{(s)}}{W^{(s-1)}}\right) \tag{79}$$

where

$$\beta^{(s-1)} = \frac{W^{(s-1)}}{W_{TO}} \tag{80}$$

When payload that weighs $W_P^{(s-1)}$ is dropped at the beginning of the leg, $\beta^{(s-1)}$ is given as

$$\beta^{(s-1)} = \frac{W^{(s-1)^-} - W_P^{(s-1)}}{W_{TO}} \tag{81}$$

where $W^{(s-1)^-}$ is the weight of the aircraft right before the payload drop.

4.3.1.2 Constant Aircraft Weight ($k = 0$)

If aircraft weight does not change in the mission leg, and the propulsion system consumes a certain type of fuel, fuel consumption is in proportion to power consumption. By dividing Eq. (66) by the aircraft weight,

$$\frac{dW_{CE}}{W} = -\sum_{i=1}^{n_{CE}} \frac{\tau^{\langle i \rangle}}{\nu_{CE}^{\langle i \rangle} \Pi_{\eta}^{\langle i \rangle}} \left(\frac{P}{W} \right) dt \tag{82}$$

Note that W is constant. By integrating Eq. (82) into the flight time or the flight distance of the s^{th} mission leg,

$$\frac{W_{CE}^{(s)}}{W} = \int_{t^{(s-1)}}^{t^{(s)}} \sum_{i=1}^{n_{CE}} \frac{\tau^{\langle i \rangle}}{\nu_{CE}^{\langle i \rangle} \Pi_{\eta}^{\langle i \rangle}} \left(\frac{P}{W} \right) dt \tag{83}$$

or

$$\frac{W_{CE}^{(s)}}{W_{TO}} = \beta^{(s-1)} \Upsilon^{(s)} \Xi_{CE}^{(s)} \tag{84}$$

The weight of the total consumable energy normalized by the take-off gross weight, Ω_{CE}, can be obtained as the sum of the normalized weight of the consumable energy of the individual leg.

$$\Omega_{CE} = \frac{W_{CE}}{W_{TO}} = (1 + \epsilon_{CE}) \sum_{s=1}^{m} \frac{W_{CE}^{(s)}}{W_{TO}} \tag{85}$$

where ϵ_{CE} is the consumable energy allowance ratio that accounts for a propulsion system with "poorer-than-normal" energy consumption and the amount of unusable energy. In the traditional aircraft sizing method, the total aircraft fuel generally includes mission fuel as well as a 5% allowance for the reserve fuel which accounts for an engine with poorer-than-normal fuel consumption and an additional 1% allowance for trapped fuel [93]. In such a case, ϵ_{CE} for the conventional aircraft is 0.06. However, the proper allowance for unconventionally-powered aircraft will differ, depending on the characteristics of the propulsion system and energy storage systems.

4.3.2 Non-consumable Energy Sizing

If the aircraft is powered on solely non-consumable energy sources, then the value of k is zero. Therefore, energy weight fraction can be computed in the same way as

done for consumable energy sizing when $k = 0$ presented §4.3.1.2. If the propulsion system consists of multiple power-paths that include consumable and non-consumable energy sources, however, aircraft weight may vary in a mission leg. In this case the amount of non-consumable energy can be computed by using the information of the amount of consumable energy in the mission leg, which can be estimated by the process described in the previous section. The amount of non-consumable energy for the j^{th} power-path is given as power multiplied by time:

$$dE_{NE}^{\langle j \rangle} = -p_o^{\langle j \rangle} dt = -\frac{\tau^{\langle j \rangle} P}{\Pi_\eta^{\langle j \rangle}} dt \tag{86}$$

Combining Eq. (65) and Eq. (66) yields

$$\nu_{CE}^{\langle i \rangle} dW_{CE}^{\langle i \rangle} = -\frac{\tau^{\langle i \rangle} P}{\Pi_\eta^{\langle i \rangle}} dt \tag{87}$$

Combining Eq. (86) and Eq. (87) yields

$$dE_{NE}^{\langle j \rangle} = \frac{\tau^{\langle j \rangle}}{\tau^{\langle i \rangle}} \frac{\Pi_\eta^{\langle i \rangle}}{\Pi_\eta^{\langle j \rangle}} \nu_{CE}^{\langle i \rangle} dW_{CE}^{\langle i \rangle} \tag{88}$$

By integrating Eq. (88) for the mission leg and dividing by the take-off gross weight, the amount of non-consumable energy normalized by the take-off gross weight required for the mission leg can be computed as follows:

$$\left(\frac{E_{NE}^{\langle j \rangle}}{W_{TO}}\right)^{(s-1)} - \left(\frac{E_{NE}^{\langle j \rangle}}{W_{TO}}\right)^{(s)} = \frac{\tau^{\langle j \rangle}}{\tau^{\langle i \rangle}} \frac{\Pi_\eta^{\langle i \rangle}}{\Pi_\eta^{\langle j \rangle}} \frac{\nu_{CE}^{\langle i \rangle} W_{CE}^{(s)}}{W_{TO}} \tag{89}$$

If the propulsion system consists of only non-consumable power-paths, this approach is not possible. However, in such a case, the aircraft weight stays unchanged during the mission segments, which leads to the following equation by modifying Eq. (86):

$$\frac{dE_{NE}^{\langle j \rangle}}{\beta W_{TO}} = -\frac{\tau^{\langle j \rangle}}{\Pi_\eta^{\langle j \rangle}} \frac{P}{W} dt \tag{90}$$

The amount of the j^{th} energy consumed in the s^{th} leg can be expressed as

$$\left(\frac{E_{NE}^{\langle j \rangle}}{W_{TO}}\right)^{(s-1)} - \left(\frac{E_{NE}^{\langle j \rangle}}{W_{TO}}\right)^{(s)} = \int_{t^{(s-1)}}^{t^{(s)}} \frac{\beta^{(s-1)} \tau^{\langle j \rangle}}{\Pi_\eta^{\langle j \rangle}} \frac{P}{W} dt \tag{91}$$

which is an equivalent equation to Eq. (89) for the propulsion system that consists of non-consumable power-paths only.

Total non-consumable energy can be calculated by summation of the consumed energy of individual segments that are computed by either Eq. (89) or Eq. (91).

$$\left(\left(\frac{E_{NE}^{\langle j\rangle}}{W_{TO}}\right)^{(0)}-\left(\frac{E_{NE}^{\langle j\rangle}}{W_{TO}}\right)^{(1)}\right)+\left(\left(\frac{E_{NE}^{\langle j\rangle}}{W_{TO}}\right)^{(1)}-\left(\frac{E_{NE}^{\langle j\rangle}}{W_{TO}}\right)^{(2)}\right)+\cdots+$$
$$\left(\left(\frac{E_{NE}^{\langle j\rangle}}{W_{TO}}\right)^{(s-1)}-\left(\frac{E_{NE}^{\langle j\rangle}}{W_{TO}}\right)^{(s)}\right)+\cdots+\left(\left(\frac{E_{NE}^{\langle j\rangle}}{W_{TO}}\right)^{(m-1)}-\left(\frac{E_{NE}^{\langle j\rangle}}{W_{TO}}\right)^{(m)}\right)=$$
$$\left(\frac{E_{NE}^{\langle j\rangle}}{W_{TO}}\right)^{(0)}-\left(\frac{E_{NE}^{\langle j\rangle}}{W_{TO}}\right)^{(m)}=\frac{E_{NE}^{\langle j\rangle}}{W_{TO}} \quad (92)$$

Therefore,

$$\frac{E_{NE}^{\langle j\rangle}}{W_{TO}}=\Upsilon^{(s)}\sum_{s=1}^{m}\left(\frac{\beta^{(s-1)}\tau^{\langle j\rangle}}{\Pi_{\eta}^{\langle j\rangle}}\right) \quad (93)$$

and

$$W_{NE}=\sum_{j=1}^{n_{NE}}W_{NE}^{\langle j\rangle}=\sum_{j=1}^{n_{NE}}\frac{E_{NE}^{\langle j\rangle}}{\nu_{NE}^{\langle j\rangle}} \quad (94)$$

The weight of the total consumable energy normalized by the take-off gross weight, Ω_{CE}, can be obtained as follows:

$$\Omega_{NE}=\frac{W_{NE}}{W_{TO}}=(1+\epsilon_{NE})\sum_{s=1}^{m}\beta^{(s-1)}\Upsilon^{(s)}\Xi_{NE}^{(s)} \quad (95)$$

Where ϵ_{NE} is the non-consumable energy allowance ratio.

As aforementioned, the formulation presented in this section has been developed with a consistent consideration for the variation of aircraft weight in a mission leg due to energy consumption. Ignoring such a weight variation results in a simpler formulation. However, the simplification may cost a significant error or require a larger number of mission segments for comparable accuracy. The following example is a simple analysis for a notional zero-emissions aircraft. The wing area and the drag polar are 500 ft^2 and $0.01489C_L^2-0.0051C_L+0.0146$. The aircraft cruises at Mach 0.6 flight speed and a 60,000 ft altitude, where the air density and TAS (true

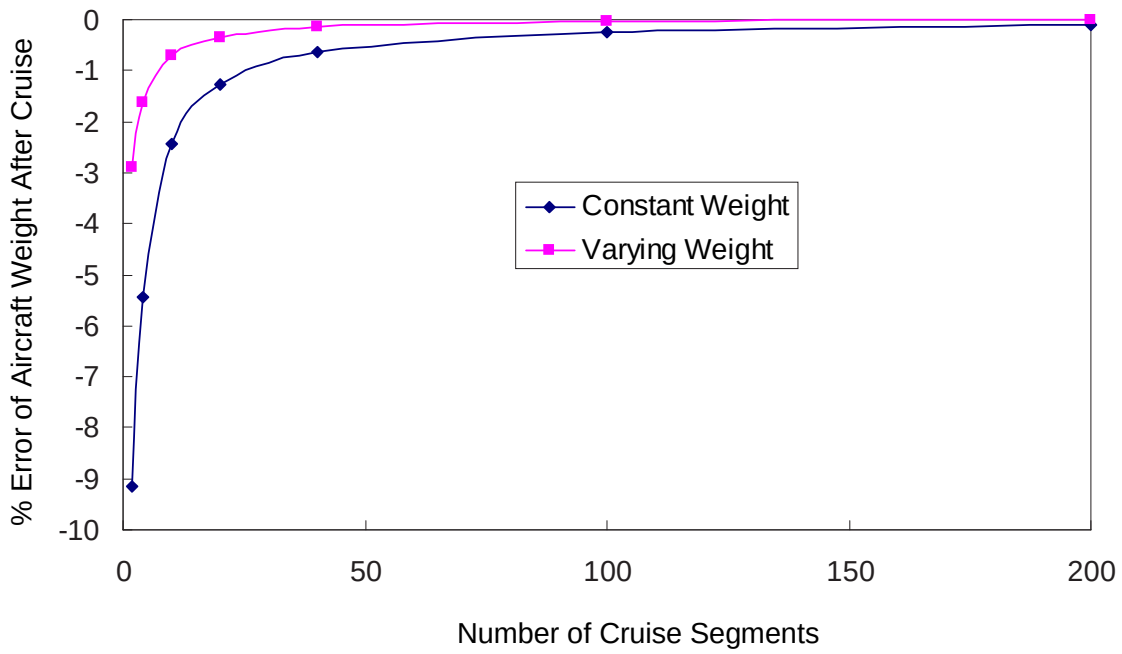

Figure 38: Comparison of numerical errors in two different approaches to mission analysis with varying number of mission legs

air speed) are the 0.000224 slug/ft^2 and 581 ft/sec, respectively. The aircraft weight after cruising 2,000 nmi is computed varying the number of segments in two ways: with and without consideration of the variation of aircraft weight. First, the cruise segment is divided into 200 small legs, and the aircraft weight at the end of the cruise segment in consideration of the variation of aircraft weight is computed at 35,736 lbs. Since two hundred is a sufficiently large number, this value is regarded as a true value for this analysis. Subsequently, the aircraft weight at the end of the cruise is computed both with and without consideration of the variation of aircraft weight lowering the number of legs from 100 to 1, and their errors with respect to the true value are depicted in Figure 38.

It is found that discretizing the mission with the coarser legs leads to underestimation of increases in aircraft weight for both methods. However, considering the variation of aircraft weight in a mission leg significantly reduces the error, which

means the method allows a lower number of mission legs for the same level of analysis accuracy.

The generalized mission analysis can estimate weight of required energy sources for various energy-propulsion system architectures. However, some cases may require more detailed supplemental analyses. First, an energy source may lose its energy capacity when it is not used for generating power. For example, a liquid hydrogen fueled aircraft that is not equipped with a cryogenic cooler will lose a certain amount of its fuel from boiling-off. Another issue is that specific energy of some energy sources may vary considerably depending on operating conditions. For example, the useful capacity of a battery changes depending on the discharge rate. Furthermore, the amount of battery storage capacity generally decreases over time.

4.4 Generalized Weight Estimation

Equation (39) can be rewritten as follows at take-off:

$$W_{TO} = W_E + W_{PL} + W_{CE} \tag{96}$$

The payload weight, W_{PL}, is usually given as a part of the customer requirements, and the consumable energy weight is determined by Eq. (85). However, empty weight cannot be estimated directly from the information derived from the constraint and mission analyses. It is the author's opinion that the estimation of empty weight is one of the greatest challenges to the sizing of revolutionary aircraft concepts. Very little information on structures and subsystems is available at the time of aircraft sizing, and hence their designs are not yet embodied. It is not possible to employ high fidelity analysis for the estimation of airframe weight with no corporeal designs. This dilemma also exists for sizing of conventional aircraft, but does not lead to a dire situation because abundant historical data allows the designer to estimate the component weight using just a handful of information about the aircraft with fairly good accuracy. However, such empirical weight equations for revolutionary aircraft

are not available and the dilemma cannot be solved simply.

One way to estimate the empty weight for revolutionary concepts is to use empirical equations for conventional aircraft with appropriate corrections that account for the repercussions of implementing an alternative energy-propulsion system architecture. In order to establish a relationship between the empty weight and the take-off gross weight, required in the proposed formulation, the empty weight is broken into subgroup weight terms as follows:

$$W_E = \acute{W}_E + W_{PS} + W_{NE} + \delta W_E \tag{97}$$

where $\acute{W}_E$ is the empty weight less the weight of installed propulsion systems estimated from a historical database; W_{PS} is the weight of the propulsion system; W_{NE} is the weight of the non-consumable energy source; and δW_E is the empty weight correction.

The fundamental idea behind this equation is that the empty weight of revolutionary aircraft can be computed as the sum of two parts: propulsion system and non-consumable energy that is certainly not available from the traditional database, and others such as structures and subsystems whose weight may still be very close to the trend of the traditional database[2]. Therefore, the latter can be obtained by computing the empty weight less the weight of installed propulsion systems from the traditional database with appropriate corrections.

This correction is necessary for several reasons. First, using an unconventional energy source may incur significant impact on structures and subsystems beyond propulsion systems. For instance, if an aircraft is powered by an electric propulsion

[2]Similar methods have been applied to aircraft design optimization problems, in which a portion of the empty weight can be computed by physics-based analyses, and the rest can be estimated only by historical guidance. For example, Muñoz and Sparkovsky [131] performed the synthesis and design optimization of a turbofan engine coupled with an environmental control system (ECS) for a military fighter. The authors estimated the weight of the airframe excluding the weight of an ECS by regression analysis, while they calculated the weight of an ECS using a separate analysis code in order to capture the variation of the ECS weight as per the changes in ECS design variables.

system that produces thrust with electric motors, engine bleed air is no longer available, which forces the designer to find a new way of integrating cooling systems into the aircraft. In addition, the aircraft is very likely not to use hydraulic systems to power actuators, which leads to elimination of centralized hydraulic pumps. Furthermore, electric generators that are driven by mechanical power extracted from IC engines are no longer necessary. These changes lead to an unavoidable conclusion of elimination of the accessory gear box, which is a mechanical interface of hydraulic pumps, generators, and engine turbine starters with IC engines. In parallel with this impact propagation, the conventional way of integrating the secondary power system will also be reexamined. In the light of inherent redundancy of electric power generation and conversion processes, conventional APU and EPU systems are likely to be eliminated. Because building distributed power generation and parallel power transformation is relatively easy for electric propulsion systems when compared to conventional IC engines, the same level of or higher reliability may be achieved without additional stand-alone secondary power systems. All of these changes in conventional subsystem integration are very likely to contribute to a reduction in aircraft empty weight, which must be accounted for by the correction weight term, δW_E.

Incorporating alternative energy sources may also incur either positive or negative impact on the airframe weight. For example, if hydrogen fuel is used, an increase in empty weight due to installing a hydrogen storage tank may be significant. In general, conventional aircraft store liquid hydrocarbon fuel inside structurally integrated fuel tanks whose structures carry load. However, the hydrogen fuel tank, either liquid or gaseous, may not be fully integrated with general structures such as bulkheads, shear webs, and skins, which will increase aircraft empty weight. Furthermore, if liquid hydrogen fuel is used, the low temperature requires the fuel tanks and associated plumbing to be insulated carefully to minimize heat leak into the fuel, thereby limiting boil-off. Not accounted for by regression equations created from traditional

Figure 39: AeroVironment WASP [134]

aircraft weight database, the hydrogen tank weight and additional weight provoked by installing the tank must be estimated by appropriate analysis and incorporated into the correction weight term, δW_E. However, it must be noted that novel approaches of integrating unconventional energy sources may not necessarily incur increases in empty weight. For example, WASP, a micro aerial vehicle developed by AeroVironment under DARPA support, is powered by two lithium-ion battery packs [132]. The conformal "spar" batteries attached to both sides of the Kevlar wing not only power the electric propulsion system, but also provide structural support to the wing. This design concept is an example of the Multifunctional Structures (MFS) design approach that pursues integrating normally stand-alone functions such as thermal management, batteries, power generation, and electronic subsystems into a composite structure thereby reducing volume and weight [133]. Such benefits in saving airframe weight incurred by the use of unconventional energy sources need to be reflected to δW_E via adequate analyses.

There is currently a lack of trusted and validated analysis capability for estimating the weight of revolutionary propulsion systems. The way of estimating propulsion system weight entirely depends on the availability of information and analysis models. The crudest way is to compute individual component's weight with weight-specific power, a measure of how much power is consumed or produced per the unit mass, of each component. The weight of a component can be computed by its reference power divided by weight-specific power. The selection of the reference power may differ on a case-by-case basis. For example, the weight-specific power of electric motors is usually measured at maximum continuous shaft power.

Then, Eq. (97) is rewritten as follows:

$$W_E = \acute{\Gamma} W_{TO} + \Phi W_{TO} + \Omega_{NE} W_{TO} + \Delta W_{TO} \tag{98}$$

where

$$\acute{\Gamma} = \frac{\acute{W}_E}{W_{TO}}, \;\; \Phi = \frac{W_{PS}}{W_{TO}}, \;\; \Omega_{NE} = \frac{W_{NE}}{W_{TO}}, \text{ and } \;\; \Delta = \frac{\delta W_E}{W_{TO}}$$

$\acute{\Gamma}$ can be estimated from a traditional database, or the following data provided by Torenbeek [104] for subsonic light aircraft: 0.45 for fixed gear, 0.47 for retractable gear, 0.50 for utility category, and 0.55 for acrobatic category.

By combining Eq. (85), Eq. (96), and Eq. (98), the take-off gross weight equation is given as follows:

$$W_{TO} = \frac{W_{PL}}{1 - \acute{\Gamma} - \Delta - \Phi - \Omega_{NE} - \Omega_{CE}} \tag{99}$$

The take-off gross weight equation, Eq. (99), cannot be solved in a closed form since $\acute{\Gamma}$, Δ, and Φ are also functions of the take-off gross weight. Therefore, an iterative process must be used to solve the equations.

The iteration process is very similar to the traditional process presented in most aircraft design books. First, make an initial guess of the take-off gross weight, $\overline{W}_{TO}$, and calculate the reference power of each power-path, $P_{ref}^{\langle i \rangle}/W_{TO}$, and wing area, S, by simply multiplying the power to weight ratio, $P_{ref}^{\langle i \rangle}/W_{TO}$, with the guessed value of the

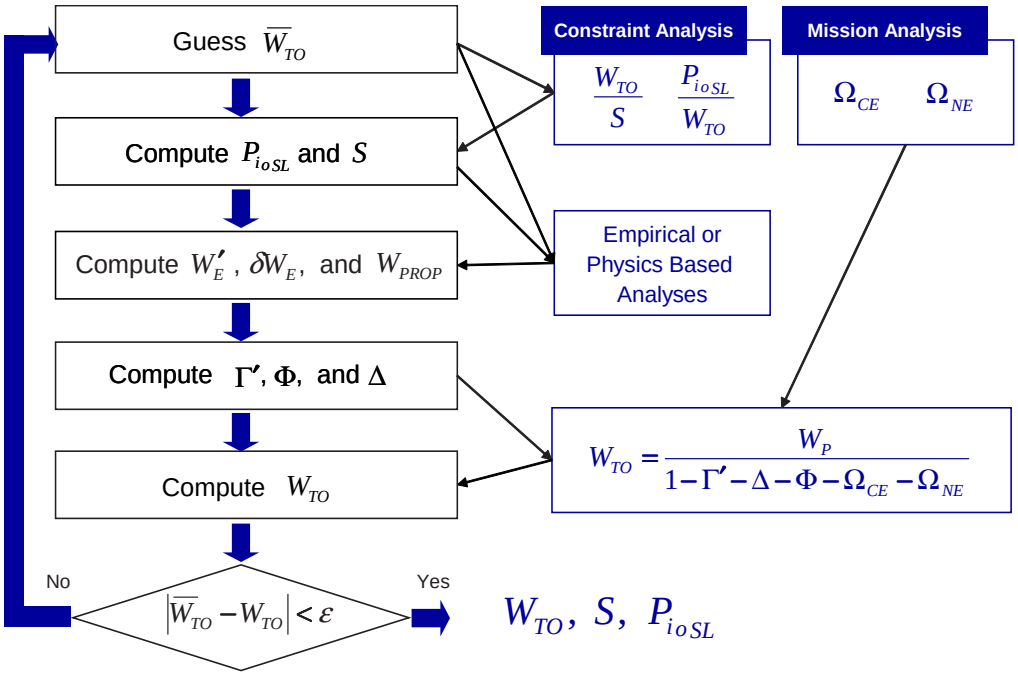

Figure 40: Weight estimation process

take-off gross weight, $\overline{W}_{TO}$, and dividing $\overline{W}_{TO}$ by wing loading, W_{TO}/S, respectively. Then, compute the group weights from empirical databases and physics-based analysis tools, if available. Next, compute updated take-off gross weight from Eq. (99). Iterate the whole process until the convergence criterion is satisfied.

4.5 The Process of AIASM

The fundamental elements that were discussed in the previous chapter are put together in AIASM. The basic structure of the method remains the same as that of the traditional method as depicted in Figure 41 which highlights the primary changes made to the traditional sizing process. First, the information of specific energy and efficiencies, in lieu of the traditional engine deck, is used to represent propulsion system performance. Secondly, the historical database is still referred to for the estimation of airframe weight. However, physics-based analysis must supplement empirical analysis. In addition, constraint analysis is changed from thrust-based to power-based, and

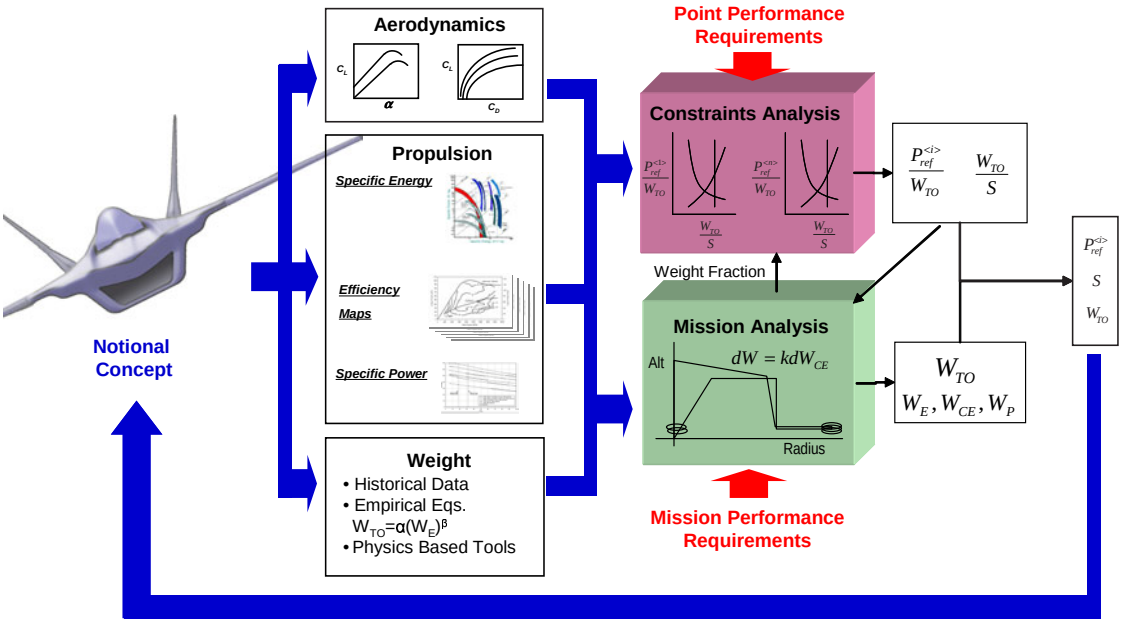

Figure 41: Overview of AIASM

power is used along the downstream analysis. The power-based constraint analysis is performed with the set of new equations presented in §4.1. Mission analysis is performed with a set of generalized equations formulated in §4.3.

The fundamental feature of this method is that, unlike general aircraft sizing tools, it does not require a set of engine deck data that describe thrust (or power) and specific fuel consumption (or fuel flow) at different flight conditions and power settings. Legacy vehicle sizing codes estimate the fuel consumption of each mission leg by interpolating the engine deck data around the specific flight condition. However, this traditional method is not appropriate when the power available and fuel consumption depend on more parameters such as power fractions of all power sources and time dependent factors (i.e. current draw for electric battery) as well as flight conditions and power setting. In contrast, AIASM directly calculates the fuel consumption or energy consumption by running the nested propulsion system model at a specific flight condition accounting for all important factors that affect fuel and/or energy consumption. Such dynamic integration is essential for sizing a hybrid power-generation system.

Similarly, the environment does not require an engine scaling law, the relationship between propulsion system weight and output power (or thrust). Because the technology behind the traditional air-breathing combustion engines has matured, a scaling law for such an engine is well established and its implementation significantly accelerates the aircraft sizing process without considerable errors. However, generic scaling laws of emerging electric propulsion architectures are not available at the same level of accuracy. Thus, the propulsion system weight must be estimated during the iterative processes of aircraft sizing, which may increase computation time and resources.

The fidelity of a sizing analysis by this method largely depends on the quality of input data. There is no distinguishable difference in preparing aerodynamic data between the traditional sizing method and AIASM. A range of methods from simple empirical equations to sophisticated computational fluid dynamics (CFD) analysis may be employed depending on required analysis fidelity and available information and resources. In contrast, the inputs for performances and weight of alternative energy-propulsion system architectures can be developed by neither traditional practices using empirical equations nor legacy codes such as NEPP[3] (NASA Engine Performance Program) [135] and WATE[4] (Weight Analysis of Turbine Engines) [136]. Therefore, appropriate analysis codes need to be acquired on a case by case basis. Due to the scarcity of reliable analysis tools for an alternative energy-propulsion system architectures, a lot of previous studies assumed a constant efficiency with flight as well as estimated propulsion system weight simply by multiplying the amount of power required by a representative value of specific power.

[3]NEPP analyzes the one-dimensional, steady state thermodynamic characteristic of an aircraft jet engine. NEPP estimates the performance of the engine in the form of an engine deck as well as detailed thermodynamic analysis results at each station and component.

[4]Originally developed by the Boeing Military Aircraft Company in 1979 and improved by NASA and the McDonnell Douglas Corporation, WATE embodies a physical engine by estimating the weight and envelope dimensions of large and small gas turbine engines using a semi-empirical method.

The equations of both this constraint analysis and the mission analysis of AIASM are described with respect to weight-specific parameters such as power-to-weight ratio, wing loading, and energy weight fraction. As discussed in §2.2.6, the weight specific parameter-based approach to solving an aircraft sizing problem significantly reduces computational efforts in a human-in-the-loop environment. If the aircraft sizing environment is automated by an optimization tool, however, the actual-value-based approach may supersede the weight specific parameter-based approach because iteration loops associated with the estimations of aircraft weight can be eliminated and absorbed in the system level optimization loop. Nevertheless, it must be noted that equations described with respect to weight-specific parameters can be still used in the actual-value-based approach with no modification. The bedrock idea of the actual-value-based approach is to use actual values for available power and energy as design variables. Whether the equations representing power balance and energy balance are described in terms of weight-specific parameters or not does not matter for the actual-value-based approach. In contrast, the weight specific parameter-based approach requires the equations described in terms of weight-specific parameters. The bottom line is that the formulation based on weight-specific parameters is applicable both for the weight specific parameter-based approach and the actual-value-based approach.

4.6 Non-dimensional Aircraft Mass (NAM) Ratio

The AIASM will enable designers to size simultaneously and optimize the airframe and revolutionary system propulsion system, and is able to support a wide range of research regarding the design of alternative energy-propulsion system architectures. First of all, the environment may aid an arbiter in selecting the most suitable propulsion system architecture for a given mission. The emergence of various alternative energy sources results in a large combinatorial space for possible propulsion system

architectures. Therefore, the selection of the *correct* propulsion system architecture becomes more challenging than before unless it can be proved that one specific type of architecture substantially outperforms others for most missions. As a case in point, Rohrschneider et al. [56] explore flight system options for the design of a long endurance Mars airplane mission. The study investigates five different alternatives with regard to the propulsion system as well as five different vehicle configuration options.[5]

Furthermore, such an architectural selection process will require numerous opportunities for decision making, including decisions on energy sources, power generation, conversion, and means of producing thrust. For example, even if fuel cells are selected as the primary power source, a variety of decision making options are still available, for example, type of fuel cells (proton exchange membrane, solid oxide fuel cells, etc.), type of fuel (methane, hydrogen, petroleum, etc.), type of fuel storage (pressurized gaseous tank, cryogenic liquid tank, etc.), and type of electric motors (general AC motor, brushless DC motor, and superconducting motor, etc.).

Such a large number of alternatives for each disciplinary design may result in a myriad of combinatorial options in terms of system-level designs, which will bring significant complications into the conceptual design phase. The problem may be alleviated by using a qualitative assessment technique such as Technique for Order Preference by Similarity to Ideal Solution (TOPSIS) that facilitates downselecting the combinatorial space into a manageable number of promising options based on a subjective ranking of some evaluation criteria. Nevertheless, the capability of quantitative assessment for different types of propulsion system architecture is crucial in the selection of the best combination, particularly when one tries to find a correct

[5]The propulsion system options includes an NTO/MMH bipropellant rocket, a battery powered propeller, a DMFC powered propeller, a beamed solar powered propeller, and a beamed microwave powered propeller. The vehicle configuration options includes a straight wing with a single vertical tail, a straight wing with two vertical tails, a wing-canard, a swept wing with a single vertical tail, and the ARES (Aerial Regional-Scale Environmental Survey) configuration (see Figure 5 in §1.1.5). Their research identified DMFC and a straight wing with two vertical tails as the best options for the on-board power system and the external configuration.

power mix for hybrid propulsion aircraft.

In addition to such *cardinal research* in which a specific mission identifies the best propulsion system, *exploratory research* in which a specific propulsion system expands available mission space will be also of importance. The history of human technology has shown that *needs promote new technology, and, in turn, the technology reveals new needs*. As illustrated in Figure 42, IC engines fueled with conventional aviation fuels have produced aircraft which have addressed the shown portions of the mission space. As revolutionary propulsion systems become tangible, however, the technology may open up new feasible and viable mission spaces that the aerospace community has previously abandoned, fettered by ineluctable logic due to obvious limitations of conventional propulsion systems. Furthermore, some alternative propulsion-energy architectures may be more attractive for such an unconventional mission. Therefore, evaluating the potential of an alternative energy-propulsion system architecture must involve investigations within a large area of the mission space that is composed by performance metrics such as flight speed, range, and payload. In addition, evaluating various concepts for alternative propulsion-energy architectures must go along with exploring the mission space in the light of their current capabilities as well as projected capabilities in the near/long term future. At present, the biggest challenge to such exploratory research is the following: it requires a rigorous survey of a *possible fleet of aircraft* for a given energy-propulsion architecture rather than a *single representative aircraft*.

Recently, Soban and Upton [137] have proposed an interactive assessment environment that can conduct a qualitative "mapping" of new propulsion technologies to their goodness for performing a mission. In order to perform such qualitative mappings, the authors developed new techniques, named IRMA (Interactive Reconfigurable Matrix of Alternatives) and IQAM (Interactive Qualitative Assessment Matrix), based on well-known qualitative assessment techniques, such as the morphological matrix

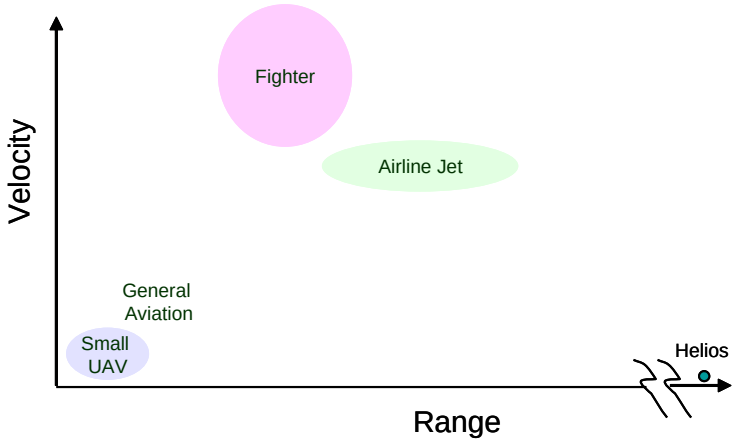

Figure 42: Mission Space Exploration

and Quality Function Deployment (QFD). The original objective of this environment is to identify the classes of air-vehicles that could best prosper from new propulsion technologies. Nevertheless, the environment would also be equally useful to compare alternative concepts embracing the options for propulsion system architectures and vehicle configurations for a given mission.

However, such a qualitative assessment is vulnerable to subjective judgments by its users. Therefore, there is a need for the capability of mapping the characteristics of a propulsion-energy system architecture into a mission space in a quantitative manner. A simple quantitative method can be developed based on aircraft weight decomposition in connection with the generalized Breguet range equations presented in §4.2. The take-off gross weight can be broken down as follows:

$$W_{TO} = \acute{W}_E + W_{PS} + W_{NE} + \delta W_E + W_{CE} + W_{PL} \tag{100}$$

By dividing Eq. (100) with W_{TO},

$$\frac{\acute{W}_E}{W_{TO}} + \frac{W_{PS}}{W_{TO}} + \frac{W_{NE}}{W_{TO}} + \frac{\delta W_E}{W_{TO}} + \frac{W_{CE}}{W_{TO}} + \frac{W_{PL}}{W_{TO}} = 1 \tag{101}$$

The correction term, δW_E, represents the collective impact on empty weight by integrating an unconventional propulsion system and an energy source, and can be further

decomposed into two terms: the change in empty weight due to the integration of an unconventional propulsion system and the change in empty weight due to the integration of an energy source. Assuming that each term is proportional to the weight of the propulsion system and the energy source, respectively, Eq. (101) reduces to the following:

$$\frac{\acute{W}_E}{W_{TO}} + (1 + e_{PS})\frac{W_{PS}}{W_{TO}} + (1 + e_{NE})\frac{W_{NE}}{W_{TO}} + (1 + e_{CE})\frac{W_{CE}}{W_{TO}} + \frac{W_{PL}}{W_{TO}} = 1 \tag{102}$$

where e_{PS}, e_{NE}, and e_{CE} represent the impact on the empty weight from integrating an unconventional propulsion system, a consumable energy source, and a non-consumable energy source, all normalized by the take-off gross weight. In the case of conventional propulsion systems, e_{PS}, e_{NE}, and e_{CE} ought to be zero. For simplicity, it is assumed that a single consumable energy source is used. Then, Eq. (102) reduces to the following:

$$\frac{\acute{W}_E}{W_{TO}} + (1 + e_{PS})\frac{W_{PS}}{W_{TO}} + (1 + e_{CE})\frac{W_{CE}}{W_{TO}} + \frac{W_{PL}}{W_{TO}} = 1 \tag{103}$$

The first term represents the ratio of airframe weight to the take-off gross weight. The airframe weight ($\acute{W}_E$) herein excludes the weight of the propulsion system, the energy source, and all components pertaining to the given energy-propulsion system architecture. For example, if liquid hydrogen is used as fuel, the hydrogen tank and cooling system are not accounted as a part of $\acute{W}_E$. This ratio is reasonably independent of the choice of propulsion system architecture and energy sources, considering structures, a major portion of an airframe, is mainly sized to sustain the aircraft load, which is strongly related to the take-off gross weight. The last term is payload-to-weight ratio, often considered a metric of the effectiveness of a transportation system. Higher payload-to-weight ratio means a lighter transportation system for the same weight of payload. As W_{PL}/W_{TO} approaches to zero, W_{PS}/W_{TO} and/or W_{CE}/W_{TO} are allowed to increase.

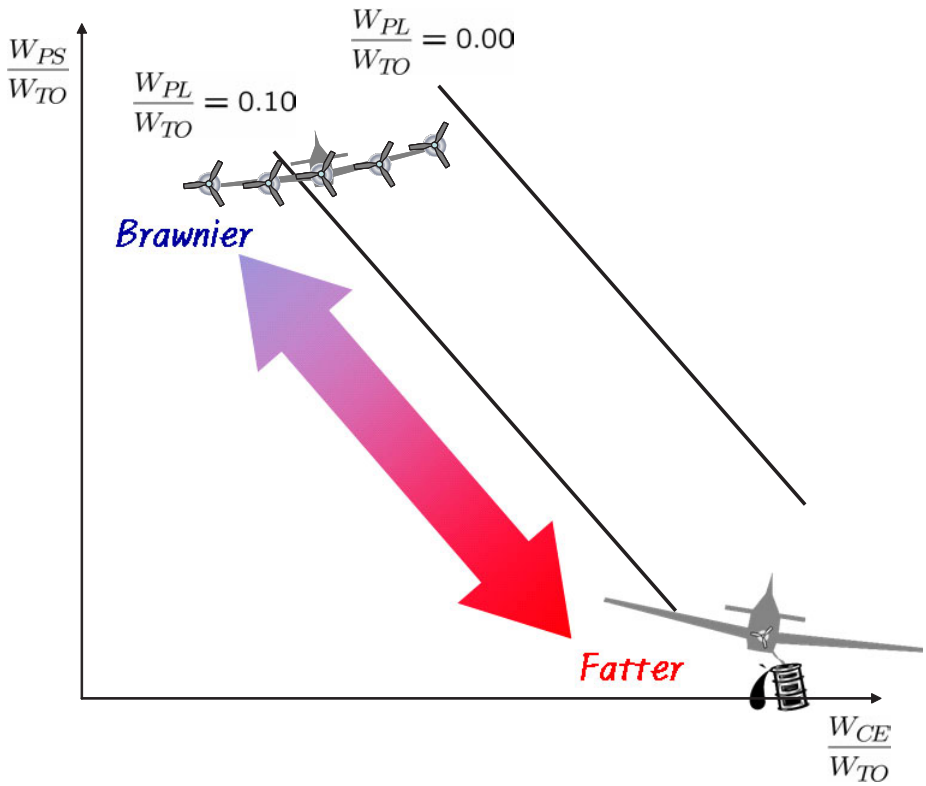

Figure 43: Dualistic relationship between energy weight fraction and propulsion system weight fraction

This equation also provides an insight to the physical limitation of a given energy-propulsion system architecture. For given values of $\acute{W}_E/W_{TO}$ and W_{PL}/W_{TO}, the remaining weight fraction $(1 - \acute{W}_E/W_{TO} - W_{PL}/W_{TO})$ must be apportioned between W_{PS}/W_{TO} and W_{CE}/W_{TO}. Therefore, Eq. (103) expresses a boundary of allowable values of the dualistic, *dichotomous* terms (W_{PS}/W_{TO} and W_{CE}/W_{TO}), which are depicted in Figure 43. The higher W_{PS}/W_{TO} and the lower W_{CE}/W_{TO} result in a "brawnier" aircraft. On the other hand, lower W_{PS}/W_{TO} and higher W_{CE}/W_{TO} produce a "fatter" aircraft.

Then, Eq. (103) expresses the linear relationship between the maximum allowable propulsion system weight and energy weight for the energy-propulsion system

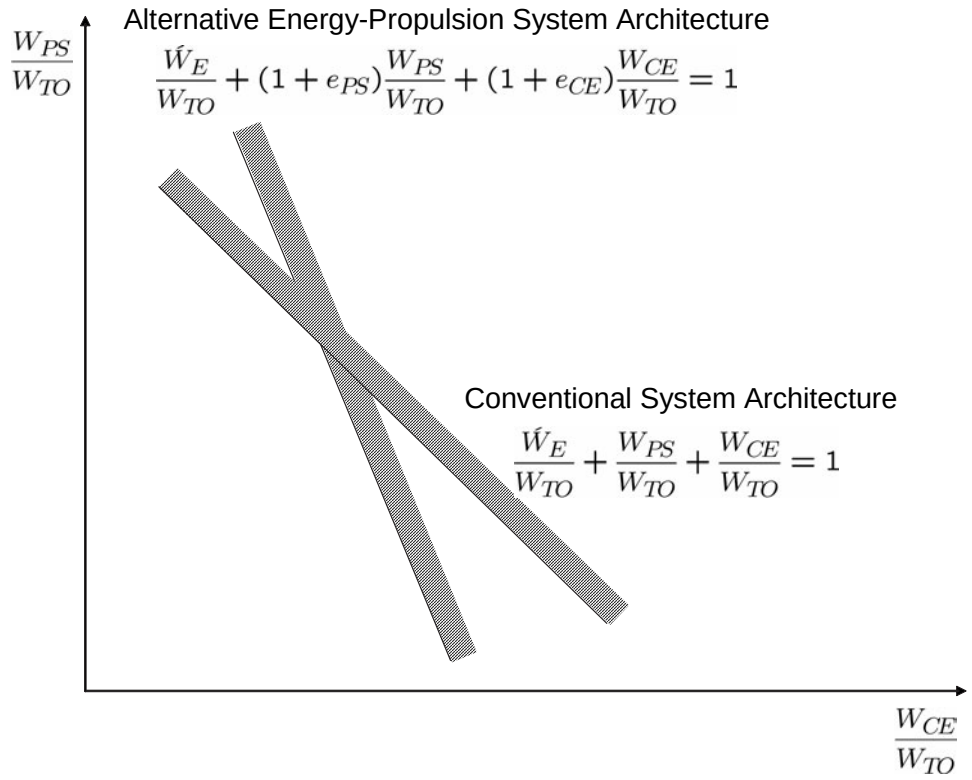

Figure 44: Comparison of an alternative energy-propulsion system architecture and a conventional energy-propulsion system architecture

architecture. The values of e_{PS} and e_{CE} are determined by the selection of an energy-propulsion system architecture. Assuming that all coefficients are constant for the variation of two variables, $\frac{W_{PS}}{W_{TO}}$ and $\frac{W_{CE}}{W_{TO}}$, the boundary is given as lines as shown in Figure 44. Note that the gradient of this boundary for the combined weight fractions of the conventional energy-propulsion system architecture is "-1," provided that e_{PS}, e_{NE}, and e_{CE} are zero. The slope of the boundary line for an alternative energy-propulsion system architecture might differ depending on e_{PS}, e_{NE}, and e_{CE}.

Treating Figure 44 as the first quadrant, another quadrant that maps the energy weight fraction to range capability is juxtaposed as shown in Figure 45. The curve in the newly added second quadrant can be obtained by the generalized Breguet range equations (Eq. (60) or Eq. (62) in §4.2). In addition, the original diagram can be

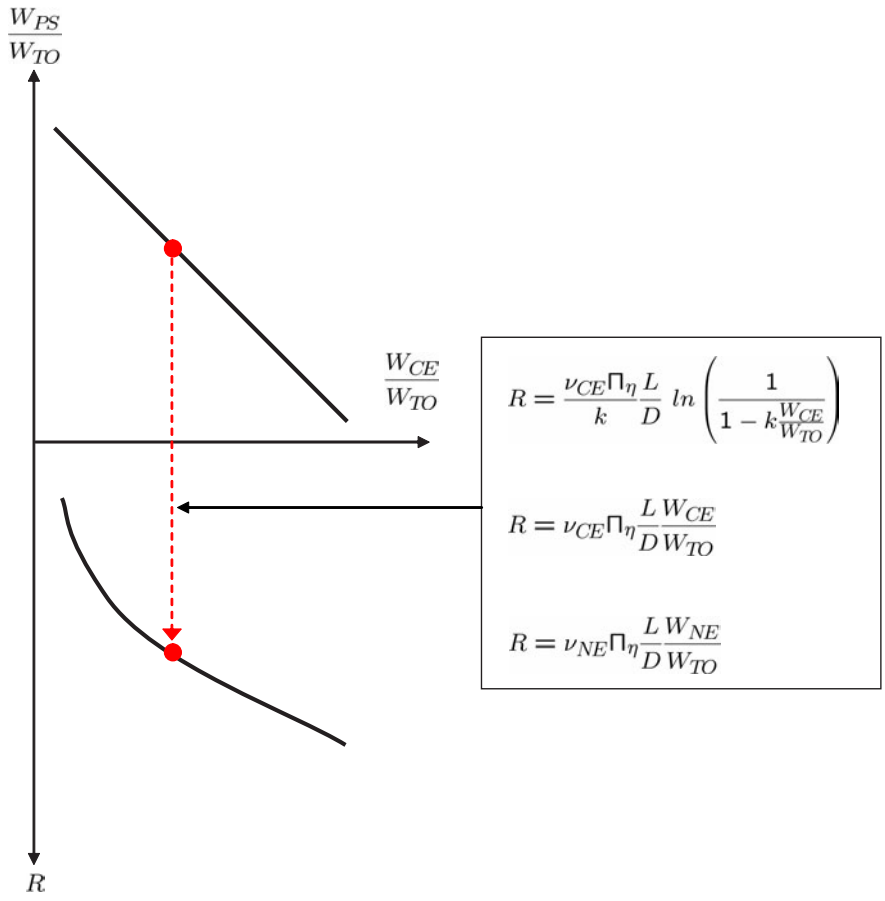

Figure 45: Mapping the energy weight fraction to the mission range

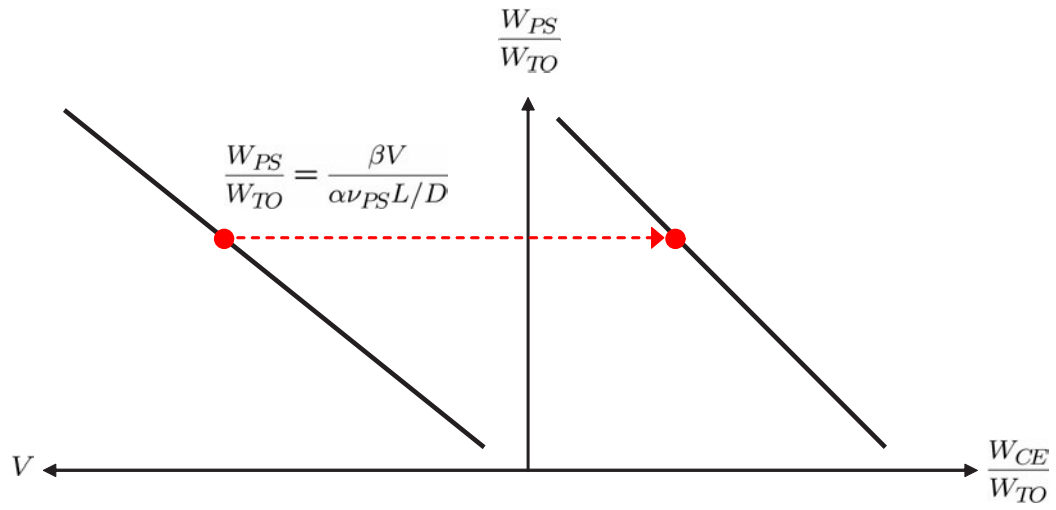

Figure 46: Mapping the cruise velocity to the propulsion system weight fraction

horizontally combined with another quadrant that relates the cruise velocity to the propulsion system weight fraction based on the specific power of the propulsion system, as shown in Figure 46. Finally, assembling Figure 45 and Figure 46 complements the development of an integrated visual environment that depicts the allowable mission capabilities in terms of cruise velocity and range for a given energy-propulsion system architecture. The resulting diagram is composed of four quadrants: each representing a design space in terms of aircraft mass, energy, mission, and power space, as shown in Figure 47.

The *mass space* describes the allowable propulsion system mass fraction and energy mass fraction, which are determined by the airframe mass fraction, including the mass fraction of the components concomitant with implementing an energy-propulsion system architecture, and a given payload mass ratio. The reduction in airframe weight due to advanced materials or better airframe integration will shift the limit state curve in the diagonal direction, which allows the aircraft to increase the amount of on-board energy sources and/or propulsive power. Alternatively, with a fixed airframe mass ratio, the limit state curve may vary with the payload mass

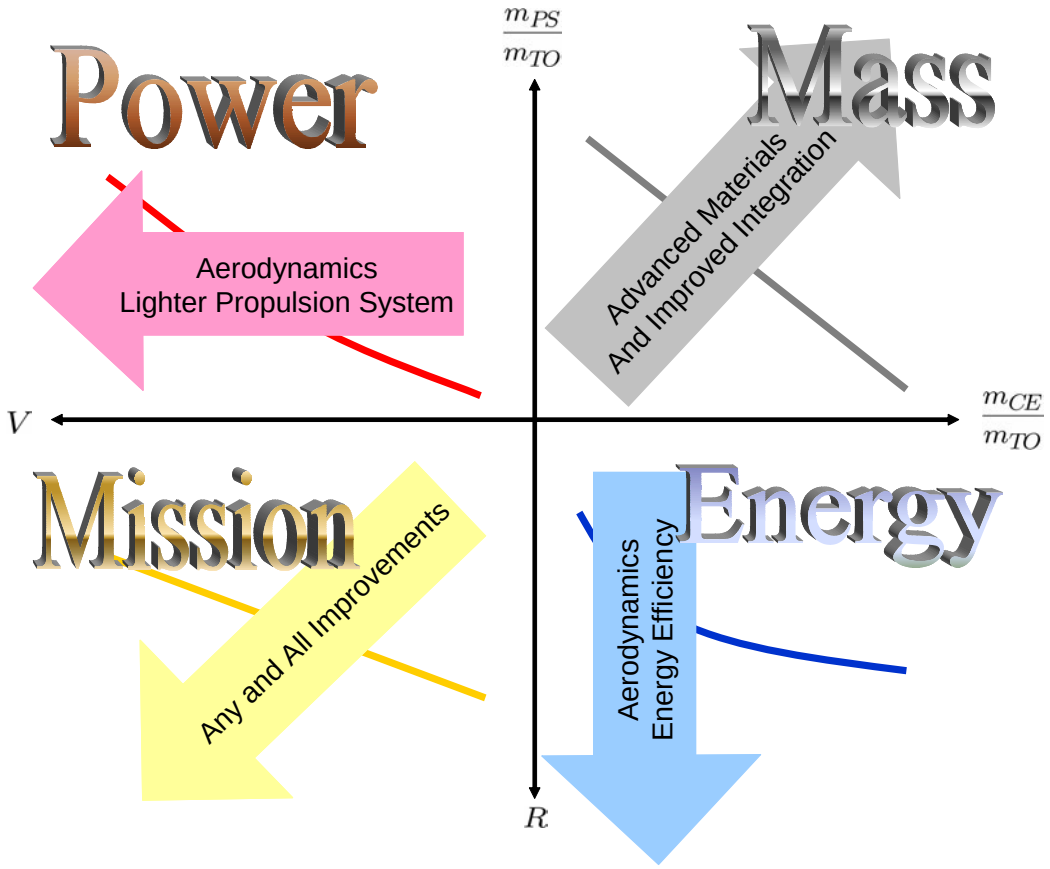

Figure 47: Illustration of a notional NAM ratio diagram

ratio. The *energy space* establishes the relationship between the allowable mission range versus the energy weight fraction. The limit state curves will be improved by the propulsion system and aerodynamic efficiencies. The *power space* depicts the allowable cruise speed versus the propulsion system mass fraction. The limit state curves will be improved by the specific power of a propulsion system and the aerodynamic efficiencies of the aircraft configuration. Finally, the *mission space* integrates velocity and range capabilities, which can be enhanced by improvements of any other spaces.

A salient feature of this diagram is that it identifies the allowable mission space for a vehicle rather than a single point design. This capability is also useful for the conceptual design of a terrestrial exploration winged platform, in which the allowable

range of the exploration per the selection of the propulsion system and energy architectures is given as an FoM rather than a design constraint. With such applications in mind, mass appears to be a more universal parameter than weight. Without any loss in generality, the first quadrant can be expressed in terms of mass ratios. In this sense, this visual environment is henceforth named as the Non-dimensional Aircraft Mass (NAM) ratio diagram.

In order to demonstrate the usefulness of the NAM ratio diagram, a simple example study has been performed, in which three alternative propulsion-energy architectures are considered for the design of a high altitude unmanned surveillance platform: a) conventional turbo prop engine fueled with jet fuel; b) PEMFC-powered electric propulsion system fueled with liquid hydrogen; and c) triggered isomer heat exchanger engine (TIHE) [83] fueled with isomers of hafnium (^{178}Hf), denoted as Architecture A, B, and C. The assumptions for each architecture are listed in Table 5. For Architecture A, it is assumed that $e_{CE} = 0$ and $e_{PS} = 0$. The value of α is estimated based on a simple equation in Ref. [103] that computes α from the density ratio. For Architecture B, the propagated impact of introducing the FC-powered electric propulsion system on other subsystems is ignored and the impact of the use of hydrogen fuel is taken into account by assuming $e_{CE} = 0.5$, which means that the weight penalty on the empty weight equals one half of the hydrogen fuel weight. For Architecture C, it is assumed that the primary impact of introducing an atomic power source on airframe weight is the addition of a radiation shield, whose weight is sensitive to design parameters such as the tolerance of equipment radiation, and the distance from the radiation source. It is assumed that the weight is reasonably proportional to the amount of output power of the TIHE engine, which is reflected in the value of $e_{PS} = 0.51$.

The weight data of several aircraft that belongs to this category are listed in Table 6. The empty weight fraction without including the propulsion system as a

Table 5: The assumptions of architecture options

Architecture	A	B	C
e_{PS}	0	0	0.51
e_{CE}	0	0.5	0
Overall efficiency at cruise	0.16 - 0.2	0.38 - 0.43	0.35 - 0.5
Specific energy (ft)	1.786×10^7	4.464×10^7	5.653×10^{11}
Specific power (ft/sec)	1400	138	421
α	0.27	0.3	0.3

Table 6: High altitude unmanned aircraft

	Predator	Dark Star	Proteus	Global Hawk
W_{TO} (lbs.)	2230	8600	13700	25600
W_E (lbs.)	1130	4286	5900	9200
W_{PS} (lbs.)	166.4	459	459	1580
W_F (lbs.)	650	3314	6000	14500
W_{PL} (lbs.)	450	1000	1800	1900
Γ	0.43	0.45	0.40	0.30
W_{PS}/W_{TO}	0.07	0.05	0.03	0.06
W_F/W_{TO}	0.29	0.39	0.44	0.57
W_{PL}/W_{TO}	0.20	0.12	0.13	0.07

part of the vehicle's empty weight ranges from 0.3 to 0.45. The payload weight fraction ranges from 0.07 to 0.2. Furthermore, values of L/D at cruise are assumed to range from 25 to 35. In order to encompass the gamut of vehicle design attributes including different empty weight fractions, payload fractions, and the aerodynamic efficiencies, Monte Carlo simulations were performed with a uniform distribution of the associated variables. A NAM ratio diagram that compares the three architectures is created from two hundred random cases, in which the cruise speed is varied from M 0.3 (290 ft/sec) to M 0.7 (774 ft/sec), as depicted in Figure 48.

In the power space of the figure, the three architectures occupy distinct regions.

The propulsion system weight fraction of Architecture A ranges from 0.03 to 0.09 for the range of cruise speed. Architecture B has higher values for the propulsion system weight fraction, ranging from 0.25 to 0.61, for the same flight speed, compared with the others. The poorer specific power of fuel cell systems makes Architecture B a heavier propulsion system than others for the same level of power. Furthermore, the maximum allowable cruise speed of aircraft equipped with Architecture B is limited to approximately 650 ft/sec. In the weight space, the three architectures also occupy different regions. Architecture B has a cluster at the region of higher power fraction and lower energy fraction, because of its heavier propulsion system and LH_2 tank, an aircraft with Architecture B is constrained to carry less fuel. Nevertheless, such an aircraft outperforms the ones with a conventional architecture in the low-speed range as shown in the mission space, because the architecture provides higher overall efficiencies of converting the more energetic fuel. The specific power characteristics of Architecture C allow higher fuel fractions when compared with Architecture B. Furthermore, the specific energy of the isomer is far greater than those of other energy sources, which allows virtually unlimited flight.

4.7 Extension to Solar-Powered Propulsion Architecture

Solar-powered aircraft obtain energy from the sun using Photovoltaic (PV) or solar cells as they are often called. This type of semiconductor device converts sunlight into direct current (DC) electricity. By collecting energy from outside of the aircraft, solar-powered aircraft may fly with less or no on-board stored energy source.

An important aspect of the sizing of solar-powered aircraft is that a solar-powered propulsion system introduces a coupling between the available power and wing geometry, creating an additional constraint in the design space. It is obvious that the maximum available solar power is limited by the wing area since PV cells are generally installed over the wing. In fact, limitation of available power is inherent for other

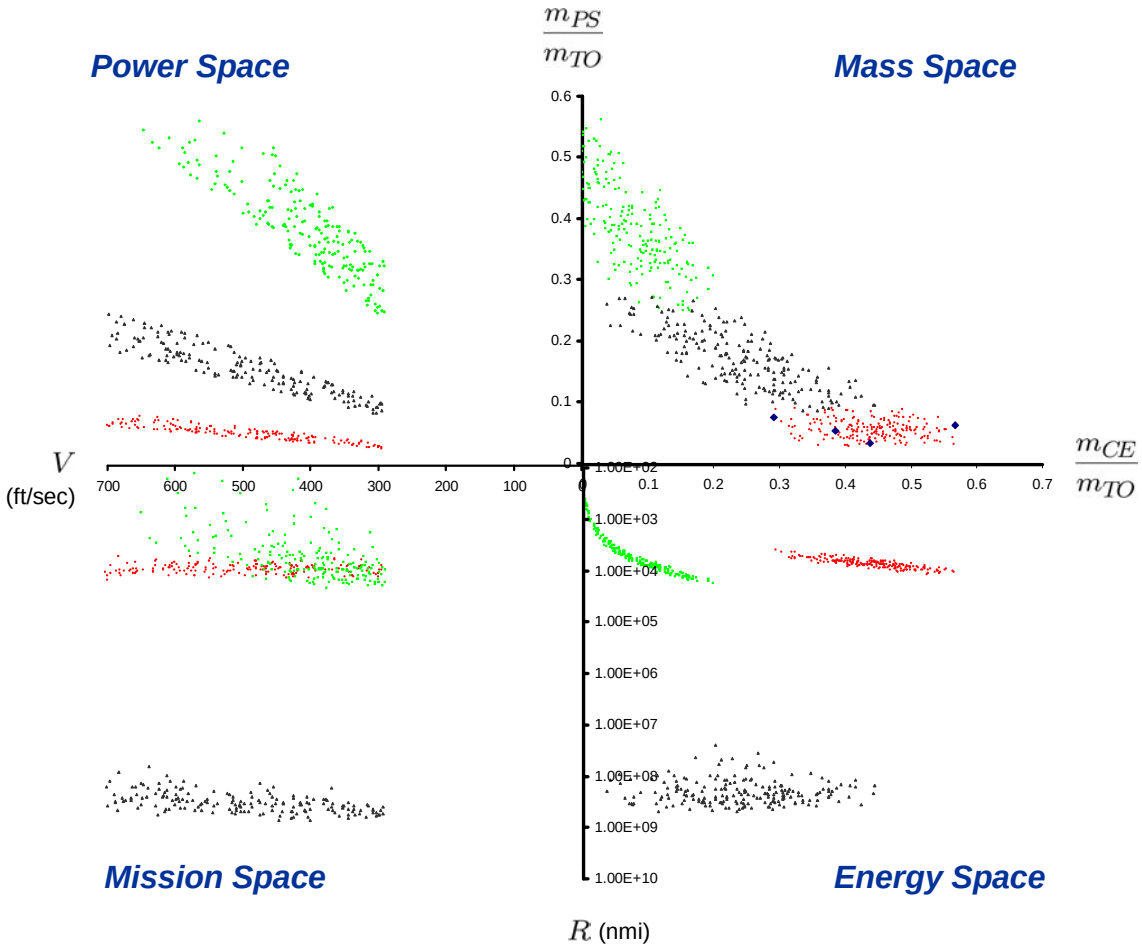

Architecture A (Turboprop + Jet Fuel)	Architecture B (PEM Fuel Cells + Hydrogen)	Architecture C (TIHE + Isomer)

Figure 48: The NAM ratio diagram of a high altitude unmanned aircraft

types of propulsion systems. As discussed in the previous section, the propulsion system weight is limited depending on the maximum allowed total aircraft weight, which underlies the limitation of available power. However, the maximum available power of other aircraft is not directly dictated by wing area.

Yet, as long as the coupling does not act as an active constraint on aircraft sizing, the coupling will be of no interest. Under the circumstances that the design power is determined to be considerably less than the maximum available power, the maximum available constraint does not act as an active constraint although the maximum available power is determined by wing area. However, the maximum available power is very likely to be an active design constraint in the design of solar-powered aircraft. The amount of vertically-aligned incoming solar radiation per unit area, often called the solar constant, is 1,352.8 watts per square meter. Both attenuation and radiation angles limit the actual energy conveyed from PV cells to much less than the solar constant. Thus, the available power from sunlight is considerably lower than the achievable power level of conventional IC engines. For example, if state-of-the art PV cells covered 541 square meters of the Boeing 747 wing shown in Figure 49, the system could deliver about 700 HP to a propeller, which equals roughly half of the maximum power of a P-51B/C Mustang's engine. The scarcity of power available from solar radiation leads to a typical integration of PV cells with wings. As shown with both the Pathfinder and Helios, PV cells are installed almost throughout the entire wing surfaces, implying that the maximum available power of solar-powered aircraft is directly limited by wing area.

In the next two sections, an additional design constraint imposed by the coupling of wing area and power available is derived for two different propulsion system architectures: a solar-powered electric propulsion system with or without regenerative fuel cells. In both cases, the constraint due to coupling of the maximum available power and aircraft size is established in terms of the maximum allowable wing loading.

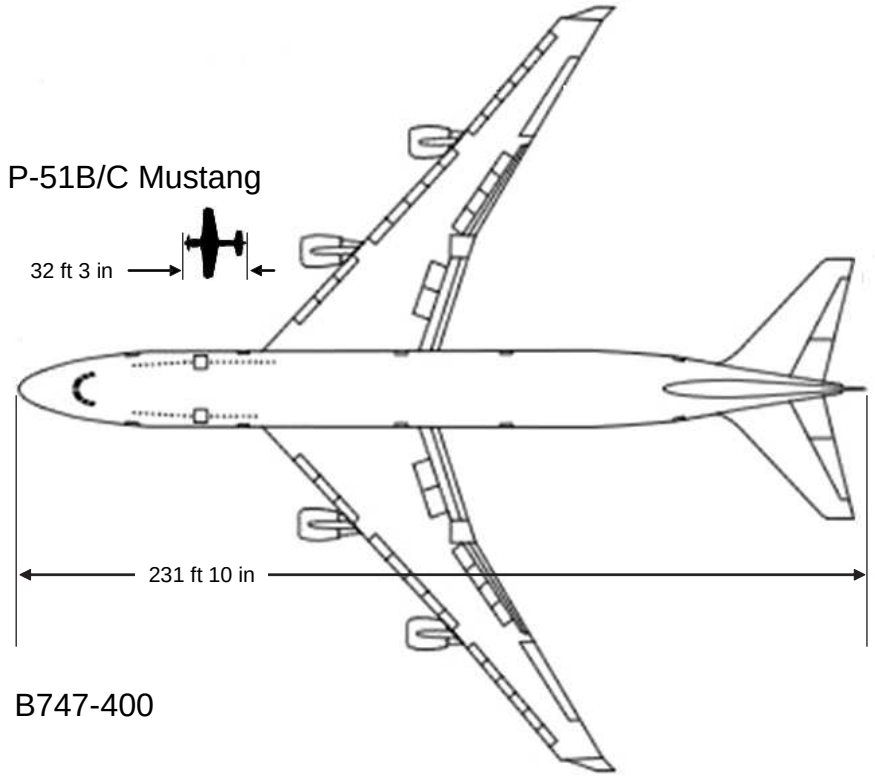

Figure 49: B747-400 vs P-51B/C Mustang

4.7.1 Application to Solar-Powered Aircraft

If the aircraft is powered by solar energy only, the flight is limited to a certain period of daytime when the PV cells provide sufficient power. Since the aircraft does not store any energy on-board, an energy balance is not included as a sizing constraint for this type of aircraft.

The available power from a photovoltaic panel varies with time of year and latitude. The total available power from the PV panels that covers $S_{ff} \times 100\%$ of the wing, is given as follows [138]:

$$P_{PV} = \sigma_{io}\tau\eta_{SC}SS_{ff}(\sin(\phi)\sin(\delta) - \cos(\phi)\cos(\delta)\cos(a)) \tag{104}$$

where τ is the solar attenuation factor, which varies with the location; η_{SC} is the PV cell efficiency; and ϕ is the latitude and δ is the earth declination angle. δ varies with

the day of the year (d_n), which is based on the vernal equinox ($d_n = 1$ is March 21st), and is given as

$$\delta = 0.4091 \sin(2\pi d_n/365) \tag{105}$$

The hour angle (a) is given by the following expression, where "i" is the instantaneous time of day in hours,

$$a = 2\pi i/23.935 \tag{106}$$

σ_{io} is the amount of incoming solar radiation per unit area on the atmosphere boundary at a given time and is given as follows:

$$\sigma_{io} = \sigma_{iom}(r_{orbm}^2/r_{orb}^2) \tag{107}$$

where r_{orbm} and σ_{iom} represent the mean distance from the earth to the sun and the amount of incoming solar radiation per unit area on the atmosphere boundary with the mean distance. The distance from the earth to the sun (r_{orb}) varies throughout the year and is computed by the following equations:

$$r_{orb} = r_{orbm}(1 - e^2)/(1 + e\cos(\theta)) \tag{108}$$

θ is given as follows:

$$\theta = 2\pi d_{n2}/365 \tag{109}$$

where the day number (d_{n2}) is based on the data of perihelion for earth's orbit, so $d_{n2} = 1$ is January 4th. The values for the constants used in the above equations are given below:

- The mean orbital radius of the Earth (r_{orbm}): 1.496 $\times$ 108 km
- The mean solar intensity at the Earth's orbital radius (S_{iom}): 1352.8 W/m^2
- The Earth's orbital eccentricity (e): 0.017
- The Earth's mean radius (r): 6.378 $\times$ 10^6 m

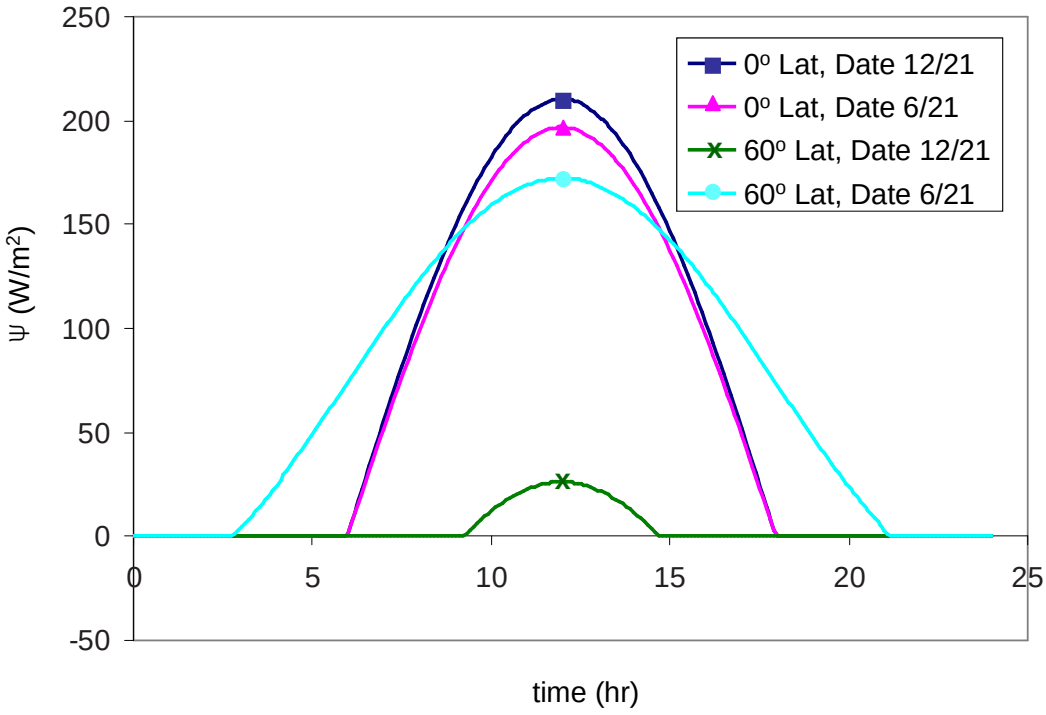

Figure 50: Available power per unit wing area for several combinations of geographic locations and dates

The available power from PV cells can then be rewritten as

$$P_{PV} = S\Psi \tag{110}$$

where Ψ stands for the amount of electric power produced by the PV cells per unit area of wing, computed by

$$\Psi = \sigma_{io}\tau\eta_{SC}S_{ff}(\sin(\phi)\sin(\delta) - \cos(\phi)\cos(\delta)\cos(a)) \tag{111}$$

The power available per unit wing area, Ψ is plotted against time in Figure 50, in which PV cell efficiency, PV cell fill factor, and solar attenuation factor(t) are 0.2, 75%, and 0.7, respectively.

The available power-to-weight ratio is given as a function of wing loading as follows:

$$\frac{P_{PV}}{W} = \Psi / \frac{W}{S} \tag{112}$$

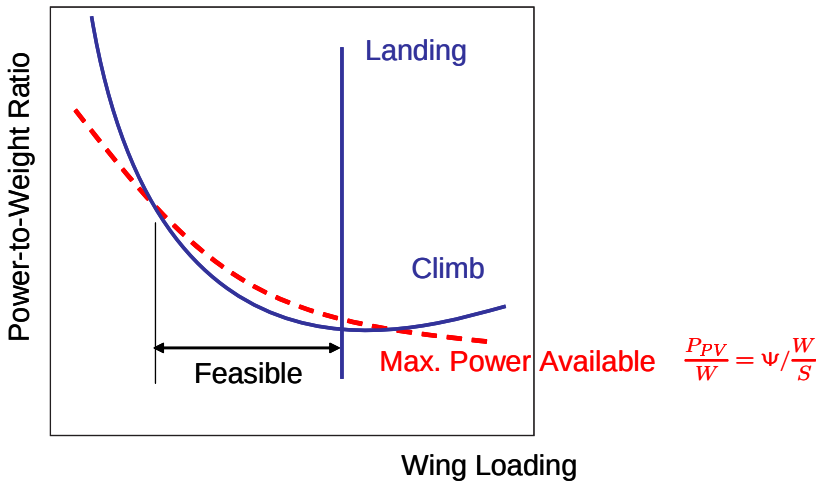

Figure 51: Constraint analysis of solar-powered aircraft

The required power-to-weight ratio for performance requirements can be computed by the power-based master constraint equation in §4.1. The available power-to-weight ratio and the required power-to-weight ratio are overlaid in Figure 51, in which the feasible design range of wing loading is determined where $\frac{P_{PV}}{W} \geq \frac{P_{required}}{W}$. Since higher wing loading reduces wing area and thus aircraft weight, the highest available wing loading value is very likely to be the optimum solution. It must be noted that the reference power in Eq. (112) is measured by the output power of the PV panels. The required power must be estimated accordingly.

4.7.2 Application to Solar-Powered Regenerative Propulsion Aircraft

Solar-powered regenerative propulsion is a type of propulsion system capable of re-generating internal energy sources such as fuel cells or an electric battery using solar energy and provides a possibility for virtually perpetual flight. Such a capability can be obtained when the PV cells provide sufficient extra energy during the day to re-generate internal energy sources for nighttime flight as illustrated in Figure 52. The on-board regenerative energy storage systems might include a Regenerative Fuel Cell

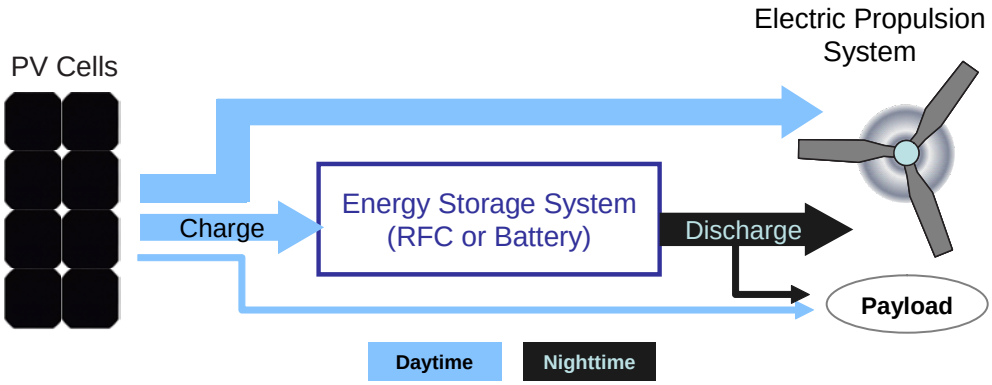

Figure 52: Illustration of a solar-powered regenerative propulsion system

(RFC) system envisioned for the AeroVironment Helios or a rechargeable lithium battery demonstrated by the AC Propulsion Solong drone [139]. Unlike aircraft powered solely by solar power, the energy balance throughout the entire 24 hour cycle must be addressed as a critical design constraint.

Figure 53 depicts the typical profile of a daily power cycle of a regenerative solar powered propulsion architecture. For the daytime period (T_d), the PV cells provide the power required for flight, payload, and regenerating an on-board energy storage. During the nighttime period (T_n), the on-board energy storage feeds the electric propulsion system. T_d, herein, is defined as a period of time within a day when the PV cells can produce the extra amount of power that can be diverted to regenerate the on-board energy storage system. Therefore, the PV cells subsidize the power demand right before and after the daytime period. The energy balance requirement can then be stated for daytime and nighttime operation.

$$\text{for daytime balance:} \qquad E_{sun}|_d = E_{flight}|_d + E_{StorIN} + E_{payload}|_d \tag{113}$$

$$\text{for nighttime balance:} \qquad E_{StorOUT} = E_{flight}|_n + E_{payload}|_n - E_{sun}|_n \tag{114}$$

A continuous flight for days or months is now possible when the total amount of daytime excess energy is at least the same as the energy required to regenerate

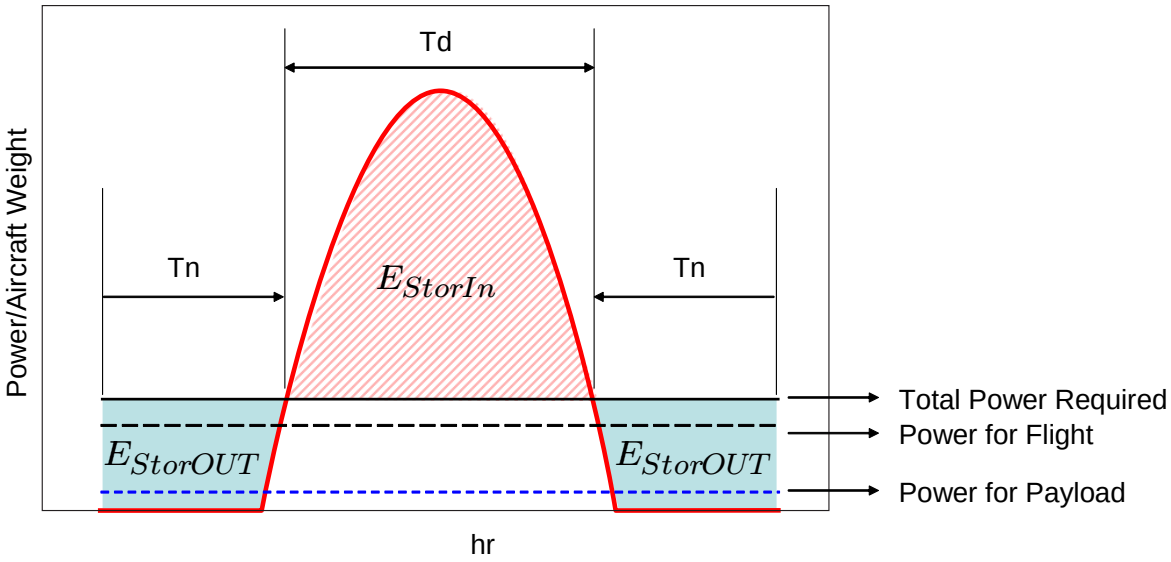

Figure 53: Power profile of solar-powered aircraft with a regenerative propulsion system

the energy storage system. Therefore, the diurnal energy balance requirement can be stated as follows:

$$E_{StorIN} \geq \frac{E_{StorOUT}}{\eta_{rt}} \tag{115}$$

where the round trip efficiency, denoted as η_{rt} is defined as the ratio of total energy output from the energy storage system to the total energy input transferred from PV cells to the energy storage system.

The physical meaning of Eq. (115) can be explained graphically with Figure 53. The gridded area that represents the total energy input must be greater or equal than the roundtrip efficiency times the shaded area that represents the total energy output from the energy storage system. Similar formulation of the diurnal energy balance has been proposed in previous research [140, 141]. Sharing the crux with previous work, this research attempts to reform the diurnal energy balance as an additional constraint with respect to wing loading.

The total energy obtained by PV panels during the daytime is given as follows:

$$E_{sun} = S \int_{T_d} \Psi dt \tag{116}$$

The energy required for level flight during the daytime is the integration of power required as follows:

$$E_{flight}|_d = \int_{T_d} \frac{D}{L} \frac{WV}{\Pi_\eta^+} dt \tag{117}$$

Combining Eq.(113)-(117), the daytime and nighttime energy balance are consolidated into the following single equation:

$$S\int_{T_d} \Psi dt \geq \int_{T_d} \left[\frac{D}{L} \frac{WV}{\Pi_\eta^+} + P_{PL} \right] dt + \frac{1}{\eta_{rt}} \int_{T_n} \left[\frac{D}{L} \frac{WV}{\Pi_\eta^+} + P_{PL} - S\int_{T_n} \Psi dt \right] dt \tag{118}$$

Finally, by rearranging Eq.(118) the maximum allowable wing loading meeting the diurnal energy balance is given as follows:

$$\left(\frac{W}{S} \right)_{\max} = \frac{\int_{T_d} \Psi dt + \frac{1}{\eta_{rt}} \int_{T_n} \Psi dt}{\int_{T_d} \left[\frac{D}{L} \frac{V}{\Pi_\eta^+} + \frac{P_{PL}}{W} \right] dt + \frac{1}{\eta_{rt}} \int_{T_n} \left[\frac{D}{L} \frac{V}{\Pi_\eta^+} + \frac{P_{PL}}{W} \right] dt} \tag{119}$$

$(W/S)_{\max}$ does not involve power-to-weight ratio, appearing as a vertical line in the constraint analysis space as illustrated in Figure 54.

This equation cannot be solved in a closed form because D/L, T_d, and T_n depend on W/S. Therefore, it requires an iterative process, in which W/S is manipulated until the equation is satisfied. In addition, there may be a need for another iteration loop to solve the equation. If payload power is given as a fixed input, the ratio of aircraft weight to payload power (P_{PL}/W) in Eq.(119) varies with the aircraft weight, which implies the constraint analysis is coupled with weight estimation. Several approaches can be taken to solve this problem. One possible approach is illustrated in Figure 55. The process begins with estimating the power profile of Ψ for a given time of year, latitude, PV cell efficiency, and PV cell filling factor. This step is followed by an iteration loop, in which aircraft weight is varied. Note that Ψ is insensitive to the sizing parameters, and thus does not have to be involved in the iteration process.

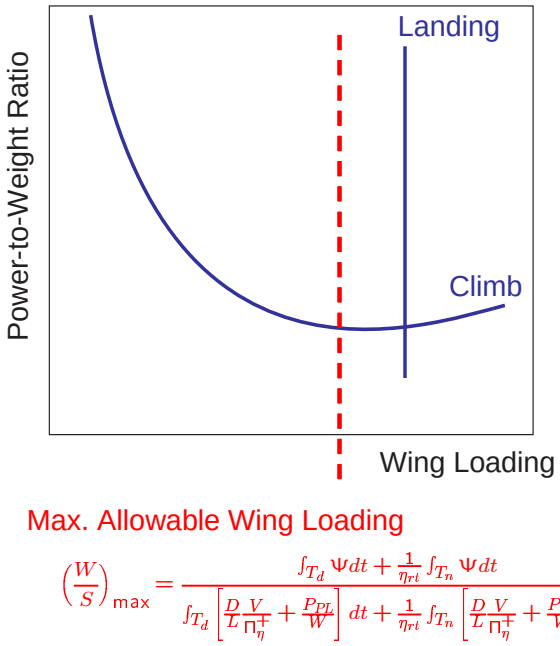

Figure 54: Constraint analysis of solar-powered aircraft with a regenerative propulsion system

The ratio of aircraft weight to payload power (P_{PL}/W) varies with every update of the aircraft's weight during its iteration process. For the given P_{PL}/W, the maximum allowable wing loading ($(W/S)_{\max}$) is computed from a nested iteration loop using Eq. (119). Subsequently, the total power to weight ratio P/W can be estimated from the constraint analysis. These analyses lead to estimations of P and S, followed by an update of aircraft weight. These steps are iterated until aircraft weight sufficiently converges.

Rizzo and Frediani [142] derived a similar wing loading constraint due to the diurnal energy balance from their work on solar powered aircraft. Zero lift drag coefficients are predicted by a simple equation that includes wing area, wetted area, and flat plate friction drag coefficient and is given as a function of the Reynolds number. The induced drag coefficient is predicted using a simple equation that includes the wing aspect ratio and Oswald's efficiency factor. However, the authors did not consider the power consumption by the payload. Another limitation is that the aerodynamic

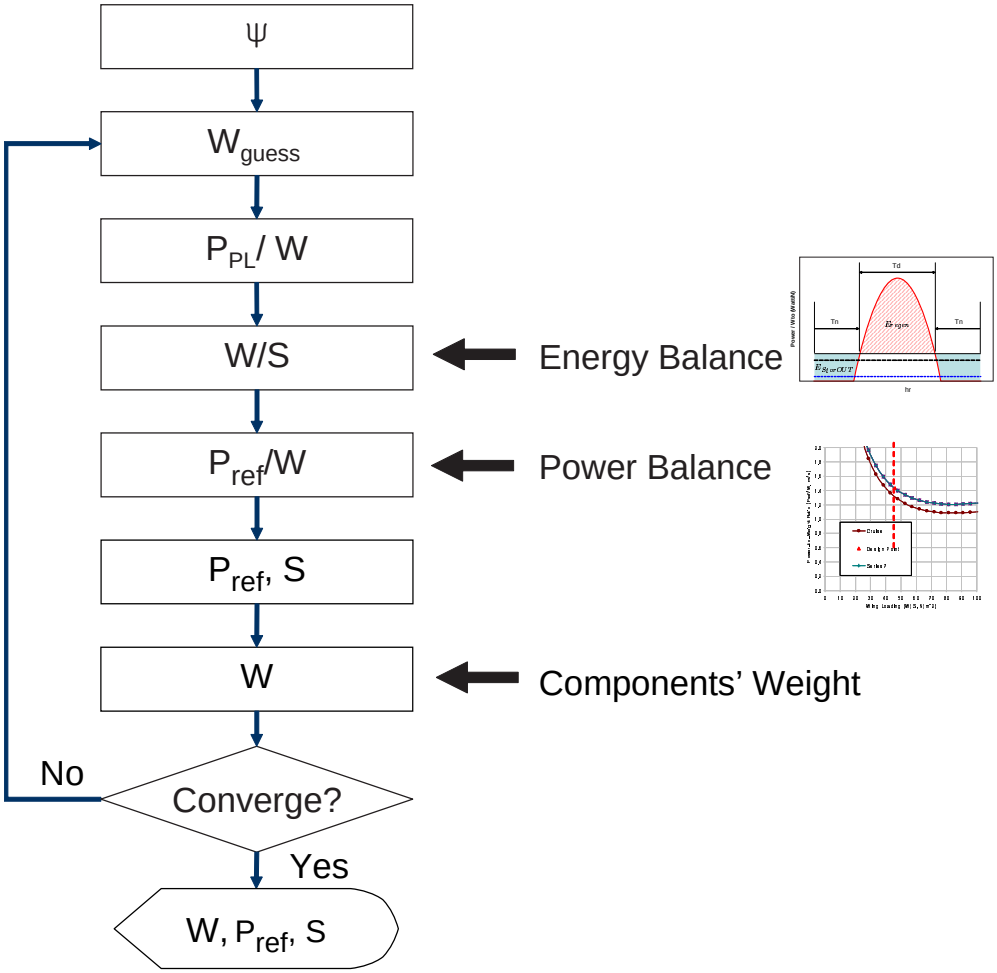

Figure 55: Sizing process of solar-powered aircraft with a regenerative propulsion system

coefficients are hard-coded into the wing loading constraint, which prevents designers from using more reliable aerodynamic analysis results when they are available.

CHAPTER V

FORMULATION OF THE PROBABILISTIC AIRCRAFT SIZING METHOD

The architecture-independent formulation presented in the previous chapter paves the way for the development of a generalized aircraft sizing environment that is capable of handling various types of unconventionally propelled aircraft in a deterministic way. Nevertheless, none of the design parameters involved in the formulation can be accurate or certain since aircraft sizing is performed during the pre-conceptual or conceptual design phase, when the least amount of knowledge about the system is available. Therefore, if an aircraft is deterministically sized without adequate design margins, any unforeseen changes to the underlying assumptions about the associated parameters will result in failure of the design to meet any or all of the design requirements [100]. On the contrary, if extraneous design margins are imparted, the cost may increase without commensurate benefits of risk mitigation. This antipodal nature of determining design margins has spawned Research Question II in §3.2: how to allocate design margins against probabilistic design constraints intelligently.

This chapter presents the probabilistic aircraft sizing method (PASM) as an attempt to solve Research Question II, beginning with discussions related to several approaches to probabilistically constrained optimization problems found in literature in §5.1. This discussion and a numerical example presented in §5.2 reveal that the chance-constrained programming (CCP) is suitable for formulating a probabilistic aircraft sizing problem under uncertainty. In §5.3, PASM is formulated as the form of the CCP, built upon the equations of AIASM, which is followed by an abridged discussion

on numerical techniques to solve the resultant problem in §5.4. §5.5 introduces several derivative formulations that can be extended from the original formulation. The last section presents two sensitivity analysis techniques that enhance the capability of PASM.

5.1 Approaches to Probabilistically Constrained Optimization Problems

Fields such as finance, management and industrial engineering have rigorously advanced various methods to solve probabilistically constrained problems. Those methods can be broadly classified into three categories. The first one is an "averaging approach" that first fixes the random variables at their mean values or any other representative value, and then solves the resultant deterministic problem. This approach seems effortless or like oversimplifying the probabilistic nature of a system. Nevertheless, it can be said that this method is implicitly exercised for every deterministic optimization problem, provided that in reality there are no truly deterministic problems.

The second method is a "penalizing approach." In certain situations, constraint violations can be corrected by appropriate compensating decisions. In such circumstances, one would rather investigate more challenging options that result in a better objective function value with an increased chance of violating the constraints. If the costs of the compensation can be quantified in the same *currency* of the objective function, the constraint violation can be considered a penalty to the objective function often modeled as a recourse function denoted as $Q(\mathbf{x}, \boldsymbol{\xi})$. The objective of this type of problem is reestablished as minimizing the total expected cost, which is a summation of the original cost function and the cost incurred by constraint violations as follows:

$$\min_{\mathbf{x}} \; f(\mathbf{x}) + \mathbb{E}[Q(\mathbf{x}, \boldsymbol{\xi})] \tag{120}$$

This is the fundamental idea of the penalizing approach, and it has been further

developed into what is known as a two-stage or multi-stage stochastic programming [143, 144].

However, the concept of compensation is not appropriate in many applications where safety-relevant restrictions are critical design constraints, or the compensation cost cannot be modeled in the same "currency" of the original objective function in any reasonable way. The aircraft sizing problem also fits into this category. Under such circumstances, one would like to insist on feasibility as much as possible. However, such an ideal solution may be difficult to obtain in actual problems for several reasons. First, one can hardly find any decision that would definitely exclude later constraint violations in the design of complex systems. Second, even if designers can identify the worst case scenario, the objective function value may be prohibitive. In general, cost and reliability conflict with each other in applications in which the optimum solution is pushed to the constraint boundaries. A more conservative decision must commit a higher cost, but it is impossible to create a perfectly safe design because of unexpected extreme events. On the other hand, it makes sense to call decisions feasible whenever they are feasible with a high enough probability. Chance-Constrained Programming (CCP) is a mathematical formulation of this type of stochastically (or probabilistically) constrained problem. A generic expression for such a probabilistic constraint as an inequality is given as follows:

$$\begin{aligned} \min_{\mathbf{x}} \quad & f(\mathbf{x}) \\ \text{s.t.} \quad & \mathbb{P}\left[g_i(\mathbf{x}, \boldsymbol{\xi}) \geq 0\right] \geq \alpha_{g_i} \end{aligned} \tag{121}$$

where $\mathbf{x}$ and $\boldsymbol{\xi}$ are the decision and random vectors, respectively, and "$g(\mathbf{x}, \boldsymbol{\xi})_i \geq 0$" is the i^{th} inequality constraint. The optimum solution to this type of problem can be found at the location of minimizing the objective function inside of the feasible set, all entities of which satisfy the probabilistic constraints with a probability of at least α_{g_i}. In some cases, the probability level is strictly set from the very beginning (e.g., $\alpha_{g_i} = 0.95, 0.99$ etc.) by management decisions. In other situations, the decision

maker may only have a nebulous idea of the properly chosen level of α_{g_i}, aware that higher values of α_{g_i} lead to higher costs. Under such circumstances, the information of the objective function trends with respect to the target reliability can assist the arbiter. As it turns out, for most cases, α_{g_i} can typically be increased over quite a wide range without significantly affecting the optimal value of the problem, until it approaches 1, and then a strong increase in costs becomes evident. In this way, models with chance constraints can also provide insights into a good compromise between *cost* and *safety*, while stochastic programming offers a trade-off between *cost at present* and *cost in the future*.

The chance-constrained approach has a long history, dating back to the work of Charnes and Cooper in linear programming in 1959 [145]. Since its conception, the method has been mainly applied to the fields of civil engineering, industrial engineering, and finance, such as inventory systems sizing [146], ecology model analysis [147], and portfolio selection [148, 149], in which uncertainty enters the inequalities that describe the proper working of a system under consideration. The earliest effort to apply the CCP approach to engineering design problems was made by Rao [150] who considered the engineering structural security of the probabilistic constraints in 1980 [151]. After that, the method has also been applied to structural optimization problems under uncertainty [152, 153, 154, 155] under the name of reliability-based design optimization (RBDO). In the RBDO problem, the probabilistic constraints are often formulated as elemental reliability indices corresponding to various limit states [156], which are essentially equivalent to the target probability in CCP. However, not much research has been performed for the application of the concept of CCP to aerospace vehicle designs so far. Smith and Mahadevan [157] applied the RBDO approach to the design of a second-generation reusable launch vehicle, in which a single probabilistic constraint was considered. However, no literature regarding CCP or RBDO approaches to airplane system designs has been found.

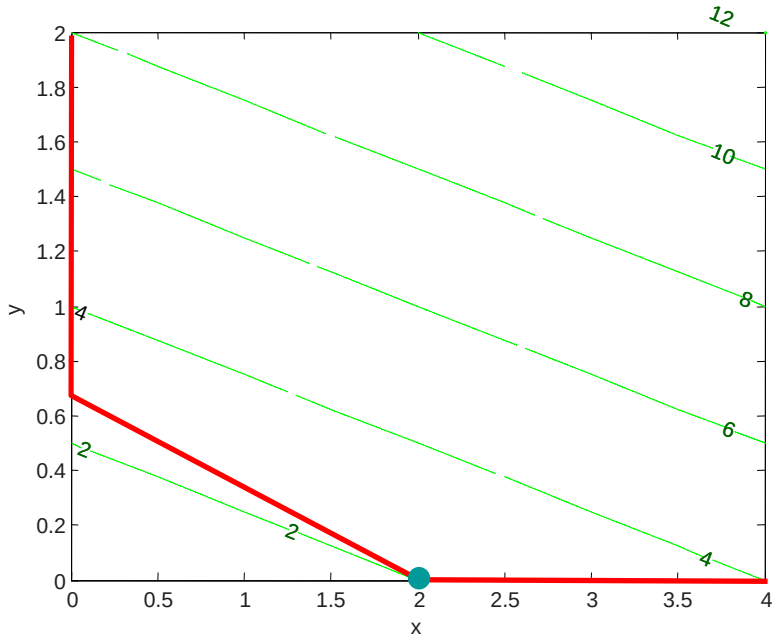

Figure 56: Design space of a deterministic optimization problem

5.2 A Numerical Example of Optimization Under Uncertainty

This section presents the application of the probabilistic approaches presented in the previous section to a numerical example problem to articulate the difference in the approaches of the methods. A simple deterministic linear programming is given as follows:

$$\begin{aligned} \min_{x,y} \quad & f = x + 4y \\ \text{s.t.} \quad & x + 3y \geq 2 \\ & x \geq 0 \\ & y \geq 0 \end{aligned} \tag{122}$$

The design space of this problem is illustrated in Figure 56. The optimum solution to this problem is found at $x = 2$ and $y = 0$, where the objective function value is 2.

Now, it is assumed that the two coefficients of x and y in the first linear constraint

are not deterministic but probabilistic, following normal distributions, the mean values of which are their deterministic values, 1 and 3, and the standard deviation values of which are 1. Then the optimization problem is given as the following statement:

$$\begin{aligned} \min_{x,y} \quad & f = x + 4y \\ \text{s.t.} \quad & \xi_1 x + \xi_2 y \geq 2 \\ & x \geq 0 \\ & y \geq 0 \\ \text{where} \quad & \xi_1 \sim N(1, 1^2) \text{ and } \xi_2 \sim N(3, 1^2) \end{aligned} \tag{123}$$

Unlike the previous deterministic system, the feasible solution area of this problem is not fixed but *amorphous*. One intuitive approach, a so-called averaging approach, is to fix the random variables at their mean value and to solve the resultant deterministic optimization problem, which results in an identical solution of the original deterministic problem. Nevertheless, the solution of the probabilistic problem can only satisfy the constraints by chance. The probability of meeting the constraint at the location of the solution can be computed by converting the linear combination of normal distributions into a standard normal distribution, yielding 0.5. However, this approach is not available when one wants to find a solution that can ensure a higher probability of success.

5.2.1 Deterministic Solution Sampling (DSS) Method

An alternative approach is the deterministic solution sampling (DSS) method which wraps the optimization process with a Monte Carlo simulation and sequentially solves a deterministic optimization problem which is set up with a set of sampled constraints. A certain number of simulations produce a set of optimum solutions, the distribution of which is shown in Figure 57 along with a set of corresponding objective function values, whose cumulative probability distribution (CDF) is depicted in Figure 58. What is the implication of the two graphs? The distribution of the objective function

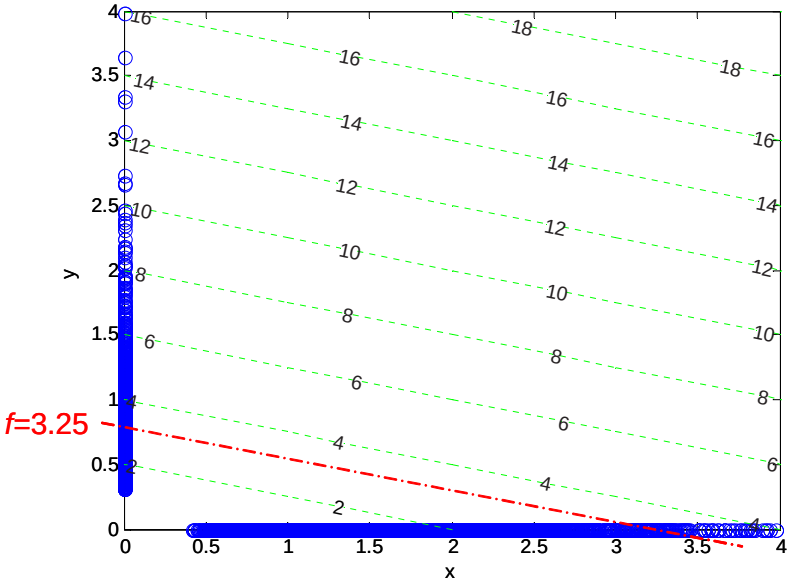

Figure 57: Optimum solutions from Monte Carlo Simulation

obtained by DSS method encompasses all possible outcomes of the objective function values from a "wait and see" type simulation, which assumes that the optimum design solution will and can be achieved after all uncertainty sources are cleared. If one wants a 90% probability of meeting the constraint, then will setting the design variables to those corresponding to 90% of the cumulative probability of the objective function in Figure 58 be the solution? The answer is "No," and even if the answer were "Yes," this approach does not provide a unique solution. From Figure 58, the objective function values at 90% of the cumulative probability is estimated at 3.25. Two solutions whose objective function value is 3.25 exist as shown in Figure 57.

5.2.2 Two-Stage Stochastic Programming Method

Two-stage stochastic programming can be used when the following assumptions are valid:

- The designer can correct constraint violation after all random variables are

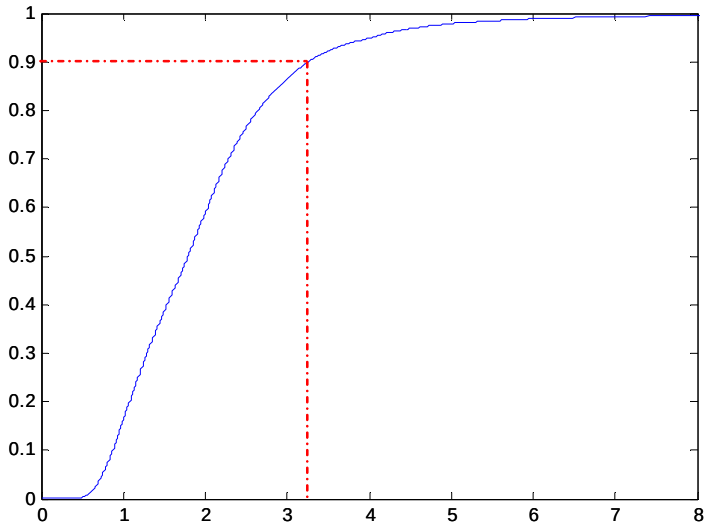

Figure 58: CDF of optimum values of the objective function of the Monte Carlo simulation

observed.

- The cost associated with the compensation is proportional to the shortage to the constraint.
- The objective is to minimize the expected total cost, the sum of the original cost function and the cost incurred by compensation.

Based upon the above assumptions, the given problem is formulated as the following two-stage stochastic programming:

$$\min_{x,y} \quad f = x + 4y + \mathbb{E}[Q(x, y, \xi_1, \xi_2)]$$

$$\text{where} \quad Q(x, y, \xi_1, \xi_2) = \begin{cases} c_p(2 - \xi_1 x - \xi_2 y) & \text{if } (2 - \xi_1 x - \xi_2 y) > 0 \\ 0 & \text{otherwise} \end{cases} \tag{124}$$

$$\xi_1 \sim N(1, 1^2) \text{ and } \xi_2 \sim N(3, 1^2)$$

Q, a recourse function representing the cost incurred by the compensation, is assumed to be proportional to the minimum amount of the adjustment required to make the

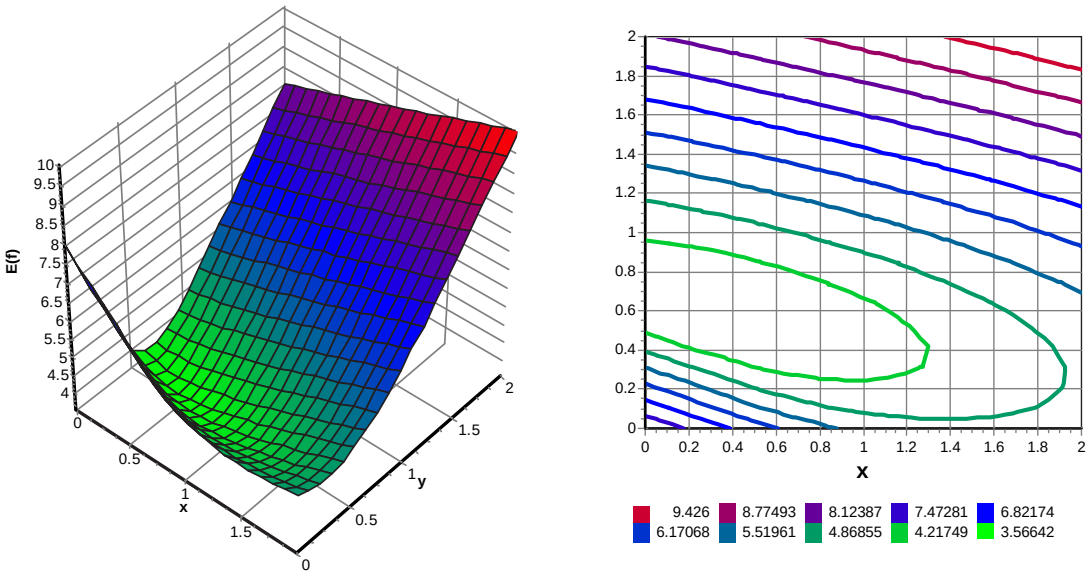

Figure 59: The total cost function of the two-stage stochastic programming problem

constraint feasible, that is, the penalty coefficient (c_p) multiplied by the amount of constraint violation ($2 - \xi_1 x - \xi_2 y$). The optimum solution to the problem, when $c_p = 4$, is found at $x^* = 0.334$, $y^* = 0.584$ and the value of the objective function is 3.567. The objective function, $f = x + 4y + \mathbb{E}[Q(x, y, \xi_1, \xi_2)]$, is plotted in Figure 59.

Optimum solutions of this problem are heavily affected by the values of c_p as shown Figure 60, which depicts the optimum values of the total cost ($x + 4y + \mathbb{E}[Q(x, y, \xi_1, \xi_2)]$) and the design variables varying the value of c_p. As c_p decreases, the optimum moves toward the point ($x = 0$, $y = 0$), where the probability of failure is the greatest, but the original objective function ($x + 4y$) is the most favorable. These results are consistent with the real world observation: wherever is less penalty incurred by a constraint violation, a more aggressive decision will appear attractive.

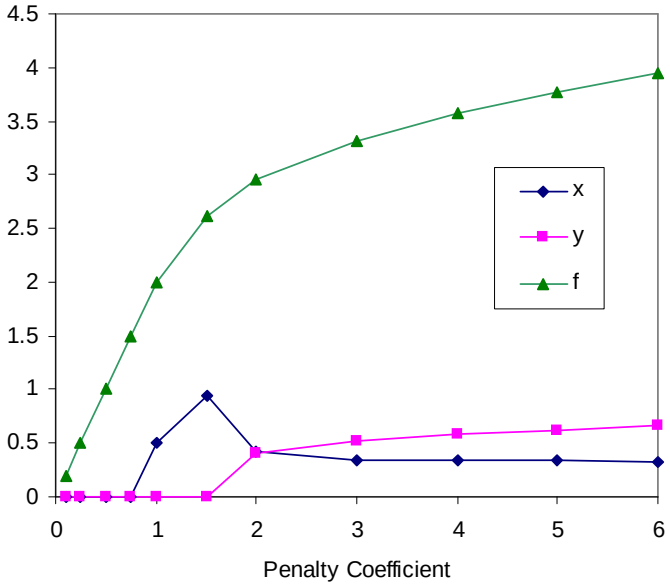

Figure 60: Optimum solutions per the value of the penalty coefficient

5.2.3 CCP Method

If any compensation is not allowed, the two-stage stochastic programming is not appropriate. Under such circumstances one would rather seek an optimum solution satisfying the probabilistic constraint with a certain level of probability, which is an intrinsic idea of the CCP. The given problem is formulated as follows:

$$\begin{aligned} \min_{x,y} \quad & f = x + 4y \\ \text{s.t.} \quad & \mathbb{P}[\xi_1 x + \xi_2 y \geq 2] \geq \alpha \\ & x \geq 0 \\ & y \geq 0 \\ \text{where} \quad & \xi_1 \sim N(1, 1^2) \text{ and } \xi_2 \sim N(3, 1^2) \end{aligned} \tag{125}$$

A linear combination of normal distributions of two random variables, $\xi_1 x + \xi_2 y$ is also a normal distribution whose mean and standard deviation are given as $x + 3y$ and $\sqrt{x^2 + y^2}$. Therefore, $\mathbb{P}[\xi_1 x + \xi_2 y \geq 2] \geq \alpha$ is true, if and only if $(\mu_1 x + \mu_2 y -$

$2)/\sqrt{x^2+y^2} \geq z_\alpha$ is true, where μ_1 and μ_2 stands for the mean value of normal distributions of ξ_1 and ξ_2, and z_α denotes the $\alpha \times 100^{\text{th}}$ percentile of the standard normal distribution. Thus, the probabilistic inequality constraints can be converted into a deterministic-equivalent constraint and the probabilistic optimization problem is transformed into an equivalent deterministic optimization problem as follows:

$$\begin{aligned} \min_{x,y} \quad & f = x + 4y \\ \text{s.t.} \quad & \frac{(\mu_1 x + \mu_2 y - 2)}{\sqrt{x^2+y^2}} \geq z_\alpha \\ & x \geq 0 \\ & y \geq 0 \end{aligned} \tag{126}$$

Using a nonlinear constrained optimization algorithm built in the MATLAB® optimization suite, the optimum solution of the above deterministic optimization problem for $\alpha = 0.9$ is found at $x = 0.4534$ and $y = 0.9748$ where the objective function is computed at $f = 4.3527$. Figure 61 shows the deterministic-equivalent constraints for different values of α. An important observation is that the linear probabilistic constraint is converted into a nonlinear constraint.

5.2.4 Lessons Learned

By DSS method, the objective function value at 90% of CDF is estimated at approximately 3.25. However, the optimum objective function value satisfying 90% of α in the CCP problem is found to be 4.2. What causes this discrepancy? In the case of DSS, the values of the design variables corresponding to 90% of the cumulative probability of the objective function are not equivalent to meeting all constraints with 90% chance. In fact, the values of α at the two design points yielding the objective function value at 90% of CDF are estimated to be approximately 65%. The bottom line is that the DSS approach is not suitable for obtaining an optimum solution to a probabilistically constrained problem although it is useful for assessing and comparing different architectures.

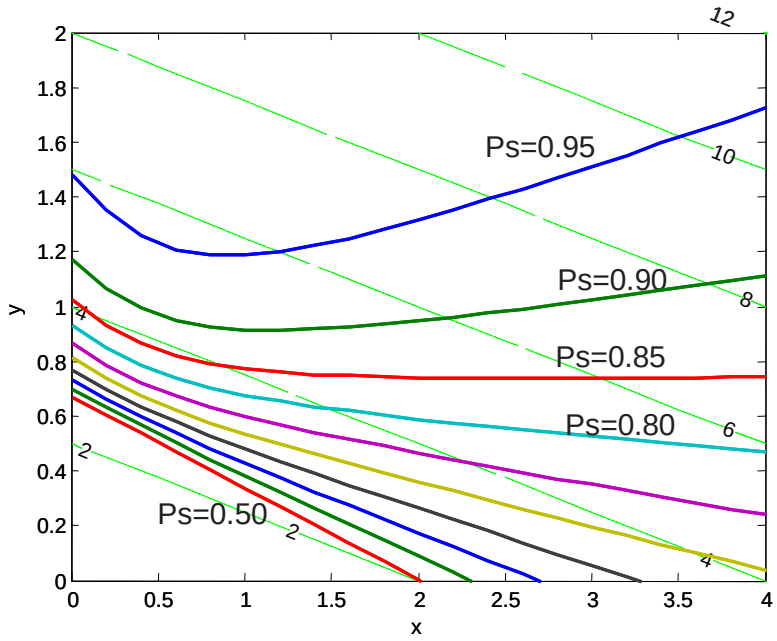

Figure 61: Equivalent deterministic constraints

The reason for highlighting the incongruousness of the DSS approach for probabilistically constrained optimization problems is that the approach may be intuitively appealing in the practice of aircraft sizing, when a deterministic aircraft sizing environment is ready to go. One would simply hook up the environment to a random number generator and run it! Nevertheless, this is essentially another practice of the DSS approach, and the implications of the output from the simulation would be the same as those of the example study.

The penalizing approach is appropriate for the application of probabilistically constrained optimization problems where the expected penalty costs, measuring the expected amount of surplus and/or shortage, can be defined. However, such penalty costs can hardly be defined in an aircraft sizing problem. For instance, how can we quantify the violation of the take-off field length by 100 ft in terms of pounds or dollars if the objective function is given as aircraft weight or cost, respectively? On the other hand, the CCP approach measures the probabilities of having any shortage

in design constraint(s), irrespective of its size [158]. From these observations the CCP approach appears the most appropriate for formulating aircraft sizing problems under uncertainty.

5.3 Standard Form of the Probabilistic Aircraft Sizing Method

The discussions of the first two introductory sections in this chapter have disclosed that the CCP is the most germane approach to formulating aircraft sizing problems in which the decision maker would compromise the associated risks with cost in a quantitative manner. This section presents a standard form of PASM. For the sake of simplicity, it is assumed that the propulsion system consists of a single power-path and single energy source. After the probabilistic formulation of the simple system is complete, the formulation will be further extended to a more complex system.

5.3.1 Integration with AIASM

A general idea regarding the application of CCP to aircraft sizing problems is contained in Eq. (46) presented in §3.4.2. The equation can be rewritten in terms of P_{ref} and W_{energy} for the use of the AIASM formulation developed in the previous chapter.

$$\begin{aligned} \min_{\mathbf{x}} \quad & \tilde{f} \\ \text{s.t.} \quad & \mathbb{P}\left[\frac{\tilde{P}_{ref}}{\tilde{W}_{TO}} \geq \tilde{\Theta}\right] \geq \alpha \\ & \mathbb{P}\left[\frac{\tilde{W}_{energy}}{\tilde{W}_{TO}} \geq \tilde{\Omega}\right] \geq \alpha \end{aligned} \tag{127}$$

where $\tilde{W}_{energy}$ is the weight of an on-board energy source, physically measured in the production aircraft, and $\tilde{\Omega}$ is the required consumable energy weight fraction estimated via mission analysis.

The power balance constraint in Eq. (127) must hold for all performance requirements such as take-off field length, climb, maximum speed, service ceiling, sustained turn, and so forth. If some of the parameters associated with the constraints are

subject to uncertainty, the required power to weight ratio is given as follows:

$$\tilde{\Theta}_i = \Theta_i\left(\frac{\tilde{W}_{TO}}{S}, \tilde{\mathbf{p}}_i, \mathbf{p}_i\right) (i = 1, \cdots, n_p) \tag{128}$$

where $\tilde{\mathbf{p}}_i$ stands for a vector of random parameters; $\mathbf{p}_i$ stands for a vector of fixed parameters; n_p represents the number of performance constraints; and Θ_i represents the required power-per-aircraft weight as a function of wing loading and other parameters for i^{th} constraints listed in Appendix A. For example, c_1 stands for take-off field length, c_2 stands for climb, and so forth.

Many newly developed aircraft, especially military aircraft, are designed to be multiple-mission capable. Usually, one driving mission appears transparently and it can be used as a sizing mission. However, as more aircraft move toward multi-mission capability, a dominant mission will become rarer. The fuel balance constraint is very likely to include a multitude of inequality constraints. Then the required energy weight fraction representing the production aircraft mission performance in the future can be expressed as the following probabilistic form:

$$\tilde{\Omega}_j = \Omega_j\left(\frac{P_{ref}}{\tilde{W}_{TO}}, \frac{\tilde{W}_{TO}}{S}, \tilde{\mathbf{p}}_j, \mathbf{p}_j\right) \ (j = 1, \cdots, n_m) \tag{129}$$

where n_p represents the number of mission fuel constraints. Then Eq. (26) changes as follows:

$$\begin{aligned} \min_{\mathbf{x}} \ & \tilde{f} \\ \text{s.t.} \ & \mathbb{P}\left[\frac{\tilde{P}_{ref}}{\tilde{W}_{TO}} \geq \Theta_i\left(\frac{\tilde{W}_{TO}}{S}, \tilde{\mathbf{p}}_i, \mathbf{p}_i\right)\right] \geq \alpha_i \\ & \mathbb{P}\left[\frac{\tilde{W}_{energy}}{\tilde{W}_{TO}} \geq \Omega_j\left(\frac{\tilde{P}_{ref}}{\tilde{W}_{TO}}, \frac{\tilde{W}_{TO}}{S}, \tilde{\mathbf{p}}_j, \mathbf{p}_j\right)\right] \geq \alpha_j \end{aligned} \tag{130}$$

where $\mathbf{x} = [\tilde{P}_{ref}, S, \tilde{W}_{energy}]$, $i = 1, \cdots, n_p$, and $j = 1, \cdots, n_m$.

5.3.2 Decision Variables as Random Variables

$\tilde{P}_{ref}$ and $\tilde{W}_{energy}$ of the three decision variables may be subject to randomness. In the sense that the wing area may vary due to manufacturing tolerances and thermal

expansions/contractions in its operation, S possesses inherent uncertainty. However, the impact of such variation on aircraft performance is deemed less significant compared with other factors. Therefore, S is considered a deterministic variable in this research. Suppose that these two quantities are functions of random parameters given as a vector form, $\tilde{\mathbf{v}}$. Then the random distribution of each parameter is replaced with a deterministic value, $\breve{v}_i$ multiplied by a normalized distribution, ζ_i as follows:

$$\tilde{v_i} = \zeta_i \breve{v_i} \tag{131}$$

The deterministic values, $\breve{\mathbf{v}}$, are the most likely values selected within the distribution of each random variable by the responsible disciplines. Notice that all necessary engineering work of the design team cannot be done or does not have to be done in a probabilistic manner. Describing technical data in probabilistic terms, for example, may bring inefficiency and inconsistency to communication and documentation. Therefore, most engineering tasks, especially disciplinary activities, are performed in a deterministic manner. Such deterministic values are the most reliable and latest engineering data which are supposed to be shared by all disciplines in a consistent manner.

It follows that the random response of the reference power of a power plant can be expressed as follows:

$$\tilde{P}_{ref} = P_{ref}|_{\breve{\mathbf{v}}} \ \zeta_P \tag{132}$$

where $P_{ref}|_{\breve{\mathbf{v}}}$ is the reference power defined by the deterministic values of the random variables, and ζ_P, given as a function of $\boldsymbol{\xi}$, is the normalized distribution of $\tilde{P}_{ref}$ to $P_{ref}|_{\breve{\mathbf{v}}}$. The random response of the amount of available energy can be expressed as follows:

$$\tilde{W}_{energy} = W_{energy}|_{\breve{\mathbf{v}}} \ \zeta_{W_{energy}} \tag{133}$$

where $W_{energy}|_{\breve{\mathbf{v}}}$ is the amount of available energy calculated with a vector of the

deterministic values of the random variables, denoted as $\breve{\mathbf{v}}$, and $\zeta_{W_{energy}}$ is the distribution of $\tilde{W}_{energy}$ normalized by $W_{energy}|_{\breve{\mathbf{v}}}$. By combining Eq. (132), the first set of constraints in Eq. (130) can be rewritten with respect to $\breve{\mathbf{v}}$ as follows:

$$\mathbb{P}\left[\frac{\zeta_P P_{ref}|_{\breve{\mathbf{v}}}}{\tilde{W}_{TO}} - \Theta_i\left(\frac{\tilde{W}_{TO}}{S}, \tilde{\mathbf{p}}_i, \mathbf{p}_i\right) \geq 0\right] \geq \alpha_i \ (i = 1, \cdots, n_p) \tag{134}$$

where n_p is the number of constraints.

Similarly, by combining Eq. (133), the second set of constraints in Eq. (130) can be expressed as follows:

$$\mathbb{P}\left[\frac{\zeta_{W_{energy}} W_{energy}|_{\breve{\mathbf{v}}}}{\tilde{W}_{TO}} - \Omega_j\left(\frac{\zeta_P P_{ref}}{\tilde{W}_{TO}}, \frac{\tilde{W}_{TO}}{S}, \tilde{\mathbf{p}}_j, \mathbf{p}_j\right) \geq 0\right] \geq \alpha_j \ (j = 1, \cdots, n_m) \tag{135}$$

5.3.3 Standard Form of PASM

One distinguishing feature of the aircraft sizing problem is that the objective function is also probabilistic as well as the constraints. The objective function in Eq. (130) may be the take-off gross weight that has been commonly used for aircraft sizing. Other candidates for the objective function are other metrics, which include total cost (acquisition cost and operating cost) or an overall evaluation criterion that represents an aggregate quantity of multiple criteria. Regardless of the choice, the quantity deemed as the objective function is very likely to involve uncertainty. One way to handle such a probabilistic objective function is a mean value-based approach [157], by which the probabilistic objective function $\tilde{f}$ is deterministically treated by converting it into the expectation of the probabilistic objective function ($\mathbb{E}[\tilde{f}]$). Such a mean value-based approach is widely used in the current RBDO practice [159].

Finally, the standard form of PASM for an energy-propulsion architecture with a single power-path is formulated as follows:

$$\begin{aligned} \min_{\mathbf{x}} \ & \mathbb{E}[\tilde{f}] \\ \text{s.t.} \ & \mathbb{P}\left[g_i(\mathbf{x}, \boldsymbol{\xi})|_{\breve{\mathbf{v}}} \geq 0\right] \geq \ \alpha_{g_i} \ \ (i = 1, \cdots, n_p + n_m) \\ \text{where} \ & \mathbf{x} = [P_{ref}|_{\breve{\mathbf{v}}}, \ S, \ W_{energy}|_{\breve{\mathbf{v}}}] \end{aligned} \tag{136}$$

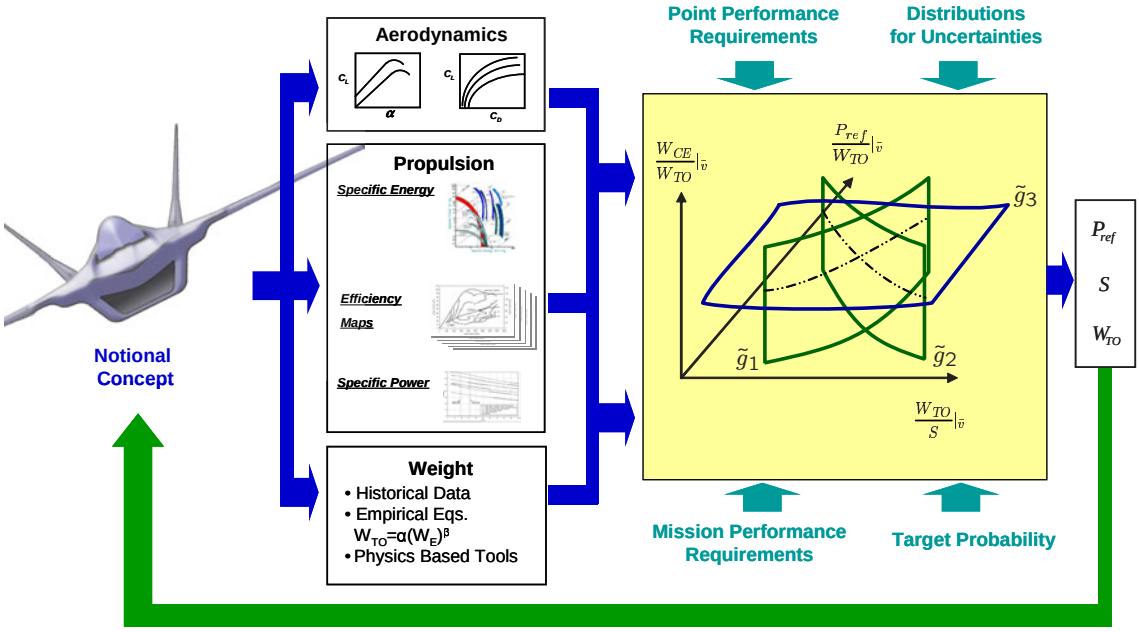

Figure 62: Overview of PASM

where $g_i(\mathbf{x}, \boldsymbol{\xi})|_{\tilde{\mathbf{v}}}$ represents i^{th} probabilistic constraint, and $\boldsymbol{\xi}$ represents a random vector that includes $\tilde{\boldsymbol{p}}$ associated with random parameters and ζ associated with random variables.

The overall concept of PASM is illustrated in Figure 62. Unlike a deterministic approach, PASM determines the optimum values of the sizing variables with target reliability. The optimization process simultaneously assesses power balance and energy balance to evaluate the sizing constraints, which are given in the form of reliability rather than a deterministic value.

It also must be noted that in PASM formulation the energy balance constraint appears explicitly, in contrast to the most classical sizing methods, in which the consideration of fuel balance is embedded in the calculation of the weight of the aircraft [160]. As mentioned in Chapter II, the classical deterministic sizing methods do not distinguish between available fuel quantity and required fuel quantity, assuming

that the former equals the latter that is determined by the mission analysis. Therefore, fuel quantity is treated as an internal variable and a response, rather than a design variable of a given aircraft sizing problem. In contrast, in PASM, the available fuel (energy) quantity appears as an independent design variable.

5.4 Solution Techniques of CCP and RBDO

Three distinctive approaches to solve the CCP and RBDO problems are found in literature. The first approach is to convert the probabilistic constraints into an equivalent deterministic function and solve the consequent deterministic optimization problem. The second approach is to approximate the feasible set with sampled constraint functions. However, these two methods are applicable to a few specific types of problems and not applicable to most complex engineering problems, where constraint functions are not given in the form of explicit mathematical expressions. The last approach is to employ a conventional design optimization loop with reliability analysis modules. This approach can be applied to a wide range of problems.

5.4.1 Deterministic Equivalent

As shown in the numerical example in §5.2, probabilistic constraints can be converted into an equivalent deterministic function. A more general form is given as a system of probabilistic constraints: $g_i(\mathbf{x}) = \boldsymbol{\xi}\mathbf{x} \geq h$, where $\boldsymbol{\xi} = (\xi_1, \xi_2, \cdots, \xi_n)^{\mathrm{T}}$ is a vector of multivariate normal distributions with $\boldsymbol{\mu} = (\mu_1, \mu_2, \cdots, \mu_n)^{\mathrm{T}}$ as their mean values and $\mathbf{V}$ as the covariance matrix. When a target value (α_g) exists for the probability of meeting the probabilistic constraints simultaneously, the deterministic equivalent of the joint probabilistic constraint is given as $\mu^T\mathbf{x} \geq h + \Phi^{-1}(\alpha_g)\sqrt{\mathbf{x}^T\mathbf{V}\mathbf{x}}$ where Φ^{-1} is the inverse normal cumulative distribution function, or so-called "Second Order Cone" constraints [161].

Another type that can be converted into a deterministic equivalent, known as the "right-hand side" problem in the context of CCP, has one or a set of constraints given

as follows:

$$\mathbb{P}\left[g_i(\mathbf{x}) \geq \xi_i)\right] \geq \alpha_{g_i} \tag{137}$$

Then the constraints can be converted into

$$g_i(\mathbf{x}) \geq F_{\xi_i}^{-1}(\alpha_{g_i}) \tag{138}$$

Aerospace system optimization problems including aircraft sizing, in which requirements are uncertain, are very likely to be formulated in this manner. Generally, the metrics related to requirements such as take-off field length, NO_x emission, and noise level are system responses, g_i as functions of decision variables, $\mathbf{x}$. When the metrics are included in a system optimization problem in the following fashion, g_i must be greater than target values given as uncertain variables, ξ_i whose distributions are known, the constraints can be formulated by Eq. (137), which is converted into its deterministic equivalent as Eq. (138). Unlike the previous form, the conversion of Eq. (137) to its deterministic equivalent does not require any information regarding g_i whose explicit expression is not available in most applications.

This method allows designers to avoid a massive analysis in order to compute the probability of failure of each constraint. However, only a few specific types of CCP problems as presented above can be converted into *exactly* equivalent deterministic optimization problems.

5.4.2 Constraint Sampling Approach

Suppose that a CCP is given as

$$\begin{aligned} \min_{\mathbf{x}} \quad & f \\ \text{s.t.} \quad & \mathbb{P}\left[g(\mathbf{x}, \boldsymbol{\xi}) \geq 0\right] \geq \ \alpha_g \end{aligned} \tag{139}$$

and the constraints cannot be converted into a deterministic equivalent. Then, one approximates the convex chance constrained problem Eq. (139) with a deterministic

optimization problem that has multiple sampled constraints as follows:

$$\begin{aligned} &\min_{\mathbf{x}} \quad f \\ &\text{s.t.} \quad \mathbb{P}\left[g_i(\mathbf{x}, \boldsymbol{\xi_i}) \geq 0\right] \quad (i = 1, \ldots, N) \end{aligned} \tag{140}$$

In other words, this approach replaces the probabilistic constraints with a large number of sampled constraints. De Farias and Van Roy [162] showed that for a special case of linear constraints, a sample size of

$$N \geq \frac{4n}{1-\alpha_g} \log\left(\frac{12}{1-\alpha_g}\right) + \frac{4}{1-\alpha_g} \log\left(\frac{2}{\delta}\right), \tag{141}$$

where $\log(\cdot)$ denotes the logarithm with base 2, ensures that the set of decision vectors feasible for the sampled problem in Eq. (140) is feasible for the chance constrained problem, Eq. (139), with a probability of at least $1-\delta$. Calafiore and Campi [163] also proposed a similar result. The authors considered general convex functions, and showed that for

$$N \geq \frac{2n}{1-\alpha_g} \ln\left(\frac{2}{1-\alpha_g}\right) + \frac{2}{1-\alpha_g} \ln\left(\frac{2}{\delta}\right) + 2n, \tag{142}$$

where $\ln(\cdot)$ denotes the natural logarithm, the optimal solution of the sampled problem Eq. (140) is feasible for $\mathbb{P}\left[g(\mathbf{x}, \boldsymbol{\xi}) \geq 0\right] \geq \alpha_g$ with a probability of at least $1-\delta$.

A notable advantage of this approach is that the set $\{\mathbf{y} | g_i(\mathbf{y}, \boldsymbol{\xi_i}) \geq 0,\ i = 1, \ldots, N\}$ is convex although the feasible set $\{\mathbf{y} | \mathbb{P}\left[g(\mathbf{y}, \boldsymbol{\xi}) \geq 0\right] \geq \alpha_g\}$ is not generally convex.

5.4.3 Optimization with Reliability Analysis

The problem stated in Eq. (121) has a complex structure that cannot be converted or approximated to an equivalent deterministic problem in any practical way. Therefore, the optimization process must be combined with a reliability analysis to compute the probability of meeting constraints. The most popular method is to employ a deterministic optimizer with a nested reliability analysis module, whereby the reliability (or probability of failure) at the current design variables set by the optimizer is estimated inside the optimization loop. The design optimization loop (outer loop) is

a deterministic nonlinear constrained optimization process and rich literature exists regarding various approaches towards nonlinear constrained optimization problems, including the Method of Feasible direction (MoFD) [164], Sequential Quadratic Programming (SQP) [165], and Sequential Linear Programming (SLP) [165]. The reliability assessment (inner loop) can be performed by simulation based methods such as Monte Carlo simulation or approximated analytical methods. In this approach, each call for constraint functions by the optimizer in the outer loop triggers a reliability assessment, which ends up becoming a computationally intensive process.

To alleviate such an impediment by nested reliability analysis, many researchers have developed single-loop RBDO methods, such as the traditional approximation method by Torng and Yang [166]; single-loop single-variable (SLSV) method by Chen et al. [167]; safety-factor approach (SFA) by Wu and Wang [168]; and a sequential optimization and reliability assessment (SORA) method by Du and Chen [169]. Those methods collapse an original two-loop optimization problem into a single-loop optimization problem, which requires fewer reliability assessments. For example, SORA decouples the RBDO process into a sequence of deterministic design optimizations and a set of reliability assessment loops. In each cycle, a deterministic design optimization is performed with a set of constraint functions, the boundaries of which are shifted in the feasible direction based on the reliability information obtained in the previous cycle. Hence, the design is improved from cycle to cycle, and computational efficiency is improved significantly.

5.4.4 Reliability Analysis

The multitude of techniques developed to assess system reliability can be broadly categorized into two groups: random sampling methods and approximated analytic methods.

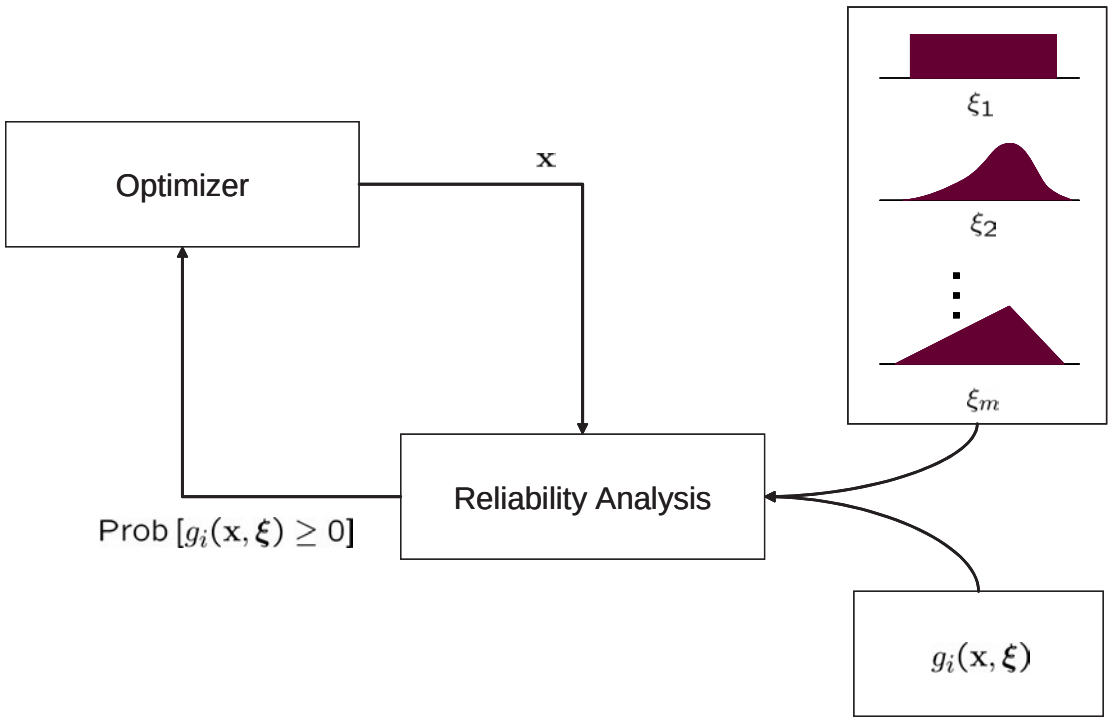

Figure 63: System optimizer integrated with a nested reliability analysis

5.4.4.1 Sampling Based Reliability Analysis

Random sampling methods have been dominated by Monte Carlo simulation, which generates a set of random values and computes the corresponding probability of failure using the following equation:

$$P_f = \frac{1}{N}\sum_{i=1}^{N} I(\boldsymbol{\xi}_i) \quad where\ I(\boldsymbol{\xi}_i) = \begin{cases} 1 & \text{if } g_i(\mathbf{x}, \boldsymbol{\xi}_i)|_{\check{\mathbf{v}}} \leq 0 \\ 0 & \text{otherwise} \end{cases} \tag{143}$$

In the above equation, N is the number of sample points and I is the indicator function. As N increases, the solution asymptotically approaches the exact solution. However, the number of sample points required to estimate small magnitudes of probability of failure is extremely high, which may lead to a computationally intractable problem formulation. This issue may be resolved by employing Quasi Monte Carlo methods such as Importance Sampling methods [170].

5.4.4.2 MPP-Based Reliability Analysis

In the application of the RBDO approach to a real engineering problem, the computational efficiency is of significance. Particularly, the efficiency associated with computing reliability is crucial because it is the most expensive part of the whole optimization process. Implementing more efficient and faster methods than MCS may greatly accelerate the overall process. Several approximation methods such as the First-Order Reliability Method (FORM) and the Second-Order Reliability Method (SORM) that are based on MPP (Most Probable Point) concepts are widely used, since these methods usually provide superior computational efficiency over the standard Monte Carlo method.

In general, RBDO methods often formulate inequality constraints in terms of the probability of failure rather than the probability of success as shown in Eq. (121), which leads to

$$\begin{aligned} &\min_{\mathbf{x}} \quad f \\ &\text{s.t.} \quad \mathbb{P}\left[g(\mathbf{x}, \boldsymbol{\xi})_i \leq 0\right] - \Phi(-\beta_{t_i}) \leq 0 \end{aligned} \tag{144}$$

where Φ is the cumulative distribution function for standard normal distribution and β_{t_i} is the target reliability index, which is given as $F_{g_i}^{-1}(\alpha_{g_i})$.

In both FORM and SORM, an MPP of failure (denoted as $\mathbf{u}^*$) is found in the standard $\mathbf{u}$-space , where the components of $\mathbf{u}$ are standard normal distributions and statistically independent from each other. The standard $\mathbf{u}$-space can be obtained by performing a Rosenblatt Transformation ($\mathbf{u} = T(\boldsymbol{\xi})$) on the set of random variables. When the random variables are statistically independent, the transformation of $\boldsymbol{\xi}$ to $\mathbf{u}$ can be performed by $u_i = \Phi^{-1}[F_i(\xi_i)]$. Transformations for several popular distributions are listed in Table 7.

The MPP lies in a limit state where $g_i(\mathbf{u}) = 0$ and has a minimum distance from

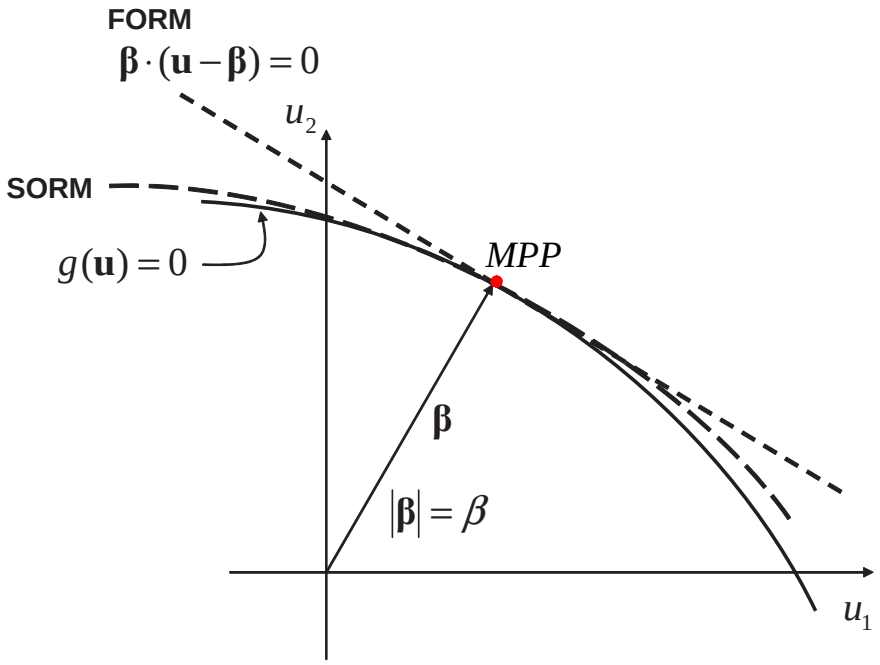

Figure 64: Approximation of the limit state function by FORM and SORM [171]

the origin of the **u**-space, which leads to

$$\begin{aligned} \min_{\mathbf{u}} \quad & \|\mathbf{u}\| \\ \text{s.t.} \quad & g_i(\mathbf{u}) = 0 \end{aligned} \tag{145}$$

The solution to this problem can be found by employing a numerical constrained optimization programming algorithm or tailored iterative methods including those developed by Hasofer and Lind [172] and extended by Rackwitz-Fiessler [173].

There exist two distinct approaches, the reliability index approach (RIA) and the performance measure approach (PMA) for implementing the probabilistic constraints in Eq. (144), which can be further reformulated in two equivalent forms through an inverse transformation as follows [175]:

$$\beta_{s_i} = -\Phi^{-1}[F_{g_i}(0)] \geq \beta_{t_i} \tag{146}$$

$$g_{p_i} = F_{g_i}^{-1}[\Phi(-\beta_{t_i})] \geq 0 \tag{147}$$

	Parameters	PDF	Transformation
Normal	$\mu =$ mean	$f(\xi) = \frac{1}{\sqrt{2\pi}\sigma} \exp\left[-0.5\left(\frac{\xi-\mu}{\sigma}\right)^2\right]$	$\xi = \mu + \sigma u$
	$\sigma =$ standard deviation	$-\infty \leq \xi \leq \infty$	
Lognormal	$\mu =$ mean		$\xi = \exp(\bar{\mu} + \bar{\sigma} u)$
	$\sigma =$ standard deviation	$f(\xi) = \frac{1}{\sqrt{2\pi}\bar{\sigma}} \exp\left[-0.5\left(\frac{\xi-\bar{\mu}}{\bar{\sigma}}\right)^2\right]$	
	$\bar{\sigma}^2 = \ln[1 + (\sigma/\mu)^2]$	$\xi > 0$	
	$\bar{\mu} = \ln(\mu) - 0.5\bar{\sigma}^2$		
Weibull	$k > 0,\ \mu = \nu\Gamma(1 + 1/k)$	$f(\xi) = \frac{k}{\nu}\left(\frac{\xi}{\nu}\right)^{(k-1)} \exp\left[-\left(\frac{\xi}{\nu}\right)^k\right]$	$\xi = \nu[-\ln(\Phi(-u)]^{\frac{1}{k}}$
	$\sigma^2 = \nu^2[\Gamma(1 + 2/k) - \Gamma^2(1 + 1/k)]$	$\xi > 0$	
Gumbel	$\mu = \nu + (0.577/\alpha)$	$f(\xi) = \alpha \exp[-\alpha(\xi - \nu) - \exp(-\alpha(\xi - \nu))]$	$\xi = \nu - \frac{1}{\alpha}\ln[-\ln(\Phi(u))]$
	$\sigma = \pi/\sqrt{6\alpha}$	$-\infty \leq \xi \leq \infty$	
Uniform	$\mu = (a + b)/2$	$f(\xi) = \frac{1}{b-a}$	$\xi = a + (b - a)\Phi(u)$
	$\sigma = (b - a)/\sqrt{12}$	$a \leq \xi \leq b$	

where $\Phi(u) = \frac{1}{\sqrt{2\pi}} \exp(-0.5u^2)$

Table 7: Transformation of the **u**-space to the $\boldsymbol{\xi}$-space [174]

where F_{g_i} denotes the cumulative distribution of g_i, and β_{s_i} and g_{p_i} are the safety reliability indices and the probabilistic performance measure for the i^{th} probabilistic constraint, respectively. RIA replaces the probabilistic constraint in Eq. (144) with the reliability index constraint given as Eq. (146), while PMA uses the performance measure constraints given as Eq. (147).

The first-order safety reliability index β_{s_i} in RIA is obtained by solving the optimization problem given as Eq. (145). The magnitude of β_{s_i} equals $\|\mathbf{u}^*\|$, and its sign is positive if the origin of the $\mathbf{u}$-space is feasible, and vice-versa. A performance measure approach (PMA) proposed by Tu et al. [153] formulates the evaluation of probabilistic constraints as an inverse problem of RIA as given in Eq. (147). PMA searches for first-order probabilistic performance g_{p_i} with the lowest performance function value on a hyper-surface determined by the target reliability index β_{t_i} within the $\mathbf{u}$-space, which can be formulated as

$$\begin{aligned} \min_{\mathbf{u}} \quad & g_i(\mathbf{u}) \\ \text{s.t.} \quad & \|\mathbf{u}\| = \beta_{t_i} \end{aligned} \tag{148}$$

where g_{p_i} equals the objective function value $g_i(\mathbf{u})$ at the optimum. PMA, in general, is more efficient than RIA, especially for high reliability problems [176] due to the simpler constraint for reliability analysis. Moreover, it has been reported that PMA converges with certain problems where RIA diverges.

5.5 Extended Formulation of PASM

The formulation presented in §5.3 provides a basic form of probabilistic aircraft sizing methods applicable for a single random objective function and multiple probabilistic constraints. This formulation can be extended to fulfill a different need depending on the application. For example, one may need to consider joint probabilistic constraints or multi-objective functions. Furthermore, one may want to find a robust solution that minimizes the mean value of the objective function as well as its variance. This

section brings to light ramifications of the standard formulation of PASM adaptive to such a purpose.

5.5.1 Joint Probabilistic Constraints

The probability of meeting all constraints simultaneously must be less than or equal the minimum of the probability level of meeting individual constraints. Particularly, if there is a strong negative correlation between any two hard constraints, the probability of meeting the joint constraints may be significantly lower than the given probability for individual constraints. Therefore, it is worthwhile to investigate the impact of implementing joint probabilistic constraints by formulating the CCP problem as follows:

$$\begin{aligned} \min_{\mathbf{x}} \quad & f \\ \text{s.t.} \quad & \mathbb{P}\left[\mathbf{G}(\mathbf{x}, \boldsymbol{\xi})|_{\breve{\mathbf{v}}} \geq \mathbf{0}\right] \geq \ \alpha_g \\ \text{where} \quad & \mathbf{x} = [P_{ref}|_{\breve{v}},\ S,\ W_{energy}|_{\breve{v}}] \text{ and} \\ & \mathbf{G} = [g_1, \cdots, g_{n_p}, g_{n_p+1}, \cdots, g_{n_p+n_m}]^T \end{aligned} \tag{149}$$

where $\mathbf{G}(\mathbf{x}, \boldsymbol{\xi})|_{\breve{v}} \geq \mathbf{0}$ is a system of inequality constraints that the design solution must satisfy simultaneously.

5.5.2 Multidisciplinary Design Optimization

The proposed probabilistic aircraft sizing method can be applied to aircraft design optimization problems in which multidisciplinary design parameters such as wing geometry, tail arrangement, and propulsion system design parameters are included as design variables. This type of problem can be solved by double-loop optimizations, in which the inner-loop optimization is performing a probabilistic sizing for fixed design parameters determined by the outer-loop optimization that drives the design parameters to an optimum solution. However, a more efficient approach is to integrate a double-loop optimization problem into a single optimization problem in which the two

groups of design variables from the inner-loop and outer-loop optimization processes are combined. In the resultant optimization problem, the design variables include disciplinary design variables, denoted as $\mathbf{x}_d$, as well as the original sizing variables. In addition, a number (n_d) of constraints resulting from decoupling the disciplinary analyses may be added. Therefore, the resultant problem can be stated as follows:

$$\begin{aligned} \min_{\mathbf{x}} \quad & \mathbb{E}[\tilde{f}] \\ \text{s.t.} \quad & \mathbb{P}\left[g_i(\mathbf{x}, \boldsymbol{\xi})|_{\check{\mathbf{v}}} \geq 0\right] \geq \ \alpha_{g_i} \quad (i = 1, \cdots, n_p + n_m + n_d) \\ \text{where} \quad & \mathbf{x} = [P_{ref}|_{\check{\mathbf{v}}},\ S,\ W_{energy}|_{\check{\mathbf{v}}}, \mathbf{x}_d] \end{aligned} \tag{150}$$

Although such efforts to enhance computational efficiencies, when the objective and/or constraint functions are evaluated by computationally-expensive analyses such as finite element methods (FEM) or computational fluid dynamics (CFD), a probabilistic design approach would be computationally intractable. To alleviate such a problem, some researchers have used surrogate models such as response surface polynomials [177, 178, 179, 175] and neural networks [180, 181] to approximate the objective function and constraint functions with respect to the decision variables as well as random parameters.

5.5.3 Probabilistic Objective Function

The basic PASM formulation seeks the design that minimizes the mean value of the probabilistic objective function responses. There are some alternative methods to handle a probabilistic objective function.

5.5.3.1 When a Target Probability Exists

An alternative approach suggested by Liu [182] is to impose a target confidence level (α_f) of the probabilistic objective as an additional constraint as follows:

$$\begin{aligned} \min_{\mathbf{x}} \quad & \bar{f} \\ \text{s.t.} \quad & \mathbb{P}[f(\mathbf{x}, \boldsymbol{\xi}) \leq \bar{f}] \geq \alpha_f \\ & \mathbb{P}[g_i(\mathbf{x}, \boldsymbol{\xi}) \leq 0] \geq \alpha_{c_i} \quad (i = 1, \cdots, n_c) \end{aligned} \tag{151}$$

where α_f and α_c are the predetermined confidence levels for the probabilistic objective and constraints, respectively.

5.5.3.2 When a Target Value Exists

If a target value for the objective function is given, an approach that maximizes the probability of achieving the target value, as shown in the RDS method, may be appropriate, leading to

$$\begin{aligned} \max_{\mathbf{x}} \quad & \mathbb{P}[f(\mathbf{x}, \boldsymbol{\xi}) \leq f_{allowable}] \\ \text{s.t.} \quad & \mathbb{P}[g_i(\mathbf{x}, \boldsymbol{\xi}) \leq 0] \geq \alpha_{c_i} \quad (i = 1, \cdots, n_c) \end{aligned} \tag{152}$$

Nevertheless, it is not common for a target value of the aircraft weight to be given for aircraft sizing. Furthermore, given as a design requirement, the aircraft weight may be incorporated as a constraint with an another metric as its substitute for the objective function. However, if another response such as a monetary metric is selected as the objective function, then this approach is suitable.

5.5.4 Multi-Objective Function

Extension to a multidisciplinary design optimization problem is very likely to call for multiple objectives in many applications. In general, maximization or minimization of a multitude of criteria concurrently in many complex system design problems results in a conflict that allows only *compromised* solutions. Under such circumstances, the conditions for "optimality" of the given problem are not apparent.

For deterministic optimization problems, two largely distinct classes of multi-objective formulation methods known as "a priori" and "posteriori" have been developed to aid in multi-objective problem definition [183]. The former, including the weighted sum method [184], goal programming [185], and ϵ-constraint method, seeks to create the single scalar substitute that aggregates multiple objectives based on the preferences of the decision makers. Once formulated, this scalar value can be optimized using traditional techniques to find a single best solution to the multi-objective problem. The most commonly used and intuitive method for converting multiple objectives ($[f_1, f_2, \cdots, f_n]$) into a single objective (f) is the weighted sum:

$$\begin{gathered} f = w_1 f_1 + w_2 f_2 + \cdots + w_n f_n \\ \text{where } \sum w_i = 1 \text{ and } w_i > 0 \end{gathered} \tag{153}$$

However, such approaches include subjective information, and can thereby be misleading concerning the nature of optimum design [186]. In contrast, the latter requires no preference or goal information before performing an optimization run [183]. Instead, these methods assist the users in forming their preferences by providing information for a set of *non-inferior solutions* [187]. A non-inferior solution, or so-called Pareto optimum, has the property that an improvement in one objective requires a degradation in at least one other. The set of all Pareto optimal solutions in the objective space creates an efficient frontier of solutions, known as the Pareto Frontier. All solutions on the Pareto Frontier are not dominated by other feasible solutions, which can provide valuable information for decision-making. The Pareto Frontier can be obtained by performing successive optimization runs using one of the "a priori" aggregation methods and different weight vectors[1].

When considering uncertainty in multiobjective optimization, computational effort becomes even larger, and as a result very few studies have been performed [190].

[1]Some alternative methods such as multiple objective Genetic Algorithms (MOGA) [188] and Non-dominated Sorting Genetic Algorithm [189] are based on the genetic algorithm.

Literature review has shown that researchers have attempted to solve a multiobjective optimization problem under uncertainty using existing multiobjective optimization methods combined with the RBDO formulation. For example, El Sayed et al. [191] have investigated a multi-objective RBDO formulation using the nonlinear goal programming method for structural design problems that involves multiple design criteria including structural weight, load induced stress, deflection, and mechanical reliability. Barakat et al. [192] formulated a multi-objective RBDO using ϵ-constraint for the designs of prestressed concrete beams (PCB). Lian and Kim [193] studied a multiobjective RBDO problem in which bi-objectives are optimized subjected to a probabilistic constraint. They used a two-loop approach. For the outer loop, they used a genetic algorithm and a gradient-based optimizer to facilitate the convergence of the genetic algorithm. For the inner loop, they used Monte Carlo simulations.

Such approaches can also be applied to the probabilistic aircraft sizing problems in which multiple objectives $F = [f_1, \cdots, f_n]$ are given. In the case of the objectives being subject to uncertainty, the approaches for a single objective subject to uncertainty discussed in §5.5.3 need to be combined. When no target values exist for the objective functions, a Pareto frontier being developed via integration of these methods with the proposed method may lead to a probabilistic method for solving complex system design optimization problems, in which both objectives and constraints are multiple and probabilistic. For example, the integration of CCP and JPDM will provide a suitable solution when one seeks an optimum solution that maximizes the probability of satisfying multiple objectives and simultaneously satisfies the uncertain constraints with a prescribed probability, which is quantitatively stated as follows:

$$\begin{aligned} \max_{\mathbf{x}} \quad & \mathbb{P}[\mathbf{F}(\mathbf{x}, \boldsymbol{\xi}) \leq \mathbf{c}] \\ \text{s.t.} \quad & \mathbb{P}[\mathbf{G}(\mathbf{x}, \boldsymbol{\xi}) \leq 0] \geq \alpha_c \end{aligned} \tag{154}$$

where $\mathbf{F}(\mathbf{x}, \boldsymbol{\xi})$ stands for a vector of multitude objectives, and $\mathbf{c}$ is a vector of criteria for each objective.

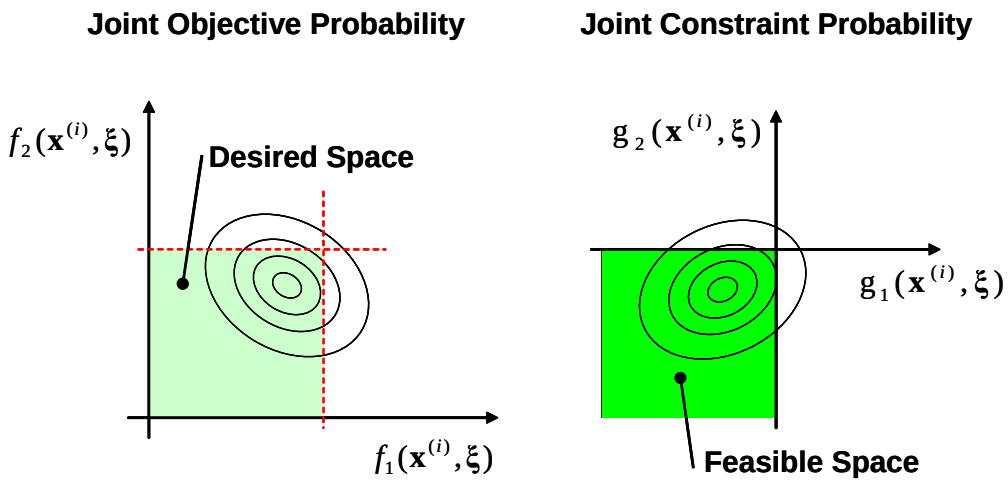

Figure 65: Simultaneous application of joint probability to the objective space and the constraint space

5.5.5 Robust Design

In general, two distinct approaches toward system design under uncertainty exist: reliability-based design and robust design. The goal of robust design is to minimize the effect of variation under controllable and/or uncontrollable factors without eliminating the sources of variations, while reliability-based design seeks a solution to ensure that system performance meets the pre-specified target with a required probability level [194].

The classical definition of robust design is *design at which the variations in performance characteristics are minimal* [195]. When it is combined with robust optimization strategies, not only the variation but also the objective function value is of interest. Therefore, implementation of robust design philosophy into a design problem is prone to yield a multi-objective problem for which the objective is to minimize both the mean and deviation of the objective function.

When uncertainty is involved in both the objective function and the constraint functions, one may want to have a solution that satisfies the reliability constraints and ensures the robustness of the objective function. A formulation that minimizes

both the mean of merit function and its variance while maintaining feasibility under uncertainty can be rewritten as follows:

$$\begin{aligned} &\min_{\mathbf{x}} \ \mu_f \\ &\min_{\mathbf{x}} \ \sigma_f \\ &\text{s.t.} \ \ \mathbb{P}[g_i(\mathbf{x}, \boldsymbol{\xi}) \leq 0] \geq \alpha_{c_i} \quad (i = 1, \cdots, n_c) \end{aligned} \tag{155}$$

Su and Renaud [194] formulated the two objectives in Eq. (155) using the weight sum method, $\mu_f + w\sigma_f$, where w is a weighting function that trades between performance and robustness to minimize (convex) weighted sums of the different objectives for various different settings of the weights. Mourelatos and Liang [159] proposed a preference aggregation method to handle the two objectives with the use of indifference points as a means of trading between performance and robustness.

5.6 Sensitivity Analysis

Although it is the end-goal of any optimization problem to seek the optimal solution, sensitivity analysis is also an important tool for designers to gain insights into the complex behavior of the system under study, thus leading to more informed decisions. Sensitivity analysis has been widely applied in engineering design to explore a model's response behavior, to evaluate the accuracy of a model, and to test the validity of assumptions [196]. Especially, sensitivity analysis provides information on the rate of change in a system's response(s) due to changes in inputs. This is usually performed by perturbing the input variables one at a time near a given central point, which involves computing the partial derivatives of the responses with respect to the input variables: an action that is known as local sensitivity analysis. Large volumes of publications are available in literature that discuss sensitivity analysis in terms of rigorous mathematical elaborations, and such is well beyond the scope of this dissertation. However, certain sensitivities can be obtained as by-products of applying PASM and result in critical information that guides a designer to a better

understanding of the sizing problem. Therefore, it is worth reviewing such sensitivities that include that of the objective function to the target probability and that of the constraint functions to the distributions of random parameters.

5.6.1 Sensitivity of Objective Function to Target Probability

It is well known that a Lagrange multiplier has implications as a sensitivity coefficient. Consider a typical constrained optimization problem

$$\begin{aligned} \min_{\mathbf{x}} \quad & f(\mathbf{x}) \\ \text{s.t.} \quad & g_i(\mathbf{x}) \leq c_i \end{aligned} \tag{156}$$

Introducing Lagrange multipliers (λ), Eq. (156) can be rewritten as follows:

$$\min_{\mathbf{x}} \; L(\mathbf{x}, \lambda) = f(\mathbf{x}) + \sum_{i=1}^{m} \lambda_i (g_i - c_i) \tag{157}$$

for a suitable set of Lagrange multipliers λ_i, $i = 1, \ldots, m$. A pair $(\mathbf{x}, \lambda)$ has to satisfy the following conditions to be a solution to the original constrained problem in Eq. (156):

$$\begin{aligned} \nabla_{\mathbf{x}} L(\mathbf{x}^*, \lambda^*) &= 0 \\ g_i(\mathbf{x}^*) &\leq c_i \\ \lambda_i^* &\geq 0 \end{aligned} \tag{158}$$

which are known as the Kuhn-Tucker conditions.

From Eq. (157) and Eq. (158), the optimum solution $\mathbf{x}^*$ must meet a necessary condition for optimality

$$0 = \nabla_{\mathbf{x}} f^* + \sum_{i=1}^{m} \lambda_i^* \nabla_{\mathbf{x}} g_i^* \tag{159}$$

The interpretation of this equation implies that at the optimum, the Lagrange multipliers are used to balance the gradients of the constraints and the objective function. With this consideration and Eq. (158), the following relation can be surmised:

$$\frac{\partial f(\mathbf{x}^*)}{\partial c_i} = \lambda_i^* \tag{160}$$

This equation states that an i^{th} Lagrange multiplier represents the sensitivity of the objective function to the i^{th} constraint. This sensitivity is known as the LHS (Left Hand Side) sensitivity [197], and its proof can be found in References [198, 199]. The relative magnitude of the i^{th} Lagrange multiplier represents the importance of the i^{th} constraint for this solution. Lagrange multipliers are the by-products of the optimization process in most gradient-based path building algorithms since the Kuhn-Tucker condition specifies optimality. In the RBDO method, the LHS sensitivity represented by the Lagrange multiplier corresponds to the sensitivity of the objective function to the target probability. This information is particularly useful to an arbiter who wants to trade reliability (probability of success) with the objective function. If the decision maker values each constraint differently, he or she may want to reduce the objective function value by accepting an increase in the probability of failure of less important constraints.

5.6.2 Sensitivity of Constraint Functions to Distributions of Random Parameters

Another useful analysis for an RBDO problem is exploring the sensitivity of the objective function(s) and constraint function(s) with respect to random parameters. When uncertainty is involved with an input variable, sensitivity analysis does not simply mean computation of a partial derivative with respective to the variable. The random parameters appear in a simulation model in the form of a distribution, rather than a single definite value. The impact of random parameters on system responses is measured by the probabilistic characteristics of the response such as its mean (μ), variance (σ), the probability density function (PDF), or the cumulative distribution function (CDF) rather than a point estimation. Correspondingly, a sensitivity analysis under uncertainty needs to be performed on the probabilistic characteristics of a model response with respect to the probabilistic characteristics of model inputs [196]. Therefore, the sensitivity of the objective function(s) and constraint function(s) with

respect to random parameters can be obtained by a different class of sensitivity analysis, known as probabilistic sensitivity analysis (PSA).

Various types of PSA techniques are found in literature. Some techniques provide information on the relative importance of random parameters on system responses, and assist a problem solver in identifying probabilistically insignificant factors. Variance-based methods including the Fourier Amplitude Sensitivity Test (FAST) [200, 201, 202], correlation ratios [203] or importance measures [204], and Sobol's indices [205] decompose the total variance of a response by the uncertainty sources (random parameters). The MPP-based method measures the relative importance of random parameters utilizing the information of the gradient with respect to random parameters at MPP.

Another widely used category of PSA techniques is the investigation of the rate of change in a probabilistic characteristic of a response Y due to the changes in the probabilistic characteristics of a random input X_i, such as $\partial\mu_g/\partial\mu_{\xi_i}$.

If an MPP-based reliability analysis is employed in solving the probabilistic aircraft sizing problem, an MPP-based sensitivity analysis can be performed with little or no additional computation. The gradient of a limit state function at MPP is construed as an index of relative contribution of the random parameters to the probability of failure as shown in Figure 66. The components of $\boldsymbol{\beta}$, decomposed to each dimension of the standard **u**-space, provide sensitivity indicators of reliability with respect to random parameters, whose mathematical expression is given as [196]:

$$S_i = \frac{\left(\frac{\partial y}{\partial x_i}\frac{\phi(u_i)}{h(x_i)}\right)^2}{\sum_{j=1}^{n}\left(\frac{\partial y}{\partial x_j}\frac{\phi(u_j)}{h(x_j)}\right)^2}|_{MPP} = \frac{(u_i^{MPP})}{\beta^2} \tag{161}$$

where y is the random performance, ϕ is the PDF of the standard normal distribution, h is the PDF of a random variable, ξ_i, u_i is the standard normal random variable transformed from ξ_i, and β is the reliability index. It should be noted that $\sum_{i=1}^{n} S_i = 1$. Moreover, S_i is the directional cosine in the gradient of the limit state at the MPP.

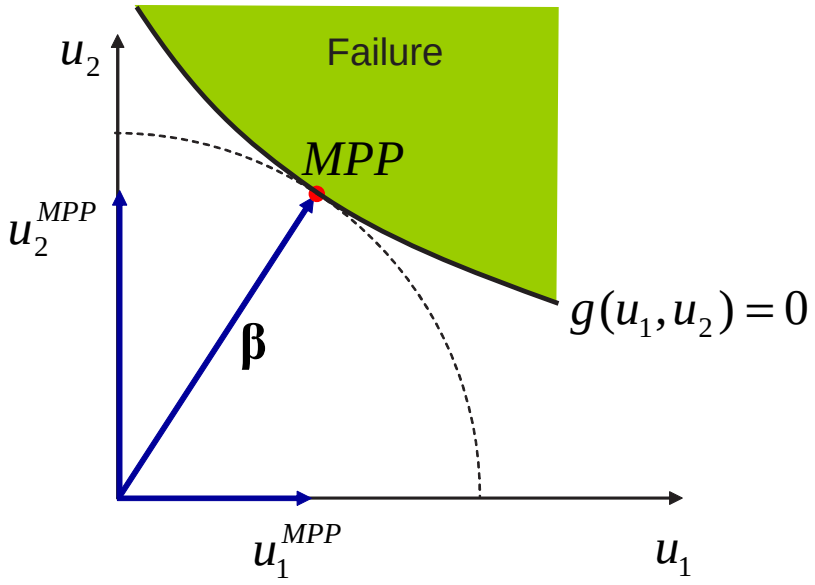

Figure 66: Illustration of the MPP-based sensitivity measure [196]

The magnitude of S_i indicates the relative significance of the uncertainty in the random parameters to the response. In PASM, this information can assist designers in various ways. Before the optimum is found, the analysis may serve as a supplemental means to check the validity of a model structure. In addition, the results may be used to reduce the dimension of a design problem by eliminating the probabilistically insignificant factors from the PASM problem. Once an optimum solution is found, the information reveals what efforts need to be pursued to reduce the variability of the response and effectively improve the reliability.

The MPP-based methods also offer potential improvement on reliability by reducing variability or by improving the mean value in random inputs, $\partial P_f/\partial \mu_{\xi_i}$ and $\partial P_f/\partial \sigma_{\xi_i}$, respectively [206].

$$\begin{aligned} \frac{\partial \beta}{\partial \mu_{\xi_i}} &= \frac{\partial \beta}{\partial u_i}\frac{\partial u_i}{\partial \mu_{\xi_i}} \\ \frac{\partial \beta}{\partial \sigma_{\xi_i}} &= \frac{\partial \beta}{\partial u_i}\frac{\partial u_i}{\partial \sigma_{\xi_i}} \end{aligned} \tag{162}$$

where $\partial\beta/\partial u_i$ is the directional cosine of the vector β, and $\partial u_i/\partial \mu_{\xi_i}$ can be obtained

from $u = T(\boldsymbol{\xi})$.

CHAPTER VI

METHOD IMPLEMENTATION

Although the objective of the proposed research is not to provide a specific solution down to the detailed design level of a specific problem, both AIASM and PASM must be verified through appropriate implementation. This chapter presents two example studies as proofs of concept, in which the proposed methods are applied to a fuel cell-powered general aviation (GA) aircraft and a Solar-Powered High Altitude Long Endurance (SPHALE) aircraft with a RFC system. These two studies are selected for different purposes. The former can be also performed with traditional aircraft sizing method if an analysis model for the fuel cell power plant can be properly integrated with a traditional sizing environment. Therefore, the comparison between the results from the traditional sizing method and the proposed method is possible. On the contrary, the latter articulates an exclusive capability of the method compared with the traditional methods. Another comparable aspect of these two studies is the incorporation of the analyses for propulsion system performance metrics and weight values. The former study employs a physics-based analysis code specially developed for electric propulsion system architectures powered by fuel cells, whereas the latter uses efficiency and specific power data available from literature.

6.1 Fuel Cell-Powered General Aviation

Both AIASM and PASM were applied to a GA aircraft configuration equipped with an all-electric aircraft propulsion system architecture powered by a PEMFC system. The baseline configuration and the sizing mission are similar to those of a Cessna 172 Skyhawk, as illustrated in Figure 67. Point performance requirements are comparable or slightly relaxed compared with those of the Skyhawk.

Point Performance

TOFL	1370 ft, Hot Day, over 35 ft obstacle clearance
Climb	150 ft/min at 8,000 ft of altitude
Level Flight	118 knot at 10,000 ft of altitude
Approach	57 knot
LDFL	1,250 ft over 50 ft obstacle clearance

Mission Profile

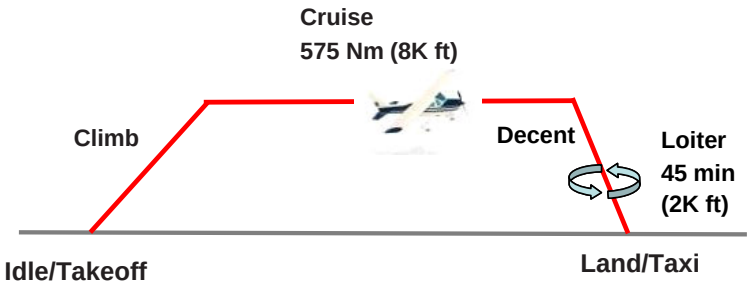

Figure 67: Mission profile of electric GA aircraft

The all-electric propulsion system architecture consists of a PEMFC stack, a power management and distribution (PMAD) system, an electric motor, and other accessories, as illustrated in Figure 68. The performance and weight of the propeller are estimated by GTPROP, which is a legacy code originally developed and validated by Hamilton Standard [207].

The performance and weight of the components of the propulsion system architecture are calculated by the design and simulation environment developed by Choi et al. [208]. The design framework consists of two main parts: an "on-design" analysis routine and an "off-design" analysis module. The on-design analysis is set up to estimate the overall efficiency and weight breakdown of the propulsion system that is designed to produce target thrust or power at a specified flight condition. The off-design analysis estimates the steady-state performance of the propulsion system whose geometric and hardware characteristics were determined by the prior on-design analysis, along the mission profile. At each mission segment, the analysis converges

on the available thrust and overall efficiency (fuel consumption) that match the required shaft power for the given flight condition. Figure 69 illustrates the integrated environment of the aircraft sizing code developed with MS EXCEL® spreadsheets and Choi et al.'s propulsion system analysis and sizing code. All codes were unified under a common GUI environment using ModelCenter® from Phoenix Integration, Inc.

The sizing reference power (P_{ref}) of the propulsion system is selected as a design shaft power at cruise (Mach 0.184 and 8,000 feet). Thus, the propulsion system weight must be estimated iteratively in conjunction with aircraft sizing, which demands significant computational effort. The new environment employs an adaptive technique for developing engine scaling law, which is capable of updating the scaling law for a specific propulsion system during the aircraft sizing process. The technique has allowed the environment to accelerate the process moderately without compromising the accuracy of estimated propulsion system weight. As identified in descendent research [65, 117, 118], the performance of off-the-shelf fuel cells and electric power components is barely sufficient to realize a flyable fuel cell airplane, mainly because of their low specific power and power density. Dramatic improvements in all sub-system components' technology readiness levels must be achieved to yield a feasible and viable aviation solution. Therefore, the weight of the fuel cell based propulsion system was estimated by consulting the hypothetical technology growth scenario reported in Ref.[117]. In addition, 10% of increase in overall efficiency of the propulsion system was assumed, resulting in 0.04 lbs/hr/lbs of TSFC at cruise. The relationship between the reference power and propulsion system weight is depicted in Figure 70, which exhibits a strong rectilinear trend.

The PEM fuel cells require pure hydrogen as fuel to carry out the electrochemical reaction. Hydrogen fuel can be stored in gaseous, gelled, or liquid form. Gaseous hydrogen fuel can be stored in a number of ways: pressure tank, metal hydride,

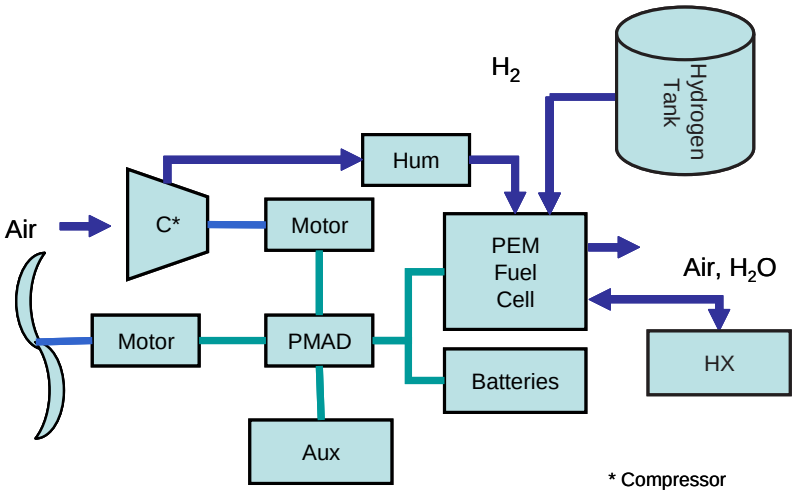

Figure 68: Notional fuel cell propulsion system architecture

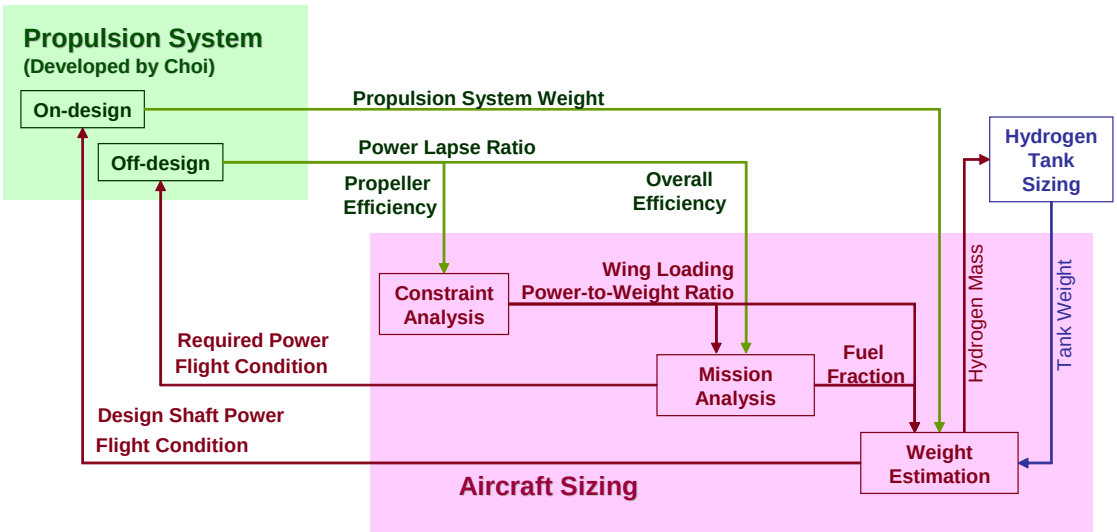

Figure 69: Integrated analysis environment

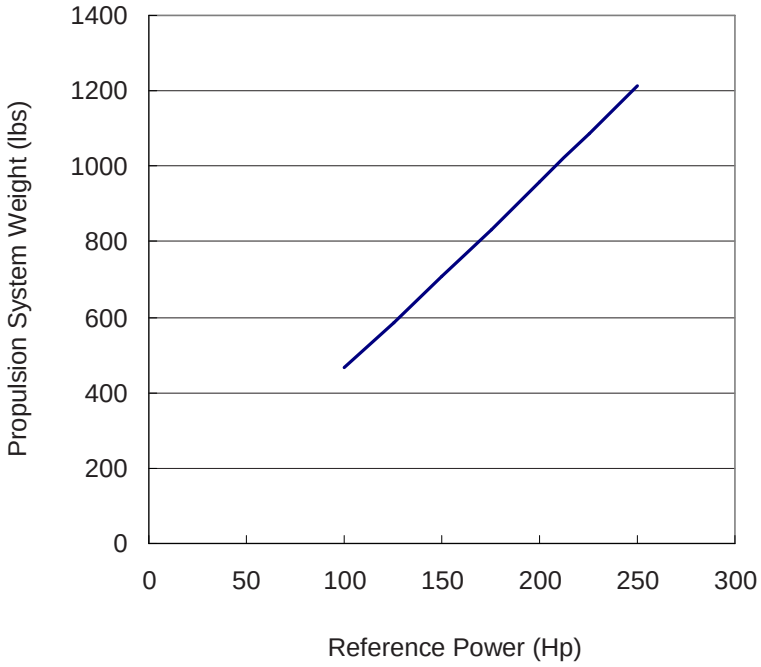

Figure 70: Power vs. weight of the electric propulsion system

carbon nanotubes, and glass microspheres. A cryogenic tanker is used for gelled or liquid hydrogen [209]. Among the options, liquid hydrogen was chosen for this study because previous studies on the options for hydrogen fuel storage [115, 119, 209] support the technology as the most promising for aircraft applications. A model that estimates the weight of the liquid hydrogen tank based on the formulation of Chambliss and Kelly [210] was used for this study.

The uncertainty sources considered for the GA study include the zero-lift drag coefficient, propulsion system efficiency, payload, and hydrogen fuel tank weight. These four random variables were assumed to have a uniform distribution as depicted in Figure 71. These distributions have been arbitrarily selected for the purpose of the demonstration. In reality, however, the distributions must be carefully selected by experts from all involved disciplines, based on their knowledge and analyses.

6.1.1 Deterministic Solutions

Three different deterministic approaches to allocating varying amounts of design margin in the presence of uncertainty were tested. The first, denoted as **D1**, represents the "voice of experience" approach that determines appropriate design margins by an expert's engineering intuition. The second, denoted as **D2**, represents a deterministic optimization approach without any design margin obtained by a numerical optimization process. The last, denoted as **D3** is also a deterministic optimization approach, but applies a safety factor to each design variable.

The first approach, **D1**, follows the steps described in §4.5. The results of the constraint analysis of the electric GA aircraft are presented in Figure 72. The input parameters for the analysis are listed in Table 21 in Appendix E. Assuming that the constraints are not deterministic, one may choose a design point within the feasible region that is removed from the constraint curves. The design point for the aircraft was selected as 11.7 lbs/ft^2 of wing loading and 37 Hp/lbs of power-to-weight ratio as marked in Figure 72. With these combinations of wing loading and power-to-weight ratio, the required fuel fraction was estimated at 2.85% by the mission analysis; detailed results are listed in Table 22 in Appendix E. The available fuel fraction was determined to be 3.4%. Such a low fuel fraction is representative of the high energy-conversion efficiency of the fuel cell power plant and the high specific energy of the hydrogen fuel. The second approach, **D2**, employs a numerical optimization process to find an optimum design resulting in the minimum take-off gross weight. During the optimization process the random parameters are set to their reference values, namely $\xi_i = 1$. The solution of **D3** was found by using the same optimization algorithm as **D2** but with a 10% pre-fixed deterministic margin to each design variable. The sizing results of the three deterministic approaches are listed in Table 8.

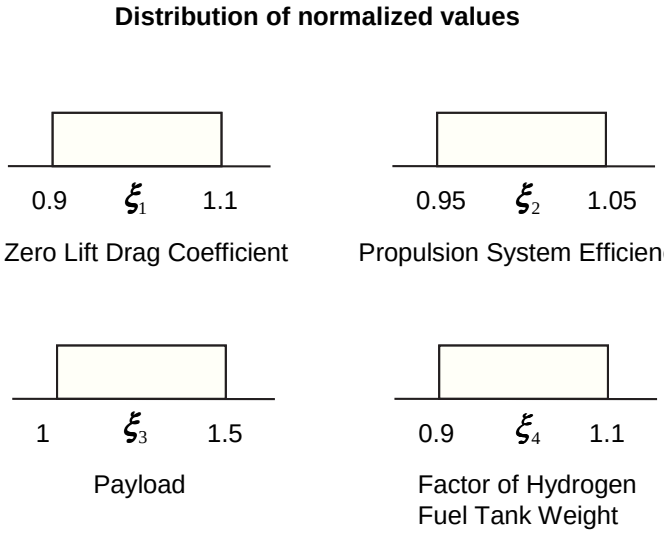

Figure 71: The distributions of random variables considered in the electric GA study

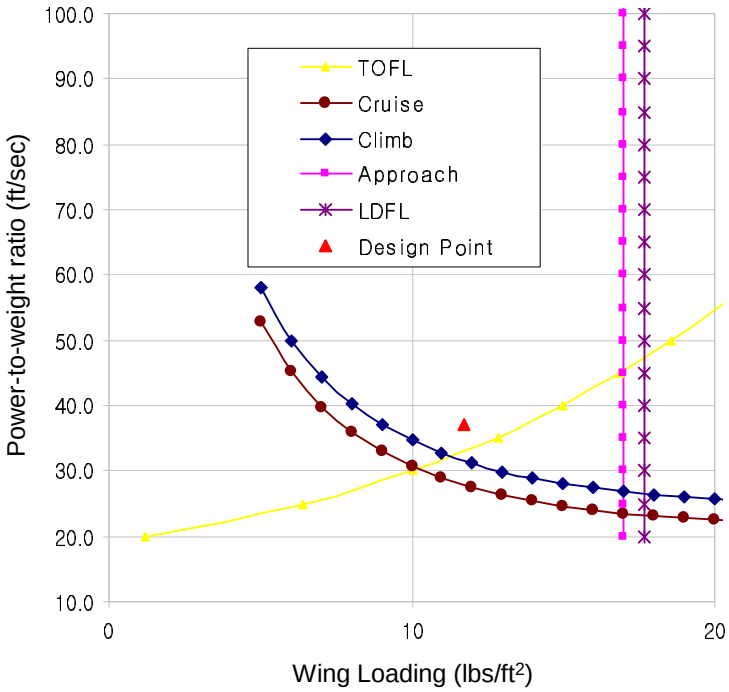

Figure 72: Constraint analysis of the electric GA Aircraft, **D1**

Table 8: Deterministic solutions

	D1	D2	D3
Power to Weight Ratio (ft/sec)	37.00	32.01	35.57
Wing Loading (lbs/ft^2)	11.70	11.45	11.45
Fuel Fraction	0.0350	0.0288	0.0323
Take-off Gross Weight (lbs)	3168	2424	2877
Wing Area (ft^2)	271	212	251
Propulsion System Power (Hp)	213	141	186

6.1.2 Code Verification

It is desired that the proposed methods are validated through their applications to existing aircraft designs before applying them to new aircraft design problems. Validation is distinguished from verification in that the former assesses the degree of representing the real-world while the latter assesses the degree of representing the developer's conceptual description. Therefore, in order to *validate* proposed methods, sufficient data of an *actual* aircraft that uses alternative energy sources are required. Validation of AIASM requires reliable, sufficient data of performance specifications and aircraft design attributes. However, very limited information of unconventionally powered aircraft can be found in the public domain. Although missing information could be estimated by manipulating or extrapolating available data, it will undermine solidity of the validation. For this reason, validation of the methods was not performed. Instead, the analysis code was verified by comparing mission analysis results of the three deterministic solutions with those obtained by FLOPS.

Although the aircraft is fueled with liquid hydrogen, FLOPS can analyze its performance if an engine deck of the propulsion system is provided. An engine deck was developed by using the same propulsion system model. The design shaft power of the engine is 171 Hp at the cruise altitude. The engine can produce 20% more shaft power at sea level because of reduced power take-out for the air compressor due to higher ambient air density. A portion of the engine deck data is pictorially described

in Figure 73, which shows the variation of thrust and fuel flow with altitude and mach number at maximum power conditions. The numeric data set also contains thrust and fuel flow for several part power conditions.

The range performance of the three deterministic designs were computed by FLOPS, which scales the engine deck based on maximum thrust at sea level static condition. The results were compared with the range values obtained by the newly developed analysis environment in Figure 74. The range values depicted in the figure include both climb and cruise segments. The difference in range performance of the three solutions was found to be less than 1%.

6.1.3 Probabilistic Sizing

Three different approaches including FORM-RIA, FORM-PMA, and MCS-based optimization, denoted as **P1**, **P2**, and **P3**, were employed to obtain the probabilistic solutions to the CCP problem per Eq. (150) in Appendix C. The confidence level of the objective function was targeted at 95%, and the probability of failure of each constraint was set to 0.05.

In applying FORM, the probability of failure was computed by RIA, whereas $\bar{f}$ can be obtained by PMA from a nonlinear optimization problem in $\mathbf{u}$-space subject to an equality constraint as

$$\begin{aligned} \max_{\boldsymbol{\xi}} \quad & f \\ \text{s.t.} \quad & \|\mathbf{u}\| = \Phi^{-1}(\alpha_f) \end{aligned} \tag{163}$$

The MCS-based optimization employs the MoFD as the system level optimizer. 10,000 random cases were simulated to compute the probability of failure of the probabilistic constraints and $\bar{f}$, which is given as the value of the objective function that corresponds to the specified percentile. The seed values of the random number generator and the number of sample points (10,000) were fixed to alleviate a discontinuity in the probability of failure and its gradients.

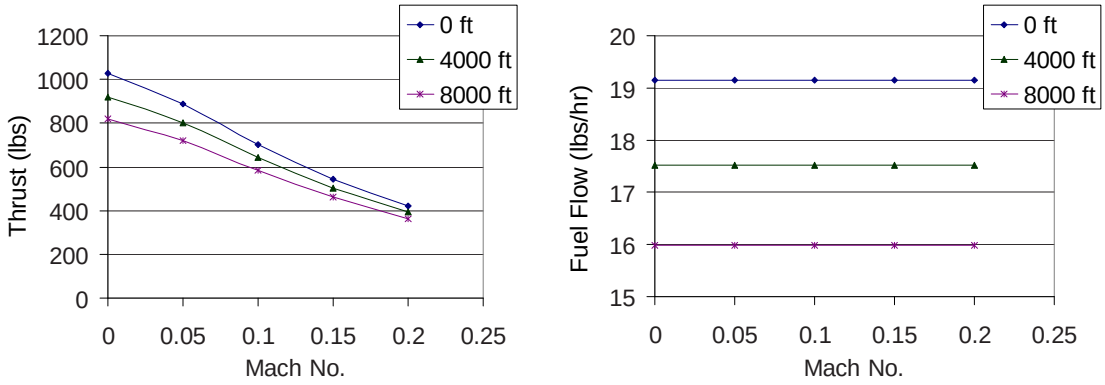

Figure 73: Thrust and fuel flow of the PEMFC propulsion system

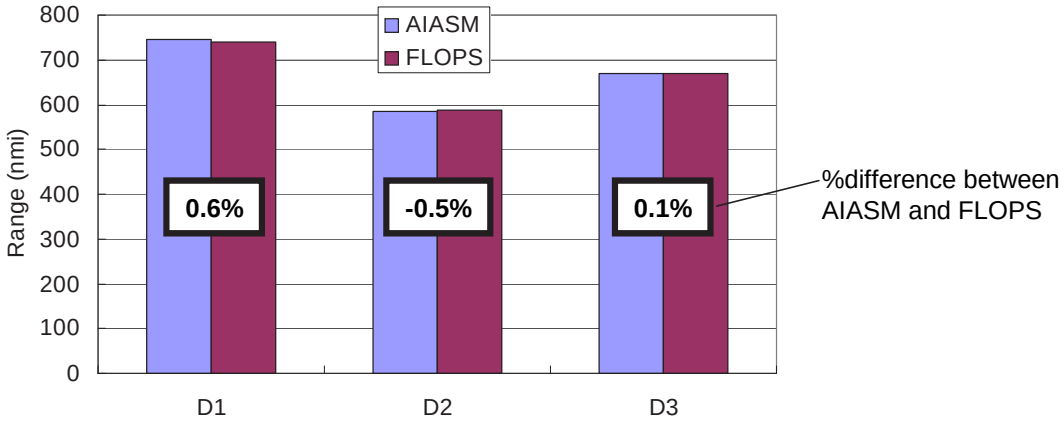

Figure 74: Comparison of range performance

Table 9: Probabilistic solutions

	P1	P2	P3
Power to Weight Ratio (ft/sec)	35.52	35.48	35.37
Wing Loading (lbs/ft^2)	11.06	11.05	11.03
Fuel Fraction	0.0341	0.0341	0.0336
Take-off Gross Weight (lbs)	2936	2933	2902
Wing Area (ft^2)	265	265	263
Propulsion System Power (Hp)	190	189	187

The results of the different approaches are listed in Table 9. All of the optimization problems resulted in the same set of active constraints: take-off field length, climb, and mission fuel. The three methods also yielded very similar optimum solutions.

The probability of failure of the constraints of all deterministic and probabilistic solutions was estimated by additional Monte Carlo simulations, as comparatively listed in Table 10. Solution **D1** is an example of the downfall of the "voice of intuition," which results in an unacceptable level of risk for the take-off field length constraint while having extraneous design margins for the other probabilistic constraints. This implies that the solution yields disproportionate amounts of reliability to the failure modes, despite yielding considerably heavier aircraft than the RBDO solutions. Solution **D2** yields a significantly high probability of failure for three hard constraints, which is not surprising because the solution is obtained without considering any design margins. Solution **D3** possesses more "balanced" reliability than **D1**. However, it does not provide the target reliability, since the amount of the fixed design margin (10%) was arbitrarily chosen. These observations lead one to surmise that, despite best intentions, the deterministic approach relying on "Rules of Thumb" may allow a *qualified success* at best.

In contrast, the solutions from the RBDO approaches yield balanced design margins to the hard constraints while minimizing the aircraft weight. The values of P_f for

Table 10: Comparison of probability of failure

	D1	D2	D3	P1	P2	P3
TOFL	0.1473	0.9879	0.3106	0.0352	0.0352	0.0507
Climb	0	0.6647	0	0.0268	0.032	0.0505
Cruise	0	0.1843	0	0	0	0
Approach	0	0	0	0	0	0
LDFL	0	0	0	0	0	0
Mission Fuel	0	0.813	0.1077	0.0258	0.0254	0.0507

the three hard constraints in FORM-RIA (**P1**) and FORM-PMA (**P2**) were smaller than the target value of 0.05. The difference beyond the tolerance of a constraint violation set for the optimization process (0.001) can be considered the error of FORM provided that the values computed by MCS are sufficiently accurate. It was observed that FORM constantly underestimates P_f in the example of this particular study. Although FORM possesses such noticeable errors, it demonstrated approximately 5 times the computational efficiency of the MCS-based optimization method for this sizing problem.

The probability of meeting all constraints simultaneously must be less than or equal the minimum of the probability level of meeting the individual constraints. Moreover, if there is a strong negative correlation between any two hard constraints, the probability of meeting the joint constraints may be significantly lower than a given probability for individual constraints. In this particular example, the solution of the MCS-based optimization method met joint probabilistic constraints by 89%. Therefore, it was deemed worthwhile to implement joint probabilistic constraints. A CCP problem, in which the six individual probabilistic constraints were consolidated into a joint probabilistic constraint, was formulated based on Eq. (149) presented in §5.5.1. The MCS-based optimization method was used for this study. The results, denoted as **P4**, are listed in Table 11. Applying the joint probabilistic constraints resulted

Table 11: The solution of joint probabilistic constraints

	P4	% Difference to P3
Power to Weight Ratio (ft/sec)	36.01	1.80
Wing Loading (lbs/ft^2)	11.22	1.72
Fuel Fraction	0.0340	1.00
Take-off Gross Weight (lbs)	2992	3.13
Wing Area (ft^2)	267	1.39
Propulsion System Power (Hp)	196	4.98

in higher required power and more fuel than applying the individual probabilistic constraints.

6.2 Regenerative Solar-powered Aircraft

In addition to the fuel cell-powered electric GA, the proposed methods were applied to the sizing of a solar-powered high altitude long endurance (SPHALE) aircraft with a regenerative PEM fuel cell system as a proof of concept. This analysis served as an excellent demonstration example of the proposed methods because such a regeneratively powered concept cannot be sized with traditional sizing methods as discussed in 4.7.2.

6.2.1 Mission and Configuration

The notional SPHALE aircraft is assumed to operate for more than six months starting on April 1st, at 38° N latitude and a design altitude of 17 km, carrying a payload that weighs 981 N[1] (100 Kg) and consumes 1,000 W of power continuously. The mission profile is depicted in Figure 75. The vehicle must be able to climb to 17 km by depending solely on solar energy and then maintain a level flight pattern. During the day, any excess energy from the sun is charged to the RFC system, while at night

[1]In this solar-powered aircraft study, the International System of Units (SI) is used because of its preference in the literature regarding this topic. For the same reason, British units are used in the general aviation study.

the platform would maintain altitude and its geostationary position by utilizing the stored energy. The aircraft maintains the flight speed that maximizes its loiter efficiency ($E = C_L^{3/2}/C_D$). In order to ensure a safe flight during periods of extremely high wind-speed jets, the aircraft must be able to sustain a level flight with a speed of 35 m/s for at least two hours per day.

On the first day starting its service, the aircraft climbs to the loitering altitude by taking advantage of the available solar insolation with tanks full of oxygen and hydrogen. Thus, no excess power is needed to be delivered to the electrolyzer during climb. It is expected that the aircraft will not require access to large numbers of public airports, and no specific rate of climb is required either, upon which take-off and climb performance are considered to be fall-outs. In addition, landing and approach speed are also treated as fall-outs, since the aircraft is very likely to have a very low wing loading, and consequently, a slow approach speed. Therefore, the maximum cruise speed is considered to be the only performance constraint in this study.

The HeliPlat shown in Figure 76 is selected as the baseline configuration for this study, because substantial analysis and experimental data for the configuration are available from Ref.[49]. The configuration has a high aspect ratio wing and a boom-mounted tail arrangement. The aspect ratio and taper ratio of the wing are 31 and 0.32, respectively. Aerodynamic coefficients of a quadratic drag polar for the configuration are obtained from regression analysis with CFD analysis data from Ref.[49] as shown in Figure 77. The regressed drag polar curve tightly matches the original wind tunnel data for $0.5 \leq C_L \leq 1.6$, which is the expected flight range of the aircraft. The coefficients of the regressed quadratic drag polar were estimated to be $K_1 = 0.0141$, $K_2 = -0.0024$, and $C_{D_o} = 0.0134$.

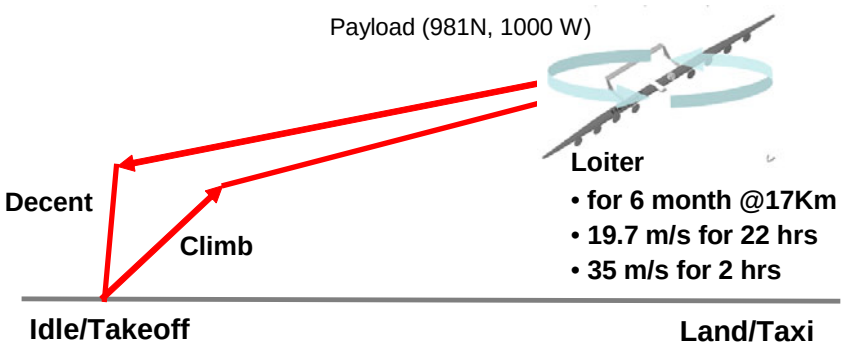

Figure 75: The mission profile of the SPHALE

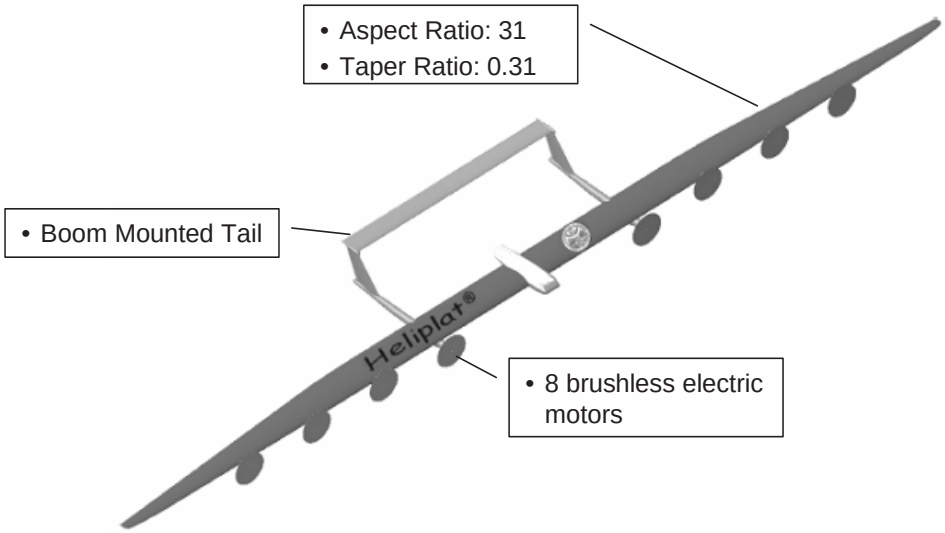

Figure 76: Baseline configuration of the SPHALE [49]

6.2.2 Deterministic Sizing

The airframe weight was computed with the following equation used in the HeliPlat study [49]:

$$W_{airframe} = 8.75 n^{0.311} AR^{0.4665} S^{0.7775} \tag{164}$$

where n is the maximum load factor, which is assumed to be 3.1 as proposed by the HeliPlat study. The avionics system weight was assumed to be fixed at 49 N. The weight and efficiency of the PV cells was estimated based on the PV cells manufactured by SunPower, which have been used in both the Pathfinder and Helios prototypes. The weight of the solar cells was computed by multiplying the weight per unit area (0.81 Kg/m^2) by the required surface area, and the collective efficiency of all panels was assumed to be 20%. The RFC system weight was computed based on its specific energy[2]. The specific energy of the state-of-the-art RFC system is reported to be 298 W-Hrs/Kg [211]. Recently, Jakupca and Wendell [211] showed that the specific energy of an RFC based on PEM fuel cells could possibly reach 359 W-Hrs/Kg by packaging the hydrogen and oxygen tanks within a common pressure vessel. For this study, the optimistic 359 W-Hrs/Kg projection was assumed to be representative current technology level. The roundtrip efficiency of the RFC system is estimated by employing an electrolysis theory and regression analyses as described in Appendix D. The electric propulsion system includes the motors, inverters, gears, and propellers, whose weight and efficiencies are estimated based on the information from the HeliPlat study. The design reference power, P_{ref}, is defined as the maximum continuous output power of the RFC system at the loiter altitude in this study,

[2]Fuel cells operates on an input fuel, and do not run down or need to be recharged, making them more similar to combustion engines in their use rather than batteries [64]. In such a sense, defining the specific energy for a fuel cell system would not make sense. In the case of RFC systems, however, the amount of energy content is part of the system properties, making them more similar to rechargeable batteries. Thus, the specific energy is apposite as a measure of the gravitational energy storage capability of the system. For this reason, the specific energy has often been used to estimate the weight of an RFC system; e.g., Ref. [49, 142]

which leads Π_η^+ to be the aggregated efficiencies of the electric propulsion system's components.

Based on the disciplinary data described above, the aircraft was sized via the iterative process illustrated in Figure 55 in §4.7.2. The initial guess of the aircraft's weight was 12,100N. The convergence history pertaining to aircraft weight, payload power-to-weight ratio, and wing loading are depicted in Figure 78 and Figure 79.

At every iteration, the 24 hour-cycle energy balance analysis and the constraint analysis are performed to update wing loading and power to weight ratio. Figure 80 shows the 24 hour-cycle energy balance analysis at the convergence point, depicting the variations in solar power, power required for flight, power required for payload, and RFC discharging power, each of which is normalized by aircraft weight. Power required for flight steps up during the first two hours of the cycle to account for the maximum headwind condition. Figure 81 depicts the constraint analysis of the SPHALE at the convergence point. The total power required is the sum of the power required for level flight and power for the payload. The maximum power required for flight occurs when headwind is at maximum, which establishes the condition of power sizing.

The sizing results of the baseline configuration are summarized in Table 12. In order to distinguish this solution from the others in subsequent investigations, it is denoted as **D1**. Figure 82 depicts the aircraft weight breakdown of solution **D1**. The airframe and propulsion system account for 39% and 52% of the aircraft weight, respectively. The lift-to-drag ratio at loiter and loiter efficiency ($C_L^{3/2}/C_D$) are estimated to be 35 and 44.3, respectively.

The actual-value-based approach is preferable for this example, since the existence of a fixed payload power significantly offsets the advantage of using weight-specific parameters, requiring a double-loop iteration. The actual-value-based approach employs an optimizer to match the performance to the target values by varying the

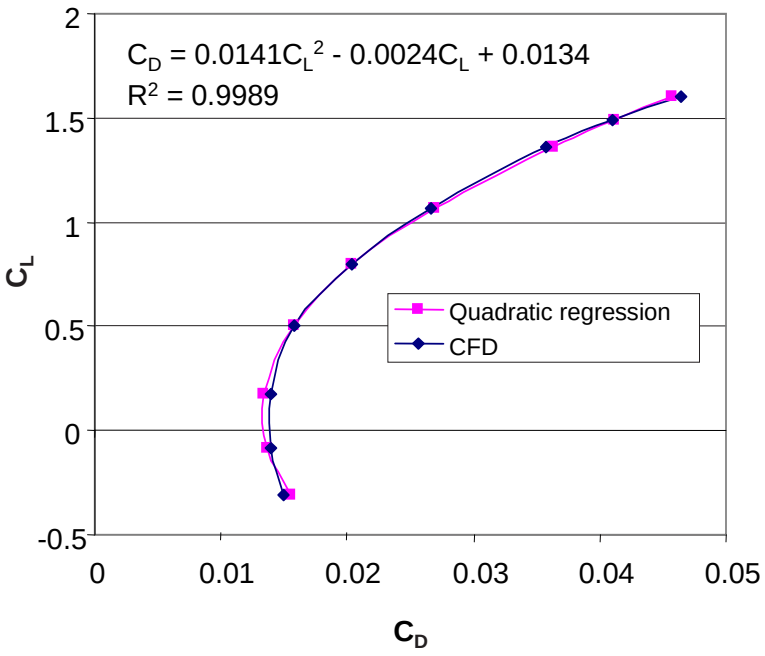

Figure 77: Comparison of drag polars

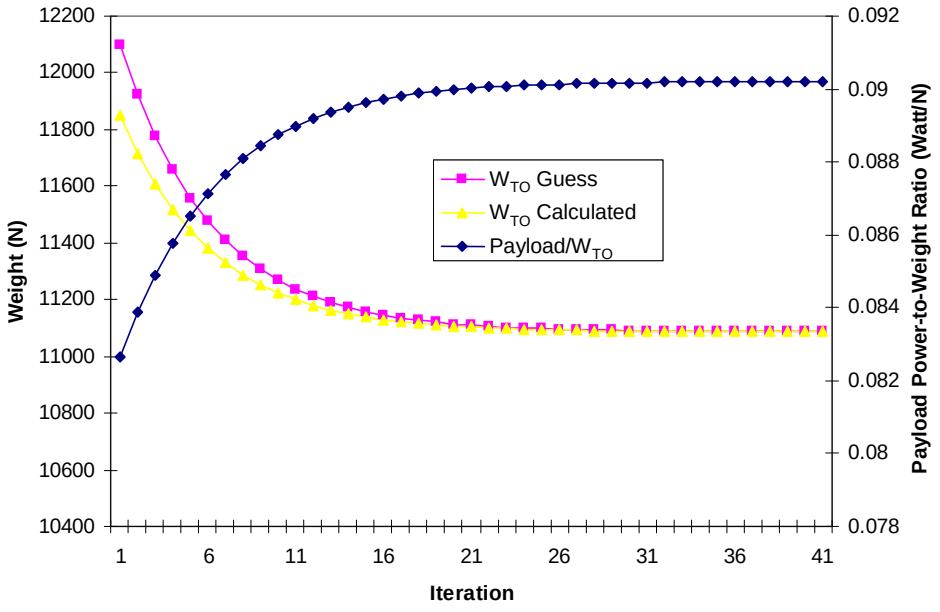

Figure 78: Convergence of weight and payload power-to-weight ratio

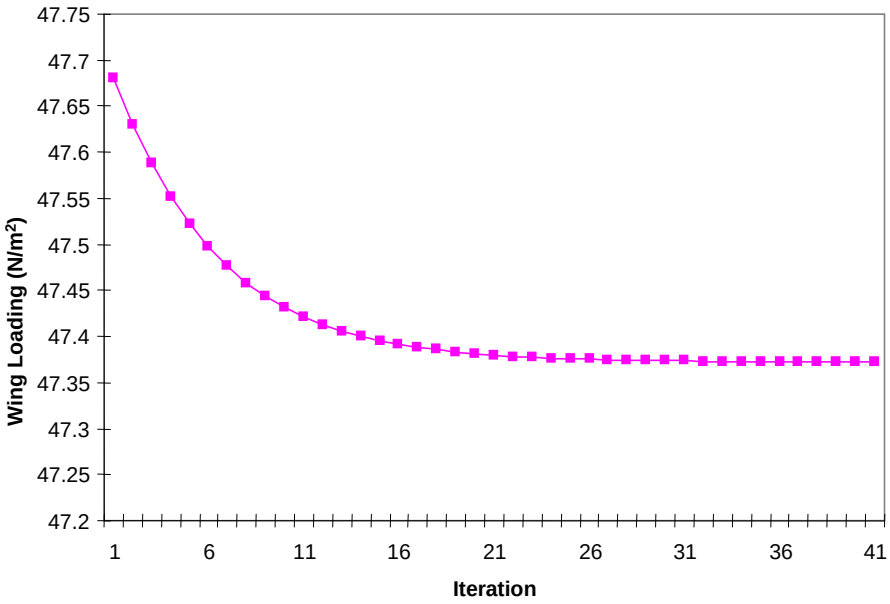

Figure 79: Convergence of wing loading

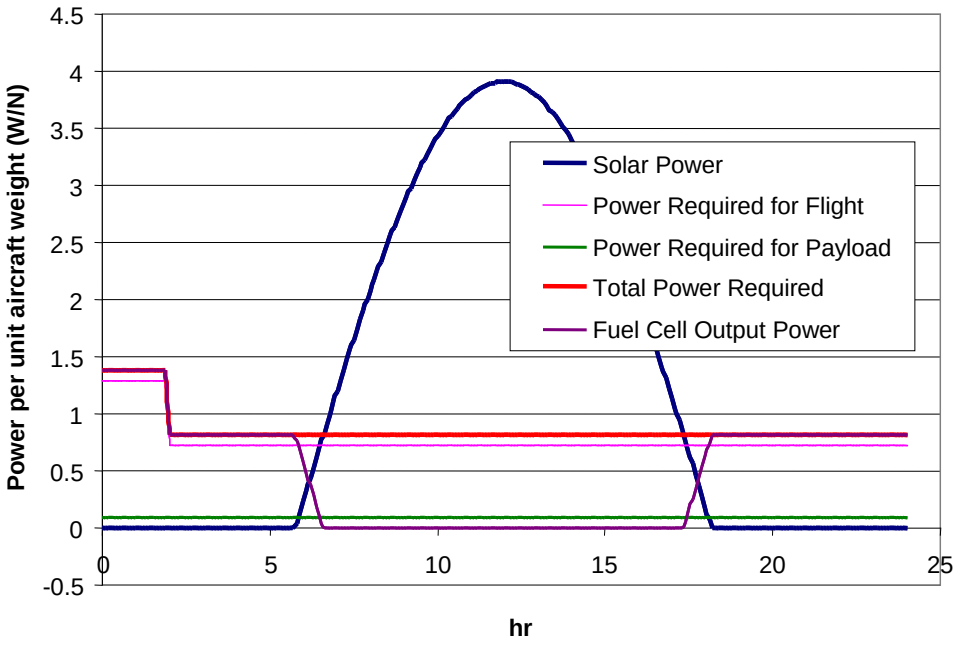

Figure 80: Power profile of the SPHALE

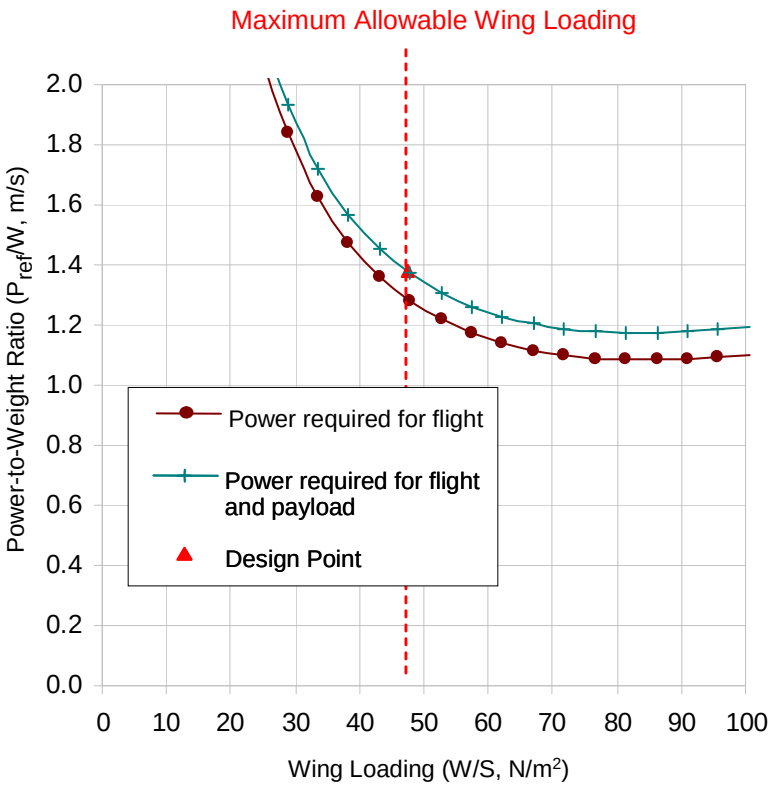

Figure 81: Constraint analysis at the converged solution

design variables (S, P_{ref}, and W_{H_2}). The design reference power (P_{ref}) for this case study is referred to as the total amount of power transferred from the PV cells and/or the RFC system to power electronics. The following constraints are considered to ensure the power balance, nighttime energy balance, and diurnal energy balance, which leads to the following nonlinear-constrained deterministic programming problem:

$$\begin{aligned} \min_{\mathbf{x}} \quad & W_{TO} \\ \text{s.t.} \quad & P_{ref} \geq \frac{DV_{\max}}{\Pi_{\eta}^{+}} + P_{PL} \\ & W_{H_2}|_{available} \geq W_{H_2}|_{required} \\ & E_{StorOUT} = \eta_{rt} E_{StorIN} \end{aligned} \tag{165}$$

Table 12: Baseline configuration sizing - solution **D1**

Aspect Ratio	31
Wing Loading (N/m^2)	47.4
Power-to-Weight Ratio (m/s)	1.378
Required RFC System Energy to Weight Ratio (Wh/N)	11.3
Wing Area (m^2)	234
Max Power required (KW)	15.3
Aircraft Weight (N)	11,086
Required RFC System Energy (KWh)	125.1
Optimum AoA	1.6
Optimum Loiter Velocity (m/s)	20.4
L/D	35.0
E	44.3

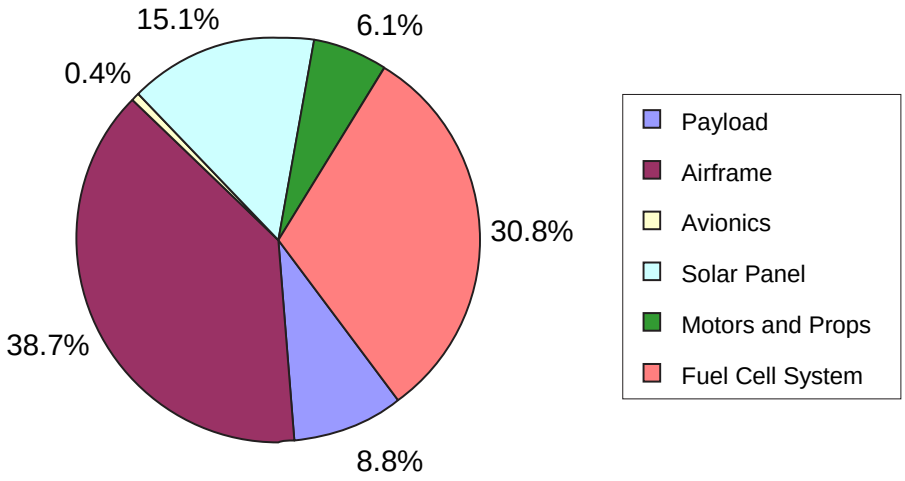

Figure 82: Weight breakdown of the design gross weight of **D1**

This problem was solved by an SLP algorithm of a commercial optimization package, DOT®, included in ModelCenter® and its solution was found to be numerically identical to **D1**, obtained by the specific parameter-based method.

6.2.3 Impact of Technology Advancement

Solution **D1** was obtained based on currently available technologies. However, relevant technologies are rapidly advancing as discussed in §1.1. Therefore, it is worthwhile to investigate the impact of technology improvement on aircraft sizing. This study considered five technology factors: 1) PV cell efficiency, 2) PV cell weight, 3) RFC system specific energy, 4) fuel cell efficiency, and 5) propulsive system specific power. The aircraft was re-sized while incorporating a series of improvements in each technology factor, between 10% and 50%, and the resultant aircraft designs are compared in Figure 83. The most significant reduction in aircraft size occurs by increasing the PV cell efficiency and the RFC specific energy, whereas the mass of the power electronics plays a marginal role in comparison[3].

Romeo et al. [49] proposed the goals of future technologies in solar-powered HALE aircraft as follows:

- PV cell efficiency increased to 25%
- RFC system specific energy increased to 550 KWh/Kg
- efficiency of fuel cells of the RFC increased to 70%

The present research accepts these hypothetical advanced technology assumptions as representative near-term goals, which are consistently applied through the subsequent studies presented in §6.2.4 to §6.2.7. To reflect the projected improvement in each technology, the baseline configuration was re-sized, and the resultant design is denoted

[3]Mission requirements also substantially affect the aircraft size. By limiting the time of year the aircraft is required to fly at high northern or southern latitudes, a significant reduction in aircraft size or increase in payload capacity can be achieved.

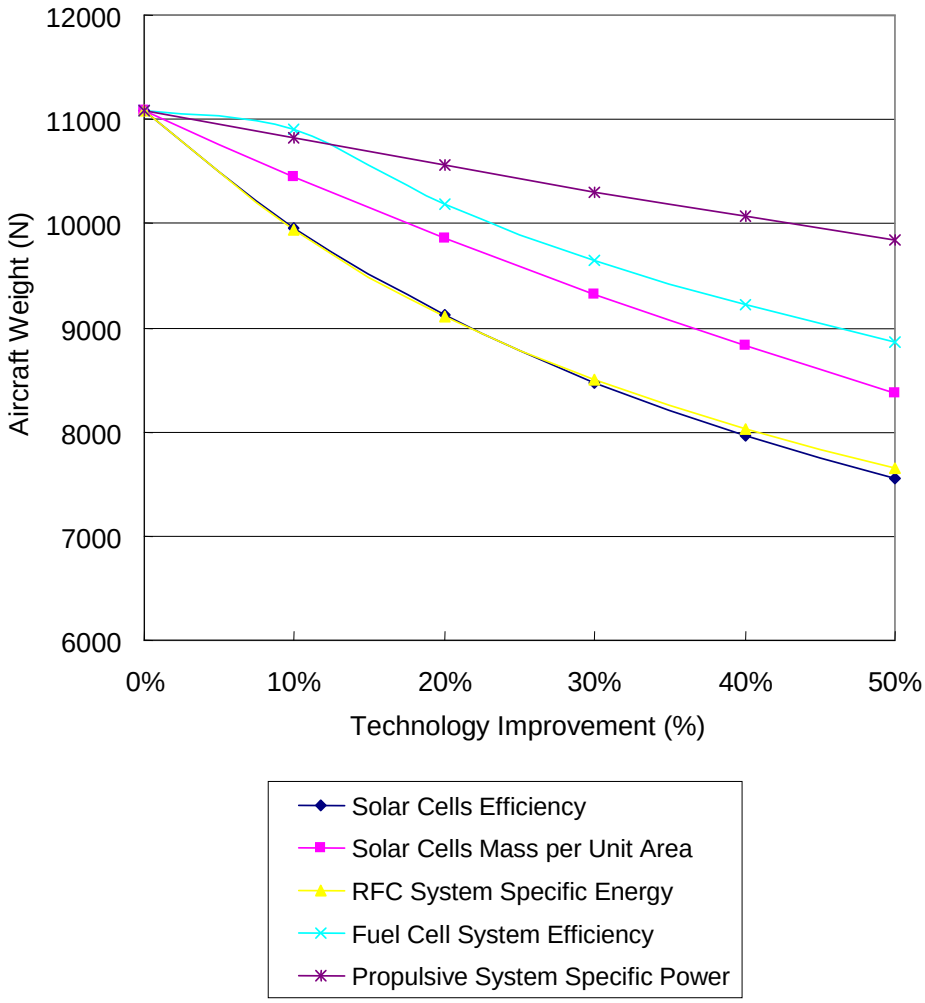

Figure 83: Sensitivity of technology impact

Table 13: Baseline configuration sizing with advanced technologies - solution **D2**

Aspect Ratio	31
Wing Loading (N/m^2)	54.7
Power-toWeight Ratio (m/s)	1.372
Required RFC System Energy to Weight Ratio (Wh/N)	12.8
Wing Area (m^2)	105
Max Power required (KW)	7.86
Aircraft Weight (N)	5729.6
Required RFC System Energy (KWh)	73.3
Optimum AoA	1.6
Optimum Loiter Velocity (m/s)	22.0
L/D	36.1
E	44.3

as **D2**. The details of **D2** are summarized in Table 13. Weight reduction in each weight group by infusing advanced technologies is illustrated in Figure 84, which shows a 46% to 52% reduction in the weight of airframe and propulsion system components, which collectively reduces the aircraft weight by 48%. The weight breakdown of the aircraft is depicted in Figure 85, which identifies, in comparison with Figure 82, that reflecting the projected technology improvements results in a considerable reduction in the RFC system weight fraction. The solar cells' weight fraction did not change considerably because the panels' weight decreases in proportion to the amount of reduction in aircraft weight. In contrast, a notable increase in the payload weight fraction was observed to be caused by aircraft weight reduction.

6.2.4 Configuration Optimization

Even when a basic concept is determined, a large number of external configuration options such as the selection of airfoil, platform, and twist distribution for wings and tails may still be altered by designers. As discussed in §5.5.2, aircraft sizing can be performed in conjunction with optimizing disciplinary design variables. For demonstration purposes, the wing aspect ratio was selected as a representative disciplinary

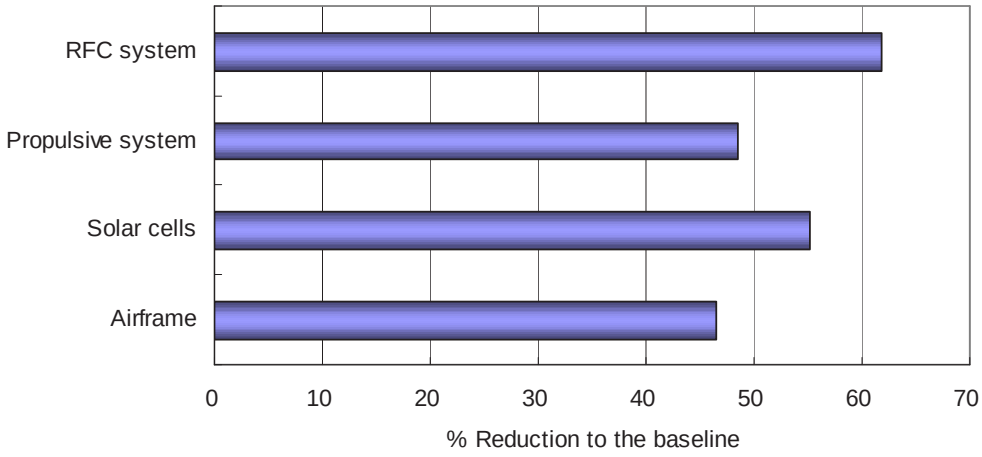

Figure 84: Weight reduction in weight groups by infusing advanced technologies

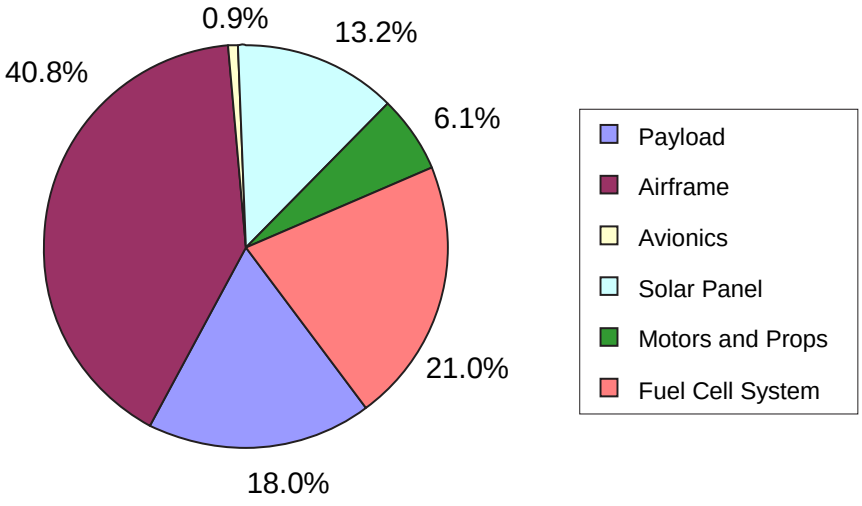

Figure 85: Weight breakdown of the design gross weight of **D2**

variable, because it is generally considered a primary design parameter that trades the aerodynamic efficiency and wing weight. As the aspect ratio increases, drag-due-to-lift reduces. Such a tendency can be captured by employing a set of empirical equations. The coefficient of drag-due-to-lift (K) can be expressed by:

$$K = 1/\pi e AR \tag{166}$$

where AR is the aspect ratio, and e is known as Oswald's efficiency of the wing of sailplanes, which was approximated as suggested in Ref. [212].

$$e = \begin{cases} 0.9 & AR \leq 20 \\ 1.2 - 0.015AR & AR > 20 \end{cases} \tag{167}$$

The variation in K as a function of aspect ratio, estimated by Eq. (166) and Eq. (167), is illustrated in Figure 86. This figure shows that the values of K decrease as aspect ratio increases, and measurements from the wind tunnel test of the baseline configuration match the empirical equation well. The variation in airframe weight with aspect ratio can be captured by Eq. (164). Figure 86 also shows the impact of aspect ratio on airframe weight for two wings of different sizes.

The optimum aspect ratio can be found by solving the optimization problem expressed as Eq. (165) in §6.2.2 by adding aspect ratio to the list of design variables. The same analysis tools and environment as used for the previous actual-value-based attempt to solve Eq. (165) were used. The results, denoted as **D3**, are listed in Table 14. The optimum aspect ratio was found to be 25.6, which results in 92 N of reduction in the total aircraft weight.

6.2.5 Probabilistic Sizing

The impact of technology improvements and wing geometry optimization presented thus far are from a deterministic aircraft sizing perspective; that is, the aircraft was sized without any additional design margins. It was assumed that the uncertainty

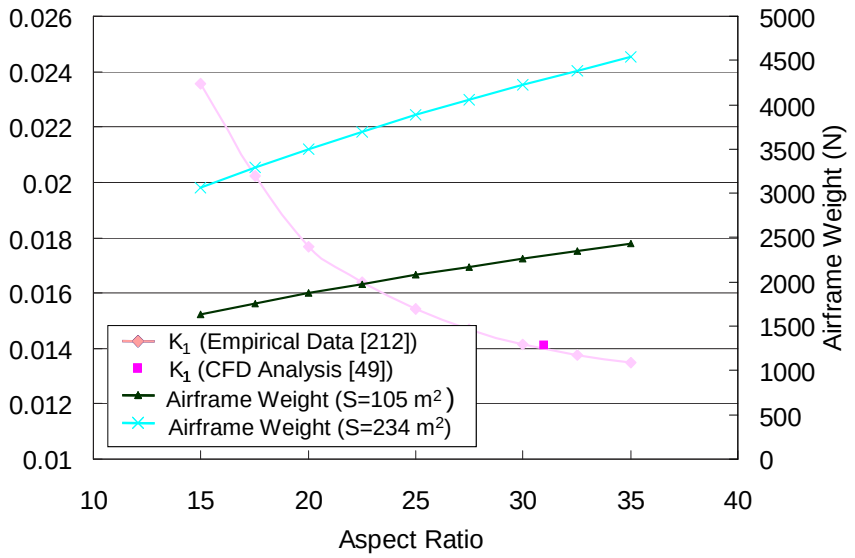

Figure 86: Impact of wing aspect ratio on drag and airframe weight

Table 14: Optimum configuration with advanced technologies - solution **D3**

Aspect Ratio	25.6
Wing Loading (N/m^2)	52.5
Power-to-Weight Ratio (m/s)	1.432
Required RFC System Energy to Weight Ratio (Wh/N)	13.3
Wing Area (m^2)	107
Max Power required (KW)	8.07
Aircraft Weight (N)	5637.6
Required RFC System Energy (KWh)	75.2
Optimum AoA	1.5
Optimum Loiter Velocity (m/s)	22.0
L/D	33.3
E	41.4

Table 15: Assumed distributions of random parameters

Normalized Random Parameter	Distribution	μ	σ	LB	UB
Induced Drag, K_1	Normal	1	0.01	0.95	1.05
Maximum Level Flight Speed	Normal	1	0.02	0.9	1.1
PV Cell Efficiency	Normal	1	0.03	0.9	1.1
Airframe Weight	Normal	1	0.02	0.9	1.1
RFC System Specific Energy	Normal	1	0.05	0.833	1.167

sources listed in Table 16 would play an important role in this design example. All random parameters were modeled as normal distributions normalized by their mean values. The upper and lower bounds (UB and LB) truncating both sides of tails were set to prevent unrealistic, extreme cases.

The three constraints included in the deterministic sizing problem per Eq. (165) are considered again, but were rearranged as follows:

$$\begin{aligned} g_1 &= P_{ref}|_{available} - P_{ref}|_{required} \geq 0 \\ g_2 &= E_{RFC}|_{available} - E_{RFC}|_{required} \geq 0 \\ g_3 &= W_{H_2}|_{regenerated} - W_{H_2}|_{required} \geq 0 \end{aligned} \tag{168}$$

Based on the assumptions of uncertainty, the probability of failure for each constraint in deterministic solution, **D3** was computed by MCS. Out of 100,000 runs, the probability of failure for all constraints was estimated at 0.5. Such a high probability of failure results from not having considered adequate design margins for the random parameters.

The target probability was set at 95% for each constraint. The design objective was established as minimizing the design gross weight (W), which is also affected by the two random parameters: the airframe weight and the specific energy of the RFC system. In order to address the probabilistic nature of the response, a target confidence level (95% for this study) was imposed on the probabilistic objective as an additional constraint as described in §5.5.3.1, which means the 95$^{\text{th}}$ percentile of

the aircraft gross weight responses were used as the objective function value by the system-level optimizer.

MCS and FORM were used to estimate the probability of success (reliability) for each design constraint. The probabilities computed by two different methods are compared at 30 points randomly selected in the design space. In Monte Carlo simulations, 100,000 cases were generated by Crystal Ball® with a fixed seed number, and the probability of meeting each constraint was computed. As shown in Figure 87, FORM estimated the reliability with comparable accuracy to the MCS. Figure 88, illustrating the differences in the 95^{th} percentile of aircraft weight responses computed by the two methods, shows that FORM was also able to estimate the objective function with comparable accuracy to MCS for this case study. It was also observed that FORM produces a higher probability of meeting the constraints and lower values of aircraft weight than MCS for most test points. It must be noted that such a tendency is valid for this particular example, since FORM does not necessarily yield a more optimistic estimation than MCS.

It was found that FORM was approximately 4 times faster than the Monte Carlo simulation for this particular example problem and the analysis environment employed. To enhance computational efficiency, the problem was solved first by using FORM for a nested reliability analysis. The solutions are denoted as **P1**. Subsequently, the problem was solved again using MCS with **P1** as an initial point for the optimization process, the solution of which is denoted by **P2**.

The SLP algorithm was used both for solving the system level optimization problem and for the MPP search. The optimization results are summarized in Table 16, showing that the solution obtained by FORM was very close to that obtained by the Monte Carlo simulation. The difference in the design variables and the objective function values was less than 1%.

For further comparison of accuracy of FORM and MCS, Monte Carlo simulations

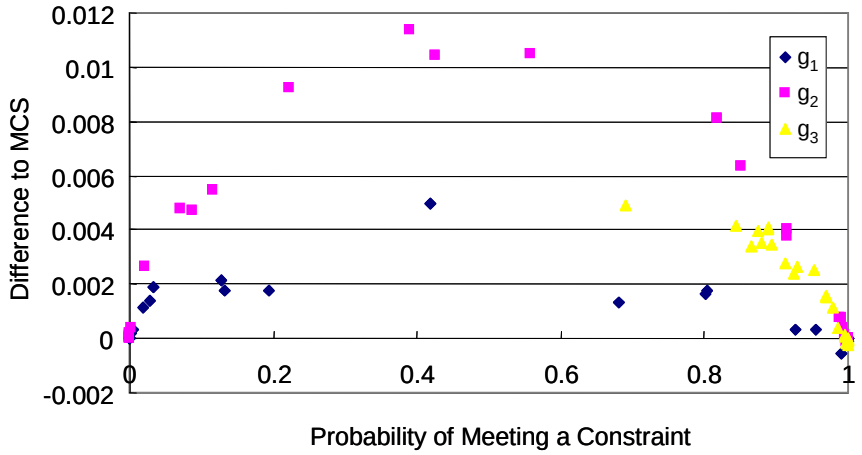

Figure 87: Differences in probabilities meeting the constraints estimated by FORM to those estimated by Monte Carlo simulations

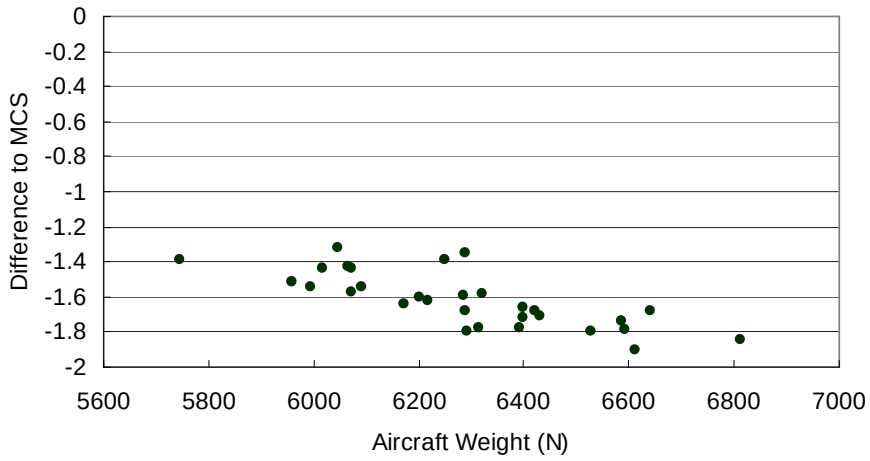

Figure 88: Differences of the objective function values (95^{th} percentile of the objective function responses) estimated by FORM to those estimated by Monte Carlo simulations

Table 16: Comparison of the results of probabilistic sizing by FORM and MCS

		P1	**P2**	% Difference
Optimum	Aspect Ratio	26.07	25.93	0.53
Solution	Wing Area (m^2)	120.02	120.38	-0.29
	Power Available (KW)	9.27	9.30	-0.27
	RFC System Energy (WKh)	81.68	81.89	-0.26
Constraints	Power Balance	Active	Active	
	Nighttime Energy Balance	Active	Active	
	Diurnal Energy Balance	Active	Active	
Objective	95^{th} percentile	6260	6269	-0.14
Function (N)	Mean	6110	6116	-0.11

were performed with **P1** while varying the number of trials from 10^2 to 10^5. For each trial number, Monte Carlo simulations were repeated ten times while varying the seed number for random number generations to produce different sets of random events. The results are depicted in Figure 89, which shows the probabilities of meeting the non-deterministic constraints and the values of the objective function for different numbers of trails. The dotted lines and the solid lines represent the probabilities computed by FORM and MCS with one million trials, respectively. The figure also shows that the clusters of Monte Carlo simulations results converge to the solid line as the number of trials increases. The figure shows that FORM slightly overestimates the reliability of the constraints. However, it is observed that some Monte Carlo simulations with less than 10^5 trials produced higher errors than FORM.

Figure 90, which compares the percentage-difference between the probabilistic solutions (**P1** and **P2**) and deterministic solution (**D3**), shows that power, wing area, and the amount of RFC system discharge energy of the probabilistic solutions are increased by 6.2%, 12.0%, and 8.9%, respectively, in order to satisfy the target probability of meeting the constraints. Such differences in design variables can be referred to as the design margins required to mitigate the risk associated with uncertainty.

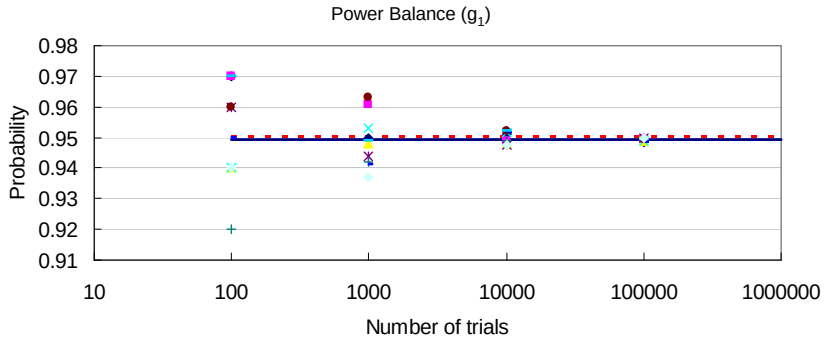

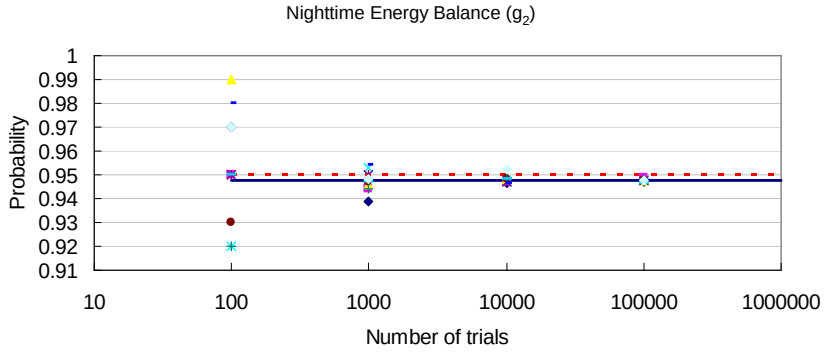

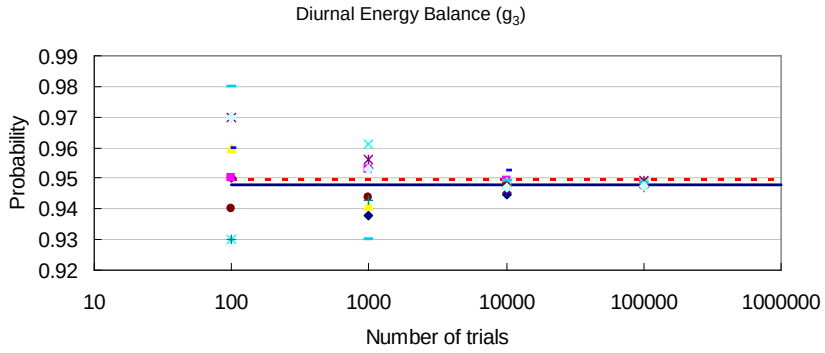

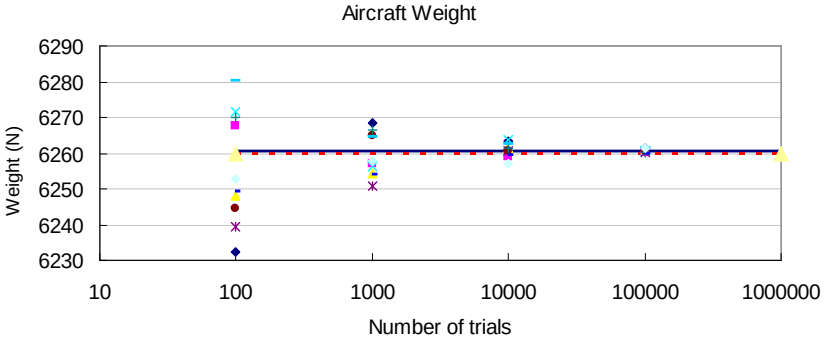

Figure 89: Monte Carlo simulations with different numbers of trials for **P1**

As shown in Figure 90, the design margin required for each design variable is not the same. Therefore, simply adding constant percentage of a design margin to all design variables may result in a non-optimal solution in the sense of CCP and RBDO.

Since the design gross weight is affected by the random parameters, the response is given as a distribution for a certain design variable setting. The distributions of the objective function and the constraint functions at **P2** are shown in Figure 91 and Figure 92, respectively. The distributions of several other responses of interest at the optimum solution, such as optimal angle of attack, loiter efficiency, flight speed, and required power at loiter, are depicted in Figures 114-117 in Appendix E.

As mentioned previously, one of the advantages of using CCP is that it allows the decision maker to trade the associated risk with the goal of the objective function. This is particularly useful when the decision maker has only a vague idea of what the appropriate confidence level is. This trade-off can be facilitated by a visual relationship between α and the value of the objective function, as illustrated in Figure 93. The objective function (the 95^{th} percentile of the design gross weight responses) increases as α increases. After α exceeds 90%, the expectation of the take-off gross weight rapidly grows, which indicates "more cost per reliability." This information assists a decision maker to determine the level of α.

6.2.6 Sensitivity Analysis

As discussed in §5.6.1, Lagrange multipliers provide an insight into the sensitivity of the objective function value with respect to the target probability. The Lagrange multipliers at the probabilistic solutions, **P1** and **P2**, are listed in Table 17. Their magnitudes identify that the diurnal energy balance constraint (g_3) is most important for both **P1** and **P2**. A Lagrange multiplier represents the variation of the objective function per unit change in the constraint function. The Lagrange multipliers listed in Table 17 were obtained by outer-loop optimization processes, in which the constraint

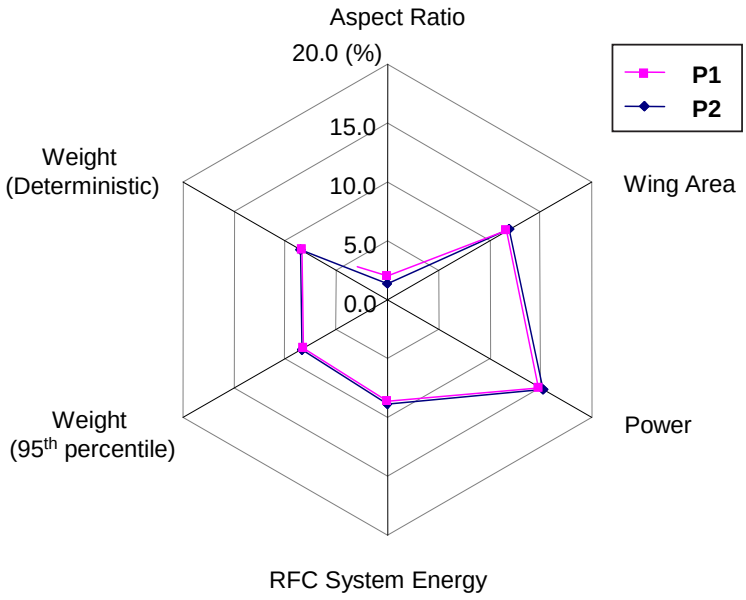

Figure 90: Difference of probabilistic solutions, **P1** and **P2** to the deterministic solution, **D3** in percentage

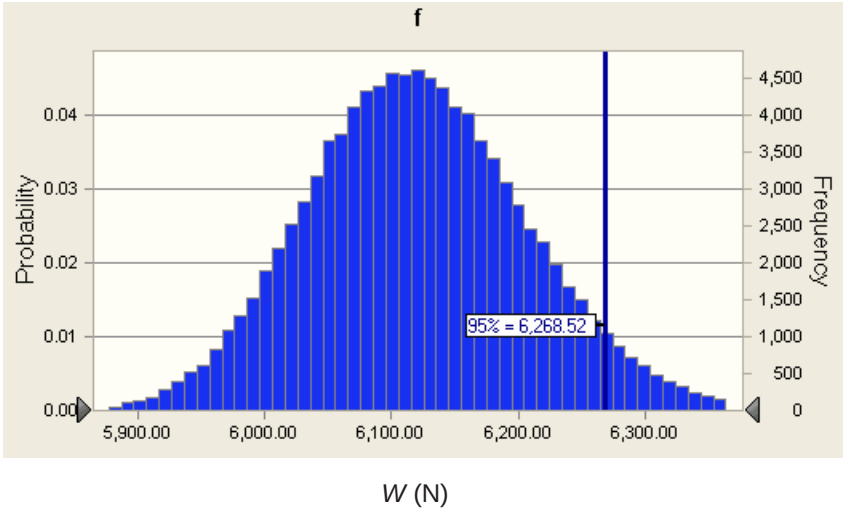

Figure 91: PDF of the objective function

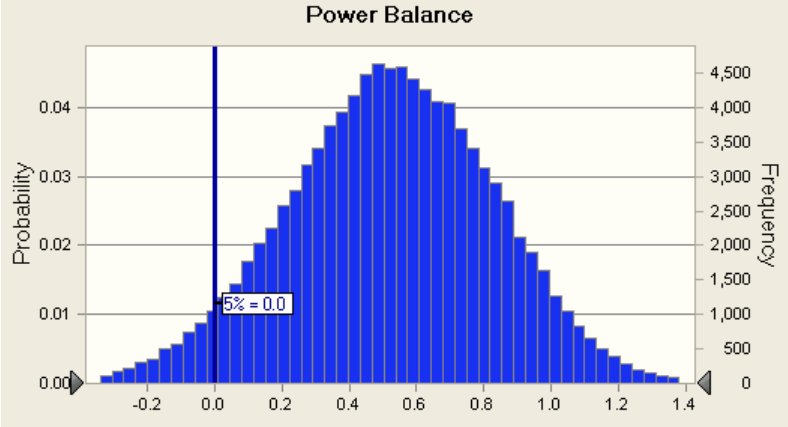

$$g_1 = P_{ref}|_{available} - P_{ref}|_{required} \text{ (KW)}$$

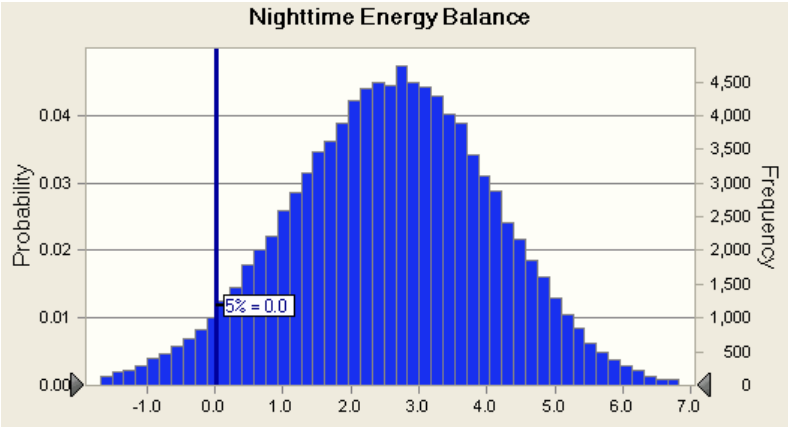

$$g_2 = E_{RFC}|_{available} - E_{RFC}|_{required} \text{ (KWh)}$$

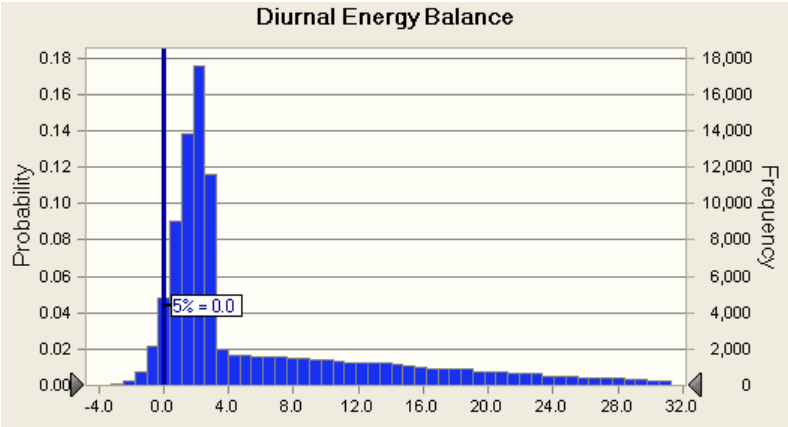

$$g_3 = W_{H_2}|_{regenerated} - W_{H_2}|_{required} \text{ (N)}$$

Figure 92: PDF's of constraint functions

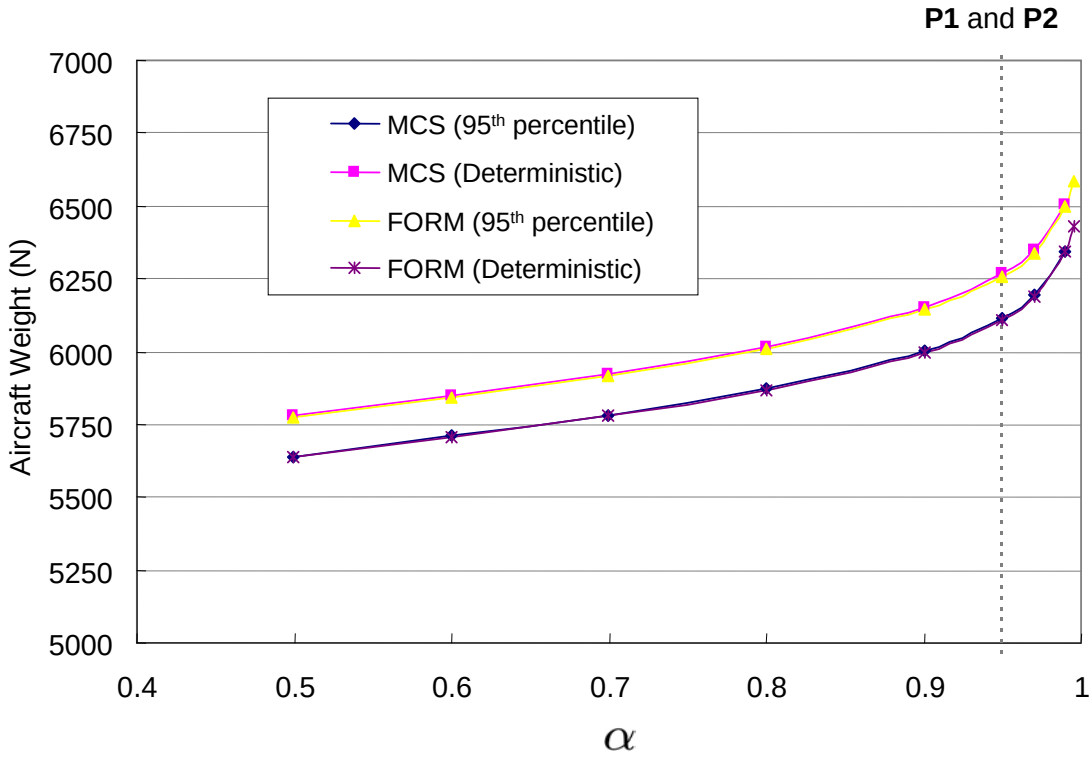

Figure 93: Objective function vs. target reliability

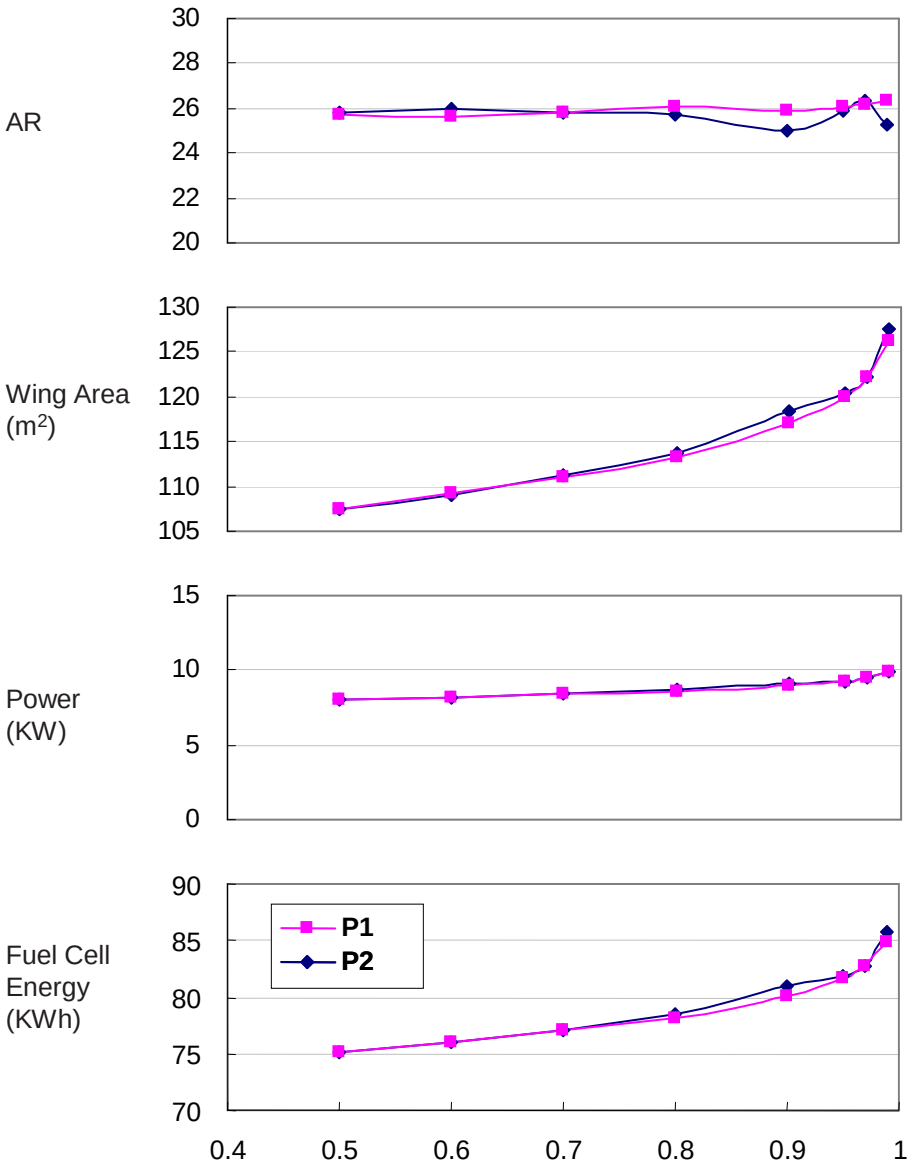

Figure 94: The optimum values of sizing variables vs. target reliability

Table 17: Lagrange multiplier

	P1	**P2**
Power Balance, g_1	420	726
Nighttime Energy Balance, g_2	889	879
Diurnal Energy Balance, g_3	1895	1732

functions were given in the form of $\mathbb{P}[g > 0] > \alpha$ instead of $g > 0$. Therefore, the sensitivity of the target probability, in terms of percentages, for a constraint can be obtained by dividing its Lagrange multiplier by 100. For example, it is expected that a relaxation of the target probability of g_3 by 0.01 (1%) will result in a reduction in the aircraft weight by 19.0 N and 17.3 N for **P1** and **P2**, respectively.

In order to assess the accuracy of Lagrange multipliers as sensitivity indices, the local sensitivities of the objective function to the target probability of constraint functions were computed by a finite difference method, and comparatively listed in Table 18. The first column lists the Lagrange multipliers of **P1** divided by 100. The second column presents the sensitivity of the objective function to the target probability obtained by subsequently solving the optimization problem while reducing the target probability of each constraint by 1% at a time. As it can be seen from Table 18, the sensitivities computed by Lagrange multipliers are in agreement with those obtained by the finite difference method. It must be noted that Lagrange multipliers provide only local sensitivities near the optimum solution. Nevertheless, they can be obtained as by-products of the optimization process, requiring no additional computational cost.

Another important sensitivity analysis was performed by the PSA discussed in §5.6.2. The sensitivities assist engineers in understanding the relative importance of the uncertainty of the probabilistic objective and constraint functions. The sensitivity of the constraint functions to the random parameters for **P1** were evaluated by the MPP-based sensitivity method presented in §5.6. Figure 95 shows the sensitivity

Table 18: Sensitivity of the objective function per target probability (%)

	By Lagrange Multiplier	Finite Difference Method	% Difference
Power Balance, g_1	4.2	4.1	0.1
Nighttime Energy Balance, g_2	8.9	7.8	1.1
Diurnal Energy Balance, g_3	19.0	18.3	0.7

indices of random parameters for each constraint. This sensitivity analysis reveals the most significant random parameter for each probabilistic constraint and objective function. The maximum cruise speed, and PV cell efficiency were found to be the dominant factors for the power balance constraint and the energy balance constraint, respectively. The energy balance and the objective function were found to be most heavily sensitive to fuel cell stack energy density. Particularly, the power balance constraint and the diurnal energy balance constraint were mostly affected by one dominant parameter, which implies that the reliability of the probabilistic constraint can be substantially improved by eliminating the uncertainty associated with the parameter.

The sensitivity for **P2** that was obtained by MCS can be obtained by an embedded feature of Crystal Ball®. This tool pairs up each assumption rank list with a corresponding forecast rank list and then calculates a Pearson correlation coefficient for each pair [213]. Figure 96 depicts the sensitivity of the responses of the objective and constraint functions of Crystal Ball®. The results are consistent with those obtained by the MPP-based analysis shown in Figure 95.

Figure 97 depicts how reducing the variance of each assumption improves the odds of meeting the non-deterministic constraints. All importance rankings listed in Figure 97 are consistent with those observed from Figure 95. For example, the probability of meeting the power balance constraint was found to be dominated by the maximum cruise speed in Figure 95. Figure 97 shows that reducing its variance

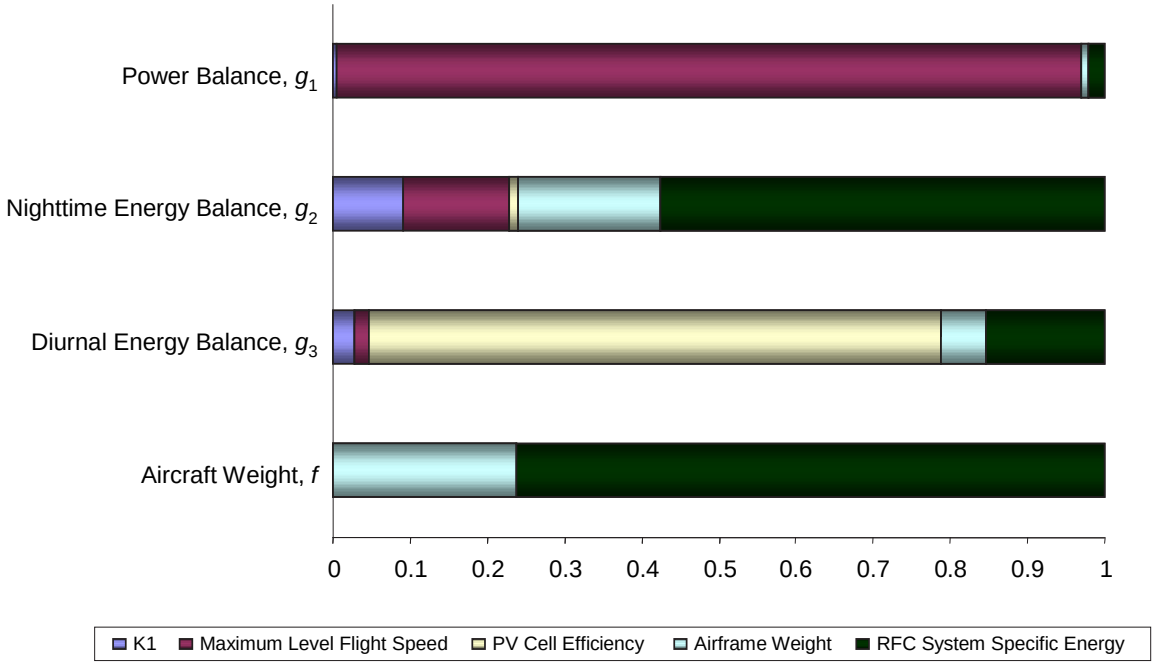

Figure 95: Sensitivity index obtained by the MPP-based sensitivity analysis

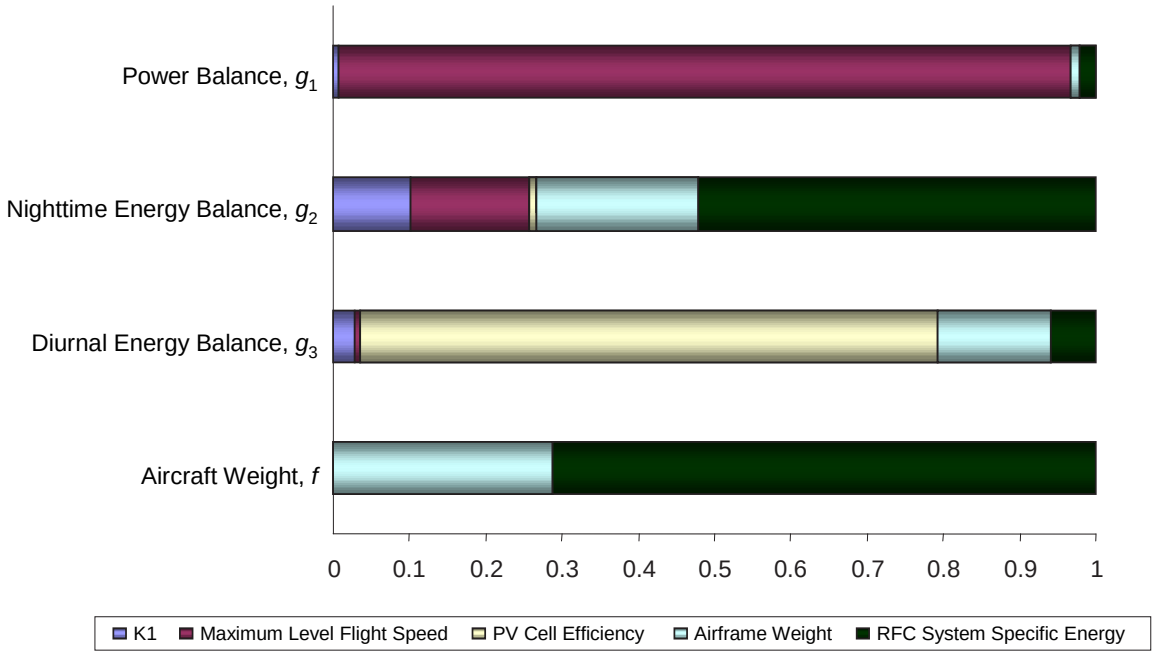

Figure 96: Sensitivity index obtained by Crystal Ball®

by 30% increases the probability from 0.95 to 0.99, while reducing the variance in other random parameters leads to a paltry improvement in reliability.

6.2.7 Joint Probabilistic Constraints

Application of the joint probabilistic constraints to the probabilistic sizing problem is preferred when the probability of simultaneously meeting the probabilistic constraints is more meaningful. As mentioned in §5.5.1, the probability of meeting all constraints simultaneously must be less than or equal the minimum of the probabilities of meeting individual constraints. In this particular example, the probability of meeting the joint probabilistic constraint at **P2**, which meets the individual constraints with 95% probability, was computed at only 0.88. This difference can easily be explained by Figure 98, which depicts the constraint function responses taken from Monte Carlo simulations with the solution. For better visuality, 3,000 random cases out of 100,000 cases are included in the figure. The problem is set up such that $g > 0$ is the feasible set. Therefore, the cases that are located in the upper right quadrant meet g_1 and g_2 concurrently. As shown, there are some random events that do not satisfy g_1 and g_2 simultaneously, while instead, satisfying only one of them. In addition, some cases marked in blue and located in the upper right quadrant fail to meet g_3, although they satisfy the energy balance and power balance constraints.

A CCP problem, in which the three individual probabilistic constraints are consolidated into a joint probabilistic constraint was formulated based on Eq. (149) presented in §5.5.1. It was observed that the SLP algorithm often fell into an infeasible region where the gradient of the constraints was computed at zero, thereby terminating the optimization process. It was conjectured that this problem was caused by the intrinsic nature of the SLP algorithm. The SLP algorithm approximates the nonlinear constraints as linear constraints at a current design point and applies a simplex method to obtain an optimum solution in the approximated design space. No optimum point

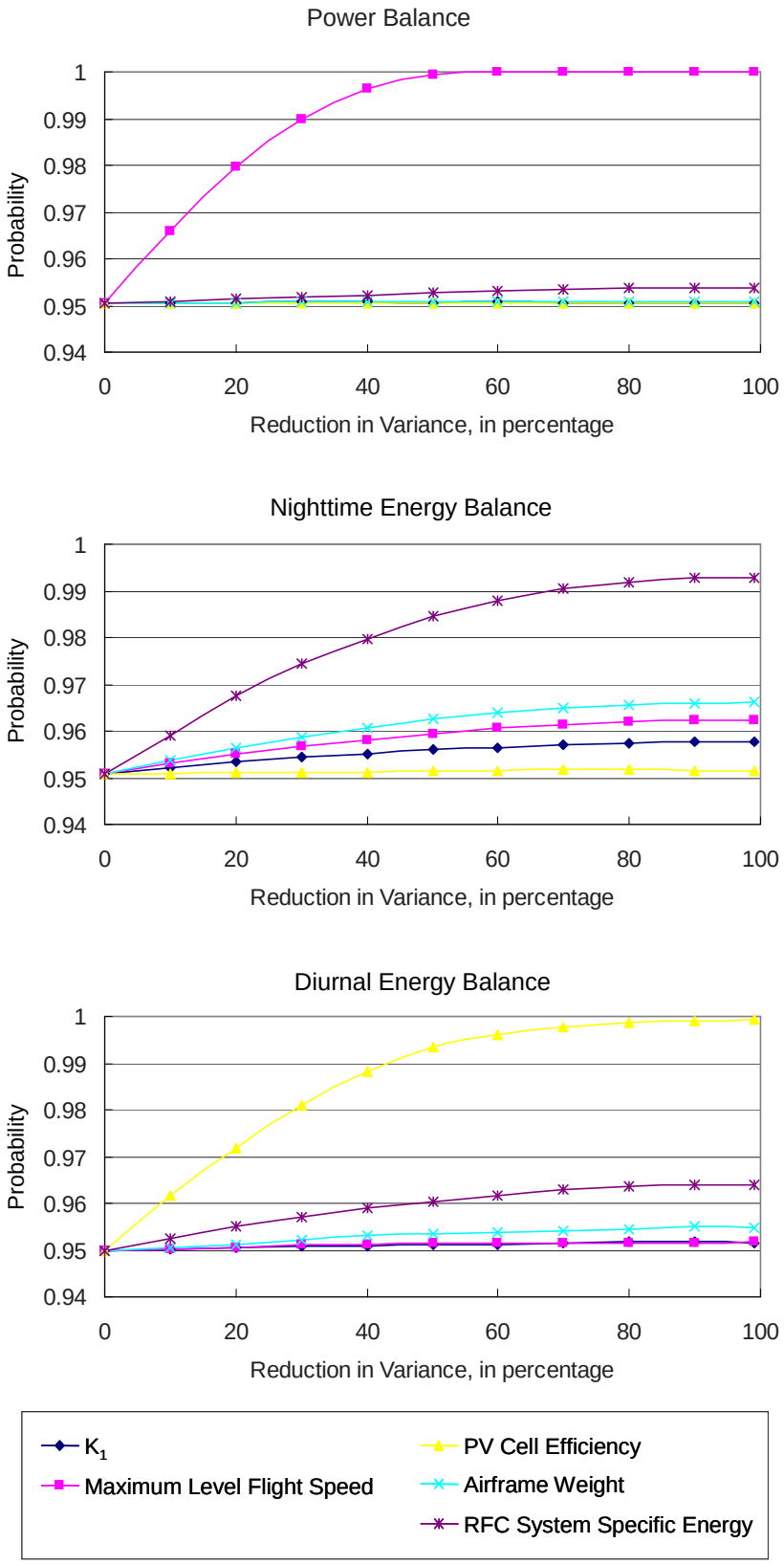

Figure 97: Reliability improvement of probabilistic constraints by variance reduction in random parameters

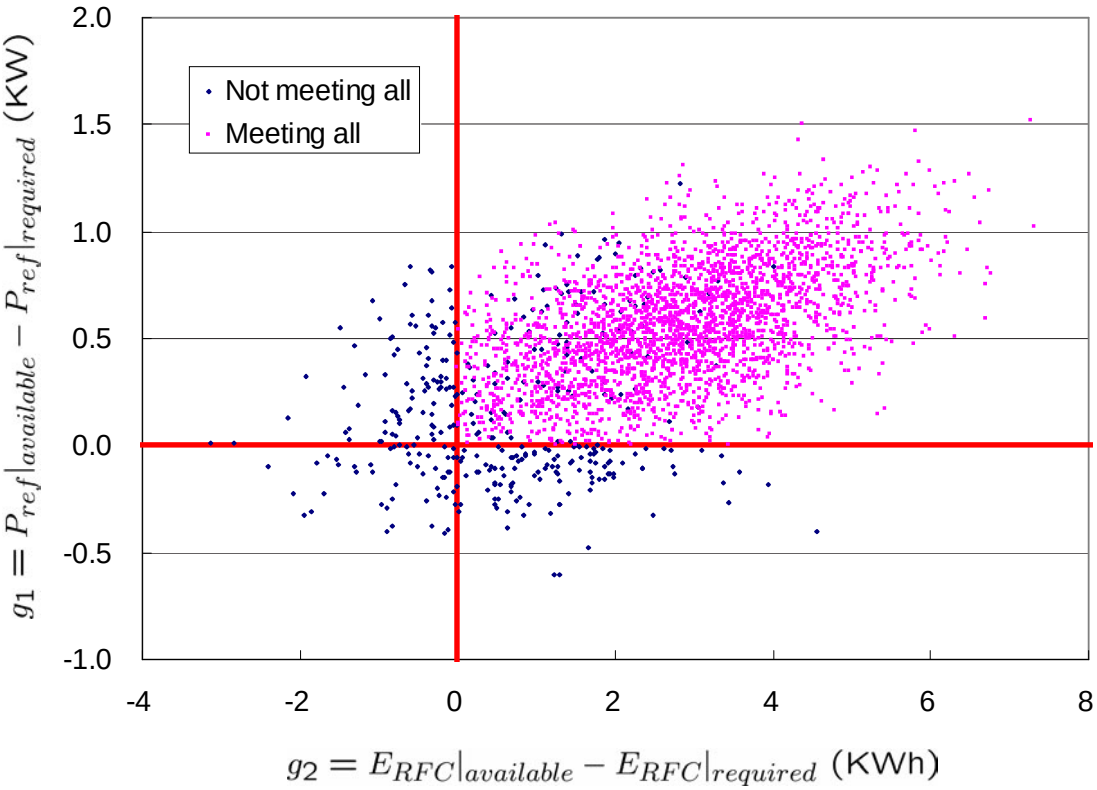

Figure 98: Illustration of samples of an MCS in the space of "power balance - energy balance"

may be found when the design space is constrained with one linear constraint. This problem can be resolved either by using an MoFD algorithm or adding individual probabilistic constraints for which target probability is the same as that of the joint probabilistic constraint. The feasible set confined by multiple individual constraints must include the feasible set that meets the joint constraint. Therefore, adding the individual constraints does not affect the optimum solution. Instead, they help to prevent the process from falling into divergence. The sizing solutions of the CCP optimization problem with joint probabilistic constraints are listed with those of the individual probabilistic constraints in Table 19.

Table 19: Comparison of the solutions of individual probabilistic constraints and joint probabilistic constraints

	Individual Probabilistic Constraint	Joint Probabilistic Constraint	% Difference
Design Variables			
Aspect Ratio	25.9	27.5	5.9
Wing Area	120.4	121.7	1.1
Power Available	9.3	9.6	2.7
Fuel Cell Energy Available	81.9	83.0	1.4
Objective Function	6268.6	6396.6	2.0
Constraints (probability)			
Power Balance	0.95	0.99	3.9
Nighttime Energy Balance	0.95	0.99	3.8
Diurnal Energy Balance	0.95	0.97	2.0
Meeting All	0.88	0.95	7.6

6.3 Lessons Learned from Implementation Studies

The AIASM has been verified via its application to two example sizing studies. The major findings obtained from these exercises are summarized below:

- The electric GA sizing study showed that the fuel cell-powered electric propulsion system architecture could result in a comparable aircraft weight and size to its counterpart, if the projected technology improvements were achieved.

- The study identified the benefit of the use of a highly efficient electric propulsion system along with a high energy content fuel. The estimated fuel fractions ranged from 2.9 to 3.5 percent, which is remarkably low compared with its conventional counterpart. However, the study also revealed that the weight penalty incurred by hydrogen fuel storage could significantly offset the advantage of the use of a high energy content fuel.

- The SPHALE study included technology impact assessments, which identified

the efficiency of the PV cells and specific energy of the RFC as the most dominant factors. Similar technology assessments have been conducted by other researchers. The impact of technology improvements, however, was evaluated in terms of performance measures for a fixed design. In contrast, AIASM offers an outstanding capability of assessing the impact on air-vehicle designs rather than performance measures. Such a *technology-to-design* capability, as opposed to a *technology-to-performance* one, is preferred for the design of a brand-new aircraft.

The PASM was also demonstrated to be capable of apportioning reasonable design margins required to ensure target reliability against probabilistic constraints. Notable lessons learned from the applications of PASM to the two example studies are abridged below:

- The GA study demonstrated that PASM could ensure the minimum cost at an admissible probability of failure, which, in general, is not expected by traditional deterministic approaches.

- The study showed that MPP-based methods may produce a considerable error in estimating reliability although their computational efficiencies surpassed those of sampling based methods. However, the MPP-based methods estimated the reliability for the SPHALE problem fairly accurately, which suggests that the MPP-based methods must be used with caution.

- Despite their inherent errors, however, the optimum solutions obtained by employing the MPP-based methods for a nested reliability analysis were found to be in close proximity to those obtained by Monte Carlo simulations. The differences in the optimum values of wing area and power were less than 2 percent, suggesting that even if their accuracy is not acceptable, MPP-based

methods might be useful in a scheme of sequential applications of two optimization processes: the first with MPP-based methods and the second with an MCS method as their nested reliability analysis. The solution to the first optimization process will serve as a good starting point for the second one.

- The present research also demonstrated another extended capability of PASM simultaneous optimization of disciplinary variables and sizing variables. In addition, it was found that the probabilistic sensitivity analysis enhanced PASM by identifying the relative significance of selected random parameters. The information may assist designers and decision makers in various ways. For example, the complexity of the problem and computational efforts could be reduced by eliminating insignificant random parameters. Engineering tasks could also be prioritized in order to validate data associated with random parameters.

CHAPTER VII

CONCLUSIONS AND FUTURE WORK

Literature review presented in Chapter I identifies the emergence of alterative energy-propulsion system architecture for future aviation as well as the need for an aircraft sizing capability to properly assess such technologies. Literature review continued in Chapter II, however, reveals the shortcomings of traditional aircraft sizing methods in their application to the conceptual design of such unconventionally-powered aircraft. The findings in these two introductory chapters formed the basis of the research objective outlined in §3.1. By advocating a couple of critical new capabilities, the objectives in turn allowed the derivation of the research questions and hypotheses, which are delineated in §3.2 and §3.3, respectively.

In closing, some critical review of the research questions in light of the accomplished thesis work is presented in the next section. The remainder of this final chapter is devoted to a section that abridges the major contributions from research of this magnitude, which is followed by a discussion of future work.

7.1 Research Questions Answered

The research questions and the hypotheses are restated below, and the answers to each question are given based on the accomplishment of this dissertation.

7.1.1 Research Questions 1

- **Question 1**: *How can a generalized aircraft sizing method, independent of the architecture of energy storage and power generation, be formulated?*

Architecture-independence demands a holistic approach toward developing a generalized method rather than creating a specific solution to a particular problem. Such

a generalized method must be able to capture the implications introduced by the utilization of alternative energy sources and revolutionary propulsion systems into aircraft sizing processes. In order to address this question, the following hypothesis has been proposed.

- **Hypothesis 1**: *A generalized aircraft sizing formulation that is independent of propulsion system architectures and energy sources can be formulated based on the traditional energy-based sizing approach by making the following modifications:*
  - *The propulsion system architecture is modeled as an integration of power-path(s), each of which is characterized by three parameters: the specific energy of the energy source, specific power, and efficiencies of power transfer devices.*
  - *Fuel is generalized as the source of energy on board a vehicle and is categorized into based on its nature of conversion: consumable and non-consumable.*
  - *Aircraft weight is decomposed into more generalized weight groups, which leads to a more general weight differential equation.*

This hypothesis propositions that the key to achieving an *architecture-independent* capability is to generalize the underlying assumptions of traditional sizing methods, which encompass the concepts of fuel, propulsion systems, and weight estimations. Mathematical interpretations of such generalized assumptions are elaborated in §3.4.1, leading to the development of AIASM in Chapter IV. Built upon such generalized assumptions, the method possesses a common structure that is applicable to any energy-propulsion system architecture and is able to capture the impact on aircraft sizing due to the choice of an architecture. Two implementation studies presented

in Chapter VI shows that AIASM is able to size revolutionary aircraft powered by alternative energy-propulsion system architectures.

7.1.2 Research Questions 2

- **Question 2**: *How can adequate design margins, required for mitigating the risk associated with uncertainty having minimal impacts on the design objective(s), be quantified in an aircraft sizing problem?*

This question seeks a method that is capable of quantifying design margins that represent a trade-off between cost and risk for an aircraft sizing problem.

- **Hypothesis 2**: *It is possible to determine adequate design margins that result in a solution satisfying all probabilistic constraints under consideration with a target probability, while searching for a design optimum.*

This hypothesis contains a supposition that the CCP and RBDO approaches are appropriate for formulating a probabilistic aircraft sizing problem under uncertainty, which is supported by the discussions in §5.1 and §5.2. The implementation of the CCP and RBDO approach into aircraft sizing formulation resulted in PASM that is capable of intelligently determining appropriate design margins as the best compromise between cost and risk. The GA sizing study presented in Chapter VI shows that PASM can find a better solution than what is obtainable with other, more routine methods.

7.2 Summary of Contributions

The primary objective of this research has been the development of new capabilities that are required for sizing an aircraft powered by alternative energy-propulsion architectures. The major contributions of this dissertation are AIASM and PASM. In

the course of the development of AIASM, a set of generalized Breguet range equations and NAM ratio diagram have also been developed, which are now summarized as follows.

- AIASM

  The architecture independent aircraft sizing method (AIASM) has been formulated. Particular emphasis is placed on ensuring *generality*, as to encompass a variety of emerging alternative energy-propulsion architectures. The method also provides a proper means to size an aircraft propelled by a hybrid energy-propulsion system architecture more effectively and efficiently.

- Generalized Breguet Range Equations

  A set of generalized Breguet range equations can estimate the ferry range of an aircraft powered by alternative energy-propulsion architectures with little information pertinent to the aircraft. The set includes three equations, each of which falls under one of the three following categories: 1) an aircraft is fueled with a consumable energy source, and its consumption leads to a change in the aircraft's weight; 2) an aircraft is fueled with a consumable energy source but its consumption does not lead to a change in the aircraft's weight; and 3) an aircraft is fueled with a non-consumable energy source.

- NAM Ratio Diagram

  Utilizing the generalized Breguet range equations as well as the intrinsic duality between the mass of on-board energy sources and the mass of propulsion systems, the NAM ratio diagram identifies performance frontiers in terms of range and velocity, achievable with a given energy-propulsion system architecture. Such a diagram enables a designer to examine rapidly a *fleet* of aircraft designs that are possible with a given energy-propulsion system architecture, hence, easily identifying the mission that appears to be the most appropriate.

- PASM

  Formulated based on the principles of CCP, PASM finds a solution of aircraft sizing variables that ensures the best objective function value with a given target probability of meeting probabilistic constraints under uncertainty. In addition, the probabilistic sensitivity analysis was found to be beneficial by providing a greater insight into the relationship between reliability and the distributions of random variables.

7.3 Future Work

Over the course of its development process, a number of secondary research areas were identified. Such areas, if pursued, would enhance the capability of the formulated sizing methods. This final section summarizes the most important lessons learned as action items for future work.

7.3.1 Comprehensive Sizing Method

The author's aircraft sizing method has its basis in balancing power and energy. However, a successfully sized configuration must achieve one more criterion: a balance between required and available aircraft volume. All three criteria will not always play equal roles in an aircraft sizing process. The relative importance of the three would depend on various parameters such as sizing requirements; configuration shapes; and characteristics of the propulsion systems and energy sources, which include the following four parameters: the specific energy and energy density of the energy source, and the specific power and power density of the propulsion system. For instance, if an aircraft is powered by an isomer energy source whose specific energy is exceptionally higher than that of conventional fuel (approximately 3×10^4 times greater), the weight of the energy source may become trivial compared to that of the entire vehicle. In such a case, the energy balance will no longer be a major concern during the aircraft sizing process, just as the weight of the cockpit instruments is not much

of a concern in conventional aircraft sizing practice. Under such circumstances, it is possible that the volumetric and power demands may begin to take precedence over the energy balance.

In general, the consideration of volume in an aircraft sizing process is encapsulated in a baseline configuration, whose volume balance is verified by an off-line internal layout study after it is initially is sized. An internal arrangement drawing, occasionally called an inboard profile, includes the occupied volume of all major components, such as the avionics bay, cockpit, landing gear, engine, passenger compartment, and fuel tank. This graphical layout of all primary components allows designers to compute the amount of usable volume for fuel, which is generally computed by multiplying fuel tank's OML volume by fuel packing factors. The surplus fuel volume - available fuel volume minus required fuel volume - is often considered as the *touchstone* of volume balance. The putative reason for measuring the surplus fuel volume as the index of volume balance is that fuel tanks of most modern aircraft are integrated with their surrounding structures such as the bulk heads, shear webs, wing skins, and spars to reduce the aircraft weight, which leads to *byzantine*-shaped fuel tank boundaries - now a striking feature of modern fighters. Therefore, measuring the *fall-out* volume with the left-over space from packing other components is usually easier than to allotting fuel tanks with the exact amount of required fuel volume.

However, such a follow-on volume assessment, performed separately from a numerical sizing process, entails an extra manual iterative step in the design process. A configuration, if sized under consideration of power and energy balance only, may not provide sufficient volume for all required systems. If it does not, then the external configuration may have to be modified so that the efficiency of the internal packaging increases, or the aircraft may need to be scaled up beyond the minimum size at which both the power balance and energy balance are achieved. Such a *human-in-the-loop* process, which can require substantial man-hours, retards the convergence of

the configuration and stymies designers from investigating alternative configurations. Therefore, an integrated sizing environment that is able to reflect volumetric demands on a sizing process concurrently, as illustrated in Figure 99, is desired, especially in the design of a revolutionary aircraft where the implicit volume balance discussed in §2.2 will not work.

Nevertheless, little literature regarding simultaneous volume assessment methods can be found. One of the most significant hindrances to the development of such an integrated power-energy-volumetric sizing environment is that it is very difficult to construct a parametric model to assess volumetric balance. Often, most internal components have yet to be designed from scratch, and they will not be designed until the later detailed design phase [214]. For this reason, an internal layout drawing at the early stage of development only includes a few major components or simply their estimated volume, while excluding structures and small equipment items such as actuators, environmental control systems, and the ducting and wiring. An experienced aircraft designer assigns a sufficient amount of volume to those "un-spoken-for" items in the aircraft, properly spaced throughout the aircraft [214]. The correct amount and shape of extra space for such items can be hardly estimated in any practical way, but may just "look right." As Raymer put it in his seminal paper [214] on volumetric sizing, "Such an intuitive measure of merit is difficult to duplicate or teach, and impossible to program."

For this reason, example studies of parametric volume assessment found in existing literature guarantee only several major subsystem components. For example, Pouchet et al. [215] developed an aircraft sizing environment that automated the volume assessment process for the design of a hydrogen-fueled jet commercial transport, called a Quiet Green Transport (QGT). The optimization environment includes a conventional sizing code (FLOPS) and two external analysis modules required for assessing volume: one computes the hydrogen tank volume for a given fuel tank geometry, and

the other estimates an appropriate fuselage length and diameter to accommodate the hydrogen fuel tank. However, these authors' volume analysis was limited to the hydrogen fuel tank.

An alternative classical approach to assess volume balance measures overall *crowdedness* of a given configuration rather than actual volume. Since Caddell [216] started a pioneering use of a volumetric density to determine a reasonable volume allocation in 1969, such density-based volume assessment has been widely used in the industry. The fundamental idea is, in fact, very simple. The aircraft density is computed by the total aircraft volume[1] divided by the aircraft weight. Historical data indicates that the density of aircraft in the same class is tightly distributed around an average value, which can be used as a touchstone to judge if a given configuration has adequate volume. The inordinately high value of this density above an average value would indicate that the design is very likely to suffer from lack of volume. This approach is relatively easy to implement into an automated sizing environment. Nevertheless, its dependence on empirical data prevents the method from being applied to the design of the alternative energy-propulsion system architecture as it is. In addition, the method is only applicable to allocating the total amount of internal volume. It is still be possible that the sized configuration could not accommodate all components, even if spacious volume was allotted, depending on the shape and the distribution of usable volume.

Raymer [214] refined the classical density-based volumetric design approach and developed the Net Design Volume (NDV) method. NDV is defined as "the internal volume of an aircraft fuselage, nacelles, and wings, less the volume dedicated to fuel, propulsion, payload, passengers, and crew." As a result, NDV more closely represents the "un-spoken-for" extra volume. Raymer showed that there is a solid relationship

[1]The volume is usually measured as the difference between the volume wrapped around by the OML and the volume of all internal diffusers.

between NDV and aircraft weight via a regression analysis of seven modern fighter aircraft. This approach has a similarity to the generalized weight estimation method presented in §4.4 in the sense that both techniques directly estimate a few selected items and rely on empirical information for all "un-spoken-for" items. Integrating the NDV method with the author's AIASM is seen as a practical way to develop an automated environment that is capable of simultaneously assessing power, energy, and volume balance.

7.3.2 Uncertainty Modeling

The numerical example study presented in §6.2 demonstrates that an improvement in the distributions of a few significant random parameters may result in considerable improvement in the reliability of associated probabilistic constraints, thereby influencing the optimum solution. On the other hand, the results accentuate that distributions of the random parameters cannot be arbitrary, and the accuracy of the assumed distributions of random parameters are of significance. Therefore, such assumptions must be carefully made[2].

In general, uncertainty that is most often encountered in engineering can be broadly classified as follows [217, 171][3]:

- Aleatory uncertainty

  Aleatory uncertainty is due to variability, which is an intrinsic property of natural phenomena or processes, thus it also referred to as uncontrollable uncertainty, irreducible uncertainty, inherent uncertainty, stochastic uncertainty, and

[2]This kind of uncertainty modeling would heavily depend on the amount of available and applicable data for constructing input probability distributions. Oberkampf et al. [217] categorize the types of uncertainty sources into three groups: 1) Strong Statistical Information, 2) Sparse Statistical Information, and 3) Intervals. If uncertainty sources are associated with the improvements in technology, then the methodical logic, which models uncertainty based on the TRL level of associated technology [218] proposed by Kirby, is recommended.

[3]In some of the literature, the concept of "error" refers to "numerical uncertainty." In the context of reliability assessment, however, "error" differs from "uncertainty" in that it is a recognizable deficiency that occurs in any phase or activity of modeling and simulation but that is not due to a lack of knowledge [219, 220].

variability.

- Epistemic uncertainty

  Epistemic uncertainty is a potential deficiency in selecting the best action in a decision (the action with the highest probability of resulting in the most desirable outcome) due to lack of knowledge or incomplete information, it is thereby also referred to as controllable uncertainty, reducible uncertainty, subjective uncertainty, model form uncertainty, or simply uncertainty.

Traditionally, both types of uncertainty have been attempted to be quantified in terms of probability theory. Such an ascendancy has been in question for sometime now as several other mathematical theories have demonstrated their capabilities of characterizing situations under uncertainty [220]. Some of the more popular quantitative theories include the theory of fuzzy sets [221], the Dempster-Shafer theory [222, 223], and the theory of upper and lower previsions [224]. Many of these new representations of uncertainty are able to more accurately represent epistemic uncertainty than is possible with traditional probability theory [225].

In reality, both aleatory and epistemic uncertainty can be present. Recently several researchers have attempted to develop RBDO methods that are able simultaneously to handle both types of uncertainty in engineering problems. Youn and Wang proposed [226] an integration of the Bayesian approach with the RBDO method, and Agarwal et al. [225] attempted to combine the Dempster-Shafer theory, also known as the evidence theory, with an RBDO method. Since an aircraft sizing problem is also very likely to involve both aleatory and epidemic uncertainty, it would thus be worthwhile to investigate the feasibility of adapting such techniques to PASM.

7.3.3 Multi-Stage RBDO with Recourse

Although proving their usefulness for numerous engineering applications, state-of-the-art CCP and RBDO methods possess a weakness to be used for a large, complex

system-level problems such as designing an aircraft. As mentioned previously, aircraft design is an iterative process, progressively moving the focus from the macro to the micro, or from conceptual to detail design. As such, designers do not determine all design variables at one time. Instead, they first prioritize the variables according to some criteria, and then progressively make decisions on how to mature the product design. In fact, in the conceptual design phase, design engineers are only considering a handful of design variables. All other variables are to be determined by further design studies, analyses, and tests. Through such decisions, the degree of design freedom gradually decreases as illustrated in Figure 100.

Along with increased design maturity, the level of uncertainty decreases as the level of knowledge increases via the applications of high fidelity analyses such as Computational Fluid Dynamics (CFD), the Finite Element Method (FEM), and 6-DoF simulations, and experiments such as wind tunnel tests, structural tests, and subsystem tests. Such increased design maturity and accrued observations of unforeseen randomness may reveal some constraint violations. Under such circumstances, designers seek to fix the problem in a way that imparts minimal impact on the overall design to prevent schedule and cost overruns. The reality is that most designers would almost always try to find an opportunity to resolve the design issues with the currently possessed design freedom, rather than start over from the beginning. However, this thesis work, as well as traditional RBDO approaches, does not reflect the reality of design progression, which motivates designers to *correct* their previous decisions and restore the balance between cost and reliability at any phase of the design. In such a sense, a solution obtained by an RBDO method is prone to be overly conservative, even if the assumptions regarding the uncertainty sources are accurate.

This issue has not attracted much attention from previous RBDO researchers. One possible reason for it may be that most RBDO research has focused on structural, component-level design problems that are most appropriate in a detail design phase,

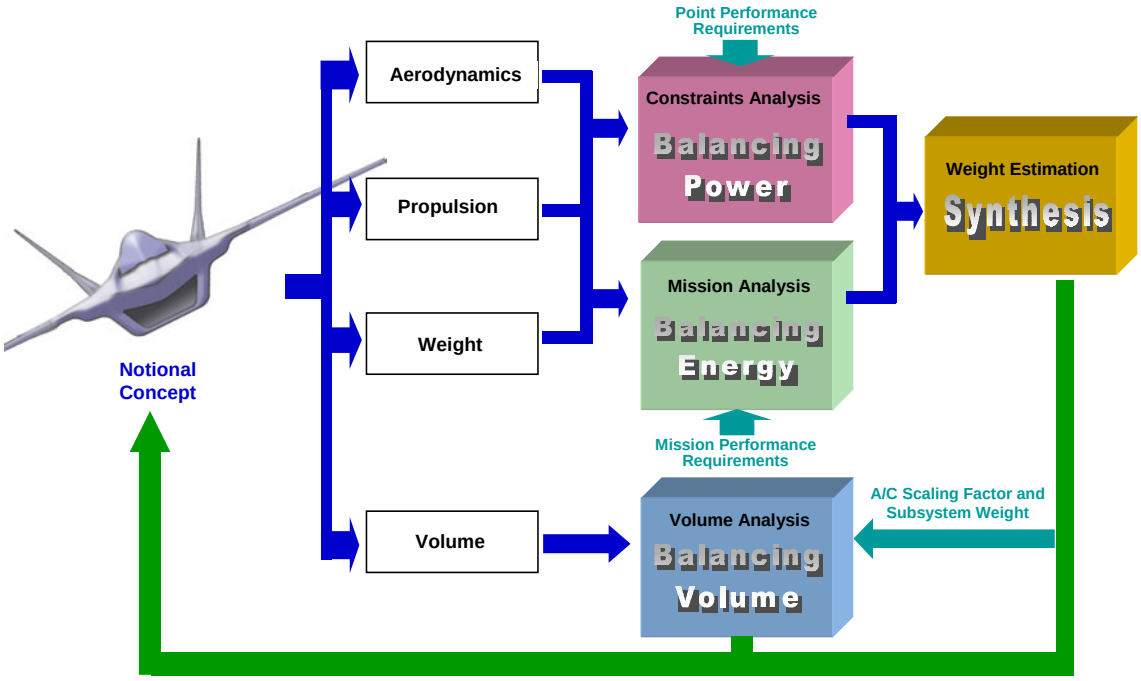

Figure 99: Comprehensive sizing method

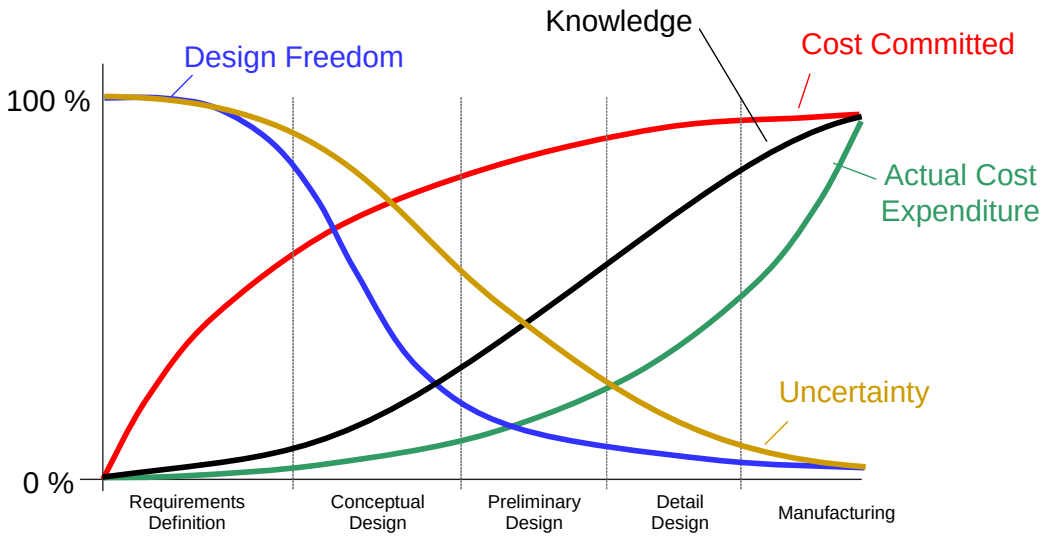

Figure 100: Distribution of knowledge, cost committed, and freedom in the design cycle [227]

when follow-on, corrective design efforts are not much expected. However, the issue may be of importance for a probabilistic optimization problem conducted in the early phases of complex systems design, including an aircraft sizing problem. Therefore, further research on this topic seems important to enhance the realism of the method.

A new RBDO method, named MSRBDO (Multi-Stage Reliability-Based Design Optimization), that addresses the above issue has been conceptualized in the course of the development of PASM. The method provides a mathematical model that represents sequential decision processes, in which the decision variables are determined progressively based on increased knowledge as well as remaining uncertainty. The formulation involves the following assumptions:

1. Designers have accumulated some knowledge, which also means cumulative reduction in uncertainty has been achieved from the previous work up to present.

2. Designers hold a certain degree of design freedom that can be used to correct the decision that was previously made.

3. Designers utilize the information obtained from previous work to make follow-on decisions for the remaining portion of the design space.

The MSRBDO method only determines a partial list of design variables in the first stage by simulating the whole process upon the above assumptions. The other design variables will be determined in follow-on stages. The designer's choice of current decision variables still affects future decisions, thus affecting the objective function value and the probability of meeting constraints also.

The simplest case of the MSRBDO formulation is a two-stage problem, in which a group of design variables, denoted as $\mathbf{x}_{s1}$, is determined at the first stage. The remaining design variables are to be determined at the second stage, when a fraction of random parameters, denoted as $\boldsymbol{\xi}_{s1}$, are observed, but the rest of random parameters, denoted as $\boldsymbol{\xi}_{s2}$, are yet uncertain. Then, a two-stage MSRBDO problem can be

expressed as

$$\min_{\mathbf{x}_{s1}} \ \mathbb{E}[f(\mathbf{x}_{s1}, \mathbf{x}^*_{s2}, \boldsymbol{\xi}_{s1}, \boldsymbol{\xi}_{s2})]$$

$$\text{s.t. } \mathbb{P}[g_i(\mathbf{x}_{s1}, \mathbf{x}^*_{s2}, \boldsymbol{\xi}_{s1}, \boldsymbol{\xi}_{s2}) \geq 0] \geq \alpha_i$$

$$\text{where } \mathbf{x}^*_{s2}(\mathbf{x}_{s1}, \boldsymbol{\xi}_{s1}) \text{ solves}$$

$$\begin{cases} \text{if } \mathbb{P}[g_i(\mathbf{x}_{s1}, \mathbf{x}^*_{s2}, \boldsymbol{\xi}_{s1}, \boldsymbol{\xi}_{s2}) \geq 0 \mid \boldsymbol{\xi}_{s1} = \overline{\boldsymbol{\xi}}_{s1}] \geq \alpha_i^{(s2)} \\ \qquad \min_{\mathbf{x}_{s2}} \ f(\mathbf{x}_{s1}, \mathbf{x}_{s2}) \\ \qquad\quad \text{s.t. } \mathbb{P}[g_i(\mathbf{x}_{s1}, \mathbf{x}^*_{s2}, \boldsymbol{\xi}_{s1}, \boldsymbol{\xi}_{s2}) \geq 0 \mid \boldsymbol{\xi}_{s1} = \overline{\boldsymbol{\xi}}_{s1}] \geq \alpha_i^{(s2)} \\ \text{else} \\ \qquad \max_{\mathbf{x}_{s2}} \mathbb{P}[g_i(\mathbf{x}_{s1}, \mathbf{x}^*_{s2}, \boldsymbol{\xi}_{s1}, \boldsymbol{\xi}_{s2}) \geq 0 \mid \boldsymbol{\xi}_{s1} = \overline{\boldsymbol{\xi}}_{s1}] \end{cases} \tag{169}$$

Figure 101 compares four different probabilistic approaches in view of the degree of uncertainty, with which a decision is made, and the degree of design freedom to which the decision commits. DSS simulates the optimum solutions obtainable with all possible random realizations. The decision on the design will be made after all the random parameters have been observed. In a two-stage stochastic programming, decisions are made for the design variables ahead of the random events, but a correction can be made afterward. Similarly, using RBDO and CCP, decisions on all the design variables are made ahead of the random events, but a possibility of later corrections is not permitted. In contrast to the classical RBDO approach, MSRBDO allows a follow-on corrective decision based on additional information obtained from the observations of a partial realization of random parameters. Unlike a two-stage stochastic programming, the decision at the second stage must still be made under (remaining) uncertainty.

In order to demonstrate the fundamental concept of the MSRBDO approach, the numeric example presented in §5.2 is re-investigated. Assuming that the design space includes an additional design variable, denoted as z, that represents *design freedom*, which the designer can retain until the second stage. The objective function and the

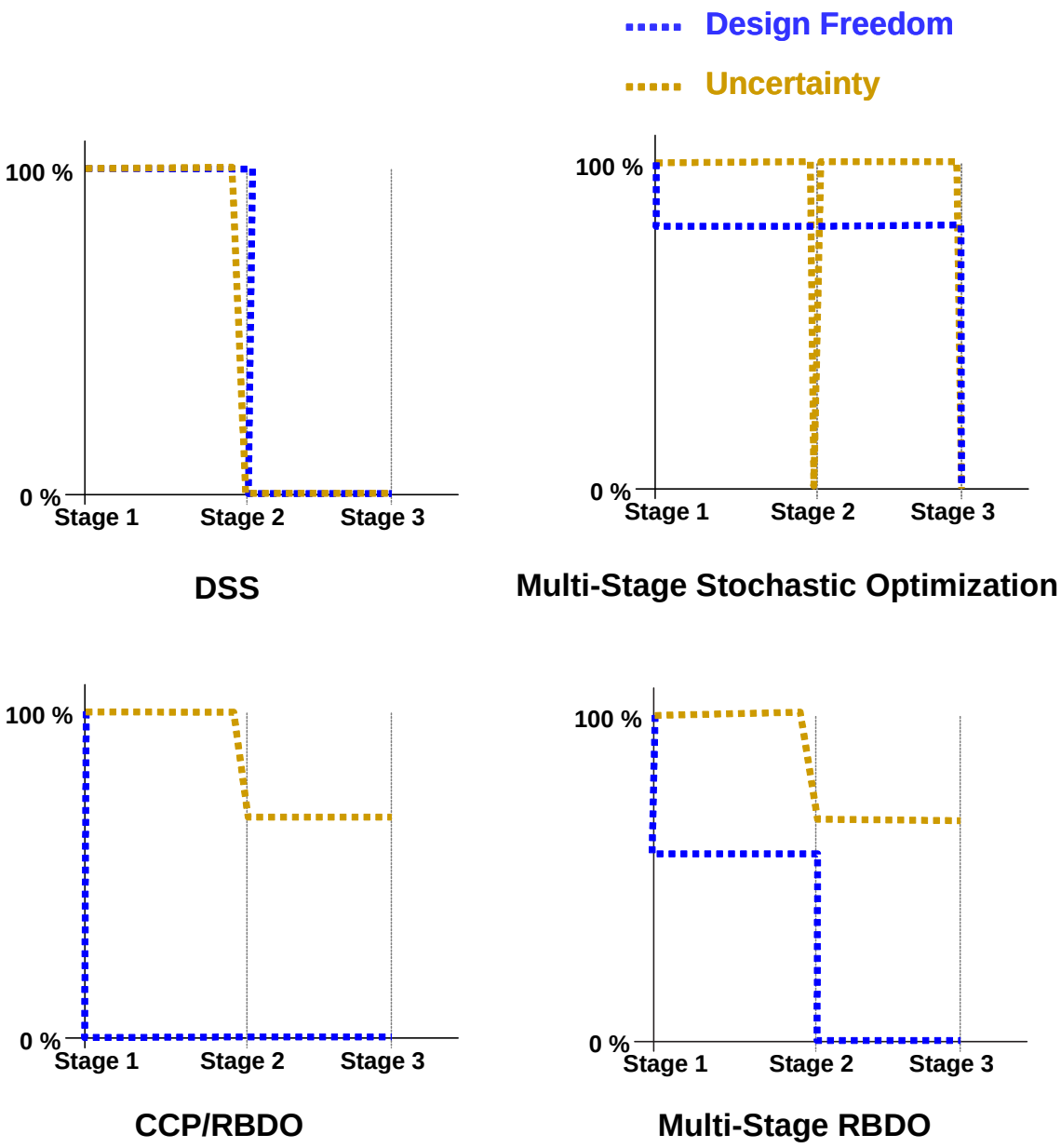

Figure 101: Comparison of nondeterministic approaches

constraint function are given as $f = x + 4y + z$ and $\xi_1 x + \xi_2 y + z \geq 2$, respectively. The following scenario is assumed for this example study:

- Designer must determine the values of x and y at the first stage.
- Designer can determine the variable z after ξ_2 is observed at the second stage. Variable z is bound to $|z| \leq 1$.
- Designer determines z such that the value of the objective function is minimized while meeting the second-stage target probability, $\alpha^{(2nd)} = 0.95$, of the probabilistic constraint.

With the above assumption, the given problem can be formalized as an MSRBDO programming as follows:

$$
\begin{aligned}
&\min_{x,y} \ \mathbb{E}[x + 4y + z^*(x, y, \xi_2)] \\
&\quad \text{s.t. } \mathbb{P}[\xi_1 x + \xi_2 y + z^*(x, y, \xi_2) \geq 2] \geq 0.9, \ x \geq 0, \ y \geq 0 \\
&\qquad \text{where } \xi_1 \sim N(1, 1^2), \ \xi_2 \sim N(3, 1^2), \text{ and} \\
&\qquad z^*(x, y, \xi_2) \text{ solves} \\
&\qquad \begin{cases}
\text{if } \mathbb{P}[\xi_1 x + \xi_2 y + z \geq 2 \mid \xi_1 = \overline{\xi_1}] \geq \alpha^{(2nd)} \\
\quad \min_z \ x + 4y + z \\
\qquad \text{s.t. } \mathbb{P}[\xi_1 x + \xi_2 y + z \geq 2 \mid \xi_1 = \overline{\xi_1}] \geq \alpha^{(2nd)}, \ |z| \leq 1 \\
\text{else} \\
\quad \max_z \mathbb{P}[\xi_1 x + \xi_2 y + z \geq 2 \mid \xi_1] \\
\qquad \text{s.t. } |z| \leq 1
\end{cases}
\end{aligned}
\tag{170}
$$

The classical RBDO approach yields the following formulation:

$$
\begin{aligned}
&\min_{x,y,z} \ f = x + 4y + z \\
&\quad \text{s.t. } \mathbb{P}[\xi_1 x + \xi_2 y + z \geq 2] \geq 0.9, \ x \geq 0, \ y \geq 0 \\
&\text{where } \ \xi_1 \sim N(1, 1^2) \text{ and } \xi_2 \sim N(3, 1^2)
\end{aligned}
\tag{171}
$$

Table 20: Comparison of the results from RBDO and MSRBDO

	RBDO	MSRBDO
x	0.229	0.087
y	0.487	0.650
z	0.999	-
f, $\mathbb{E}[f]$	3.176	2.689

The optimum solutions of the MSRBDO approach and the ordinary RBDO approach for the given problem are compared in Table 20. In this particular example, the objective function of the RBDO approach is deterministically defined, while that of the MSRBDO approach is given as a random response. Thus, for the MSRBDO approach, a mean value is listed for the objective function value in the table. The solution from the MSRBDO method is expected to yield a lower value of the objective function. The RBDO approach determines the optimum value of z at the first stage. In the case of the MSRBDO formulation, z is classified as a second-stage variable, which will be determined by solving a sub-optimization problem upon observation of the random parameter ξ_1. In other words, z^*, the solution of the second stage optimization problem, is essentially a function of ξ_2 and plays as a random parameter in the first stage. The distributions of z^* and f are depicted in Figure 102. In this particular example, an increase in z raises both the feasibility of the constraint and the value of the objective function, which means a higher value of z yields more design margin with a higher penalty on the objective function. The MSRBDO approach takes advantage of the retained design freedom: z is determined upon the observation of ξ_2.

Another interesting quantity is the probability of meeting the target feasibility (0.95) of the second stage, which can be computed by separate MCSs. The solutions from the RBDO and MSRBDO approaches are expected to meet the target feasibility of the second stage by 0.85 and 0.94, respectively. In an actual engineering

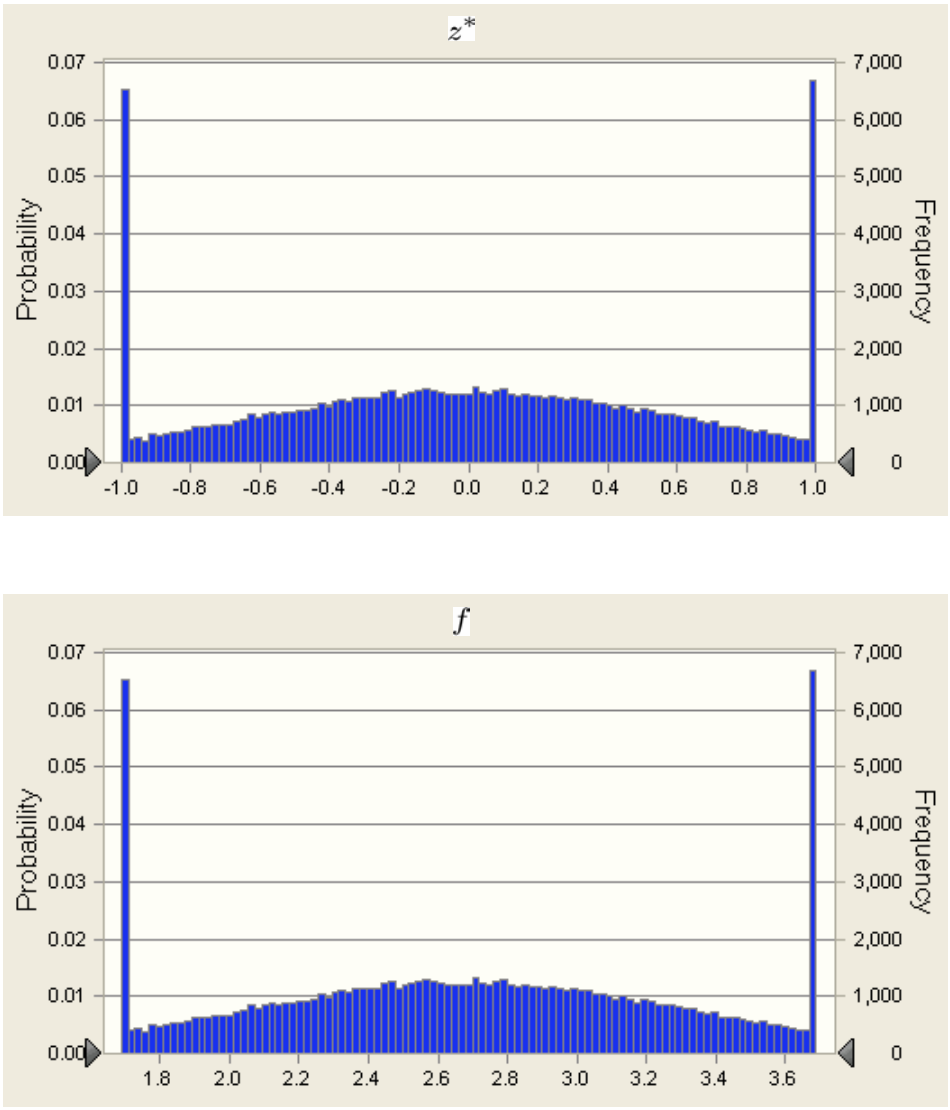

Figure 102: Distributions of z^* and f from the application of the MSRBDO

development program, this quantity can be used as an FoM, with which, the program director can decide whether the product design can successfully proceed to the next development stage or not.

When the diagram of the MSRBDO in Figure 101 is extended to a multi-stage problem, it will appear as shown in Figure 103. The two dotted lines represent the

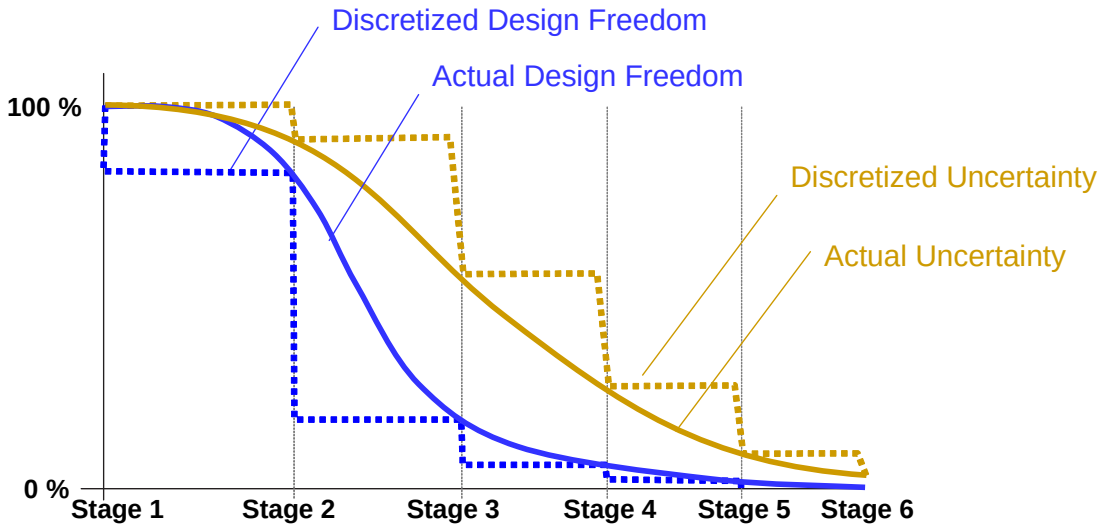

Figure 103: The MSRBDO simulates a decision making process of a complex system design problem

degree of uncertainty and design freedom, which continues to diminish after every stage, where a decision is made based on increased information as well as remaining uncertainty. In an actual aircraft development program, the design evolution is a continuous process, where the degree of uncertainty and design freedom gradually diminishes as depicted by the solid lines in Figure 103, which were originally shown in Figure 100. In this sense, the MSRBDO imitates the decision making process of a complex system design problem, but consolidates the continuous process into a number of discrete moments in time.

Although the numerical example shows the potential of the MSRBDO approach,

much further research must be performed to assess its effectiveness in practical engineering problems. It is conjectured that one of the foreseeable challenges would be a prohibitive level of computational cost. The MSRBDO determines the design variables of the first stage by simulating all the decisions that will be made upon the observations of random parameters at every subsequent stage. Thus, the computational effort is projected to a near exponential rate as the number of stages grows.

7.4 Concluding Remarks

Considering the readiness of revolutionary technologies, infrastructure, and economics, the dominance of IC engines consuming conventional aviation fuels will be likely to persist for the next couple of decades. However, this should not lead to the downplaying of the significance and urgency of the search for alternative-energy flight. Worldwide petroleum supplies will eventually be depleted. If no viable alternative is orchestrated on a *timely basis*, the economic and environmental ramifications could be appalling.

Achieving alternative-energy flight is only a part of the odyssey to a "post-oil economy" that we as world citizens must complete within this century. Fortunately, the arduous journey has already begun, although the destination is yet to be determined. The expedition must be carefully guided by strategic plans that are premeditated by the collective efforts of all societies. It is this author's hope that the work contained in this dissertation could contribute towards a project of such importance and magnitude.

APPENDIX A

CONSTRAINT EQUATIONS

A constraint equation for a particular maneuver of an aircraft can be derived from the master equations, given as Eq. (11) and Eq. (52) of the Mattingly's method and AIASM, respectively. Such tailored constraint equations of Mattingly's method and AIASM are listed below. Most of the equations, except for take-off and landing, can be easily derived by simply applying the flight conditions of the maneuver.

A.1 Constant Altitude/Speed Cruise

The condition of constant altitude and speed yields $dh/dt = 0$, $dV/dt = 0$, and $n = 1$. Cruise altitude, h, and cruise speed, V, are given. Under these conditions,

Mattingly's Equation

$$\frac{T_{SL}}{W_{TO}} = \frac{\beta}{\alpha}\left\{K_1\left(\frac{\beta}{q}\frac{W_{TO}}{S}\right) + K_2 + \frac{C_{D_o} + C_{DR}}{\left(\frac{\beta}{q}\frac{W_{TO}}{S}\right)}\right\} \tag{172}$$

AIASM's Equation

$$\frac{P_{ref}^{\langle i\rangle}}{W_{TO}} = \frac{\tau^{\langle i\rangle}\beta V}{\Pi_\eta^{+\langle i\rangle}\alpha^{\langle i\rangle}}\left\{K_1\left(\frac{\beta}{q}\frac{W_{TO}}{S}\right) + K_2 + \frac{C_{D_o} + C_{DR}}{\left(\frac{\beta}{q}\frac{W_{TO}}{S}\right)}\right\} \tag{173}$$

A.2 Constant Speed Climb

The condition of constant speed climb yields $dV/dt = 0$. Assuming $L \approx W$, $n \approx 1$. The rate of climb, dh/dt, and the flight speed, V, are given. Under these conditions,

Mattingly's Equation

$$\frac{T_{SL}}{W_{TO}} = \frac{\beta}{\alpha}\left\{K_1\left(\frac{\beta}{q}\frac{W_{TO}}{S}\right) + K_2 + \frac{C_{D_o} + C_{DR}}{\left(\frac{\beta}{q}\frac{W_{TO}}{S}\right)} + \frac{1}{V}\frac{dh}{dt}\right\} \tag{174}$$

AIASM's Equation

$$\frac{P_{ref}^{\langle i\rangle}}{W_{TO}} = \frac{\tau^{\langle i\rangle}\beta V}{\Pi_{\eta}^{+\langle i\rangle}\alpha^{\langle i\rangle}}\left\{K_1\left(\frac{\beta}{q}\frac{W_{TO}}{S}\right) + K_2 + \frac{C_{D_o} + C_{DR}}{\left(\frac{\beta}{q}\frac{W_{TO}}{S}\right)} + \frac{1}{V}\frac{dh}{dt}\right\} \tag{175}$$

A.3 Horizontal Acceleration

By definition, $dh/dt = 0$ and $n = 1$. The requirement is typically described in terms of values of altitude, h, the initial velocity, $V_{initial}$, the final velocity, V_{final}, and the allowable time for the acceleration, $\Delta t_{allowable}$.

Mattingly's Equation

$$\frac{T_{SL}}{W_{TO}} = \frac{\beta}{\alpha}\left\{K_1\left(\frac{\beta}{q}\frac{W_{TO}}{S}\right) + K_2 + \frac{C_{D_o} + C_{DR}}{\left(\frac{\beta}{q}\frac{W_{TO}}{S}\right)} + \frac{1}{g_o}\frac{dV}{dt}\right\} \tag{176}$$

AIASM's Equation

$$\frac{P_{ref}^{\langle i\rangle}}{W_{TO}} = \frac{\tau^{\langle i\rangle}\beta V}{\Pi_{\eta}^{+\langle i\rangle}\alpha^{\langle i\rangle}}\left\{K_1\left(\frac{\beta}{q}\frac{W_{TO}}{S}\right) + K_2 + \frac{C_{D_o} + C_{DR}}{\left(\frac{\beta}{q}\frac{W_{TO}}{S}\right)} + \frac{1}{g_o}\frac{dV}{dt}\right\} \tag{177}$$

A.4 Sustained Turn

Sustained turn performance is the aircraft's ability to make a turn maintaining constant altitude and flight speed for an extended period of time, which leads to $dh/dt = 0$ and $dV/dt = 0$. Under these conditions, Eq. (11) and Eq. (52) can be rewritten as follows:

Mattingly's Equation

$$\frac{T_{SL}}{W_{TO}} = \frac{\beta}{\alpha}\left\{K_1 n^2\left(\frac{\beta}{q}\frac{W_{TO}}{S}\right) + K_2 n + \frac{C_{D_o} + C_{DR}}{\left(\frac{\beta}{q}\frac{W_{TO}}{S}\right)}\right\} \tag{178}$$

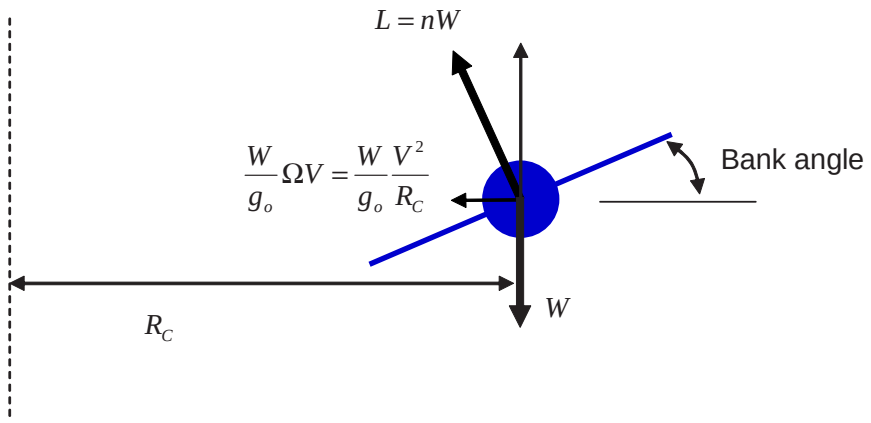

Figure 104: Forces on aircraft in a sustained level banked turn [100]

AIASM's Equation

$$\frac{P_{ref}^{\langle i \rangle}}{W_{TO}} = \frac{\tau^{\langle i \rangle}\beta V}{\Pi_{\eta}^{+\langle i \rangle}\alpha^{\langle i \rangle}} \left\{ K_1 n^2 \left(\frac{\beta}{q}\frac{W_{TO}}{S} \right) + K_2 n + \frac{C_{D_o} + C_{DR}}{\left(\frac{\beta}{q}\frac{W_{TO}}{S} \right)} \right\} \tag{179}$$

Sustained turn performance is also measured in terms of turn rate (Ω) and turn radius (R_c) rather than load factor (n), (e.g. maximum sustained turn rate, minimum sustained turn radius). From the Pythagorean Theorem, n in Figure 104 is related to Ω and R_c for a given value of V as follows:

$$n = \sqrt{1 + \left(\frac{\Omega V}{g_o} \right)^2} \tag{180}$$

$$n = \sqrt{1 + \left(\frac{V^2}{g_o R_c} \right)^2} \tag{181}$$

A.5 Service Ceiling

The service ceiling is the density altitude where the flying at the best rate of climb airspeed for that altitude, and with all engines operating and producing maximum continuous power, will produce a certain climb rate, usually 100 feet per minute of climb, which leads to $dV/dt = 0$ and $n = 1$. For given h and $dh/dt > 0$, and C_L, Eq. (11) and Eq. (52) become

Mattingly's Equation

$$\frac{T_{SL}}{W_{TO}} = \frac{\beta}{\alpha}\left\{K_1 C_L + K_2 + \frac{C_{D_o} + C_{DR}}{C_L} + \frac{1}{V}\frac{dh}{dt}\right\} \tag{182}$$

AIASM's Equation

$$\frac{P_{ref}^{\langle i\rangle}}{W_{TO}} = \frac{\tau^{\langle i\rangle}\beta V}{\Pi_{\eta}^{+\langle i\rangle}\alpha^{\langle i\rangle}}\left\{K_1 C_L + K_2 + \frac{C_{D_o} + C_{DR}}{C_L} + \frac{1}{V}\frac{dh}{dt}\right\} \tag{183}$$

A.6 Take-off Distance

In general, an aircraft takes-off in the three steps: acceleration, rotation, and transition. The take-off field length is the total distance to complete the all steps.

A.6.1 Take-off Ground Roll

Given that $dh/dt = 0$,

Mattingly's Equation

When $T_{SL} \gg (D + R)$, Eq. (11) becomes

$$\frac{T_{SL}}{W_{TO}} = \frac{\beta}{\alpha g_o}\frac{dV}{dt} = \frac{\beta}{\alpha g_o}\frac{dV}{\frac{ds}{V}} \tag{184}$$

which can be rearranged to yield

$$ds = \frac{\beta}{\alpha g_o}\frac{W_{TO}}{T_{SL}} V dV \tag{185}$$

Integrating the equation from static where $s = 0$ and $V = 0$ to take-off, where $s = s_G$ and $V = V_{TO}$, with the use of representative take-off values of α and β.

$$s_G = \frac{\beta}{\alpha}\frac{W_{TO}}{T_{SL}}\frac{V_{TO}^2}{2g_o} \tag{186}$$

The take-off velocity (V_{TO}) is usually defined as the stall speed multiplied by a constant k_{TO}, which is greater than one and specified by regulations or military standards. V_{stall} is the minimum speed at which the airplane flies at $C_{L_{\max}}$, then

$$\frac{V_{TO}^2}{2} = k_{TO}^2\frac{V_{stall}^2}{2} = \frac{\beta k_{TO}^2}{\rho C_{L_{\max}}}\frac{W_{TO}}{S} \tag{187}$$

Finally,

$$\frac{T_{SL}}{W_{TO}} = \frac{\beta^2}{\alpha} \frac{k_{TO}^2}{s_G \rho g_o C_{L_{\max}}} \frac{W_{TO}}{S} \tag{188}$$

AIASM's Equation

$$\frac{P_{ref}^{\langle i \rangle}}{W_{TO}} = \frac{\beta V}{\Pi_\eta^{+\langle i \rangle} \alpha g_o} \frac{dV}{dt} = \frac{\beta V}{\Pi_\eta^{+\langle i \rangle} \alpha g_o} \frac{dV}{\frac{ds}{V}} \tag{189}$$

which can be rearranged to yield

$$ds = \frac{\beta}{\Pi_\eta^{+\langle i \rangle} \alpha^{\langle i \rangle} g_o} \frac{W_{TO}}{P_{ref}^{\langle i \rangle}} V^2 dV \tag{190}$$

or

$$s_G = \frac{\beta}{\Pi_\eta^{+\langle i \rangle} \alpha^{\langle i \rangle}} \frac{W_{TO}}{P_{ref}^{\langle i \rangle}} \frac{V_{TO}^3}{3 g_o} \tag{191}$$

Assuming that $\Pi_\eta^{+\langle i \rangle}$ is constant, the equation leads to

$$\frac{P_{ref}^{\langle i \rangle}}{W_{TO}} = \frac{2}{3} \frac{\beta^2 \tau^{\langle i \rangle} k_{TO}^2}{\Pi_\eta^{+\langle i \rangle} \alpha^{\langle i \rangle} s_G \rho g_o} \left(\frac{W_{TO}}{S} \right)^{\frac{3}{2}} \tag{192}$$

A.6.2 Total Takeoff Distance

The total takeoff distance consists of four parts: (1) the ground-roll distance (s_G), (2) the rotation distance (s_R), (3) the transition distance (s_{TR}), and (4) the climb-out distance over an obstacle (s_{CL}).

Mattingly's Equation

(1) The ground-roll distance (s_G)

A simplified version of the equation regarding the ground-roll distance is given as Eq. (188). A more accurate equation can be derived by accounting for the impact of D and R. Then,

$$\frac{T_{SL}}{W_{TO}} = \frac{\beta}{\alpha} \left(\xi_{TO} \frac{q}{\beta} \frac{S}{W_{TO}} + \mu_{TO} + \frac{1}{g_o} \frac{dV}{dt} \right) \tag{193}$$

where $\xi_{TO} = C_D + C_{DR} - \mu_{TO} C_L$. Integrating Eq. (193) results in

$$s_G = -\frac{\beta (W_{TO}/S)}{\rho g_o \xi_{TO}} \ln \left\{ 1 - \xi_{TO} / \left[\left(\frac{\alpha}{\beta} \frac{T_{SL}}{W_{TO}} - \mu_{TO} \right) \frac{C_{L_{\max}}}{k_{TO}^2} \right] \right\} \tag{194}$$

(2) The rotation distance (s_R)

The rotation distance can be computed by

$$s_R = t_R V_{TO} = t_R k_{TO} \sqrt{2\beta/(\rho C_{L_{\max}})(W_{TO}/S)} \tag{195}$$

where t_R is a total aircraft rotation time based on experience (normally 3 seconds),

(3) The transition distance (s_{TR})

The transition distance can be computed by

$$s_{TR} = R_c \sin\theta_{CL} = \frac{V_{TO}^2 sin\theta_{CL}}{g_o(n-1)} \tag{196}$$

where θ_{CL} is the angle of climb, which is given as

$$\sin\theta_{CL} = \frac{1}{V}\frac{dh}{dt} = \frac{T-D}{W} \tag{197}$$

Given that $n = 0.8k_{TO}^2$,

$$s_{TR} = \frac{k_{TO}^2 \sin\theta_{CL}}{g_o(0.8k_{TO}^2 - 1)} \frac{2\beta}{\rho C_{L_{\max}}} \frac{W_{TO}}{S} \tag{198}$$

(4) The climb-out distance over an obstacle (s_{CL})

There are two different cases, depending on h_{obs} and h_{TR}, each of which is depicted in Figures 105 and 106, respectively.

If $h_{obs} > h_{TR}$,

$$s_{CL} = \frac{h_{obs} - h_{TR}}{\tan\theta_{CL}} \tag{199}$$

$$h_{TR} = \frac{V_{TO}^2(1-\cos\theta_{CL})}{g_o(0.8k_{TO}^2 - 1)} = \frac{k_{TO}^2(1-\cos\theta_{CL})}{g_o(0.8k_{TO}^2 - 1)} \frac{2\beta}{\rho C_{L_{\max}}} \frac{W_{TO}}{S} \tag{200}$$

Plugging Eq. (194), (195), (198), (199), and (200) into $s_{TO} = s_G + s_R + s_{TR} + s_{CL}$, results in a quadratic equation with respect to $(W_{TO}/S)^{1/2}$ as follows:

$$a\left(\frac{W_{TO}}{S}\right) - b\left(\frac{W_{TO}}{S}\right)^{1/2} + c = 0 \tag{201}$$

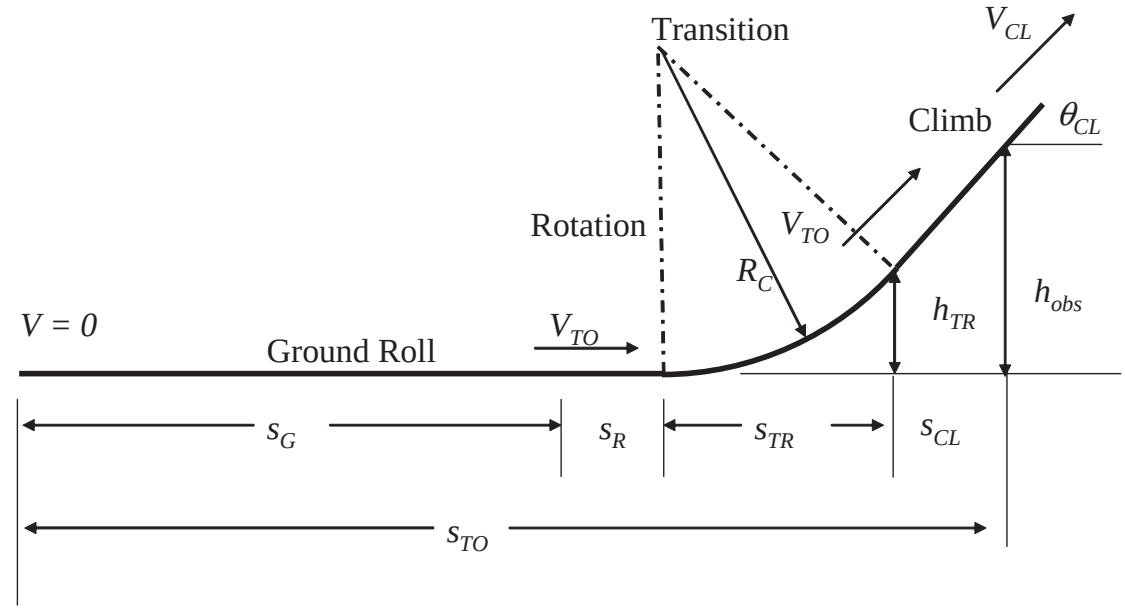

Figure 105: Takeoff terminology ($h_{TR} < h_{obs}$) [100]

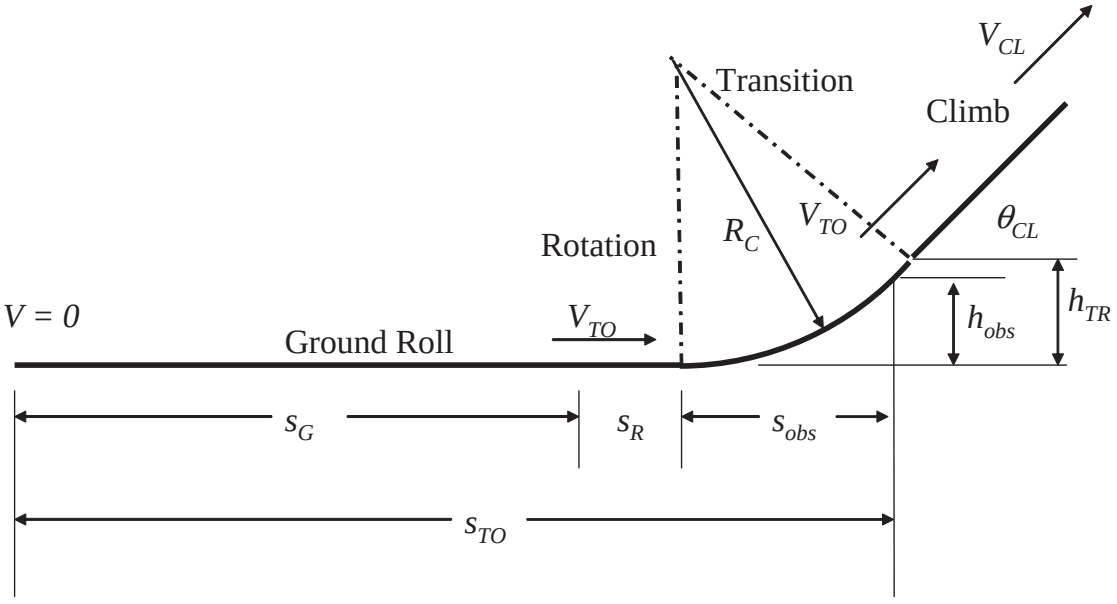

Figure 106: Takeoff terminology ($h_{TR} > h_{obs}$) [100]

where

$$
\begin{aligned}
a =& -\frac{\beta}{\rho g_o \xi_{TO}} \ln\left\{1 - \xi_{TO} / \left[\left(\frac{\alpha}{\beta}\frac{T_{SL}}{W_{TO}} - \mu_{TO}\right)\frac{C_{L_{\max}}}{k_{TO}^2}\right]\right\} \\
&+ \frac{k_{TO}^2 \sin\theta_{CL}}{g_o(0.8k_{TO}^2 - 1)}\frac{2\beta}{\rho C_{L_{\max}}} - \frac{k_{TO}^2(1-\cos\theta_{CL})}{g_o(0.8k_{TO}^2-1)}\frac{2\beta}{\rho C_{L_{\max}}}\frac{1}{\tan\theta_{CL}} \\
&\text{(obstacles considered and } h_{obs} < h_{TR}) \\
=& -\frac{\beta}{\rho g_o \xi_{TO}} \ln\left\{1 - \xi_{TO} / \left[\left(\frac{\alpha}{\beta}\frac{T_{SL}}{W_{TO}} - \mu_{TO}\right)\frac{C_{L_{\max}}}{k_{TO}^2}\right]\right\} \\
&\text{(no obstacles considered)}
\end{aligned}
\tag{202}
$$

$$
\begin{aligned}
b =& t_R k_{TO}\sqrt{2\beta/(\rho C_{L_{\max}})} \\
c =& S_{TO} - \frac{h_{obs}}{\tan\theta_{CL}}
\end{aligned}
$$

Therefore, for a given T_{SL}, W_{TO}/S can be obtained from Eq. (201)

$$
\frac{W_{TO}}{S} = \left\{\frac{b + \sqrt{b^2 - 4ac}}{2a}\right\}^2 \tag{203}
$$

If $h_{obs} < h_{TR}$, s_{TO} is given as the summation of s_G, s_R, and s_{obs} as shown in Figure 106. Note that unlike the previous case s_{TR} is not included in s_{TO}. From Figure 106, s_{obs} is given as

$$
s_{obs} = R_c \sin\theta_{obs} = \frac{V_{TO}^2 \sin\theta_{obs}}{g_o(0.8k_{TO}^2 - 1)} \tag{204}
$$

where

$$
\theta_{obs} = \cos^{-1}\left(1 - \frac{h_{obs}}{R_c}\right) \tag{205}
$$

Even if $h_{obs} < h_{TR}$, the same quadratic equation per Eq. (201) as used for the case of $h_{obs} > h_{TR}$ can be used for computing W_{TO}/S for a given T_{SL}, but the coefficients are now modified as follows:

$$
\begin{aligned}
a =& -\frac{\beta}{\rho g_o \xi_{TO}} \ln\left\{1 - \xi_{TO} / \left[\left(\frac{\alpha}{\beta}\frac{T_{SL}}{W_{TO}} - \mu_{TO}\right)\frac{C_{L_{\max}}}{k_{TO}^2}\right]\right\} \\
&+ \frac{k_{TO}^2 \sin\theta_{obs}}{g_o(0.8k_{TO}^2 - 1)}\frac{2\beta}{\rho C_{L_{\max}}} \\
b =& t_R k_{TO}\sqrt{2\beta/(\rho C_{L_{\max}})} \\
c =& S_{TO}
\end{aligned}
\tag{206}
$$

In fact, Eq. (204) and (205) cannot be solved without knowing W_{TO}/S, because θ_{obs}, V_{TO} and R_c are functions of W_{TO}/S. Mattingly et al. did not address this issue in Ref. [100]. The present study employs an interactive scheme to find the quantities that are interdependent upon one another. First, a value for θ_{obs} is assumed. Now, wing loading can be computed by Eq. (201) and Eq. (206). Once W_{TO}/S is obtained, V_{TO} and R_c can be computed by Eq. (187) and Eq. (204), respectively. Subsequently, θ_{obs} can be updated by Eq. (205). These steps are repeated until θ_{obs} converges.

AIASM's Equation

Considering $\frac{T_{SL}}{W_{TO}} = \frac{\eta_p(V)}{V}\frac{P_{ref}}{W_{TO}}$ and $dt = ds/V$,

$$\frac{\Pi_\eta^{+\langle i\rangle}(V)}{V}\frac{P_{ref}}{W_{TO}} = \frac{\beta}{\alpha}\left(\xi_{TO}\frac{\frac{\rho V^2}{2}}{\beta}\frac{S}{W_{TO}} + \mu_{TO} + \frac{V}{g_o}\frac{dV}{ds}\right) \tag{207}$$

$$ds = \frac{\frac{V}{g_o}dV}{\frac{\alpha}{\beta}\frac{\Pi_\eta^{+\langle i\rangle}(V)}{V}\frac{P_{ref}}{W_{TO}} - \xi_{TO}\frac{\rho V^2}{2\beta}\frac{S}{W_{TO}} - \mu_{TO}} \tag{208}$$

$$s_G = \int_0^{S_G} ds = \int_0^{V_{TO}} \frac{\frac{V}{g}dV}{\frac{\alpha}{\beta}\frac{\Pi_\eta^{+\langle i\rangle}(V)}{V}\frac{P_{ref}}{W_{TO}} - \frac{\xi_{TO}\rho V^2}{2\beta}\frac{S}{W_{TO}} - \mu_{TO}} \tag{209}$$

When the reference power, P_{ref} is given as the shaft power, then $\Pi^+_{\eta^{\langle i\rangle}}$ is simply the efficiency of a propeller η_P, which varies with V. When $V_{TO} \ll V(\eta_{P_{\max}})$, V_{TO} can be assumed to linearly vary with V as follows:

$$\Pi_\eta^{+\langle i\rangle}(V) = \eta_P(V_{TO})V \tag{210}$$

where $\eta_P(V_{TO})$ is the propeller efficiency at take-off speed (V_{TO}). The take-off ground roll is given as

$$s_G = -\frac{\beta(W_{TO}/S)}{\rho g_o \xi_{TO}} \ln\left\{1 - \xi_{TO}/\left[\left(\frac{\alpha^{\langle i\rangle}\eta_P(V_{TO})}{\beta\tau^{\langle i\rangle}}\frac{P_{ref}^{\langle i\rangle}}{W_{TO}} - \mu_{TO}\right)\frac{C_{L_{\max}}}{k_{TO}^2}\right]\right\} \tag{211}$$

The other distances, s_R, s_{TR}, s_{CL}, and s_{obs} can be computed by the same equations as Mattingly's method.

A.7 Landing Distance

The total landing distance (s_L) consists of three parts: (1) the distance to clear an obstacle of given height (s_A), (2) a free roll traversed before the brakes are fully applied (s_{FR}), and (3) braking roll (s_B) as illustrated in Figure 107.

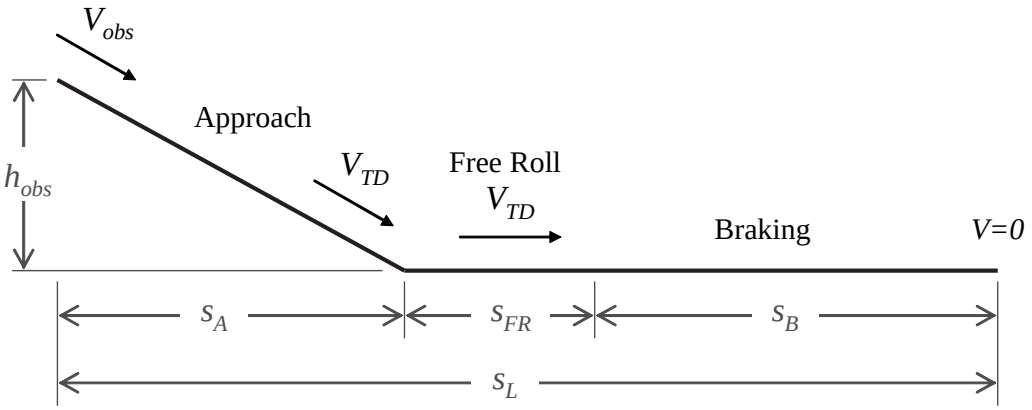

Figure 107: Landing terminology [100]

(1) Distance to clear an obstacle of given height (s_A)

$$s_A = \frac{2\beta}{\rho g_o (C_D + C_{DR})} \left(\frac{W_{TO}}{S}\right) \left(\frac{k_{obs}^2 - k_{TD}^2}{k_{obs}^2 + k_{TD}^2}\right) + \frac{C_{L_{\max}}}{(C_D + C_{DR})} \frac{2h_{obs}}{(k_{obs}^2 + k_{TD}^2)} \tag{212}$$

where h_{obs} is the height of the obstacle and the velocity at the obstacle is

$$V_{obs} = k_{obs} V_{STALL} \tag{213}$$

(2) Free roll traversed before the brakes are fully applied (s_{FR})

$$s_{FR} = t_{FR} V_{TD} = t_{FR} k_{TD} \sqrt{\{2\beta/(\rho C_{L_{\max}})\}(W_{TO}/S)} \tag{214}$$

(3) Braking roll (s_B)

$$\frac{T_{SL}}{W_{TO}} = \frac{\beta}{\alpha} \left(\xi_L \frac{q}{\beta} \frac{S}{W_{TO}} + \mu_B + \frac{1}{g_o} \frac{dV}{dt}\right) \tag{215}$$

where $\xi_L = C_D + C_{DR} - \mu_B C_L$.

$$s_G = \frac{\beta(W_{TO}/S)}{\rho g_o \xi_L} \ln \left\{1 + \xi_L / \left[\left(\mu_B - \frac{(-\alpha)}{\beta} \frac{T_{SL}}{W_{TO}}\right) \frac{C_{L_{\max}}}{k_{TD}^2}\right]\right\} \tag{216}$$

Then, the constraint curve of T_{SL}/W_{TO} and W_{TO}/S for landing distance performance can be obtained in a similar way that for take-off distance performance is derived. If thrust reversers are not equipped in the aircraft, that is $\alpha = 0$, then landing distance no longer depends on thrust, yielding a second order algebraic equation for W_{TO}/S, which is applicable in both thrust-based and power-based approaches. The equation was used for developing landing distance constraints in the GA study presented in §6.1.

APPENDIX B

WEIGHT FRACTION EQUATIONS

B.1 Mattingly's Equation

The ratio of the final to the initial weight for a mission leg can be computed as follows:

- Constant Speed Climb

$$\exp\left\{\frac{-c_t}{V}\left[\frac{\Delta h}{1-u}\right]\right\} \tag{217}$$

- Horizontal Acceleration

$$\exp\left\{\frac{-c_t}{V}\left[\frac{\Delta(V^2/2g)}{1-u}\right]\right\} \tag{218}$$

- Climb and Acceleration

$$\exp\left\{\frac{-c_t}{V}\left[\frac{\Delta(h+V^2/2g)}{1-u}\right]\right\} \tag{219}$$

- Constant Altitude/Speed Cruise

$$\exp\left\{\frac{-c_t}{V}\left(\frac{D}{L}\right)\Delta s\right\} \tag{220}$$

- Constant Altitude/Speed Turn

$$\exp\left\{-c_t \cdot n \cdot \left(\frac{D}{L}\right)\frac{2\pi NV}{g\sqrt{n^2-1}}\right\} \tag{221}$$

- Loiter

$$\exp\left\{-c_t \cdot n \cdot \left(\frac{D}{L}\right)\Delta t\right\} \tag{222}$$

- Warm-up

$$1 - c_t\left(\frac{T_{SL}}{W_{TO}}\right)\Delta t \tag{223}$$

- Take-off Rotation

$$1 - c_t\left(\frac{T_{SL}}{W_{TO}}\right)\Delta t_R \tag{224}$$

B.2 AIASM's Equation

As depicted in Figure 108, the energy weight fraction for the s^{th} mission leg ultimately depends on $\beta^{(s-1)}$, $\Upsilon^{(s)}$ and $\Xi_{CE}^{(s)}$ ($\Xi_{NE}^{(s)}$ for a non-consumable energy source). The expressions for $\beta^{(s-1)}$ and $\Xi_{CE}^{(s)}$ are provided as Eq. (80), Eq. (81), and Eq. (71).

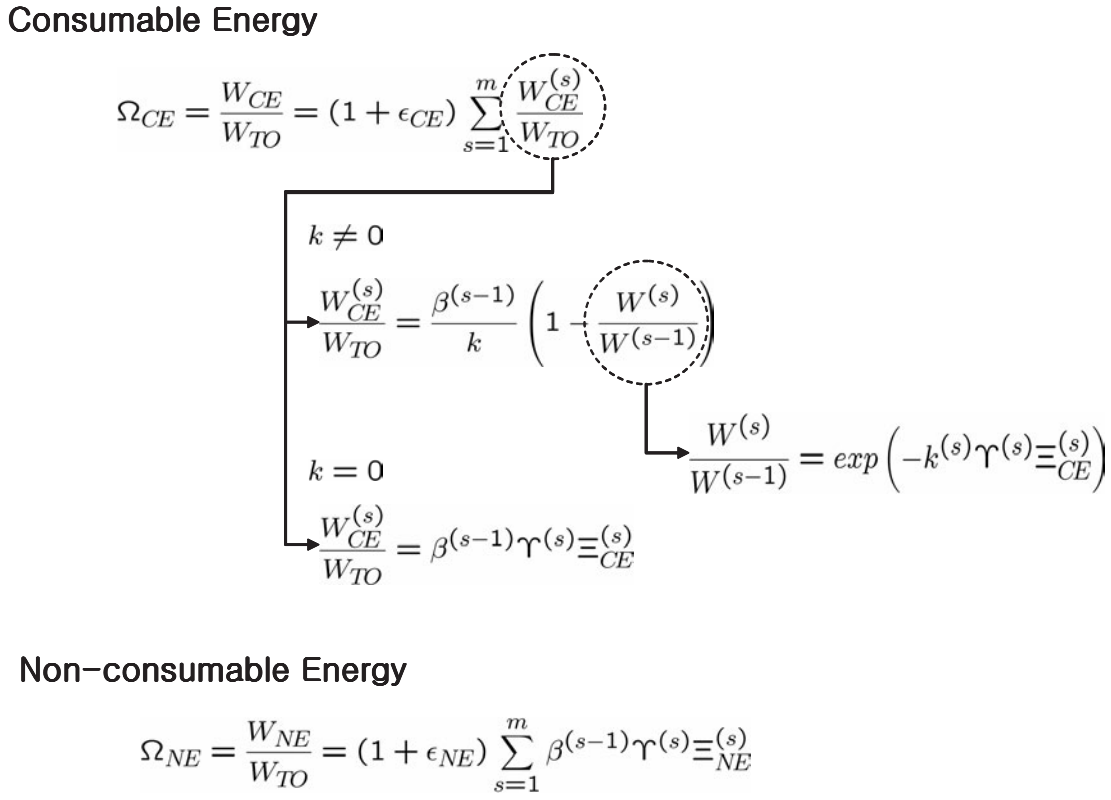

Figure 108: Equations associated with generalized mission analysis

In addition, general expressions for $\Upsilon^{(s)}$ are given as Eq. (74) for positive excess power and Eq. (77) or Eq. (78) for zero excess power. The aerodynamic coefficients and flight conditions of the equations are assumed to be constant at some representative values so that the integration can be accomplished explicitly. The resulting $\Upsilon^{(s)}$ for different cases are listed as follows:

- Constant Speed Climb

$$\frac{\Delta h}{1-u} \tag{225}$$

- Horizontal Acceleration

$$\frac{\Delta(V^2/2g)}{1-u} \tag{226}$$

- Climb and Acceleration

$$\frac{\Delta(h+V^2/2g)}{1-u} \tag{227}$$

- Constant altitude/speed cruise

$$\left(\frac{D}{L}\right)\Delta s \tag{228}$$

- Constant altitude/speed turn

$$\left(\frac{D}{L}\right)\frac{2\pi NV}{g\sqrt{n^2-1}} \tag{229}$$

- Loiter

$$\left(\frac{D}{L}\right)\Delta t \tag{230}$$

APPENDIX C

WEIGHT-SPECIFIC PARAMETERS AS DECISION VARIABLES

If power to weight ratio ($\frac{P_{ref}}{W_{TO}}$), energy weight fraction($\frac{W_{energy}}{W_{TO}}$), and wing loading ($\frac{W_{TO}}{S}$) are chosen as the design variables in the replacement of power, fuel, and thrust, the distributions of the random variables are not given in a explicit form. Each of the random variables can be decomposed into a static decision variable and a random distribution by the similar process as presented in §5.3.2. The random response of take-off gross weight can be expressed as follows:

$$\tilde{W}_{TO} = W_{TO}|_{\check{\mathbf{v}}} \zeta_{W_{TO}} \tag{231}$$

where $W_{TO}|_{\check{\mathbf{v}}}$ is the take-off gross weight calculated with the deterministic values of the random variables, $\check{\mathbf{v}}$, and $\zeta_{W_{TO}}$ is the actual take-off gross weight distribution normalized to $W_{TO}|_{\check{\mathbf{v}}}$.

By combining Eq. (132) and Eq. (231), the first set of the constraints in Eq. (130) can be rewritten with respect to the deterministic values, $\check{\mathbf{v}}$, as follows:

$$\frac{\zeta_P}{\zeta_{W_{TO}}} \frac{P_{ref}}{W_{TO}}|_{\check{\mathbf{v}}} - \Theta_i\left(\zeta_{W_{TO}} \frac{W_{TO}}{S}|_{\check{\mathbf{v}}}, \tilde{\mathbf{p}}_i, \mathbf{p}_i\right)|_{\check{\mathbf{v}}} \geq 0 \quad (i = 1, \cdots, n_p) \tag{232}$$

where n_p is the number of constraints. Similarly, by combining Eq. (133) and Eq. (231) the second set of the constraints in Eq. (130) can be expressed as follows:

$$\frac{\zeta_{W_{energy}}}{\zeta_{W_{TO}}} \frac{W_{energy}}{W_{TO}}|_{\check{\mathbf{v}}} - \Omega_j\left(\frac{\zeta_P}{\zeta_{W_{TO}}} \frac{P_{ref}}{W_{TO}}|_{\check{\mathbf{v}}}, \zeta_{W_{TO}} \frac{W_{TO}}{S}|_{\check{\mathbf{v}}}, \tilde{\mathbf{p}}_j, \mathbf{p}_j\right) \geq 0 \ (j = 1, \cdots, n_m) \tag{233}$$

Finally, a PASM problem whose design variables are weight-specific variables can be

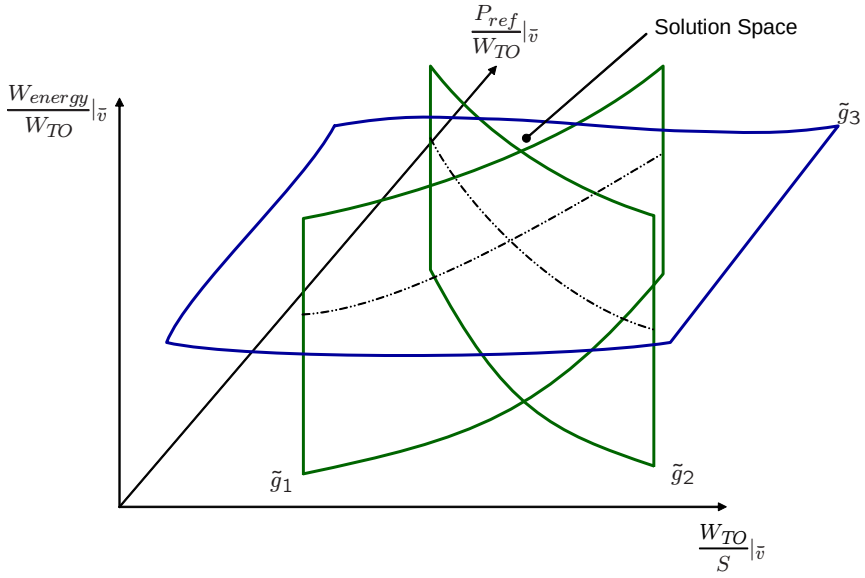

Figure 109: Design space of probabilistic aircraft sizing

formulated as follows:

$$\begin{aligned} &\min_{\mathbf{x}} \ \mathbb{E}[\tilde{f}] \\ &\quad \text{s.t.} \mathbb{P}\left[g_i(\mathbf{x}, \boldsymbol{\xi})|_{\breve{\mathbf{v}}} \geq 0\right] \geq \ \alpha_{g_i} \\ &\qquad \text{where } \mathbf{x} = \left(\frac{P_{ref}}{W_{TO}}|_{\breve{\mathbf{v}}}, \frac{W_{TO}}{S}|_{\breve{\mathbf{v}}}, \frac{W_f}{W_{TO}}|_{\breve{\mathbf{v}}}\right) \end{aligned} \tag{234}$$

The probabilistic constraint, $g_i(\mathbf{x}, \boldsymbol{\xi})|_{\breve{\mathbf{v}}} \geq 0$ is given either Eq. (232) or Eq. (233). A notional design space of a PASM problem established as Eq. (234) is illustrated in Figure 109. The three-dimensional design space includes two power-balance constraints and the single energy-balance constraint for simplicity's purpose.

APPENDIX D

ELECTROLYZER MODEL AND ROUND TRIP EFFICIENCY

The RFC system considered in the SPHALE aircraft consists of an electrolyzer component and a fuel cell component as illustrated in Figure 110. Excess energy from PV cells during the daytime provides the electricity to decompose water into hydrogen and oxygen by the process of electrolysis in the electrolyzer. The stored energy is discharged via a redox reaction process of PEM fuel cells at night time.

The electrolyzer begins to electrolyze water to produce hydrogen above the calculated theoretical open circuit potential, 1.23V at 25°C. The rate of hydrogen flow can be determined by electrochemistry as follows [228]:

$$\dot{m}_{H_2} = \frac{I n_{cell} M_{H2}}{2F} \tag{235}$$

where I is the current (A), n_{cell} is the number of cells in the electrolyzer, M_{H2} is the molar mass of hydrogen (2g/mol), F is Faraday's constant (96,485°C/mol), and $\dot{m}$ is a mass flow rate in grams per second of hydrogen. Therefore, hydrogen production is proportional to the current applied to the load.

The voltage applied to the electrolyzer can be modeled using

$$V_{stack} = n_{cells}\left(1.23 + \frac{RT}{2\alpha F}\ln\left(\frac{I}{I_0}\right) + IR_0\right) \tag{236}$$

where 1.23V is the theoretical open circuit voltage at 25°C; R is the gas constant 8.314; T is the temperature in Kelvin (298°K); α is the charge transfer coefficient (approximately 0.325 from the experimental data); I is the current; I_0 is the cathode exchange current (approximately 0.5mA); and R_0 is the cell resistance (0.0107Ω).

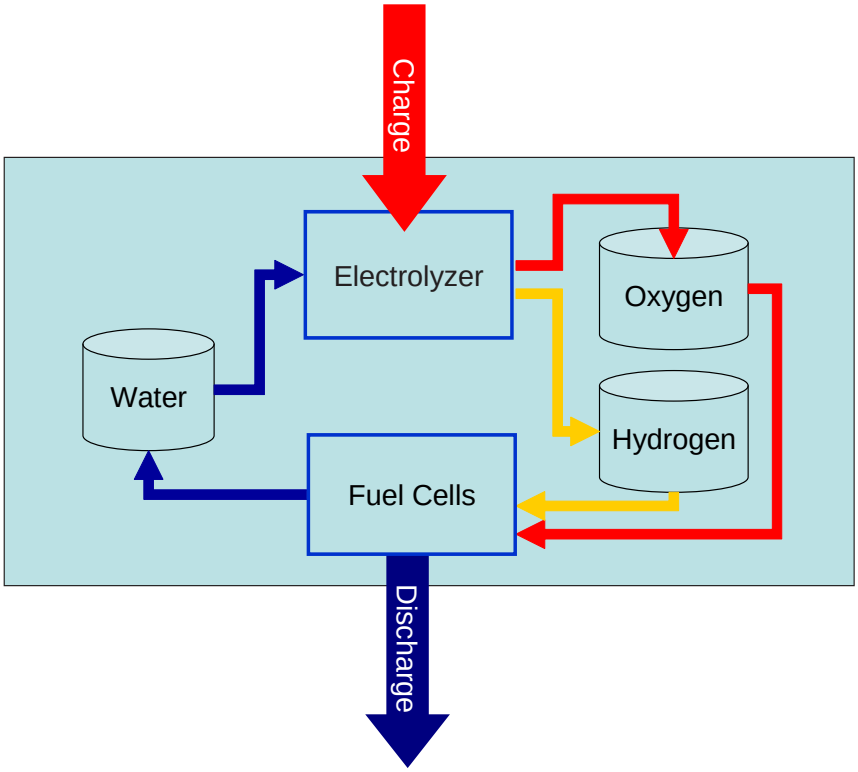

Figure 110: Illustration of a regenerative fuel cell system

The electrolyzer efficiency is given by the simple relationship

$$\eta_{electrolyzer} = \frac{1.48 n_{cells}}{V_{stack}} \tag{237}$$

Since the electrolyzer efficiency is affected by voltage, the number of cells, and operating temperature, an accurate estimation can be obtained through a comprehensive simulation with detailed models that are able to capture the voltage and the current behavior and environmental changes such as pressure and temperature. However, a simple model that is acceptable for the conceptual design phase can be constructed through a regression analysis. Figure 111 depicts the current and hydrogen mass flow versus the voltage for two different numbers (four and ten) of cell stacks.

The hydrogen mass flow versus power for the two different stacks is plotted in Figure 112, which shows a strong linear relationship between the hydrogen mass flow

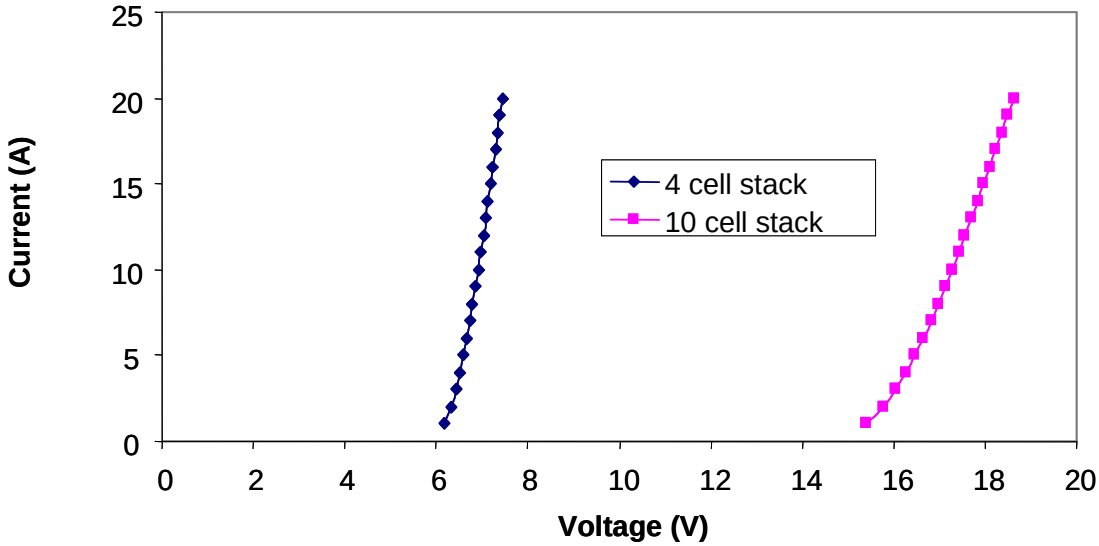

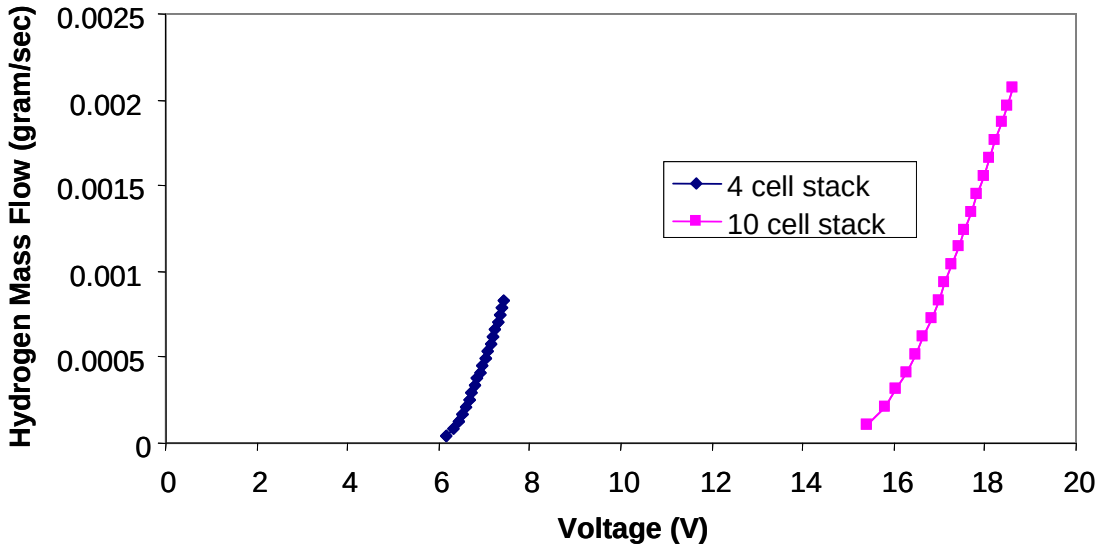

Figure 111: Performance of the electrolyzer model

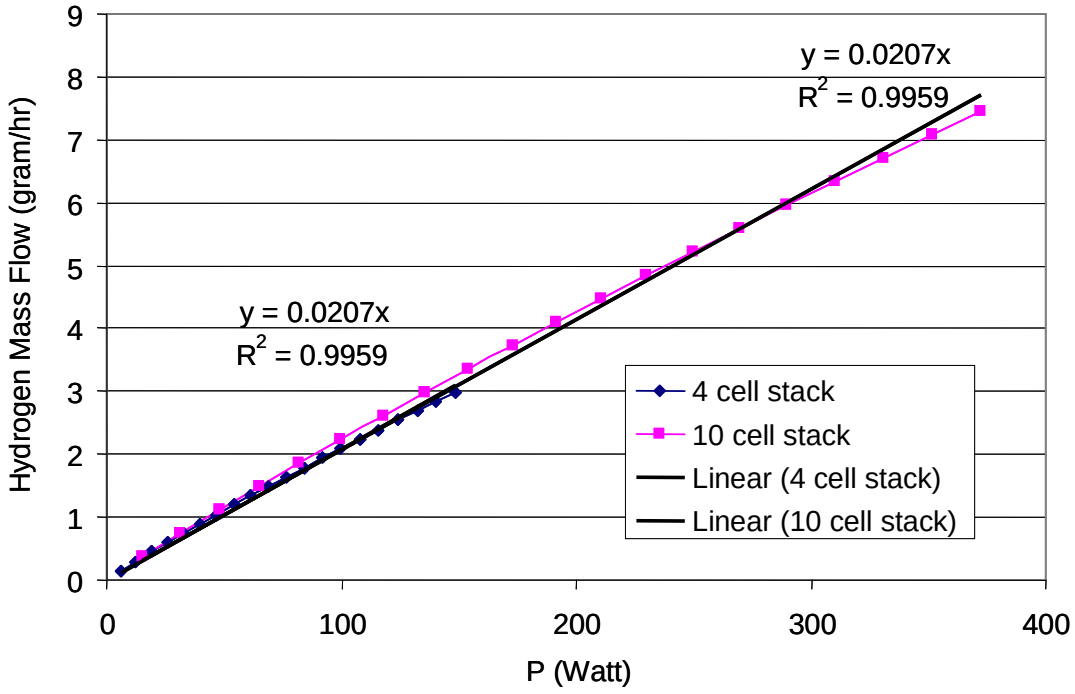

Figure 112: Hydrogen mass flow versus power

and input power. Regression analyses for the two cases yield an identical linear equation as follows[1]:

$$\dot{m}_{H_2} = 0.0207P \text{ (gram/hr)} \tag{238}$$

The total discharge energy of the fuel cell system is

$$\eta_{fc}\nu_{H_2}g\int_{T_D}\dot{m}_{H_2}dt = \eta_{fc}\nu_{H_2}g\left(0.0207\int_{T_D}Pdt\right) \tag{239}$$

The total input energy from PV cells to the fuel cell system is

$$\int_{T_D}Pdt \tag{240}$$

Therefore, the roundtrip efficiency is given as follows:

$$\eta_{rt} = 0.0207\eta_{fc}\nu_{H_2}g \ = 0.4895 \tag{241}$$

[1]Note that this equation holds only for the specific temperature 25°C. The numeric constant must be revised by another regressions at different operating temperatures.

which is comparable with 0.42 estimated by Jakupca et al. [211].

APPENDIX E

SUPPLEMENTAL CHARTS

This appendix includes additional charts developed in the course of the example studies presented in Chapter VI.

Table 21: Inputs of the constraint analyses of the GA study

		TOFL	Climb	Cruise	Approach	LDFL
User Inputs	**PA (Pressure Altitude, ft)**	0	8,000	10,000	0	0
	β (Weight Fraction to TOGW)	1	0.99	0.97	0.96	0.96
	M (Mach Number)	0.1	0.185	0.185	0.09	0.09
For Constant Speed Climb Only	**Climb Rate (ft/min)**		150			
For Field Performance Only	**T (Tempreture, R)**	554.7	490.2	483.0	516.7	516.7
	C_{Lmax} (Maximum Lift Coefficient)	2.0			2.5	2.0
	k_{TD} (Touch Down Speed Ratio to Stall Speed)	1.2				1.15
	k_{CL} (Climb Speed Ratio to Stall Speed) or k_{APP} (Approach Speed Ratio to Stall Speed)	1.2			1.3	1.3
	μ (Friction Coefficient)	0.05				0.18
	Δt_{ROT} (Rotation Time of Take-Off, sec) Δt_{FR} (Free Roll Time of Landing, sec)	3.0				3.0
	h_{obs} (Obstacles Height, ft)	35.0				50.0
	S_{TO} (Take-off Field Length) S_L (Landing Field Length)	1370.0				1500
Air Properties & Thrust Lapse Rate	**α (Installed Full Throttle Power Lapse)**	1.2000	1.1000	1.0000	1.0000	1.0000
	ρ (Air Density, slug/ft^3)	0.002223	0.001868	0.001755	0.002386	0.002386
	Θ (Temperature Ratio)	1.06940	0.94500	0.93125	0.99614	0.99614
	σ (Density Ratio)	0.9351	0.7860	0.7385	1.0039	1.0039
	δ (Pressure Ratio)	1.0000	0.7428	0.6877	1.0000	1.0000
	a (Speed of Sound, ft/sec)	1154.4	1085.2	1077.2	1114.1	1114.1
Velocity & Dynamic Pressure	**V (Speed, ft/sec)**	115	201	199	96	96
	V (Speed, knot)	68	119	118	57	57
	q (Dynamic Pressure)	14.8	37.7	34.9	11.0	11.0
Drag Coefficients	**K1 (K' + K'')**	0.0565	0.0565	0.0565	0.0565	0.0565
	K2 (-2K''(C_{Lmin})^2)	0.0136	0.0136	0.0136	0.0136	0.0136
	C_{Do} (C_{Dmin} +K''C_{Lmin}^2)	0.0281	0.0281	0.0281	0.0281	0.0281
	C_D (Drag Coefficient)	0.1560				0.1273
	C_{DR} (Drag Coeeficient of Protuburances)	0.0694				0.2178
	C_{DRc} (Drag Coeeficient of Drag Parachute)					0.0000
	ξ_{TO} (= C_D+ C_{DR} - $\mu_{TO}C_L$)	0.1560				0.1273
Others	**g (Gravity Constant, ft/sec^2)**	32.17				32.17

		q	Alt.	Δ_{z_e}	Δ_t	Δ_s	θ	C_L	L/D	u	β_i	β_f	Weight Fraction
			ft.	ft.	min.	mi.	deg.		–	–	–	–	–
s01	Warm up	0.0	0	0	15	0			–		1.00000	0.99911	0.99911
s02	Take-off Accel.	2.4	0	126	0.51	0.23	0		2	0.5	0.99911	0.99907	0.99996
s03	Take-off Rotation	9.6	0	0	0.05	4.50	–		3	0.5	0.99907	0.99907	1.00000
s04	Climb	10.6	500	1030	0.86	0.79	12.1	1.11	9.9	0.3	0.99907	0.99895	0.99988
s05	Climb	11.4	1795.5	1594	1.49	1.45	10.2	1.03	10.1	0.3	0.99895	0.99877	0.99982
s06	Climb	11.3	2862	546	0.51	0.51	10.1	1.03	10.1	0.3	0.99877	0.99871	0.99994
s07	Climb	11.4	3269	274	0.26	0.26	9.9	1.03	10.1	0.3	0.99871	0.99868	0.99997
s08	Climb	11.6	3533.5	264	0.25	0.25	9.8	1.01	10.2	0.3	0.99868	0.99865	0.99997
s09	Climb	11.8	3798.5	274	0.25	0.26	9.8	0.99	10.2	0.3	0.99865	0.99862	0.99997
s10	Climb	11.8	4209	551	0.53	0.54	9.5	0.99	10.2	0.4	0.99862	0.99855	0.99994
s11	Climb	11.7	4759	553	0.53	0.55	9.4	1.00	10.2	0.4	0.99855	0.99849	0.99993
s12	Climb	11.5	5517.5	966	0.93	0.96	9.4	1.02	10.1	0.4	0.99849	0.99837	0.99988
s13	Climb	11.1	6500	1000	0.97	1.00	9.3	1.05	10.0	0.4	0.99837	0.99825	0.99988
s14	Climb	22.3	7500	1445	1.34	2.02	6.7	0.52	10.3	0.4	0.99825	0.99809	0.99983
s11	Cruise	37.4	8000	0	48.52	95.83	0	0.31	8.3	1	0.99809	0.99412	0.99602
s12	Cruise	37.4	8000	0	48.52	95.83	0	0.31	8.2	1	0.99412	0.99016	0.99601
s12	Cruise	37.4	8000	0	48.52	95.83	0	0.31	8.2	1	0.99016	0.98620	0.99601
s13	Cruise	37.4	8000	0	48.52	95.83	0	0.31	8.2	1	0.98620	0.98226	0.99600
s13	Cruise	37.4	8000	0	48.52	95.83	0	0.31	8.2	1	0.98226	0.97832	0.99599
s13	Cruise	37.4	8000	0	48.52	95.83	0	0.31	8.2	1	0.97832	0.97438	0.99598
s14	Descent	28.7	5000	−6338	10.00	0.00	0	0.40	9.4	1	0.97438	0.97371	0.99931
s15	Loiter	20.4	2000	0	10.00	0.00	0	0.56	10.5	1	0.97371	0.97330	0.99959
s16	Loiter	20.4	2000	0	45.00	0.00	0	0.56	10.5	1	0.97330	0.97149	0.99814

Table 22: Mission analysis of the electric GA

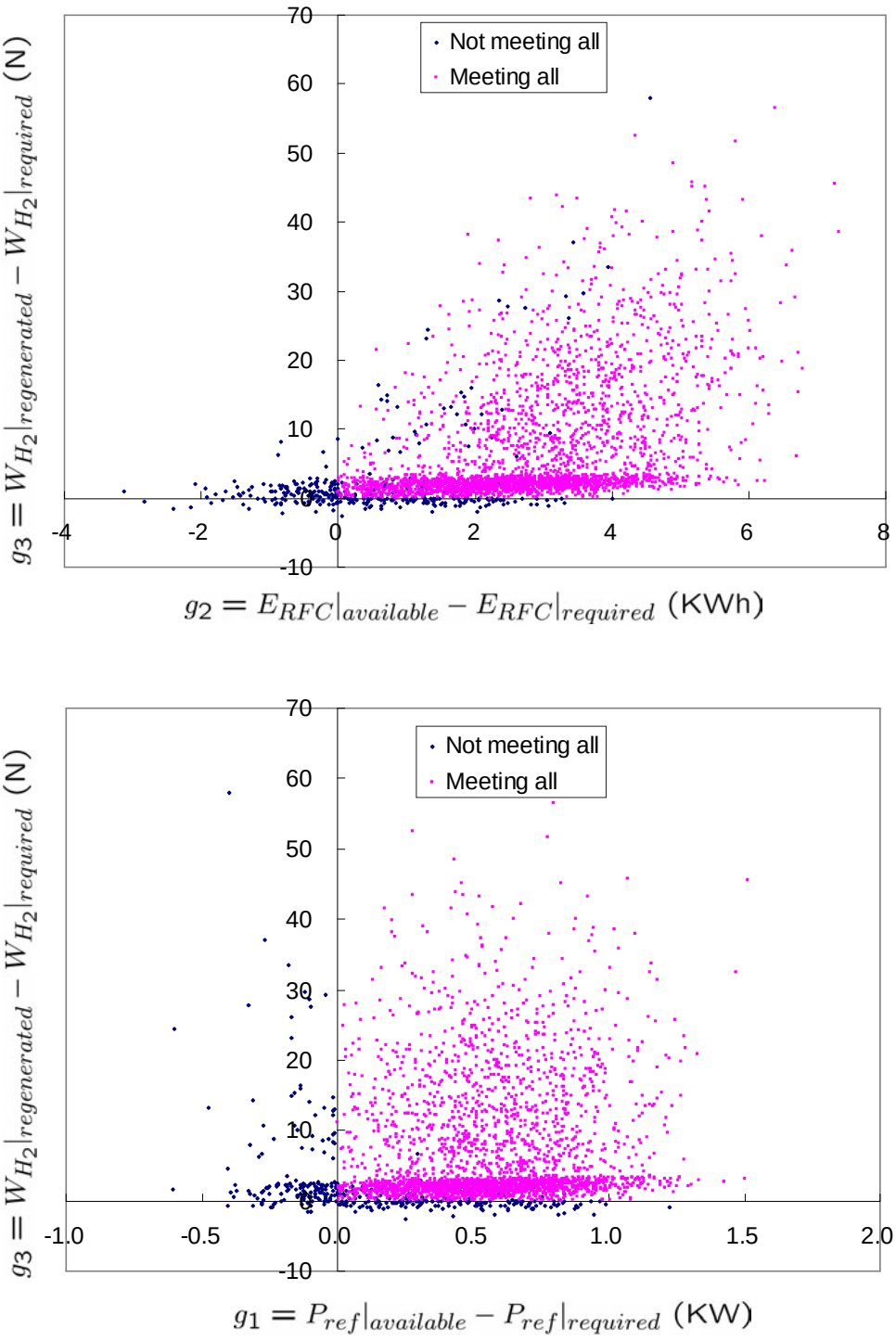

Figure 113: Illustration of samples of an MCS (**P2**)

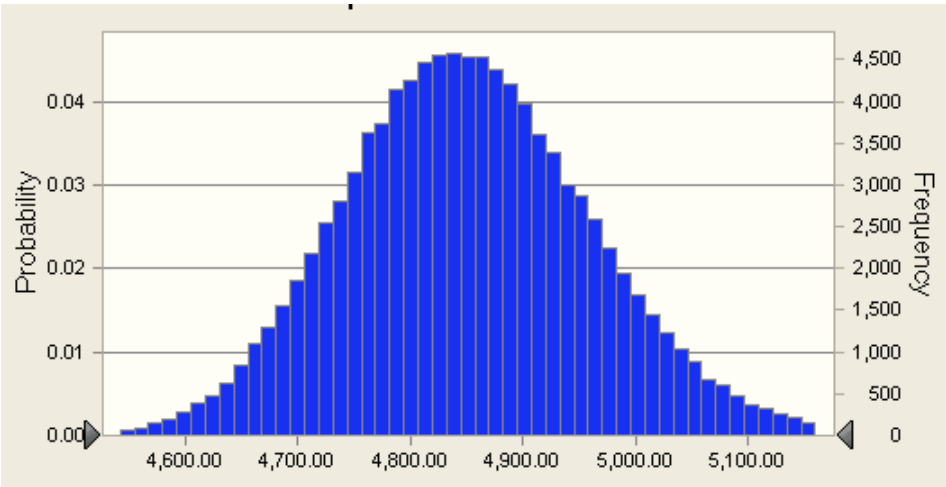

Figure 114: PDF of total power required at loiter (W)

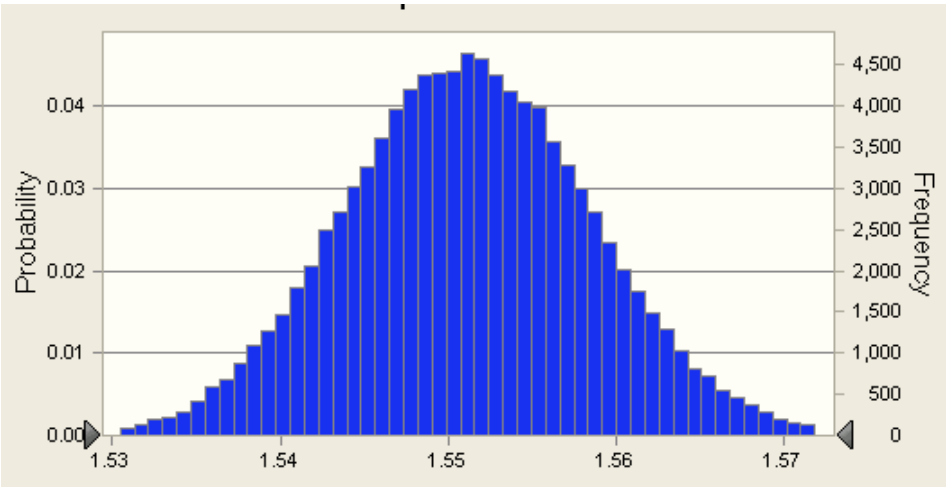

Figure 115: PDF of angle of attack at loiter

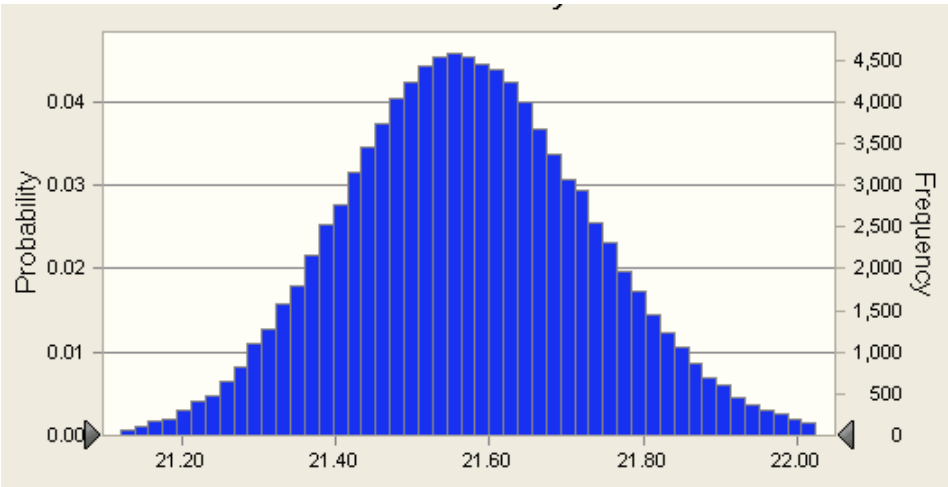

Figure 116: PDF of loiter velocity (m/sec)

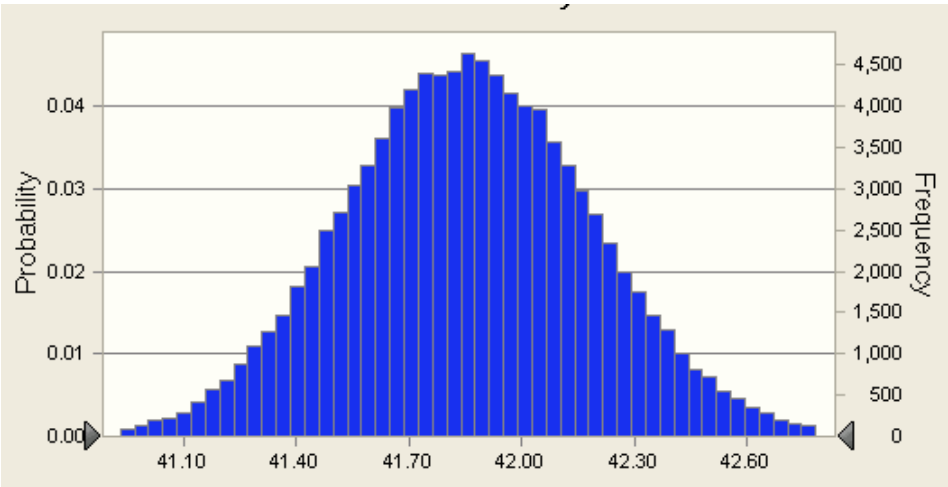

Figure 117: PDF of loiter efficiency

REFERENCES

[1] Fred L. Robson, G. T. P., "Engine Technology for Large Subsonic Nuclear Powered Aircraft," in *American Institute of Aeronautics and Astronautics and Society of Automotive Engineers, Joint Propulsion Specialist Conference*, 1972.

[2] Brewer, G. D., *Hydrogen Aircraft Technology*. CRC Press, 1991.

[3] John A. Wise, Todd Denning, J. B. and McMullen, T., "General Aviation in 2050," in *Aircraft, Technology Integration, and Operations Forum*, 2001.

[4] Garot, J.-M., "The Future Air Transport System in Europe: Vision and Perspectives," in *AIAA/ICAS International Air and Space Symposium and Exposition: The Next 100 Y*, 2003.

[5] Sehra, A. K. and Shin, J., "Revolutionary Propulsion Systems for 21st Century Aviation," Tech. Rep. NASA/TM2003-212615, NASA Glenn Research Center, 2003.

[6] NASA, "Past Projects - Helios Prototype." `http://www.nasa.gov/centers/dryden/history/pastprojects/Erast/helios.html`. [Online; accessed 26-October-2006].

[7] Westenberger, A., "Hydrogen Fuelled Aircraft," in *AIAA/ICAS International Air and Space Symposium and Exposition: The Next 100 Y*, 2003.

[8] Panel on Reconciling Temperature Observations, "Reconciling Observations of Global Temperature Change," tech. rep., National Research Council, 2000.

[9] J. Hansen, R. Ruedy, M. S. and Lo, K., "GISS Surface Temperature Analysis, Global Temperature Trends: 2005 Summation." `http://data.giss.nasa.gov/gistemp/2005/`, Jan 2006. [Online; accessed 15-October-2006].

[10] Penner, J. E., Lister, D. H., Griggs, D. J., Dokken, D. J., and McFarland, M., "IPCC Special Report, Aviation and the Global Atmosphere," tech. rep., the Intergovernmental Panel on Climate Change, 1999.

[11] Hansen, J., Sato, M., Ruedy, R., Lo, K., Lea, D. W., and Medina-Elizade, M., "Global Temperature Change," *Proceedings of the National Academy of Sciences*, vol. 103, pp. 14288–14293, 2006.

[12] Clarkin, J., "Hydrogen: Opportunities and Challenges," in *AIAA/ICAS International Air and Space Symposium and Exposition: The Next 100 Y*, 2003.

[13] United States General Accounting Office, "Aviation and the Environment, Aviation's Effects on the Global Atmosphere Are Potentially Significant and Expected to Grow." Report to the Honorable James L. Oberstar, Ranking Democratic Member, Committee on Transportation and Infrastructure, House of Representatives, February 2000.

[14] Penner, J. E., Lister, D. H., Griggs, D. J., Dokken, D. J., and McFarland, M., *Aviation and the Global Atmosphere*. Cambridge University Press, 1999.

[15] National Research Council, *A Review of NASA's Atmospheric Effects of Stratospheric Aircraft Project*. National Academies Press, 1999.

[16] Leary, N., "Aviation and the Global Atmosphere, A Special Report of IPCC Working Groups I and III," in *Presentation for the IPCC Symposium*, 1999.

[17] National Research Council (NRC), *Commercial Supersonic Technology: The Way Ahead*. National Academic Press, 2001.

[18] Kawa, S.R., J.G. Anderson, S.L. Baughcum, C.A. Brock, W.H. Brune, R.C., Cohen, D.E. Kinnison, P.A., Newman, J.M. Rodriguez, R.S. Stolarski, D. Waugh, and S.C. Wofsy, *Assessment of the Effects of High-Speed Aircraft in the Stratosphere: 1998*. Greenbelt, Md., National Aeronautics and Space Administration, Goddard Space Flight Center, 1999.

[19] Shindell, D., "Climate and Ozone Response to Increased Stratospheric Water Vapor," *Geophysical Research Letters*, vol. 28, pp. 1551–1554, April 2001.

[20] Daniel B. Kirk-Davidoff, Eric J. Hintsa, J. G. A. and Keith, D. W., "The Effect of Climate Change on Ozone Depletion through Changes in Stratospheric Water Vapor," *Nature*, vol. 402, pp. 399–401, 1999.

[21] Waitz, I. A., Lukachko, S. P., and Lee, J. J., "Military Aviation and the Environment: Historical Trends and Comparison to Civil Aviation," *Journal of Aircraft*, vol. 42, pp. 329–339, 2005.

[22] Nam, T., Shih, K.-C., and Mavris, D. N., "Assessment of Environmental and Regulatory Uncertainty Impacts on Propulsion System Design," in *AIAA's 3rd Annual Aviation Technology, Integration, and Operations (ATIO) Forum, Denver, Colorado, Nov. 17-19*, 2003.

[23] United States Environmental Protection Agency, "Environmental Fact Sheet Adopted Aircraft Engine Emission Standard." `http://www.epa.gov/OMS/regs/nonroad/aviation/aircr-fr.pdf`, April 1997. [Online; accessed 8-May-2004].

[24] The U.S. Environmental Protection Agency (EPA), "New Emission Standards for New Commercial Aircraft Engines." Regulatory Announcement, EPA420-F-05-015, `http://www.epa.gov/otaq/regs/nonroad/`

aviation/420f05015.htm, November 2005. [Online; accessed 27-November-2006].

[25] Guynn, M. D. and Olson, E. D., "Evaluation of an Aircraft Concept With Over-Wing, Hydrogen-Fueled Engines for Reduced Noise and Emissions," tech. rep., NASA Langley Research Center, Hampton, Virginia, 2002.

[26] Guynn, M. D., Freeh, J. E., and Olson, E. D., "Evaluation of a Hydrogen Fuel Cell Powered Blended-Wing-Body Aircraft Concept for Reduced Noise and Emissions," Tech. Rep. NASA/TM-2004-212989, NASA, 2004.

[27] Wikipedia, "Solar cell — Wikipedia." http://en.wikipedia.org/wiki/Solar_cell, 2006. [Online; accessed 25-November-2006].

[28] California Energy Commission, "Energy Time Machine." http://www.energyquest.ca.gov/time_machine/1950ce-1960ce.html, 2006. [Online; accessed 22-December-2006].

[29] Energy Information Administration, U.S. Department of Energy, "July 2006 Monthly Energy Review." http://tonto.eia.doe.gov/FTPROOT/multifuel/mer/00350607.pdf, July 2006. [Online; accessed 27-November-2006].

[30] "Strategic Significance of Americas Oil Shale Resource, Volume I Assessment of Strategic Issues." Office of Deputy Assistant Secretary for Petroleum Reserves, U.S. Department of Energy Washington, D.C., March 2004.

[31] Tester, J. W., Drake, E. M., Driscoll, M. J., Golay, M. W., and Peters, W. A., *Sustainable Energy: Choosing Among Options*. The MIT Press, 2005.

[32] J. Brand, S. Sampath, F. S., "Potential Use of Hydrogen in Air Propulsion," in *AIAA/ICAS International Air and Space Symposium and Exposition: The Next 100 Y*, 2003.

[33] Bentley, R. W., "Global Oil & Gas Depletion: an Overview," *Energy Policy*, vol. 30, pp. 189–205, 2002.

[34] Laherrere, J., "Hydrocarbons Resources," in *The Fifth International Petroleum Conference and Exhibition - Petrotech 2003*, 2003.

[35] Wayne, E. A., "Energy Security - A Global Challenge." Released by The United States Mission to the European Union, http://www.state.gov/e/eb/rls/rm/2006/66715.htm, May 2006. [Online; accessed 16-August-2006].

[36] Feder, B. J., "A Different Era for Alternative Energy," *The New York Times*, May 29, 2004 Saturday Late Edition - Final, Section C; Column 4.

[37] U.S. Department of Energy, "Hydrogen, Fuel Cells & Infrastructure Technologies Program - Multi-Year Research, Development and Demonstration Plan." http://www1.eere.energy.gov/hydrogenandfuelcells/mypp/index.html, May 2006. [Online; accessed 5-January-2007].

[38] Energy Information Administration, "Annual Energy Outlook 2006 With Projections to 2030." www.eia.doe.gov/oiaf/aeo/, February 2006. [Online; accessed 22-July-2006].

[39] Smith, D., "Pain at the pump." National Geographic News, http://news.nationalgeographic.com/news/2000/03/0302_oil.html, March 2 2000. [Online; accessed 29-July-2006].

[40] Greene, D. L. and Tishchishyna, N. I., "Costs of Oil Dependence : A 2000 Update," tech. rep., U. S. DEPARTMENT OF ENERGY, 2000.

[41] U.S. Environmental Protection Agency, "Strengthen National Energy Security." http://www.fueleconomy.gov/feg/oildep.shtml. [Online; accessed 24-October-2006].

[42] "Energy Dependence and Oil Security, Statement of Senator Joseph R. Biden." http://www.senate.gov/~foreign/testimony/2006/BidenStatement060516.pdf, May 16 2006. [Online; accessed 29-July-2006].

[43] The National Energy Policy Development Group, "National Energy Policy." http://www.whitehouse.gov/energy/, May 2001. [Online; accessed 20-September-2006].

[44] Office of the Press Secretary, "President bush signs into law a national energy plan." http://www.whitehouse.gov/news/releases/2005/08/20050808-4.html, August 2005. [Online; accessed 9-September-2006].

[45] The Department of Energy, "U.S. Department of Energy Strategic Plan." http://www.energy.gov/about/strategicplan.htm, 2006. [Online; accessed 11-January-2007].

[46] National Economic Council, "Advanced Energy Initiative," February 2006. [Online; accessed 16-August-2006].

[47] Cowell, A., "Sweden Offers Itself as a Model on Energy," *The New York Times*, February 3, 2006.

[48] Vidal, J., "Sweden Plans to be World's First Oil-Free Economy," *The Guardian*, February 8, 2006.

[49] Romeo, G., Frulla, G., Cestino, E., and Corsino, G., "HELIPLAT: Design, Aerodynamic, Structural Analysis of Long-Endurance Solar-Powered Stratospheric Platform," *Journal of Aircraft*, vol. 41, pp. 1505–1520, 2004.

[50] Herwitz, S. R., Johnson, L. F., Arvesen, J. C., Higgins, R. G., Leung, J. G., and Dunagan, S. E., "Precision Agriculture as a Commercial Application for Solar-Powered Unmanned Aerial Vehicles," in *AIAA's 1st Technical Conference and Workshop on Unmanned Aerospace Vehicles*, 2002.

[51] Jr, C. E. K. M., "Microwave-Powered, Unmanned, High-altitude Airplanes," *Journal of Aircraft*, vol. 21, pp. 966–970, 1984.

[52] Ritter, D., "Aerial Refueling," *Code One*, vol. 7, no. 4, 1993.

[53] Guynn, M. D., Croom, M. A., Smith, S. C., Parks, R. W., and Gelhausen, P. A., "Evolution of a Mars Airplane Concept for the Ares Mars Scout Mission," in *2nd AIAA "Unmanned Unlimited" Systems, Technologies, and Operations*, 2003.

[54] The Researcher News, NASA Langley Research Center, "First Stop Langley, Next Stop Mars: Bringing Aeronautics and Space Together with Developmental Model of Airplane to Explore Mars." `http://www.nasa.gov/centers/langley/news/researchernews/rn_ares_100506.html`. [Online; accessed 23-October-2006].

[55] Lorenz, R. D., "Post-Cassini Exploration of Titan: Science Rationale and Mission Concepts," *Journal of the British Interplanetary Society*, vol. 53, pp. 218–234, 2000.

[56] Reuben R. Rohrschneider, John R. Olds, R. D. B. and Virgil Hutchinson, J., "Flight System Options for a Long-Duration Mars Airplane," in *AIAA 3rd "Unmanned Unlimited" Technical Conference, Workshop and Exhibit*, 2004.

[57] "Artist's Concept of the ARES Mars Airplane Flying over Mars." `http://marsairplane.larc.nasa.gov/multimedia.html`. [Online; accessed 25-October-2006].

[58] Bacha, J., Barnes, F., Franklin, M., Gibbs, L., Hemighaus, G., Hogue, N., David Lesnini, J. L., Maybury, J., and Morris., J., "Technocal Review, Aviation Fuel." `http://www.chevron.com/products/prodserv/fuels/bulletin/aviationfuel/pdfs/aviation_fuels.pdf`, 2000. [Online; accessed 28-August-2006].

[59] Day, D. A., "Aviation Fuel." `http://www.centennialofflight.gov/essay/Evolution_of_Technology/fuel/Tech21.htm`. [Online; accessed 14-January-2007].

[60] The ChevronTexaco Energy Research & Technology Company, "Material Safety Data Sheet, Product Number(s): CPS201000." `http://msds.ohsah.bc.ca/msds_ws/MSDS_Files/7656.pdf`. [Online; accessed 15-March-2007].

[61] Wikipedia, "Jet fuel — Wikipedia." http://en.wikipedia.org/wiki/Jet_fuel, 2007. [Online; accessed 12-January-2007].

[62] Silverstein, A. and Hall, E. W., "Liquid Hydrogen as a Jet Fuel for High-Altitude Aircraft," Tech. Rep. NACA RM E55C28a, National Advisory Committee for Aeronautics-Lewis Flight Propulsion Laboratory, 1955.

[63] EG&G Services Parsons, Inc. Science Applications International Corporation, "Fuel Cell Handbook (Fifth Edition)." Contract report sponsored by U.S. Department of Energy, Office of Fossil Energy, National Energy Technology Laboratory, http://www.fuelcells.org/info/library/fchandbook.pdf, October 2000. [Online; accessed 22-September-2005].

[64] Yacobucci, B. D. and Curtright, A. E., "A Hydrogen Economy and Fuel Cells: An Overview." CRS Report for Congress, http://ncseonline.org/NLE/CRSreports/04Jan/RL32196.pdf, January 2004. [Online; accessed 20-November-2006].

[65] Freeh, J. E., Liang, A. D., Berton, J. J., and Wickenheiser, T. J., "Electrical Systems Analysis at NASA Glenn Research Center: Status and Prospects," tech. rep., NASA Glenn Research Center, 2003.

[66] Lopez, R., "ENERGIZED; Search for Alternative Energy Drives Fuel-Cell Research," *Aviation Week & Space Technology*, vol. 164 No. 21, p. 519, 2006.

[67] Bradley, T. H., Moffitt, B. A., Parekh, D. E., and Mavris, D. N., "Flight Test Results for a Fuel Cell Unmanned Aerial Vehicle," in *45th AIAA Aerospace Sciences Meeting and Exhibit, 8 - 11 January 2007, Reno, Nevada*.

[68] Parent, B. and Jeung, I.-S., "Quasi One-Dimensional Performance Analysis of a Magnetoplasma Jet Engine," in *40th AIAA/ASME/SAE/ASEE Joint Propulsion Conference and Exhibit*, 2004.

[69] Eccles, L., George, J., Tsukamoto, M., and Han, H. Y., "Comparison Study of Current Photovoltaic Technologies for Use on a Solar Electric Vehicle," tech. rep., Oregon State University.

[70] BOUCHER, R. J., "Sunrise, the World's First Solar-Powered Airplane," *Journal of Aircraft*, vol. vol.22, pp. 840–846, 1985.

[71] NASA, "Solar-Power Research and Dryden." http://www.nasa.gov/centers/dryden/news/FactSheets/FS-054-DFRC_prt.htm. [Online; accessed 12-June-2006].

[72] NASA, "Past Project ERAST - Pathfinder/Pathfinder Plus." http://www.nasa.gov/centers/dryden/history/pastprojects/Erast/pathfinder.html. [Online; accessed 27-October-2006].

[73] "Sunny Prospect," *Aviation Week & Space Technology*, vol. 163, p. 13, 2005.

[74] Landis, G. A., "Exploring Venus by Solar Airplane," *AIP Conference Proceedings*, vol. 552, pp. 16–18, 2001.

[75] Colozza, A. and Landis, G. A., "Long Duration Solar Flight on Venus," in *Infotech@Aerospace*, 2005.

[76] Parlos, A. G. and Metzgert, J. D., "Feasibility Study of a Contained Pulsed Nuclear Propulsion Engine," *Journal of Propulsion and Power*, vol. 10, pp. 269–278, 1994.

[77] Martinez, J. S. and Plebuch, R. K., "Nuclear Propulsion Applications," in *American Inst. Of Aeronautics And Astronautics, Annual Meeting And Technical Display, 4th*, no. AIAA-1967-781, 1967.

[78] The Comptroller General of the United States, "Review of Manned Aircraft Nuclear Propulsion Program." `http://www.fas.org/nuke/space/anp-gao1963`, February 1963. [Online; accessed 14-January-2005].

[79] Rom, F. E., "Status of the Nuclear Powered Airplane," *Journal of Aircraft*, vol. 8, pp. 26–33, 1971.

[80] Lange, R., "Design Concepts for Future Cargo Aircraft," *Journal of Aircraft*, vol. 13, pp. 385–392, 1976.

[81] "What the Nuclear Field Program is all about...." `http://www.cnrc.navy.mil/nucfield/`. [Online; accessed 25-October-2006].

[82] Bennett, G. L., "Space Nuclear Power: Opening the Final Frontier," in *4th International Energy Conversion Engineering Conference and Exhibit*, 2006.

[83] Hamilton, C. E., King, P. I., and Franke, M. E., "Isomer Energy Source in Hybrid Jet Engines for High Altitude Reconnaissance Flight," *Journal of Aircraft 2004*, vol. 41, no. 1, pp. 151–155, 2004.

[84] Frisbee, R. H., "Advanced Space Propulsion for the 21st Century," *Journal of Propulsion and Power*, vol. 19, no. 6, pp. 1129–1154, 2003.

[85] Bulman, M. J. and Borowski, S., "Deep Space Propulsion Requirements Development," in *39th AIAA/ASME/SAE/ASEE Joint Propulsion Conference and Exhibit, Huntsville, Alabama, July 20-23*, no. AIAA-2003-5129, 2003.

[86] Saynor, B., Bauen, A., and Leach, M., "The potential for Renewable Energy Sources in Aviation," tech. rep., Imperial College, London, 2003.

[87] NASA Dryden Flight Research Center, "Beamed Laser Power For UAVs." NASA Facts Sheet FS-2004-03-087 DFRC, `http://www.nasa.gov/centers/dryden/news/FactSheets/FS-087-DFRC.html`, March 2004. [Online; accessed 13-October-2005].

[88] Hertzberg, A. and Sunt, K. C., "A Laser-Powered Flight Transportation System," in *American Institute of Aeronautics and Astronautics, Aircraft Systems and Technology Conference, Los Angeles, Calif., August 21-23, 1978*, 1978.

[89] Friend, M. G. and Daggett, D. L., "Fuel cell demonstrator airplane," in *AIAA International Air and Space Symposium and Exposition: The Next 100 Years, Dayton, Ohio, July 14-17*, 2003.

[90] Dornheim, M. A., "Perpetual Motion," *Aviation Week & Space Technology*, vol. 162 No. 26, p. 48, 2005.

[91] AC Propulsion, "AC Propulsions Solar Electric Powered SoLong UAV." `http://www.acpropulsion.com/solong/ACP_SoLong_Solar_UAV_2005-06-05.pdf`, June 2005. [Online; accessed 22-December-2006].

[92] Taeyun P. Choi, T. N. and Soban, D. S., "Novel Synthesis and Analysis Methods Development towards the Design of Revolutionary Electric Propulsion and Aircraft Architectures," in *Infotech@Aerospace*, 2005.

[93] Raymer, D. P., *Aircraft Design: A Conceptual Approach*. AIAA, 1999.

[94] DeLaurentis, D. A., *A Probabilistic Approach to Aircraft Design Emphasizing Stability and Control Uncertainties*. PhD thesis, Georgia Institute of Technology, November 1998.

[95] Roth, B. A., *A Theoretical Treatment of Technical Risk in Modern Propulsion System Design*. PhD thesis, Georgia Institute of Technology, 2000.

[96] Soban, D. S., *A Methodology for the Probabilistic Assessment of System Effectiveness as Applied to Aircraft Survivability and Susceptibility*. PhD thesis, Georgia Institute of Technology, 2001.

[97] Jenkinson, L. R., Simpkin, P., and Rhodes, D., *Civil Jet Aircraft Design*. Aiaa.

[98] Wood, K., *Aerospace Vehicle Design*, vol. I. Johnson Publishing Company, thrid ed., 1968.

[99] Ibrahim, K., "Selecting Wing Loading and Thrust to Weight Ratio for Military Jet Trainers," in *20th AIAA Applied Aerodynamics Conference*, 2002.

[100] Mattingly, J. D., Heiser, W. H., and Daley, D. H., *Aircraft Engine Design*. AIAA Education Series, second ed., 2002.

[101] Howe, D., *Aircraft Conceptual Design Synthesis*. Professional Engineering Publishing, 2000.

[102] Arjomandi, M. and Liseytsev, N., "A Simplified Method for Estimating the Take-off Weight for Short-haul Transports," *Aircraft Design*, vol. 3, pp. 49–56, 2000.

[103] Anderson, J. D., *Aircraft Performance and Design.* McGraw-Hill, 1999.

[104] Torenbeek, E., *Synthesis of Subsonic Airplane Design: An Introduction to the Preliminary Design of Subsonic General Aviation and Transport Aircraft, With Emphasis on Layout, Aerodynamic Design, Propulsion and Performance.* Delft Univeristy Press, 1976.

[105] Crisler, W. P. and Brandt, S. A., "Teaching the Nine Technologies of Conceptual Aircraft Design," in *1998 World Aviation Conference, Anaheim, CA, Sept. 28-30*, no. AIAA-1998-5531, AIAA and SAE, 1998.

[106] Jun, Y., "Special Report Golden Eagle Flies High - Waht's the next step?," *Aerospace Korea*, October 2005.

[107] Roth, B. and Mavris, D. N., "Commercial Engine Architecture Selection in the Presence of Uncertainty and Evolving Requirements," in *The 15th International Society of Air Breathing Engines, Bangalore, India, September 2-7*, 2001.

[108] Mavris, D. N., DeLaurentis, D. A., Hale, M. A., and Tai, J. C., "Elements of an Emerging Virtual Stochastic Life Cycle Design Environment," in *The 4th World Aviation Congress and Exposition, San Francisco, CA, October 19-21*, 1999.

[109] Nam, T., Soban, D. S., and Mavris, D. N., "A Generalized Aircraft Sizing Method and Application to Electric Aircraft," in *The 3rd International Energy Conversion Engineering Conference, San Francisco, California, Aug. 15 - 18*, 2005.

[110] Mavris, D. N., Bandte, O., and DeLaurentis, D. A., "Robust Design Simulation: A Probabilistic Approach to Multidisciplinary Design," *Journal of Aircraft*, vol. 36, no. 1, pp. 298–307, 1999.

[111] Bandte, O., *A Probabilistic Multi-Criteria Decision Making Technique for Conceptual and Preliminary Aerospace Systems Design.* PhD thesis, Georgia Institute of Technology, 2000.

[112] Baker, A., *The Role of Mission Requirements, Vehicle Attributes, Technologies and Uncertainty in Rotorcraft System Design.* PhD thesis, Georgia Institute of Technology, 2002.

[113] Linderoth, J., "Stochastic Programming Modeling." Lecture Notes, `http://www.lehigh.edu/~jtl3/teaching/ie495/lecture2.pdf`, January 2003. [Online; accessed 23-July-2005].

[114] Holder, B. and Wallace, M., *Range Unlimited - A History of Aerial Refueling.* A Schiffer Military History Book, 2000.

[115] Wickenheiser, T. J., Sehra, A. K., Seng, G. T., Freeh, J. E., and Berton, J. J., "Emissionless Aircraft: Requirements and Challenges," in *AIAA/CAS International Air and Space Symposium and Exposition: The Next 100 Y, 14-17 July 2003, Dayton, Ohio*, no. AIAA 2003-2810, July 2003.

[116] Alexander, D. S., "Advanced Energetics for Aeronautical Applications," Tech. Rep. NASA/CR-2003-212169, MSE Technology Applications, Inc., 2003.

[117] Berton, J. J., Freeh, J. E., and Wickenheiser, T. J., "An Analytical Performance Assessment of a Fuel Cell-Powered, Small Electric Airplane," Tech. Rep. NASA/TM2003-212393, NASA Glenn Research Center, June 2003.

[118] Kohout, L. L. and Schmitz, P. C., "Fuel Cell Propulsion Systems for an All-Electric Personal Air Vehicle," Tech. Rep. NASA/TM2003-212354, NASA Glenn Research Center, July 2003.

[119] Alexander, D., Lee, Y.-M., Guynn, M., and Bushnell, D., "Emissionless Aircraft Study," in *38th AIAA/ASME/SAE/ASEE Joint Propulsion Conference & Exhibit*, no. AIAA-2002-4056, 2002.

[120] Smith, J. R., Batish, P. G., Brandt, S. A., and Morton, S. A., "A Student Developed Sizing Methodology for Electric Powered Aircraft Applied to Small UAVs," in *2000 World Aviation Conference, San Diego, CA*, 2000.

[121] Harmats, M. and Weihs, D., "Hybrid-Propulsion High-Altitude Long-Endurance Remotely Piloted Vehicle," *Journal of Aircraft*, vol. 36, no. 2, pp. 321–331, 1999.

[122] L. Zhou, K. C., "Uncertainty Analysis in the Preliminary Design Stage for a Robust Multidisciplinary Methodology," in *10th AIAA/ISSMO Multidisciplinary Analysis and Optimization Conference*, 2004.

[123] Tomsic, J. L., ed., *SAE Dictionary of Aerospace Engineering.* Society of Automotive Engineers, Inc, 1998.

[124] Wikipedia, "Higher heating value — Wikipedia." `http://en.wikipedia.org/wiki/Higher_heating_value`, 2007. [Online; accessed 4-April-2007].

[125] Wikipedia, "Heating value — Wikipedia." `http://en.wikipedia.org/wiki/Heating_value`, 2007. [Online; accessed 4-April-2007].

[126] Cumpsty, N., *Jet Propulsion.* The Press Syndicate of the University of Cambridge, 1997.

[127] Spenser, J., "International Fuel Cell Efforts Include Boeing," *Boeing Frontiers*, vol. 3, Issue 3, July 2004. `http://www.boeing.com/news/frontiers/archive/2004/july/ts_sf7b.html`, [Online; accessed 14-December-2005].

[128] Bayles, G., "New Power Source Technologies for Electric Wheelchairs," tech. rep., University of Pittsburgh RERC on Wheelchair Mobility, 9 1996.

[129] "Boeing Company, Image Gallery." http://www.boeing.com/companyoffices/gallery/images/commercial/777200-01.html. [Online; accessed 26-March-2007].

[130] "Hades: Suppression of Enemy Air Defense for the Future Combat Arena - Morphing Unmanned Combat Aerial Vehicle, American Institute of Aeronautics and Astronautics 2004-2005 Graduate Team Aircraft Design Competition," tech. rep., Georgia Institute of Technology, 2005.

[131] Muñoz, J. R. and von Spakovsky, M. R., "The Use of Decomposition for the Large Scale Synthesis/Design Optimization of Highly Coupled, Highly Dynamic Energy Systems, Part II - Applications," in *Proceedings of the ASME, Advanced Energy System Division*, vol. 40, pp. 231–249, The American Society of Mechanical Engineers, 2000.

[132] Pines, D. J. and Bohorquez, F., "Challenges Facing Future Micro-Air-Vehicle Development," *Journal of Aircraft*, vol. 43, no. 2, pp. 290–305, 2006.

[133] Barnett, D. M., Rawal, S., and Rummel, K., "Multifunctional Structures for Advanced Spacecraft," *Journal of Spacecraft and Rockets*, vol. 38, no. 2, pp. 226–230, 2001.

[134] "AeroVironment's "WASP" Micro Air Vehicle Sets World Record." http://www.aerovironment.cn/news/news-archive/wasp62.html, August 2002. [Online; accessed 14-October-2006].

[135] Klann, J. L. and Snyder, C. A., "NASA Engine Performance Program." Aeropropulsion Analysis Office, NASA Lewis Research Center, Cleveland Ohio, March 1997.

[136] "WATE User's Guide." NASA Lewis Research Center, 1999.

[137] Soban, D. and Upton, E., "Design of a UAV to Optimize Use of Fuel Cell Propulsion Technology," in *Infotech@Aerospace*, 2005.

[138] Colozza, A. J., "Effect of Date and Location on Maximum Achievable Altitude for a Solar Powered Aircraft," Tech. Rep. NASA/CR-202326, NASA, March 1997.

[139] Dornheim, M. A., "Get Me Through the Night," *Aviation Week & Space Technology*, vol. 159, pp. 66–70, September 15, 2003.

[140] Colozza, A., "Effect of Power System Technology and Mission Requirements on High Altitude Long Duration Aircraft," Tech. Rep. NASA/CR-194455, NASA, 1994.

[141] Reinhardt, K. C., Lamp, T. R., Geis, J. W., and Colozza, A. J., "Solar-Powered Unmanned Aerial Vehicles," in *IECEC 96. Proceedings of the 31st Intersociety Energy Conversion Engineering Conference*, vol. 1, pp. 41–46, 1996.

[142] Rizzo, E. and Frediani, A., "A Model for Solar Powered Aircraft Preliminary Design," in *XVIII Congresso Nazionale Aidaa*, 2005.

[143] Kall, P. and Wallace, S. W., *Stochastic Programming*. Wiley John & Sons, 1995.

[144] Birge, J. R. and Louveaux, F., *Introduction to Stochastic Programming*. Springer, 2000.

[145] Charnes, A. and Cooper, W. W., "Chance-Constrained Programming," *Management Science*, vol. Vol. 6, pp. 73–79, 1959.

[146] Bollapragada, R., Rao, U., and Zhang, J., "Managing Two-stage Serial Inventory Systems under Demand and Supply Uncertainty and Customer Service Level Requirements," *IIE Transactions*, vol. 36, no. 1, p. 73, 2004.

[147] Kandlikar, M. and McRae, G. J., "Inversion of the Global Methane Cycle Using Chance Constrained Programming: Methodology and Results," *Chemosphere*, vol. 30, no. 6, pp. 1151–1170, 1995.

[148] Agnew, N. H., Agnew, R. A., Rasmussen, J., and Smith, K. R., "An Application of Chance Constrained Programming to Portfolio Selection in a Casualty Insurance Firm," *Management Science*, vol. 15, no. 10, p. B512 (9 pages), 1969.

[149] Li, S. X., "An Insurance and Investment Portfolio Model Using Chance Constrained Programming," *Omega (International Journal of Management Science)*, vol. 23, no. 5, pp. 577–585, 1995.

[150] Rao, S., "Structural Optimization by Chance Constrained Programming Techniques," *Computers and Structures*, vol. 12, pp. 777–781, 1980.

[151] Shih, C. J., Wang, C. S., and Lin, Y.-Y., "Hasofer-Lind's Reliability-Based Optimization for Multiobjective Fuzzy and Stochastic Design Problem," in *the Sixth IEEE International Conference on Fuzzy Systems*, vol. 3, 1997.

[152] Enevoldsen, I. and Sorensen, J., "Reliability-Based Optimization in Structural Engineering," *Structural Safety*, vol. 15, pp. 169–196, 1994.

[153] Tu, J., Choi, K. K., and Park, Y. H., "A New Study on Reliability-Based Design Optimization," *Journal of Mechanical Design*, vol. 121, pp. 557–564, 1999.

[154] Rais-Rohan, M. and Xie, Q., "Probabilistic Structural Optimization Under Reliability, Manufacturability, and Cost Constraints," *AIAA Journal*, vol. 43, pp. 864–873, 2005.

[155] Ba-abbad, M. A. and Kapania, R. K., "Reliability-Based Structural Optimization of an Elastic-Plastic Beam," *AIAA Journal*, vol. 41, pp. 1573–1582, 2003.

[156] Madsen, H. and Hansen, P. F., "Comparison of Some Algorithms for Reliability-Based Structural Optimization and Sensitivity Analysis," in *Brebbia CA, Orszag SA (eds) Reliability and Optimization of Structural Systems*, pp. 443–451, 1991.

[157] Smith, N. and Mahadevan, S., "Probabilistic Methods for Aerospace System Conceptual Design," *Journal of Spacecraft and Rockets*, vol. 40, pp. 411–418, 2003.

[158] Haneveld, W. and Vlerk, M., "Integrated Chance Constraints: Reduced Forms and an Algorithm," *Computational Management Science*, vol. 3, issue 4, pp. 245–269, 2006,.

[159] Mourelatos, Z. P. and Liang, J., "A Methodology for Trading-off Performance and Robustness under Uncertainty," *Journal of Mechanical Design, Transactions of the ASME*, vol. 128, pp. 856–863, 2006.

[160] Raymer, D. P., "Vehicle Scaling Laws for Multidisciplinary Optimization (Preliminary Report)," in *Aerospace Sciences Meeting and Exhibit, 39th, Reno, NV*, 2001.

[161] Linderoth, J., "Chance Constrained Programming." Lecture Notes, `http://www.lehigh.edu/~jtl3/teaching/ie495/lecture22.pdf`, January 2003. [Online; accessed 30-June-2005].

[162] de Farias, D. P. and Roy, B. V., "On Constraint Sampling in the Linear Programming Approach to Approximate Dynamic Programming," *Mathematics of Operations Research*, vol. 29, pp. 462–478, 2004.

[163] Calafiore, G. and Campi, M., "Uncertain Convex Programs: Randomized Solutions and Confidence Levels," *Mathematical Programming*, vol. 102, no. Number 1, pp. 25–46, 2005.

[164] Zoutendijk, G., *Methods of Feasible Directions: A Study in Linear and Nonlinear Programming*. Elsevier Pub. Co, Amsterdam, 1960.

[165] Luenberger, D., *Linear and Nonlinear Programming*. Addison-Wesley, 1984.

[166] Torng, T. and Yang, R., "Advanced Reliability Based Optimization Method for Robust Structural System Design," *Collection of Technical Papers - AIAA/ASME Structures, Structural Dynamics and Materials Conference*, pp. 1198–1206, 1993.

[167] Chen, X., Hasselman, T. K., and Neill, D. J., "Reliability Based Structural Design Optimization for Practical Applications," *Collection of Technical Papers - AIAA/ASME/ASCE/AHS/ASC Structures, Structural Dynamics & Materials Conference*, vol. 4, pp. 2724–2732, 1997.

[168] Wu, Y.-T. and Wang, W., "Efficient Probabilistic Design by Converting Reliability Constraints to Approximately Equivalent Deterministic Constraints," *Journal of Integrated Design and Process Sciences*, vol. 2, pp. 13–21, 1998.

[169] Du, X. and Chen, W., "Sequential Optimization and Reliability Assessment Method for Efficient Probabilistic Design," *Journal of Mechanical Design*, vol. 126, pp. 225–233, 2004.

[170] Padmanabhan, D. and Tappeta, R. V., "Monte Carlo Simulation in Reliability Based Optimization Applied to Multidisciplinary System Design," in *44th AIAA/ASME/ASCE/AHS Structures, Structural Dynamics, and Materials Conference*, 2003.

[171] Nikolaidis, E., Ghiocel, D. M., and Singhal, S., eds., *Engineering Design Reliability Handbook*. CRC, 2004.

[172] Hasofer, A. M. and Lind, N. C., "An Exact and Invariant First-Order Reliability Format," *Journal of Enginnering Mechanics*, vol. 100, pp. 111–121, 1974.

[173] Rackwitz, R. and Fiessler, B., "Structural Reliability Under Combined Random Load Sequences," *Computers and Structures*, vol. 9, pp. 489–494, 1978.

[174] Choi, K. and Youn, B., "Advances in Reliability-Based Design Optimization and Probability Analysis." Lecture notes, NASA/ICASE Series on Risk-Based Design, December, 10-11, 2001.

[175] Youn, B. D. and Choi, K. K., "A New Response Surface Methodology for Reliability-Based Design Optimization," *Computers and Structures*, vol. 82, pp. 241–256, 2004.

[176] Youn, B., "Hybrid Analysis Method for Reliability-Based Design Optimization," *Journal of Mechanical Design*, vol. 125, pp. 221–232, 2003.

[177] Tandjiria, V., Teh, C. I., and Low, B. K., "Reliability Analysis of Laterally Loaded Piles Using Response Surface Methods," *Structural Safety*, vol. 22, pp. 335–355, 2000.

[178] Gayton, N., Bourinet, J. M., and Lamaire, M., "CQ2RS: A New Statistical Approach to the Response Surface Method for Reliability Analysis," *Structural Safety*, vol. 25, pp. 99–121, 2003.

[179] Agarwal, H. and Renaud, J. E., "Reliability Based Design Optimization Using Response Surfaces in Application to Multidisciplinary Systems," *Engineering Optimization*, vol. 36, pp. 291–311, 2004.

[180] Burton, S. A. and Hajela, P., "Variable Complexity Reliability-Based Optimization with Neural Network Augmentation," in *43rd AIAA/ASME/ASCE/AHS/ASC Structures, Structural Dynamics, and Materials Conference*, 2002.

[181] Papadrakakis, M. and Lagaros, N. D., "Reliability-Based Structural Optimization Using Neural Networks and Monte-Carlo Simulation," *Computer Methods in Applied Mechanics and Engineering*, vol. 191, pp. 3491–3507, 2002.

[182] Liu, B., *Uncertain Programming*. Wiley, 1999.

[183] Buonanno, M. A., *A Method for Aircraft Concept Exploration Using Multicriteria Interactive Genetic Algorithms*. PhD thesis, Georgia Institute of Technology, 2005.

[184] Geoffrion, A. M., "Proper Efficiency and the Theory of Vector Maximization," *Journal of Mathematical Analysis & Applications*, vol. 22, pp. 618–630, 1968.

[185] Charnes A., Cooper WW, F. R., *Management Models and Industrial Applications of Linear Programming*. Wiley, New York, 1961.

[186] Athan, T. W. and Papalambros, P. Y., "Note on Weighted Criteria Methods for Compromise Solutions in Multi-objective Optimization," *Engineering Optimization*, vol. 27, pp. 155–176, 1996.

[187] Zadeh, L., "Optimality and Non-Scalar-Valued Performance Criteria," *Automatic Control, IEEE Transactions on*, vol. 8, pp. 59– 60, 1963.

[188] Fonseca, C. M. and Fleming, P. J., "Genetic Algorithms for Multiobjective Optimization: Formulation, Discussion and Generalization," *Proceedings of the Fifth International Conference on Genetic Algorithms*, pp. 416–423, 1993.

[189] Srinivas, N. and Deb, K., "Multiobjective Optimization Using Nondominated Sorting in Genetic Algorithms," *Evolutionary Computation*, vol. 2, pp. 221–248, 1994.

[190] Zou, T. and Mahadevan, S., "Multiobjective Reliability-Based Optimization," in *45th AIAA/ASME/ASCE/AHS/ASC Structures, Structural Dynamics and Materials Conference*, 2004.

[191] Sayed, M. E., Edghill, M., and Housner, J., "Multi-objective optimization in reliability based design," *International Conference on Computer Aided Optimum Design of Structures, OPTI, Proceedings*, vol. 5, pp. 161 – 169, 1999.

[192] Samer Barakat, Khaldoon Bani-Hani, M. Q. T., "Multi-Objective Reliability-Based Optimization of Prestressed Concrete Beams," *Structural Safety*, vol. 26, pp. 311–342, 2004.

[193] Lian, Y. and Kim, N.-H., "Reliability-Based Design Optimization of a Transonic Compressor," *AIAA Journal*, vol. 44, pp. 368–375, 2006.

[194] Renaud, J. E., "Automatic Differentiation in Robust Optimization," *AIAA Journal*, vol. 35, pp. 1072–1079, 1997.

[195] Phadke, M., *Quality Engineering Using Robust Design*. Prentice Hall, Englewood Cliffs, NJ, 1989.

[196] Liu, H. and Chen, W., "Probabilistic Sensitivity Analysis Methods for Design under Uncertainty," in *10th AIAA/ISSMO Multidisciplinary Analysis and Optimization Conference*, 2004.

[197] Gal, T. and Greenberg, H. J., eds., *Advances in Sensitivity Analysis and Parametric Programming*. Boston: Kluwer Academic Publishers, 1997.

[198] Luenberger, D. G., *Linear and Nonlinear Programming*. Addison-Wesley, 2004.

[199] Bertsekas, D. P., *Nonlinear Programming*. Athena Scientific, 1999.

[200] Cukier, R.I.and Fortuin, C., Shuler, K., Petschek, A., and Schaibly, J. D. I., "Study of the Sensitivity of Coupled Reaction Systems to Uncertainties in Rate Coefficients. I. Theory," *Journal of Chemical Physics*, vol. 59, pp. 3873–3878, 1973.

[201] Schaibly, J. and Shuler, K., "Study of the Sensitivity of Coupled Reaction Systems to Uncertainties in Rate Coefficients. II. Applications," *Journal of Chemical Physics*, vol. 59, pp. 3879–3888, 1973.

[202] Cukier, R., Schaibly, J., and Shuler, K., "Study of the Sensitivity of Coupled Reaction Systems to Uncertainties in Rate Coefficients. III. Analysis of the Approximations," *Journal of Chemical Physics*, vol. 63, pp. 1140–1149, 1975.

[203] McKay, M., Morrison, J., and Upton, S., "Evaluating Prediction Uncertainty in Simulation Models," *Computer Physics Communications*, vol. 117, pp. 44–51, 1999.

[204] Homma, T. and Saltelli, A., "Importance Measures in Global Sensitivity Analysis of Nonlinear Models," *Reliability Engineering & System Safety*, vol. 52, pp. 1–17, 1996.

[205] Sobol', I. M., "Sensitivity Analysis for Nonlinear Mathematical Models," *Mathematical Modeling & Computational Experiment*, vol. 1, pp. 407–414, 1993. [translation of Sobol, Sensitivity Estimates for Nonlinear Mathematical Models, Matematicheskoe Modelirovanie, 2, 1990, pp. 112-118 (in Russian)].

[206] Madsen, H. O., Krenk, S., and Lind, N. C., *Methods of Structural Safety (Prentice-Hall International Series in Civil Engineering and Engineering Mechanics)*. Prentice Hall, 1986.

[207] Worobel, R. and Mayo, M., "Advanced General Aviation Propeller Study," Tech. Rep. NASA CR 114289, NASA CR 114289, 1971.

[208] Choi, T., Soban, D., and Mavris, D., "Creation of a Design Framework for All-Electric Aircraft Propulsion Architectures," in *3rd International Energy Conversion Engineering Conference and Exhibit*, 2005.

[209] Colozza, A. J., "Hydrogen Storage for Aircraft Applications Overview," Tech. Rep. NASA/CR-2002-211867, Analex Corporation, September 2002.

[210] Chambliss, K., Kelly, S., and Kimble, J., "Cryogenic Fluid Storage for the Mission to Mars," tech. rep., Texas Tech University, 1999.

[211] I. Jakupca, J. W., "Self-Contained Aerospace Pressure Following Regenerative Fuel Cell Energy Storage System," in *3rd International Energy Conversion Engineering Conference*, 2005.

[212] Youngblood, J., Talay, T., and Pegg, R., "Design of Long-Endurance Unmanned Airplanes Incorporating Solar and Fuel Cell Propulsion," in *20th SAE, and ASME, Joint Propulsion Conference*, no. AIAA-1984-1430, 1984.

[213] "How does crystal ball calculate sensitivity?." Technical Note cbl-gen-004A, `http://www.crystalball.com/support/simulation/cbl_gen_004A.html`, April 1998. [Online; accessed 20-November-2006].

[214] Raymer, D. P., "Vehicle Scaling Laws for Multidisciplinary Optimization - Use of Net Design Volume to Improve Optimization Realism," in *AIAA Aircraft, Technology Integration, and Operations Forum, 1st*, 2001.

[215] Pouchet, C. F., Forbes, E. T., DeLaurentis, D. A., and Mavris, D. N., "An Exploration and Study of a Novel Approach to Aircraft Volumetric Sizing," in *AIAA's 3rd Annual Aviation Technology, Integration, and Operations (ATIO) Forum*, 2003.

[216] Caddell, W. E., "On the Use of Aircraft Density in Preliminary Design," *SAWE Paper 813*, 1969.

[217] Oberkampf, W., Helton, J., Joslyn, C., Wojtkiewicz, S., and Ferson, S. S., "Challenge Problems: Uncertainty in System Response Given Uncertain Parameters," *Reliability Engineering & System Safety*, vol. 85, pp. 11–19, July-Sept 2004.

[218] Kirby, M. R. and Mavris, D. N., "Forecasting Technology Uncertainty in Preliminary Aircraft Design," in *The 4th World Aviation Congress and Exposition, San Francisco, CA, October 19-21*, 1999.

[219] Oberkampf, W. L., Helton, J. C., and Sentz, K., "Mathematical Representation of Uncertainty," in *AIAA/ASME/ASCE/AHS/ASC Structures, Structural Dynamics, and Materials Conference and Exhibit, 42nd, Seattle, WA, Apr. 16-19*, 2001.

[220] Agarwal, H., *Reliability Based Design Optimization: Formulations and Methodologies*. PhD thesis, University of Notre Dame, 2004.

[221] Zimmerman, H.-J., *Fuzzy Set Theory and its Applications*. Springer, 4th ed., 2005.

[222] Yager, R. R., Kacprzyk, J., and Fedrizzi, M., eds., *Advances in the Dempster-Shafer Theory of Evidence*. Wiley, 1994.

[223] Nikolaidis, E., Chen, S., Cudney, H., Haftka, R. T., and Rosca, R., "Comparison of Probability and Possibility for Design Against Catastrophic Failure under Uncertainty," *Journal of Mechanical Design, Transactions of the ASME*, vol. 126, pp. 386–394, May 2004.

[224] Walley, P., *Statistical Reasoning With Imprecise Probabilities (Monographs on Statistics and Applied Probability)*. Chapman & Hall, 1991.

[225] Agarwal, H., Renaud, J. E., Preston, E. L., and Padmanabhan, D., "Uncertainty Quantification Using Evidence Theory in Multidisciplinary Design Optimization," *Reliability Engineering and System Safety*, vol. 85, pp. 281–294, July/September 2004.

[226] Youn, B. and Wang, P., "Bayesian Reliability Based Design Optimization under Both Aleatory and Epistemic Uncertainties," in *11th AIAA/ISSMO Multidisciplinary Analysis and Optimization Conference, Portsmouth, Virginia, Sep. 6-8*, 2006.

[227] Mavris, D. and DeLaurentis, D., "Methodology for examining the simultaneous impact of requirements, vehicle characteristics, and technologies on military aircraft design," in *22nd Congress of the International Councilon the Aeronautical Sciences (ICAS)*, 2002.

[228] Chemistruck, A., Papadhima, E., Palmer, E., Zwolinski, C., and Fox, M., "Photovoltaic Power Interface." University of Connecticut, Research project report sponsored by PROTON Energy Systems, `http://www.engr.uconn.edu/ece/SeniorDesign/projects/ecesd53/`, 2005. [Online; accessed12-May-2006].

VITA

Taewoo Nam was born in Busan, South Korea in 1969. He attended Seoul National University and graduated with his Bachelor of Science in 1993. He remained at Seoul National University to pursue his Master of Science in Aerospace Engineering. After receiving his MS in 1995, he started working for Samsung Aerospace Industries as a structural analysis engineer. He was assigned to a research project, "Experimental Analysis of Bird Strike Characteristics," which was funded by the Korean government.

In 1996, he participated in the development of the Korea Air Force T-50 and A-50 Advanced Jet Trainer as a configuration design engineer. He continued to work for the program after Korea Aerospace Industries Ltd. was established in 1999 with the consolidation of Samsung Aerospace, Daewoo Heavy Industries, and Hyundai Space and Aircraft Company.

In 2002, he joined the Aerospace Systems Design Laboratory at the Georgia Institute of Technology to pursue his doctorate. He has been an active member of a subtask group of the University Research, Engineering and Technology Institutes (URETI) program. His group is responsible for formulation and development of physics-based methods for analysis and design of revolutionary concepts, architectures, and technologies. His area of interest is development of sizing and synthesis methods for revolutionary concepts that use alternative energy sources including zero-emissions aircraft and regenerative solar-powered aircraft. He has also worked on intelligent design margin allocation for risk mitigation. He currently resides in Alpharetta, Georgia with his wife Joung Yun, daughter Jihye, and son Jiung.